IN-SITU BEHAVIOR OF GEOSYNTHETICALLY STABILIZED FLEXIBLE PAVEMENT

By

Alexander Kwasi Appea

Thesis submitted to the Faculty of the
Virginia Polytechnic Institute and State University
Charles E.Via Department of Civil Engineering
In partial fulfillment of the requirements for the degree of

MASTER OF SCIENCE
in

Civil Engineering

APPROVED:

_____

Dr. Imad L. Al-Qadi, Chairman

_____ _____

Dr. Brian J D Coree, Co-Chairman

Dr. Thomas Brandon

Blacksburg, Virginia

June 20th, 1997

Keywords: geosynthetics, geotextiles, geogrid, stabilization, dynamic loading, flexible pavement, falling weight deflectometer.

IN-SITU BEHAVIOR OF GEOSYNTHETICALLY STABILIZED PAVEMENT SECTIONS

By

ALEXANDER KWASI APPEA

(ABSTRACT)

The purpose of a geotextile separator beneath a granular base, or subbase in a flexible pavement system is to prevent the road aggregate and the underlying subgrade from intermixing. It has been hypothesized that in the absence of a geotextile, intermixing between base course aggregate and soft subgrade occurs. Nine heavily instrumented flexible pavement test sections were built in Bedford County Virginia to investigate the benefits of geosynthetic stabilization in flexible pavements. Three groups of different base course thicknesses (100, 150 and 200mm) test sections were constructed with either geotextile or geogrid stabilization or no stabilization. Woven geotextile was used in sections 2, 5 and 8. Geogrids were used in sections 3, 6 and 9, and sections 1, 4 and 7 were controls.

Six Falling weight deflectometer (FWD) tests were performed on all the nine sections over 30 months. The nine sections were subjected to at least 5 load drops with wide loading range each time. The measured deflections were analyzed using the MODULUS back-calculation program to determine layer moduli. The measured deflections were used together with elastic, viscoelastic and the MODULUS program to determine the extent of intermixing at base-subgrade interface. The study concluded that a transition layer would develop when a separator is absent, especially in the weak sections (designed to fail in three years). Other measurements such as in-situ stresses, rut depth, and subsurface profiling (using ground penetrating radar) support the conclusion of the development of a transition layer.

ACKNOWLEDGEMENT

I would like to express my appreciation to my committee members, Dr. Brian Coree, Dr. Tom Brandon, and especially my major advisor, Dr. Imad Al-Qadi for his keen interest and untiring efforts in the progress of this work.

I also would like to express my gratitude to the Civil Engineering Fabrics Division of the Amoco Fabrics and Fibers Co. (AMOCO) for sponsoring this study and the Virginia Department of Transportation (VDOT) for the their help in conducting the FWD measurements.

The efforts and helpful insights from my colleagues, Salman Bhutta and Amara Loulizi are greatly appreciated.

TABLE OF CONTENTS

TABLE OF FIGURES

LIST OF TABLES

CHAPTER 1 – INTRODUCTION

1.1 BACKGROUND

The United States has one of the largest highway system in the world with over 6.2 million km of roads, however many of the existing roads are becoming structurally inadequate because of the rapid growth in traffic volume and axle loadings. The National Highway Needs Report in the mid-seventies indicated that the deterioration is 50% faster than the road replacement. In the nineties, this statistic could be worse (Guram *et al.*, 1994). The escalating costs of materials and energy and a general lack of resources provide an incentive for exploring alternatives to existing methods of building and rehabilitating roads. Stabilizing paved and unpaved roads with fabrics offers one such alternative. If it can reduce the thickness of the various road layers or extend pavement service life and simultaneously be both cost and performance effective, such a technique would provide a viable alternative.

Geosynthetic materials have been used to stabilize soils in road construction and have proved in several cases to be successful (van Zanten, 1986). The addition of materials possessing properties that would enhance the behavior of the soil itself was no doubt done long before our first historical records. It seems reasonable to assume that the first attempts were made to stabilize swamps and marshy soils using tree trunks, small bushes and the like. Such stabilization attempts were undoubtedly continued with the development of a more systematic approach in which timbers of nearly uniform size and length were lashed together to make a mattressed surface. Such split-log "corduroy" roads over peat bogs date back to 3000 BC (Dewar, 1962). This art progressed to the point where the surface ridges were filled in smooth. Some of these systems were surfaced with a stabilized soil mixture or even paved with stone blocks. However, the deterioration of the timber and its lashings over time was an obvious problem.

The concept of stabilizing poor soils has continued until the present day. The first recorded use of fabrics in roads was attempted by the South Carolina Highways Department in 1926 (Becham, 1935). A heavy cotton fabric was placed on a primed earth base, hot asphalt was applied to the fabric, and a thin layer of sand was placed on the asphalt. The Department built eight separate field experiments. Until the fabric deteriorated, the results showed that the roads were in good condition and that the fabric reduced cracking, raveling and localized road failures. That project was certainly the forerunner on the incorporation of geosynthetic materials in flexible pavements.

In recent years polymer geotextiles and geogrids have been proposed and used to improve the performance of paved roadways and to reduce base course thickness. Performance improvements have been demonstrated for design conditions where relatively large rut depths are acceptable (unsurfaced roads) and where relatively weak pavement sections have been used. Incorporation of geosynthetic materials in the design of paved and unpaved road systems has been shown to improve the performance and service life of pavement.

The major functions of geosynthetic materials are separation, reinforcement, filtration, drainage and liquid barrier (Koerner, 1994). In providing reinforcement, the geosynthetic material

structurally strengthens the pavement section by changing the response of the pavement to loading. In providing separation it prevents contamination of an aggregate layer by the underlying subgrade and hence maintains a clean interface. In providing filtration and drainage, it aids in improving subsurface drainage and allows the rapid dissipation of excess subgrade pore pressures caused by traffic loading (Barksdale *et al.*, 1989). However, the geosynthetic must minimize the possibility of erosion of the drainage layer and resist clogging of the filter over the design life of the pavement.

The most commonly used types of geosynthetics are geogrids, geotextiles, geocomposites, geonets, and geomembranes. Geotextiles and geogrids are mostly used in roads for separation and reinforcement in flexible pavement systems.

For many years, the principal use of geotextiles has been as a separator during the construction of roadworks and in the area of stabilization (Ruddock, 1978). Usually geotextiles are placed directly on the soft soil formation followed by layers of increasingly well compacted aggregate to build up a stabilized layer. Generally, the benefits of a separator in the reduction of the loss of granular material into the subgrade and the prevention of contamination of sub-base are greatest over soft subgrades, e.g. California Bearing Ratio (CBR) < 3% (Lawson, 1992). Over very weak soils, using a separator may be a particularly viable technique for fill placement, particularly in bad weather.

All road systems, whether temporary or permanent, ultimately derive their strength and support from the subgrade. The misconception in conventional layered roadway designs, such as AASHTO, is that respective layers of various pavement components will remain unchanged over the existing subgrade throughout the service life of the pavement. Changes in load and environment cause pavement system failures to occur at the aggregate base subgrade interface. This is a result of the intrusion of low strength subgrade material into the aggregate base and base materials into the subgrade (Hayes *et al.*, 1994).

Research programs have largely concentrated on unpaved roads and have been able to identify benefits in terms of either reduced plastic deformation or the ability to have reduced aggregate thickness (Potter and Currer, 1981). Dawson and Milligan (1989) also concluded that geotextiles can reduce the stresses on the subgrade by preventing premature local shear failure in the subgrade through the provision of lateral restraint within the base aggregate, thus effecting design savings. Other design procedures (Giroud *et al.*, 1981; Hausmann, 1987) developed for stabilizing unpaved roads suggest that the membrane effect of higher modulus geotextiles may permit considerable reduction in designed aggregate thickness where large rut depths, greater than 75mm, are acceptable.

Work by Barenburg *et al.* (1975) clearly showed that incorporation of a geotextile could significantly improve the stability of the roadway system or would allow the system to be constructed using a thinner structural section. In addition, Guram and Hayes (1994) found that the use of geotextiles provided a less expensive alternative to the use of chemically stabilized subgrades in the routine maintenance and reconstruction of roadways. A study by Jorenby and Hicks (1986) shows that base contamination by as little as 10% soil fines can significantly alter the structural value of the base layer.

Geogrids are high-strength extruded sheets of polyethylene or polypropylene with holes punched in a regular pattern producing a grid-like pattern. Geogrids are quite stiff compared to the fibers of geotextiles and have a higher modulus. Some reinforcing restraint has been observed from geogrids within the subbase below thin asphalt layers (Kennepohl *et al.*, 1985; Chan. *et al.*, 1989), improving load distribution and acting as a reinforcement membrane. Laboratory research on geosynthetic reinforcement of base courses in flexible pavements was conducted by Barksdale *et al.* (1989) at the University of Nottingham, the analytical studies were conducted at the Georgia Institute of Technology. Some of the variables investigated in the laboratory study included types and stiffness of reinforcement, reinforcement position, pavement strength, geosynthetic prestressing and prerutting of the aggregate base both with and without reinforcement. The laboratory and analytical results indicated that geosynthetic reinforcement of an aggregate base can, under the proper conditions, improve pavement performance with respect to both permanent deformation and fatigue.

Barksdale *et al.* (1989) recommended additional research be conducted consisting of carefully instrumented, full-scale field test sections. They recommended geogrid reinforcement as the primary reinforcement since it was found to perform better than woven geotextile. Geotextile reinforcement however has the advantage of providing an additional separation function that can help maintain original performance characteristics. A comprehensive laboratory study by Al-Qadi *et al*. (1994) was performed on stabilized paved sections. In this study, cyclic circular plate loading tests were performed on laboratory-built secondary road pavement sections. The sections were stabilized with geotextiles or geogrids placed between the subgrade and base layer. Section failure was defined as a permanent deformation of 25mm under the loading plate. They reported that more cycles (almost twice) were needed to reach a deformation of 25mm for the geotextile stabilized as compared with the geogrid stabilized and control sections. Details of different research studies on geosynthetics in flexible pavement systems are presented in Chapter Two.

Studies to date have found that incorporation of geosynthetics in flexible pavement provides a degree of performance improvement. A few studies have tried to quantify the benefits of geosynthetic reinforcement/separation, but no firm conclusions can be drawn due to differences of results. Although geogrids may have a higher tensile strength than geotextiles, migration of fines from the subgrade and penetration of the aggregate from the base course may occur through the larger openings. Some of the findings reported by Austin and Coleman (1993) showed that no significant correlation could be made between the geosynthetic tensile strength of geogrids and the measured performance. Thus, an important need exists to quantify the benefits derived from stabilizing flexible pavements with geosynthetics and the conditions necessary for successful geosynthetic stabilization if an adequate cost comparison is to be made.

1.2 PROBLEM STATEMENT

In recent years polymer geotextiles and geogrids have been proposed to improve the performance of paved and unpaved roadways and to reduce base course thickness. Existing literature shows that laboratory and analytical studies performed in the past have shown promising

results, however, conflicting and sometimes inconclusive results have been reported with regards the degree of improvement provided by geosynthetics.

One of the principal applications of geotextiles in road pavements has been as a separator between the base course or subbase and subgrade. The main purpose of the granular base is to dissipate the stress imposed by vehicles on the underlying soil to a safe level and thereby control the life of the pavement. At the absence of a geotextile, intermixing of the base and subgrade (base contamination) may occur under the influence of traffic loading due to the pumping of fines from the subgrade into the base course. The intermixing between two dissimilar materials causes a net reduction of base course thickness and weakening of that layer. A transition layer at the subgrade-base course interface may develop. Contamination changes the gradation of the base and causes the effected base to become overstressed, thereby limiting the life of the pavement. There has been limited research on the effect of base contamination on the structural capacity of the pavement system.

1.3 OBJECTIVES

The construction and monitoring of a well instrumented pavement section comprising control sections and geosynthetic stabilized sections with real traffic providing real field conditions provides the basis to address the lack of understanding of the contamination mechanism. The objective of this research is to confirm the occurrence of base contamination (intermixing of subgrade and base course) in sections without geosynthetics, and to quantify its progress over time.

1.4 HYPOTHESIS

It is hypothesized that geosynthetics improve pavement performance by preventing subgrade contamination of granular base course or subbase layers, and that in the absence of a geotextile at the subgrade/ base course or subbase interface, aggregate contamination by the subgrade fines occurs thereby weakening the overall strength of the pavement system. It is further hypothesized that the effects of this mechanism can be identified and quantified by analyzing the data by falling weight deflectometer (FWD).

1.5 RESEARCH APPROACH

Nine test sections of flexible pavements have been constructed in Bedford County, Virginia as part of the realignment of Route 757. For three different base course thickness (100, 150 and 200mm) test sections were constructed with either geotextile or geogrid stabilization or with no stabilization. The woven geotextile used in sections 2, 5, and 8 was manufactured by the Amoco

Fabrics and Fibers Corporation, and the geogrid used in test section 3, 6 and 9 was manufactured by the Tensar Corporation. The total length of the test section was 150 m. The site is a typical secondary road section with an average daily traffic (AADT) of less than 800 vehicles per day. The pre-construction average CBR of the subgrade soil was measured to be 2-3%. The CBR of the subgrade soil after construction was in the range of 6-8%. The road test sections were instrumented with earth pressure cells, strain gages, temperature sensors, soil moisture sensors and piezoelectric polymer traffic sensors. The majority of the instruments were placed in the right side wheel path of the inside lane of the test sections, 0.53-0.69m from the shoulder.

The pressure cells measured the vertical pressures developed in the subgrade and base course due to dynamic traffic loading. Two different types of earth pressure cells were installed in the pavement sections; Kulite and Carlson type earth pressure cells. The strain gages measured strains in the subgrade and Hot-mix asphalt (HMA).

Thermocouples were installed in the HMA layer, base course and subgrade to record daily temperatures in the layers. Periodic rut measurements were also taken on all the sections. Calibration runs using a test vehicle were conducted to record the responses of the strain and pressure gages under specified axle loads, speeds and tire pressures. Tire pressures of 420, 490, 560, 630 and 700 kPa and speeds of 40, 56, 64 km/h were used. The calibration tests conducted in March 1995, August 1995 and April of 1996, were used in the research analysis.

Seasonal deflection measurements were determined from FWD tests performed on all nine sections. Subgrade resilient moduli were back-calculated for all sections. These tests were performed periodically to monitor changes and seasonal trends in the subgrade resilient moduli of the sections. An analysis of the deflection values (from FWD tests) of all sections will be used to determine if any intermixing is taking place and its rate if any occurs.

Using elastic and viscoelastic layered pavement analysis programs such as ELYSYM5, VESYS and KENLAYER, the surface deflections and stress values in the base and subgrade layers were determined. A comparison of these results with deflection results (from FWD tests) and pressure cell responses in the base and subgrade layers from the calibration runs would help in determining the elastic properties and the extent of base contamination.

1.6 SCOPE OF THESIS

This thesis is divided into five chapters and five appendices. Chapter Two gives the present state of knowledge, manufacturing and applications of geosynthetics; a detailed review of literature on field and laboratory evaluation of geosynthetics is presented. Chapter Three gives a description of the site infrastructure, instrumentation and the research program carried out in Bedford County. A brief description of the use of nondestructive evaluation techniques, such as the FWD and Ground Penetration Radar (GPR) to determine the transition zone is also presented in Chapter three. Chapter Four discusses the data from FWD and other methods used in determining the transition layer development, as well as analyses of this data. Conclusions and summary of findings of the research program are given in Chapter Five.

CHAPTER 2- LITERATURE REVIEW

2.1 GEOSYNTHETICS

Geosynthetics is the collective term applied to thin and flexible sheets of synthetic polymer material incorporated in or about soil to enhance its engineering performance. Applications of geosynthetics fall mainly within the discipline of civil engineering and are closely associated with geotechnical, transportation, and environmental engineering.

The American Society for Testing and Materials (ASTM) has defined geosynthetics in D 4439 as follows: "A planar product manufactured from polymeric material used with soil, rock, earth, or other geotechnical engineering related material as an integral part of a man-made project, structure, or system."

Common types of geosynthetics are geogrids, geotextiles, geocomposites, geonets, and geomembranes and our review would concentrate on geotextiles and geogrids.

2.1 1 GEOTEXTILES

2.1.1.1 Early Use of Geotextiles

Geotextiles, as known and used today were first used in connection with erosion control applications and were intended to be an alternative to granular soil filters. Thus the original, and still sometimes used, term for geotextiles is filter fabrics. Barrett (1966) in his classic paper, tells of work originating in the late 1950's using geotextiles behind precast concrete seawalls, under precast concrete erosion control blocks, beneath large stone riprap, and in other erosion control situations. He used different styles of woven monofilament fabrics, all characterized by a relatively high percentage of open area (varying from 6% to 30%). He discussed the need both for adequate permeability and soil retention, along with adequate fabric strength and proper elongation. Barrett set the stage for geotextile use in filtration situations.

In the late 1960's, Rhone-Poulenc Textiles in France began working with non-woven fabrics for different applications. Emphasis was on reinforcement for unpaved roads, beneath railroad ballast, within embankments and earth, and the like. The primary function in many of these applications was that of reinforcement and separation.

Credit for early work in the use of geotextiles should also be given to the Dutch and the English (van Zanten,1985). Table 2.1 shows the utilization of geotextiles in the early nineties in North America in various civil engineering applications.

Table 2.1 Utilization of Geotextiles in North America by Use in km^2 (after Jagielski, 1995)

Application	**1989**	**1990**	**1991**	**1992**
Asphalt overlays	7550	7340	7340	7340
Separation	6781	7130	7130	7271
Drainage	2936	2936	3006	3076
Protection (membranes)	1748	1258	1328	1328
Erosion control	1188	1258	1258	1328
Reinforcement (wall, subgrade, slopes)	1188	1328	1396	1468
Protection for geomembranes	1748	2517	3426	4824
Total Market	23039	23767	24884	26635

2.1.1.2 Geotextiles Manufacturing

The polymers used in the manufacture of geotextile fibers are made from polypropylene (83%), polyester (14%), polyethylene (2%) and polyamide, nylon (1%). The basic polymers are made into fibers (or yarns, which may consist of one or more fibers) by melting them and forcing them through a spinneret, similar in principle to a bathroom showerhead. The resulting fiber filaments are then hardened or solidified by one of three methods: wet, dry or melt. The melt process accounts for most geotextile fibers; these include polyolefins, polyester, and nylon. Hardening is by cooling and simultaneously stretching the fibers. Stretching reduces the fiber diameter and causes the molecules to arrange themselves in a more orderly fashion. In so doing, the fibers gain strength, the elongation at failure decreases, and modulus increases. A wide range of stress-strain patterns can be achieved. These monofilaments can also be twisted together to form a multifilament yarn.

Geotextiles may be used for separation, reinforcement, filtration and drainage:

1- Separation of dissimilar materials; such as between subgrade and stone base in paved and unpaved roads and airfields, subgrade and ballast in railroads, foundation and embankment soils for roadway fills, and beneath curb areas.

2- Reinforcement of weak soils and other materials; such as over soft soils for unpaved, airfield and railroads, for lateral containment of railroad ballast, to enhance the bearing capacity of shallow foundations, to reinforce embankments, to reinforce jointed flexible pavements, and to bridge over cracked or jointed rock.

3- Filtration (cross-plane flow); such as beneath base course for paved and unpaved roads and air fields, around crushed stone surrounding underdrains and perforated underdrain pipe, and as a filter beneath stone riprap.

4- Drainage; to dissipate seepage water from exposed soil or rock surfaces, as a drainage interceptor for horizontal flow, and as a drain behind a retaining wall.

2.1.1.3 Mechanical Properties

The mechanical properties of a geotextile depend on the mechanical properties of the fiber material and fiber structure, the yarn structure and the structure of the geotextile. Further, the properties depend on direction because of the anisotropy of the material. In general, two directions have to be differentiated: the machine direction and cross direction.

Depending on the application, a geotextile must be able to bear a load or to undergo deformation. A load will cause deformation but also a deformation will mobilize a tension in the geotextile. The relationship between load and deformation is generally considered as a mechanical behavior. Loading can be perpendicular to the plane of the geotextile, e.g. water and soil pressures. Tensile forces and, to a much lesser extent, shear forces can be borne in the plane of the geotextile. A geotextile does not bear compression forces in its plane because both the constituting elements (fibers and yarns) and the geotextile itself are very flexible and tend to buckle in compression. Forces perpendicular to the plane of the geotextile can only be counteracted by a bulge deformation resulting in tensile forces in the plane of the geotextile. External loads can be applied in the form of areas (soil mass, friction, etc.), lines (e.g. seams), or points (stones, pegs, hooks, etc.).

In addition to tensile tests in which the geotextile is subjected to loads and/or displacements, tests have been devised in which the load is applied perpendicular to the geotextile as occurs in many practical cases. These are the burst test and puncture test. When stress concentrations occur, the geotextile is likely to tear. Table 2.2 gives a summary of the various project phases and the relative importance of the geotextile properties.

Non-woven geotextiles are often referred to as being isotropic, however, in most cases these fabrics show some degree of anisotropy. A first approximation of the relationship between load and deformation in the plane of a geotextile can be found by assuming it to be a homogeneous anisotropic layer. The visco-elastic behavior of fiber material becomes manifest under long-term as creep and relaxation.

Mechanical properties of geosynthetics indicate the resistance of the fabric to mechanical forces mobilized under applied loads and installation conditions. Tensile strength is a very important property of geotextiles. Most geosynthetic materials rely on this property when performing the functions of separation, reinforcement, filtration and drainage (Koerner 1990). In determining the tensile strength, the geotextile material is placed within a set of clamps or jaws and stretched until failure occurs. During this extension process the load (or stress) and deformation (or strain) are measured and recorded. From the resulting stress-strain curve the fabric strength, maximum elongation (strain at failure), toughness, modulus of elasticity and secant modulus may be evaluated. In general, geotextile tensile strengths are less than that those of geogrids. Fatigue strength of a geotextile reflects the ability of the fabric to withstand repetitive loading before undergoing failure. In the fatigue test, the tensile test specimen is stressed longitudinally at a constant strain rate to a predetermined length and then relaxed back to zero load. This sequence is repeated cyclically until failure occurs.

Table 2.2 Relation between properties and applications (after van Zanten,1985)

Working phase	Execution	Temporary Construction	Permanent Construction
Relevant	1 month	1/4-year	> 3 years
Tensile strength/strain	+	+	+
Creep, time to failure	–	–	–
Burst and puncture strength	++	O	O
Wear	+	-	+
Shear	+	-	+
Crimp	+*	-	-

* Only when constructing with warm materials, for example asphalt.

++ Of vital importance; +=important; O= possibly influenced by,

- Insignificant

2.1.2 GEOGRIDS

The relatively recent discovery of methods of preparing high-modulus polymer materials by tensile drawing has raised the possibility that such materials may be used in the reinforcement of a number of construction materials, including soil, such as geogrid (Koerner,1990). Today, the major function of geogrids is in the area of reinforcement. Geogrids are relatively high strength, high-modulus, low-creep-sensitive polymers with apertures varying from 10 to 100mm. The holes are either elongated ellipses, near squares with rounded corners, squares, or rectangles.

The key feature of geogrids is that the openings between the longitudinal and transverse ribs, called the apertures, are large enough to allow soil strike through from one side of the geogrid to the other. The ribs of the geogrids are often quite stiff compared to the fibers of geotextiles. The rib strength and junction strength are important parameters. The reason for this is that the soil strike-through within the apertures bears against the transverse ribs, which transmit the forces to the longitudinal ribs via the junctions. The junctions are where the longitudinal and transverse ribs meet and are connected.

The polymer materials used in the manufacture of oriented geogrids are typically high-density polyethylene or polypropylene. Geogrids are manufactured as sheets; holes are then punched into the sheeting in a regular pattern, and the sheet is then drawn uniaxially or biaxially. Geogrids use polyester for strength and are coated with any one of a number of materials.

Drawing is done under controlled temperatures and strain rates to avoid fracture while allowing ductile flow of the molecules into an elongated condition. The key variable in the process is the draw ratio, but other variables, such as molecular weight, molecular weight distribution, and degree of branching or cross-linking, are also important (Koerner, 1995). Aside from marked increases in modulus and strength, the creep sensitivity of the ribs is greatly reduced by the drawing process.

Geogrids has been used beneath aggregate in unpaved roads, beneath ballast in railroad construction, as asphalt reinforcement in pavements, and as inserts between geotextiles**.**

2.1.3 GEONETS

These are the most recently introduced members of the geosynthetic family. They are grid-like materials, however, distinct, from geogrids by virtue of their function. They do have considerable strength but are used mostly for drainage purposes. All geonets are made of polyethylene. The specific gravity of most geonets is in the range of 0.935 to 0.942. The only other materials in geonets are carbon black and a processing package.

In manufacturing, the ingredients are mixed and passed through an extruder, which injects the melt into a die with slotted counter-rotating segments. Over these, the melt flows at angles forming discrete ribs in two planes. As pressure forces the semi-solid mass forward, it is pushed over an increasing diameter core, which forces the ribs apart and opens the net. Diamond-shaped apertures are formed that are typically 12mm long by 8mm wide. Geonets are typically 5.0 to 7.2mm thick. Thickness is a key factor in determining drainage capability. Adding a foam agent to the ingredients can increase thickness of geonets.

2.1.4 GEOMEMBRANES

Geomembranes are thin, two-dimensional sheets of material with very low permeability. This makes them ideal for forming waterproof or gasproof barriers between adjacent bodies of soil or soil and fluid. Some of their potential applications include sealing against fluid percolation along the coasts, river banks, reservoirs and in water storage. They are also used as buffers against pollutants.

The manufacturing of geomembranes begins with the production of raw materials. These are polymer resin, plasticizer accelerators or retarders, filters, and processing aids. The raw materials are blended together and compounded before being extruded in sheet or cylindrical form. Extruders both melt the above materials and homogenize them into a consistent fluid mass in a

partial vacuum. The vacuum eliminates air bubbles in the final product. They are mainly used as canal linings and beneath HMA overlays as a waterproofing layer.

2.2 THE USE OF GEOSYNTHETICS IN FLEXIBLE PAVEMENTS

A national road-system does not only consist of highways for the fast and comfortable movement of high speed traffic but also low volume roads whose principal function is to open up the country. Traffic volume and loads on low volume roads are generally limited, and less strict requirements are usually set for both horizontal and vertical alignments than on highways, which must guarantee a fast flow of the traffic. However, laying out such a road construction on a soft subgrade, which can only support relatively small loads, can be a problem. With a weak subgrade it is often impossible to build a stable base course without punching expensive base material into the subgrade. The base course material is usually pressed into the soft subgrade by the trucks which deliver the material and the machines, which spread it.

In the past, straw, branches, woven rushes and even hides have been used to stabilize weak subgrades. The development of geotextiles, has stimulated the whole of soil improvement process. Because of its fundamental properties, such as tensile strength, filtering and permeability to water, a geotextile inserted between the base course or subbase material and the subgrade may function as reinforcement, a filter medium, a separation layer, a drainage medium or a sealing layer.

2.2.1 Filtration

A common problem with existing pavements is inadequate internal drainage which may result in mud pumping. The mixture being pumped is a combination of fine particles from the subgrade and water trapped beneath the base course. The action of mud pumping is to move this mixture towards the surface and/or shoulder because of traffic load repetitions which may then deposit fines into the base course and sometimes into the HMA layer. The placement of geosynthetics below the base course reduces this problem by preventing the movement of fine particles while allowing the water to drain.

The filtering function is similar to the separation function in that the migration of fines into the base course is reduced. If this migration were permitted to occur, it would make the base course susceptible to frost action, ultimately rendering the pavement structure unstable. The placement of geosynthetic at the base course-subgrade interface permits the drainage of water which is vital to preventing deterioration, and reduces the contamination of the base course with fines.

2.2.2 Reinforcement

The term ”reinforcing” implies the mobilization of tension in the plane of the membrane or membrane reinforcing. It is the ability to distribute a concentrated load over a larger area of the subgrade, thus avoiding local overloading of the bearing capacity. This reinforcement can be classified as base and subgrade restraint, lateral restraint, and membrane type support (Christopher and Holtz, 1985; Giroud, 1987; Haliburton and Barron, 1983; Hausmann, 1987). It has also been suggested that interlocking (friction) between the aggregate-geosynthetic and soil-geosynthetic surfaces may minimize lateral spreading of the aggregate and soil.

Carrol *et al (*1987) carried out a comprehensive program at the University of Waterloo, Ontario on granular base reinforcement of flexible pavements using geogrids. Some of their objectives were to analyze and explain geogrid reinforcement mechanisms in paved road applications through the use of stress, strain, and deflection measurements. They found that grid reinforcement reduced permanent deformation in flexible pavement systems and allowed up to 50% reduction in the thickness requirements of granular base based on equal load-deformation performance. Webster *et al. (*1991) performed studies on geogrid reinforcement of flexible pavements for light aircraft. Their research indicated that geogrid reinforcement improved the performance of the pavement system as a whole and should be placed between the aggregate and subgrade layers for best performance. Based on a literature review, full-scale tests have verified that for CBR strengths in the range of 1.5 to 5.0, geogrid reinforced aggregate surfaced pavements can carry about 3.5 times more traffic repetitions than non-reinforced pavements before 37mm in rut depth is reached (Webster, 1991).

2.2.2.1 Base and Subgrade Constraint

Haliburton *et al.* (1983) suggested that under load, the stress conditions in the base are analogous to those of a loaded beam. Due to bending, the base is subjected to compression at the top and tension at the bottom. The cohesionless materials that make up the base have little tensile resistance and generally depend on the subgrade to provide lateral restraint. In weak subgrades, very little lateral restraint is provided. Thus, the aggregate particles at the bottom of the base tends to move apart, allowing intrusion of the soft subgrade. According to Haliburton *et al.* (1983) a geosynthetic at the bottom of the base course can provide tensile reinforcement, which restrains aggregate movement. However, an extremely high strength, high modulus fabric with good friction or interlocking with the aggregate would be required.

2.2.2.2 Membrane Reinforcement

Membrane reinforcing is mobilized when the subgrade deforms. This type of reinforcing is especially important when laying a base course on soft subgrade with a limited load bearing capacity or in case of an unpaved road after repeated loading. As the subgrade deforms under loading the geosynthetic material stretches like a membrane. The loading is distributed over a wider area as a result of the vertical component of the tension, which develops in the geosynthetic material. Rutting and the resulting spread of the load by the geotextile continues until equilibrium

is reached, that is, until the subgrade can bear the distributed load without further plastic deformation.

Membrane reinforcing is in fact the structural interaction between loading, geotextile and subgrade. With geotextile membrane reinforcing, a road can be constructed on subgrades with low load-bearing capacity and in wet climatological conditions without excessive loss of base material. Membrane reinforcing at the same time reduces the general development of rutting, caused by traffic on an unbound base course. In areas where the subgrade has a strongly varying load-bearing capacity, a geotextile can relieve stresses at weaker points and thus promote and reduce more uniform deformation of the subgrade. The membrane reinforcing function makes it possible to reduce the thickness of the base course required for initial construction. For this type of reinforcement to be significant, the subgrade CBR should be less than 3% (Barkdsdale *et al.*, 1989; Bell, 1980; Robnett and Lai, 1982b). Several research attempts were undertaken to develop an appropriate design procedure for construction involving geotextiles (Giroud and Noiray., 1980, Sellmeijer, 1990).

Membrane reinforcing is greater with high modulus geotextiles (van Zanten, 1986). Many researchers indicate that geotextiles which possess high modulus will provide more load spreading ability for the same degree of deformation (De Groat *et al*., 1986; Hausmann, 1987; Holtz and Harr, 1983; Robnett and Lai, 1982a). Higher tension forces are developed in these materials with smaller elongation compared to low modulus. Creep behavior of geosynthetic materials is important for construction designed for static loads such as stationary trucks. If the material has a limited creep resistance, deformation, including that in the subgrade, will continue under the effect of constant load. After a wheel has passed, the stresses in the material will not be completely removed. Tension forces will remain as a result of the weight of the overlying base course and the structure will remain to some extent pre-stressed.

2.2.2.3 Lateral Restraint

Horizontal reinforcing, often referred to in international literature as ‘lateral restraint’, reduces the horizontal deformation of the base course and the subgrade where these are in contact with the geosynthetic. It has been reported that geosynthetics hold the base material and the subgrade together by developing friction forces between it and the other two materials. This action of the geosynthetic and the base material is referred to as base restraint and that between the geosynthetic and the subgrade as subgrade restraint.

Carrol *et al*. (1987) described lateral restraint as the confinement of the base course through geosynthetic reinforcement thus reducing strain. They stated that “the principle of confinement is best illustrated by a pyramid of billiard balls held together at their base by a plastic ball rack. Without a rack at the base, the pyramid of balls would collapse under its own weight, the rack provides confinement against lateral movement at the pyramid’s base.” The author disagree with this analogy as the pavement system is confined.

2.2.3 Separation

The separation function, which is considered by many (Barsvary and Korgemagi, 1979; Christopher and Holtz, 1985; US Dept of Transportation, 1989b; Al-Qadi *et al.*, 1994) to be the primary function of geotextiles in road construction, prevents contamination of the base coarse aggregate by the subgrade soil, thus preserving the original pavement design. An intermixing occurs by either the aggregate being forced into the subgrade by the action of the applied loads or the migration of the subgrade into the aggregate layer. The load-spreading ability of the aggregate depends on continuous contact between individual aggregate. Under applied loads such as those from vehicle wheels, the aggregate layer deforms. Christopher and Holtz (1985) state that after a sufficient number of load repetitions, the particles at the surface of the layer in contact with the subgrade begins to separate, since the individual aggregate cannot resist the tension forces. Initially, these separations are small; however, they accumulate as the load repetitions continue. As a result, the space between particles increases and the soft subgrade material may intrude into the base course material. A geotextile can prevent this from happening. The effect, therefore, of the separation function is to ensure that the base or sub-base course, (aggregate layer) can be placed as required for initial construction, and will continue to function by remaining separate. Milligan *et al.* (1989) state that when vertical loads are applied to a granular layer, high horizontal stresses develop within that layer. In the absence of a geotextile separator, outward shear stresses occur on the surface of the subgrade. The presence of this outward shear reduces the bearing capacity of the subgrade. Thus, pumping of fines from the subgrade to the base course occurs.

Al Qadi *et al.* (1994) stated that in the absence of separation, two mechanisms tend to occur simultaneously over time in pavements: Soil fines attempt to migrate into the voids between the base course stones, thereby affecting the drainage capability of the pavement and its structural capacity; and the stones tend to penetrate into the soil, compromising the strength of the pavement system.

Jorenby and Hicks (1986) evaluated the separation mechanism in roadways with higher strength soils (CBR > 3%). The performance of a geotextile as a separation layer and its contribution to the road structure was found to be largely dependent on the subgrade material, the magnitude and number of loading during the service life of the road and environmental conditions. With regard to the subgrade soil, the most important factors are the subsoil grain size and the grain size distribution. For the separation function, a geotextile must fulfill the following requirements (van Zanten 1986):

- Soil tightness: The size of openings in the geotextile should be such that subsoil particles cannot intrude into base course and the aggregate cannot be pressed through.
- Water permeability: If the groundwater level rises it should not be possible for water to build up under a separation layer to such an extent that the structural stability is endangered. Any water in the base course must be able to drain through the geotextile, otherwise the base may become unstable. The water permeability of the geotextile should, therefore, be equal to or larger than that of the subgrade. This property is required in both

the short and long-term and it should be verified in the design whether or not the geotextile can be allowed to become blocked.

- Puncture strength: When the base course is loaded, the aggregate is pressed against the geotextile, which therefore must be strong enough to resist puncturing.
- Tearing strength: If the geotextile for any reason is damaged or torn, the tears should not propagate in size under normal loads.
- Breaking strength, breaking strain, stress-strain relation: in order to continue functioning as a separation layer, it is of primary importance that the geotextile remains intact, especially if the subgrade and base course are deformed during construction.

2.3 LABORATORY AND FIELD STUDIES

Literature review revealed that a considerable amount of research has been conducted by various individuals and groups on the use of geotextiles and geogrids in flexible pavements. However, a majority of the research has dealt with geogrid reinforcement in pavements. A summary of five of such tests and reports is presented. A report by White (1991) summarized unpublished data from tests on unsurfaced roads performed by Webster. Full-scale traffic tests on geogrid and geotextile reinforced aggregate layers over sand (SP) subgrade were conducted by Webster using a truck, a tank and a simulated C-130 aircraft tire traffic. These tests included a 100mm aggregate base layer with and without reinforcement placed at the top of the subgrade. Reinforcement materials were as follows:

Test Section	Reinforcement	Test Section	Reinforcement
1	None	4	Geotextile
2	Geotextile	5	Geotextile
3	Geogrid	6	Geotextile

Test traffic loads were as follows:

TRUCK	C-130	TANK
5 ton military	Single tire	77.16 ton
Payload at 9091 kg	Load at 15909 kg	
Gross weight at 19045 kg		
Tire pressure at 490 kPa	Tire pressure at 700 kPa	

Webster's test results show that under truck traffic the geogrid test section performed better than the control. For truck traffic, the unreinforced control section reached a rut depth of 50mm after 2600 passes while it took 5200 passes on a geogrid-reinforced section. The three geotextile sections (2, 5 and 6) performed significantly worse than the control section, indicating aggregate slippage on the geotextiles. Under the C-130 gear traffic all reinforcement performed much worse than the control section. Under tank traffic, performance was mixed. The geogrid section (3) performed best followed by the two strongest geotextiles sections (6 and 5), the control (1), and the two weaker geotextiles sections (4 and 2). For all three types of traffic, test results showed that geogrids performed better than geotextiles. These results showed that reinforcement material friction properties are critical to performance and that more work needs to be done regarding placement depths of reinforcement materials.

In 1989 Barksdale *et al.* performed a study dealing with the performance of geogrids and geotextiles in flexible pavements. Analytical studies were carried out at the Georgia Institute of Technology, and laboratory studies were performed at Nottingham University in England. Analytical studies were performed using the finite element method in order to identify the parameters to be varied in the experimental studies. In the experiment, the major parameters studied were the influence of different geosynthetic types, the placement locations of the geosynthetic, and the effects of prestressing and pre-rutting.

An important finding from the analytical study was that the performance of reinforced flexible pavement sections was not improved when the subgrade CBR was greater than 3%. The large-scale test were performed in a test facility 4.9 by 2.4m in plan using a 7kN wheel loading moving at a speed of 4.8 km/h. Up to 70,000 repetitions of wheel loading were applied to the test sections at a constant temperature. Pressure cells were installed in each section, and strain gages were used to measure strains in each layer of the flexible pavement sections and in the geogrids.

Four series of experiments were carried out, each consists of three pavement sections. The first series was made up of a 25mm HMA surface with a 150mm base course. The other three sections had a 37.5mm asphalt HMA surface with a 200mm base course. The effects of geosynthetic type, geosynthetic position, pre-rutting and prestressing reinforcement in each series were investigated.

Barksdale *et al.* (1989) reported the minimum stiffness of 700 kN/m at 5% elongation, for a woven geotextile and 260 kN/m for geogrids must be used if the geosynthetics are to be used as pavement system reinforcement. They concluded that a woven geotextile must have a stiffness of 2.5 times greater than that of a geogrid to provide the same reinforcing capacity.

They indicated that improvement of pavement performance was clearly shown in the fourth test series. However, based on the data presented the non-prestressed geotextile reinforced section had a permanent strain 30% greater than the prestressed geogrid reinforced section at 10,000 load repetitions. By 70,000 repetitions, however, the difference in measured strain was only about 5%. These results are insufficient to conclude that the geogrid performed better than the geotextile. In addition, the unreinforced section of series two had over twice the permanent deformation of the unreinforced section series three at 10,000 passes. The experimental test results in test series three showed that when the very stiff geotextile was placed at the bottom of

the aggregate base, a reduction of 57 percent in permanent deformation was observed in the subgrade. In test series two when a geogrid was placed at the bottom of the base there was also a 52 percent reduction in permanent subgrade deformation. In his literature review, Barksdale seemed predisposed to the benefits of geogrids over geotextiles. Much of the literature he reviewed involved a lot of work on the benefits of geogrids as reinforcement as opposed to geotextiles.

Concerning the location of the reinforcement, Barksdale *et al*. (1989) concluded that for light pavement sections constructed with low quality aggregate bases, the preferred position for the reinforcement should be in the middle of the base, particularly if a good subgrade is present. For pavements constructed on soft subgrades, the reinforcement should probably be placed at or near the bottom of the base. This is particularly true if the subgrade was known to have rutting problems and the base is of high quality and well compacted.

Barksdale *et al*. (1989) suggested that an HMA surface of thickness between 64mm to 90mm is necessary for the reinforcement to be most effective. Very weak bases, however, could show some improvement under even greater thicknesses of HMA. They stated that light sections on weak subgrades reinforced with geosynthetics with effective thicknesses of 700 to 1050 kN/m could provide reductions in base thickness of 10 to 20 percent . This is based on equal strain levels in the subgrade and bottom of the HMA surfacing. For weak subgrades (CBR < 3%), total rutting in the base and subgrade could be reduced by 20 to 40 percent. Some of the factors that could have influenced the results of Barksdale *et al*. (1989) are the magnitude and duration of the load used in their study. The moving load used was 7 kN, which is small, compared to 40 kN load from a typical 80 kN axle. The speed of 4.8 km/h is relatively slow compared to typical vehicle traffic. It is known that the slower the speed of test traffic, the greater the damage imparted to a flexible pavement. This should have been considered in the analysis and performance evaluation.

Austin and Coleman (1993) conducted a full-scale field study to evaluate the effectiveness of polypropylene geogrids and woven/nonwoven geotextiles as reinforcement in aggregate placed over soft subgrades. The test initial soil strengths were too high for the desired field evaluation conditions. Therefore, the test site was flooded with water and allowed to remain exposed to the environment for almost eight months in order to soften the soil. The resulting subgrade CBR of almost 1% was estimated from correlations with the Dynamic Cone Penetrometer data. The subgrade of the test road was covered with either geogrid or geotextile sections and overlaid with aggregate of varying thickness. The granular subbase of the test sections was constructed with crushed limestone at depths between 150mm to 260mm.

Four geogrids and two geotextiles were used as reinforcement in the study. The test vehicle used in this study had a front axle loaded to 25.1kN and rear dual axle loaded to approximately 81.4kN. A rut depth of 75mm was chosen as the failure criterion. Test sections were trafficked until the failure criterion was reached. Austin and Coleman (1993) found that contamination of the failed granular subbase by the soft subgrade clay was evident in those sections without a geotextile separator. The degree of contamination however varied.

Excavation of the geogrid sections revealed that individual stones from the aggregate subbase had penetrated and interlocked with the apertures of the geogrid. The base layer had been contaminated for thickness ranging from 35mm to 190mm above the original subgrade. The geotextile reinforced sections performed the role as separators and had no evidence of actual tensile failure.

Results from the field study showed that two to three times the number of Equivalent Single Axle Load (ESAL) passes were carried by the reinforced sections than the similar unreinforced (control) sections of same thickness. Austin and Coleman (1993) concluded that geosynthetics provide an effective way of reinforcing and stabilizing aggregate/surface roads (unpaved) built on soft cohesive soils with a CBR less 1%. The separation function of geosynthetics is demonstrated in their data.

Le (1982) in his Ph.D. thesis describes the use of various geotextile fabrics in the construction of streets in New Orleans. The fabrics were placed between the subgrade and base, between the base and the HMA layer or between HMA layers for overlays. All the applications pertained to soft clay subgrades. Strain gages within the subgrade, moisture sensors and FWD measurements were used to monitor the performance of constructed roadways. FWD results from his studies showed an increase in pavement stiffness in sections where geotextiles were placed as a separator. His conclusion was that the inclusion of fabric provided an increase in pavement strength by improving load distribution and acting as a separating membrane. No analytical modeling was performed to predict the observed behavior. Comparisons were made to predictions from existing design procedures.

Jorenby and Hicks (1986) conducted a laboratory study to evaluate the effect of added subgrade fines on the resilient modulus of an aggregate base. By illustrating the effect of subgrade intrusion on resilient modulus, the benefits of using geotextiles to limit intrusion can be demonstrated. The gradations they used were those typical of specified for aggregate base course used with flexible pavements. Resilient modulus tests were performed on the crushed aggregate mixture. The aggregate tested was a 25mm crushed aggregate with 5.5 percent passing the 75 μm (No. 200) sieve. The aggregate was blended with subgrade fines using 2, 4, 6, 8, and 19.5% of added fines. Resilient modulus tests on the aggregate-subgrade fines mixtures compacted to approximately 95% maximum density were performed. The tests were performed with an MTS testing machine. The influence of added fines on the life of a pavement structure was evaluated. Jorenby and Hicks (1986) expressed the amount of contamination as percent increase in fines content of the aggregate base (S) or by the soil contamination value (SCV). An S value of 19.5 represented a situation in which the aggregate base is contaminated to the point where it acts as a subgrade.

Jorenby and Hicks (1986) found that the resilient modulus of the aggregate-subgrade mixture increased as the percentage of fines increased. A peak in resilient modulus was observed at 6 percent added fines. At 8%-added fines, a dramatic drop in resilient modulus occurred. From stiffness standpoint, a 6% added fines could be tolerated when the initial aggregate has 5.5% passing the 75 μm (No 200) sieve.

The work by Jorenby and Hicks (1986) showed the reduction of resilient modulus due to subgrade intrusion in the absence of a separation mechanism at the base/subgrade interface. Taking this into account during design can extend the life of a pavement by the provision of a thicker pavement or thicker aggregate base. A cost-effective alternative was the use of geotextiles as a separation layer. Jorenby and Hicks (1986) estimated potential cost savings between $\$3.50/m^2$ to $\$4.75/m^2$.

Guram *et al*. (1984) conducted a study on the relative performance of Supac 8NP, a nonwoven needle-punched polypropylene geotextile; nominal weight $271g/m^2$ and lime-treated subgrade soil. The subgrade soil was of poor quality and low bearing capacity. The same pavement structure was placed over the lime-treated and the geotextile-covered sections. The durability and performance of both sections were monitored over a period of 9 years. The durability and performance of the geotextile was evaluated by soil sampling, fabric sampling, evaluating roadway conditions, ride quality and roadway maintenance history. In 1986 the lime-treated section had experienced extensive pothole damage and underwent repairs. Guram *et al*. (1984) found that, from a pavement life-cycle analysis, the geotextile section required less maintenance and should continue to show a longer pavement life due to its long-term establishment of a separation and stabilization layer compared with the lime-stabilized system. The research concluded that the non-woven geotextile did not lose any strength properties during 9 years of service life.

In 1992, Al-Qadi *et al*. (1994) performed experimental and analytical investigations to evaluate the performance of pavements with and without geotextile or geogrid reinforced materials. Eighteen pavement sections were tested in three groups: one unreinforced that served as a control, geotextile-stabilized and geogrid-reinforced sections. The geogrids and geotextiles were placed between the subgrade and base course. The test sections were built to model typical secondary roads constructed on a weak granular material. Following the construction of each section, the pavement surface was dynamically loaded using a rigid plate and the resulting displacement was continuously monitored and recorded. Loading of the pavement sections was accomplished using a computer-controlled pneumatic system that delivered approximately 550 kPa through a 300mm rigid plate at a frequency of 0.5 Hz. This loading simulated the dual tire load from a 80 kN axle with a tire pressure of 550 kPa . A 44.5 kN load cell was placed directly on the top of the loading plate to monitor the loading that were applied. Deformation of the pavement surface was monitored and recorded through an array of linear variable displacement transducers (LVDT).

The subgrade was a weak silty sand (CBR of 2-5.5%). The base was a dense granite aggregate (VDOT classification 21-A). Performance of the test sections was evaluated by studying the effect of loading cycles on deformation, the deformation profile at 800 cycles and the rate of deformation. Visual observations and measurements of the excavated profiles were also useful in the evaluation. Performance of the test sections was compared by studying deformation beneath the center of the loading plate as a function of loading cycles. The AASHTO pavement design procedure was used in the study by Al-Qadi *et al*.(1994*)* as the basis for converting loads to equivalent single axle loads as part of the service life prediction. The KENLAYER computer program developed by Huang (1993) was also used to determine the frequency of applied load.

The predicted equivalent single axle loads (ESALs) to failure were calculated and presented for a speed of 64 and 96 km/hr.

Experimental results showed the geotextile stabilized sections sustained 1.7 to over 3 times the number of load repetitions of the control sections for 25mm of permanent deformation. An interesting observation was also made regarding the base course-subgrade interface in the excavated profiles. In the control and geogrid-reinforced sections the granite aggregate material had penetrated into the silty sand subgrade material and the silty sand had migrated into the granite aggregate layer. The geotextile material was effective in preventing fines migration between the base course and subgrade layers. This agrees with field studies conducted by Austin and Coleman (1993). Al-Qadi *et al*. (1994) concluded that geotextiles and geogrids offered substantial improvement to the performance of pavement sections constructed on a low CBR subgrade. They also concluded that geotextiles offer substantial improvement to pavement service life due to separation between the subgrade and aggregate layers.

Although the majority of the investigations into the performance of geosynthetics in pavements have led to the conclusion that the key performance factor of geosynthetics is reinforcement which is based on the tensile strength of geosynthetics. However, recent studies have shown that separation mechanism appears to be more important in improving pavement structure capacity than has been reported previously in the literature.

CHAPTER 3 - PROJECT DESCRIPTION

3.1 SITE INFRASTRUCTURE, INSTRUMENTATION AND MATERIAL PROPERTIES

3.1.1 Site Infrastructure

This research was conducted on pavement test sections constructed on the intersection of Routes 575 and 616 in Bedford County, VA. The selection of the site was as the result of a joint effort between Virginia Tech personnel and representatives of the Virginia Department of Transportation (VDOT).

Selection of the research site was based on several factors:

- A secondary road section approximately 150m in length. This length would allow building nine individual test sections (at least 15m in length).
- An annual average daily traffic (AADT) of less than 800 representing a secondary road.
- A low subgrade CBR value.
- Redirection of traffic during instrument installation at test site.

The nine test sections differed in the type of geosynthetic stabilization used and thickness of the base course layers. Table 3.1 shows the initial design of each of the instrumented test sections. The thickness of the HMA averaged 89mm. Figure 3.1 shows the original road, and the new alignment of the instrumented sections. A detailed view of the test sections and support structures is shown in Figure 3.2.

Table 3.1 Initial design of instrumented sections

Section No	Stabilization	Base Course Thickness (mm)
1	Control	100
2	Geotextile	100
3	Geogrid	100
4	Control	150
5	Geotextile	150
6	Geogrid	150
7	Control	200
8	Geotextile	200
9	Geogrid	200

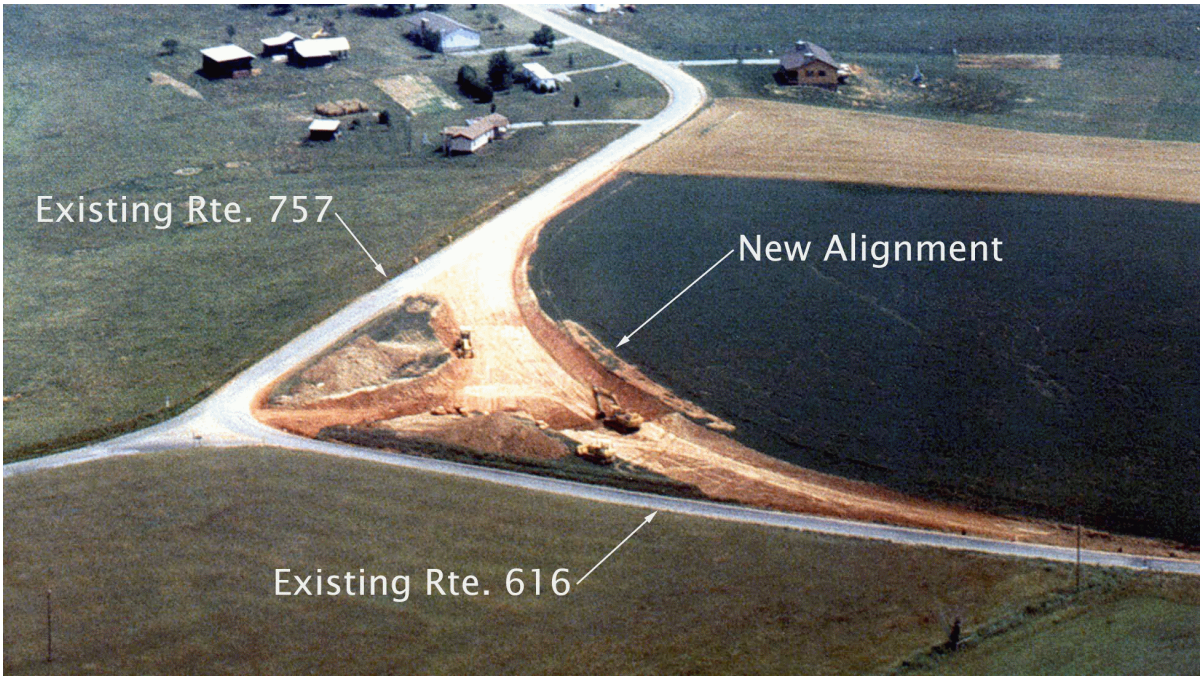

Figure 3.1 Original road and new alignment section

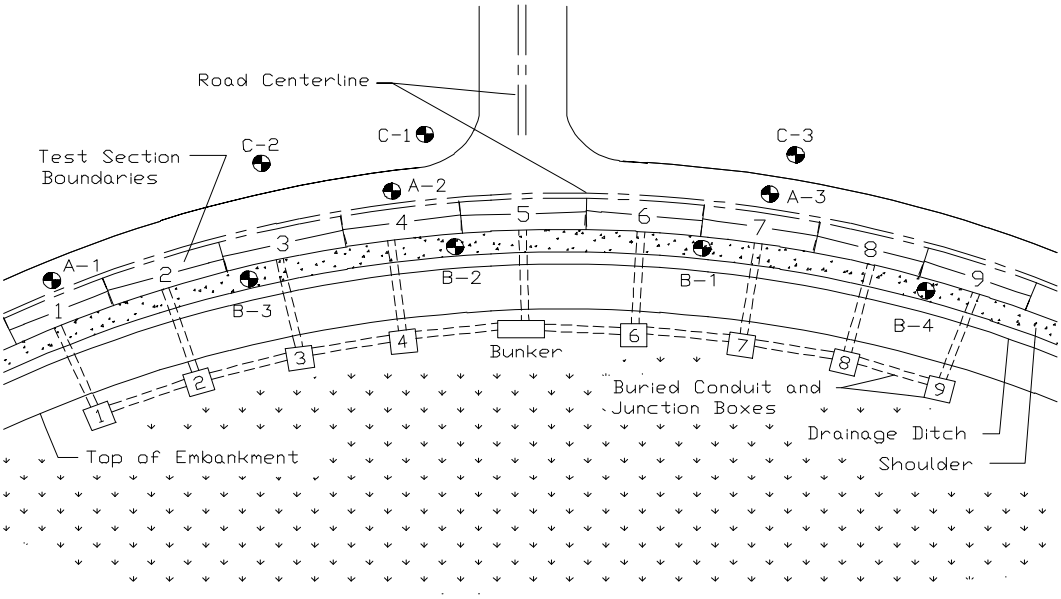

Figure 3.2 Layout of the test sections and support facilities

Construction activities started in early June, 1994 and ended in mid August, 1994. The infrastructure installed included a service pole for the phone and electric power, PVC conduits for channeling the instrumentation wiring system, data acquisition system housed in a bunker, and instrumentation in the pavement layers.

The service pole housed the phone and electric services. Prior to the completion of the bunker, the service pole was equipped with a circuit breaker panel and outdoor outlets to provide power, eliminating the need for on-site generators.

All nine sections were instrumented. The subgrade and base course were instrumented with Kulite earth pressure cells, Carlson earth pressure cells, soil strain gages, thermocouples and moisture sensors. The HMA was instrumented with strain gages and thermocouples. Four piezoelectric traffic sensors were installed in the HMA wearing surface along the length of the pavement test sections. All the instruments were wired from the road to the data acquisition in the bunker.

The data acquisition system comprised both hardware and software. The software component was run on a Microsoft QuickBasic 4.5 program. This program handled the switching from the data acquisition program to the communications software in order to download the data files.

3.2 SITE MATERIALS CLASSIFICATION

3.2.1 Subgrade

Samples of the residual subgrade soil were taken before test section construction at several locations along the proposed road realignment. Auger samples were taken at 45m intervals, at depths of 1, 2, and 3m at each sampling location. The auger samples were taken in accordance with test method ASTM D 1452 -95, and were used for subgrade soil classification purposes and for performing the initial soaked CBR tests on reconstituted specimens. The locations of the auger samples taken are shown in Figure 3.2.

Index and physical property test performed on the subgrade to determine its material properties include:

- Standard test method for classification of soils for engineering purposes, (ASTM D 2487-93)
- Standard test method for particle-size analysis of soils, (ASTM D422-90)
- Standard test method for liquid limit, plastic limit, and plasticity index of soils, (ASTM D 854-92)
- Standard test method for specific gravity of soils, (ASTM D 854-92)
- Standard test methods for moisture-density relations of soils and soil aggregate

mixtures using 2.49 kg hammer and 305mm drop, (ASTM D 698-91)

- Standard test method for moisture-density relations of soil and soil-aggregate mixtures using 4.54 kg hammer and 457mm drop, (ASTM D 1557- 91)
- Standard test method for water content of soil and rock in place by nuclear methods (shallow depths), (ASTM D 3017-96)

Soil Classification: The subgrade is primarily composed of two different residual soil types across the length as reported by Brandon *et al*. (1996). These are a reddish brown material found throughout the majority of the test sections, and a yellowish brown material found mostly in test sections 4 and 5. The reddish brown material was classified as CH using ASTM D 2487-93, and as an A-7-6 by the AASHTO classification method. The subgrade in test sections 4 and 5 is a yellowish brown silt and classifies as an ML using ASTM D 2487-93, and predominantly as an A-5 by the AASHTO classification method.

Soil Gradation: The results of the gradation analyses on the subgrade soil is shown in Appendix A, Figure A 1. CH subgrade material of the test sections has about 80% passing the 75μm (#200) sieve. The ML material found predominantly in sections 4 and 5 has approximately 73% passing the 75μm (#200) sieve.

Atterberg limits tests performed on samples of the CH subgrade material indicated liquid limits (LL) of 56 to 68% and plasticity indices (PI) of 28 to 37%. The ML subgrade material in sections 4 and 5 had liquid limits of approximately 41% and a plasticity index range of 4 to 6%. Results of Atterberg limits are given in Appendix A, Table A 1

The CH material has a specific gravity of 2.77 and the ML material has a specific gravity of 2.74. The results of the specific gravity tests are given in Appendix A, Table A 2.

Laboratory Compaction Characteristics: A modified Proctor effort of 17.1 kN/m^3 at an optimum water content of 17% was obtained for the ML soil and 15.8 kN/m^3 maximum dry density at 24.4% optimum moisture content for the CH soil. The results of the compaction test are shown in Appendix A, Figure A 2. In the field, a nuclear gage was used to determine the dry densities and the moisture contents of the subgrade soil before placement of the base course layer. Tests were performed in accordance with ASTM D 3017 -96. The results are shown in Appendix A, Table A3. Measurements of moisture content were verified using microwave and conventional oven.

3.2.2 Base Course

Samples of the base course material were taken at 30m (100 ft) intervals during placement of the material. The samples were collected for laboratory tests to determine the material properties of the aggregate. The base course material used in construction of the test sections is type 21-B in accordance with VDOT specifications.

Index and physical property tests were performed on the base course aggregate to determine its material properties. These tests include:

- Standard test method for classification of soils for engineering purposes, (ASTM D 2487 - 93).
- Standard test method for particle-size analysis of soils, (ASTM D 422-90)
- Standard test method for moisture-density relations of soils and soil-aggregate mixtures using 4.54 kg hammer and 457mm drop. (ASTM D 1557-91)
- Standard test method for water content of soil and rock in place by nuclear methods, shallow depths, (ASTM D 3017-96).
- Base Course Classification: The base course material is composed of limestone aggregate quarried by W. W. Boxley in Roanoke, Virginia. The material is found to be a GW by the USCS and is classified as a 21-B by VDOT.

Base Course Gradation: The base course aggregate was found to have approximately 50% by weight of its coarse fraction retained on the 4.75mm (No.4) sieve, with a coefficient of uniformity (C_u) of 16, and a coefficient of curvature (C_z or C_c) of 1.5. The results of the gradation analysis on the base course material for pre- and post-construction samples is shown in Figure A 3 (Appendix A).

The specific gravity of the base course aggregate was found to be 2.78. The results of the specific gravity tests on the base course material are given in Table A 2 (Appendix A).

Compaction Characteristics: Modified Proctor test were performed on the base coarse aggregate specimens. The optimum moisture content of 6.1% corresponds to a maximum dry density of 22.4 kN/m^3. Figure A 4 (Appendix A) shows these results along with values obtained from nuclear gage measurements made in the field. A nuclear gage was used to determine the dry densities and the moisture contents of the base course before placement of the HMA layers. The testing was performed in accordance with ASTM D 2922-96.

Nuclear density tests were conducted on the base course and subgrade soils using the nuclear density gage. Moisture contents for the subgrade ranged from 29% to 36%. Average dry densities ranged from 12.3 to 14.0 kN/m^3 for the subgrade. Moisture contents for the base course ranged from 2.0% to 3.2%. The average dry density of the base course layer was 22.5kN/m^3.

Resilient Modulus Tests: The resilient modulus of the base course aggregate sampled from the test sections was determined in the laboratory for remolded specimens. Specimens were tested in accordance with interim test method AASHTO T 294-92-I. The samples were tested at confining stresses of 21, 35, 69, 103, and 138 kPa.

The vertical stresses used in the resilient modulus testing correspond to the responses of pressure cells within the base course of test sections. The responses were recorded during instrument calibrations performed at the project site. Table A 4 (Appendix A) shows the final resilient modulus values as determined based on field instrumentation response (field moisture content at 5.5%). Field instrument response for the calibration runs of 80 kN axle load, 560 kPa tire pressure and 56 km/h speed were used for calculation of resilient modulus.

3.2.3 Geosynthetic Layer

Geosynthetic material layers installed at the base/subgrade interface were polypropylene based polymer materials. The woven geotextile placed in test sections 2, 5, and 8 was manufactured by Amoco Fabrics and Fibers Corporation, product number 2002. The geogrid used in test sections 3, 6 and 9 was manufactured by the Tensar Corporation, product number BX1200. The material properties for the geosynthetics are shown in Tables A 5 and A 6 (Appendix A).

3.2.4 HMA Surface

Properties of HMA layer were determined from samples taken at approximately 30m (100 ft) intervals during construction of the field sections. Specimens were also taken by coring samples of the HMA along the length of the test section by VDOT personnel after construction.

Index and physical property test performed on the HMA layer were the following:

- Bulk specific gravity test, paraffin film method (ASTM D 1188- 89)
- Theoretical maximum specific gravity of the laboratory specimens (ASTM D70 - 90)
- Volumetric properties of the HMA
- Creep compliance for the field specimens
- Resilient modulus of field specimens (ASTM D 4123- 87)
- Asphalt content, ashing method (ASTM D 2172-93)

Laboratory Test Specimens: Marshall specimens were compacted from the HMA samples taken during placement of the HMA layer in the field. Specimens were used in the determination of the volumetric properties of the HMA on the project site. Cored specimens were taken from the inside wheel path along the road test section by VDOT (Virginia Department of Transportation) personnel after the road was constructed. Some of the material properties determined were the bulk specific gravity, resilient modulus and creep compliance.

The average value of the bulk specific gravity for the asphalt was determined to be 2.25. the test results are shown in Table A 7, Appendix A. Volumetric properties such as voids in total mix (VTM), voids in mineral aggregate (VMA), voids filled with asphalt (VFA) as well as the HMA density were determined (Table A 8, Appendix A). The stability and flow of six Marshall specimens were also determined and the results are shown in Table A 9, Appendix A. Asphalt cement content was determined in accordance with the ASTM D 2172-93 procedure using the Ashing method. Two Marshall specimens from each lot were tested. Average asphalt cement contents are summarized in Tables A 10 through A 12, Appendix A.

Resilient modulus tests of the HMA were performed in accordance with ASTM D 4123- 87 on specimens fabricated in laboratory and on core samples taken from the test sections. The 100mm diameter core samples taken from the test sections were trimmed to a length of 64mm for resilient

modulus testing. A cyclic dynamic load of 2 kN was applied during testing with a seating load of 0.09kN. The tests were run at 4, 25, and 40°C.

Three different sweeps of 3, 2, and 1 second of dynamic loading (0.1 second loading and 2.9, 1.9, and 0.9 seconds relaxation, respectively) were performed on each Marshall specimen. Each loading and unloading sweep consisted of 200 cycles; measurements were averaged from the last five cycles of each sweep. Specimens were conditioned for at least one hour before testing at a specific temperature. Results of the resilient modulus testing are shown in Table A 13, Appendix A.

A total of twenty seven, 1000-sec creep tests were performed on field-cored HMA specimens from the nine sections. The creep tests were performed at 40ºC , 25ºC and 5ºC using an MTS machine. A 353N load was applied for 1000 sec with a corresponding relaxation period of 1000 sec. Creep compliance curves as a function of time for the field specimens are presented in Appendix A (Figures A 5 through A 13).

3.3 LAYER INSTRUMENTATION

Five types of instruments were used at the research site: earth pressure cells, strain gages, temperature sensors, soil moisture sensors, and piezoelectric polymer traffic sensors.

Kulite type 0234 and Carlson type TP-101 earth pressure cells were installed in the base and subgrade layer. Their primary functions were to monitor the change in the stress state of the overlaying layers. They also measured the increase in vertical pressure due to dynamic traffic loading. The pressure cells were installed 25mm below the subgrade surface and base layer surface. The Carlson and Kulite earth pressure cells were designed to operate within a vertical pressure range of 0 to 690 kPa. The Kulite pressure cells had a thickness of 14.3mm. The stainless steel pressure head of the Carlson type TP-101 is 114mm diameter and 6.4mm thick, and is welded to a 15.9mm outside diameter stainless steel tube that is attached to a silicon pressure transducer.

Strain gages (Kyowa KM type) were installed in the HMA to monitor strain at the bottom of the HMA wearing surface layer. Strain gages were also installed at the bottom of the geotextile (Measurement Group N2A 06 40 CBY foil strain gages) and geogrid (Texas Measurement FLK-6-1L foil type strain gages). These strain gages were used to monitor the changes in horizontal strains under the geotextile and geogrid material. The strain gages were checked for circuit integrity, and their zero values recorded for later use in instrument calibration.

Thermocouple temperature sensors were installed in the pavement subgrade layer at a depth of 152mm, in the middle of the base layers and the HMA. The thermocouples recorded temperature variations in the various pavement layers. The temperature sensors consisted of a twisted, welded pair of T type thermocouple wire. T type thermocouples are composed of a constantan and copper wire.

Gypsum blocks were installed in the base and subgrade layers for moisture measurement. The moisture block was equipped with steel electrodes, surrounded by nylon impregnated gypsum. As the gypsum is exposed to moisture, the resistance between the electrode decreases, indicating an increase in moisture content of the soil. Laboratory calibrations were performed on the gypsum blocks for the subgrade and base course materials. Water contents and dry densities were varied on soil samples brought to determine the possible range of resistance readings expected in the field. Calibration curves for the base and subgrade material were developed. In this way impedance bridge measurements from the field could always be converted to their respective moisture levels.

Piezoelectric Polymer traffic sensors were installed across the pavement test section and were used for vehicle classification and counting. The sensors were AMP Sensor Inc. Roadtrax Series P Traffic Sensors. Two of the sensors were used as triggers for the data acquisition system and two were used as weigh-in-motion sensors. The sensor installed before section 1 triggers the data acquisition for the instruments for all the nine sections. The piezoelectric sensor installed before section 7 triggers the data acquisition for test sections 7 through 9 when a vehicle enters from the intersecting road. The two weigh-in-motion sensors are installed between test sections 4 and 5, and between test sections 5 and 6.

3.4 DATA COLLECTION

A Keithley Metrabyte Instruments, Inc. KDAC500 data acquisition system was installed on the project site . It was responsible for data collection and storage of all the raw data from the field test sections. The data acquisition system communicates with a personal computer through a cable and IBIN interface card. The software for operation of the data acquisition system was written by the research personnel utilizing subroutines and libraries supplied by the manufacturer. The software was written using Microsoft QuickBASIC 4.5 and software from Keithley Instruments Inc. (KDAC500/M) which is a compiler version of their data acquisition software.

Once the system was triggered, the instrumentation was sampled continuously at a frequency of 200Hz for a period of either six or ten seconds. The length of time used for sampling was dependent on where a vehicle enters the road section. If a vehicle enters at section 1, data is collected for ten seconds. If a vehicle enters the test section in the middle at the intersection, data is collected for seven seconds. The thermocouples were sampled by the system only once, immediately after the data acquisition system trigger was activated. The triggering system received signals from a vehicle traveling between 50 and 80 km/h. The data files created by the data acquisition software were appended for the vehicle triggering system. The data files were compressed for each vehicle triggering the system. At the end of every day the data is downloaded via a modem telephone to the Civil Engineering Materials Laboratory at Virginia Tech. A program was used to view the instrument responses and to eliminate non-reading gages and bad data from the data file.

The processed data could then be imported into a spreadsheet computer program, MS Excel. On importing the reduced data files into MS Excel, separate workbooks were created for pressure, strain, temperature and piezoelectric strip responses. The pressure, strain, temperature, and piezoelectric strip workbooks are each saved after each vehicle pass has been processed.

3.5 TRAFFIC

A Traffic counter was installed across the pavement section for vehicle counting. During installation and initial calibration, this counter was found to count 3 for every 2 axle passes. The reading on the counter during each visit to project site was recorded. Table 3.2 shows the recorded counter readings, the maximum reading on the counter is 99,999. When the reading was of lesser magnitude than the preceding reading, it meant the count had exceeded the maximum count. A count of 100,000 was added to the second reading.

Table 3.2 : Traffic volume on the instrumented lane of Bedford project

Date	Volume Counter reading	Traffic in the Instrumented Lane/ day
9/19/95	85476	250
10/30/95	20736	172
11/14/95	32586	160
1/17/96	76811	145
3/15/96	29821	186
4/17/96	58461	179
5/9/96	81781	212
6/20/96	30776	239
7/20/96	75416	288
8/19/96	28516	354

In the traffic analysis it was assumed that there were two axles per vehicle. The initial count difference was mapped to an estimated vehicle count as follows:

$$\frac{\text{Vehicles}}{\text{Day}} = \frac{(A - B)}{15C} \tag{3.1}$$

Where,

A = count on date 2;

B= count on date 1; and

C= number of days between dates 1 and 2.

As indicated earlier there were four piezoelectric sensors installed on the pavement section in addition to the traffic counter. These sensors were also used in counting vehicles passing the test section. The average traffic ranges from 250 to 350 vehicles per day up to 700 vehicles per day in the summer. With the aid of responses of the other piezoelectric sensors the amount of trucks passing the test section was evaluated. An analysis of the traffic data gave 8%-10% truck traffic passing the test section.

3.6 FIELD CALIBRATION

Field calibrations were performed on the instrumented test sections. A dual-wheeled, single-axle truck with known load configurations was driven over the test sections at known speeds. This permitted the recorded data from the embedded instrumentation to be calibrated to known conditions of loading. Three calibration runs were made: April 1995, August 1995 and April 1996.

In a typical calibration run, single-axle loads of 22, 53, 80 and 102kN ; tire pressures of 420, 490, 550, 630 and 700kPa ; and speeds of 40, 56 and 64km/h (25, 35 and 40 mph) were used. Much of the data collected in the calibration runs was used and reported for purposes out of scope of this investigation and can be found in Al-Qadi *et al*. (1996). However, in examining the development of a transition layer hypothesis, the pressure responses in the base course and subgrade under a standard load of 40kN (a standard half axle), a tire pressure of 550 kPa at a speed of 56km/h were used in the FWD analysis. These parameters correspond closely to the conditions of loading under an FWD.

3.7 RUT DEPTH MEASUREMENTS

Surface rut measurements on all pavement test sections have been recorded semi monthly to monthly since the test section was opened to traffic. The ruts were measured using the straight edge method. In this method, a straight edge aluminum bar of 2m long and 53.2mm thickness and scale is used. Rut measurement of each section was taken at a specific distance before and after the instrumented areas. The average of the two readings was recorded and designated as the rut depth for each section.

The magnitude of rutting was defined as the greatest gap between the straight-edge, laid upon the pavement transverse to the direction of traffic, and the pavement surface. This method would not distinguish between settlement or compaction rutting and plastic flow/heave rutting, however, it is noted that there was no indication of plastic flow/heave distortion of the pavement surfaces.

Figures 3.3, 3.4 and 3.5 summarize rut depths during the monitoring period for sections 1 through 3, 4 through 6 and 7 through 9, respectively.

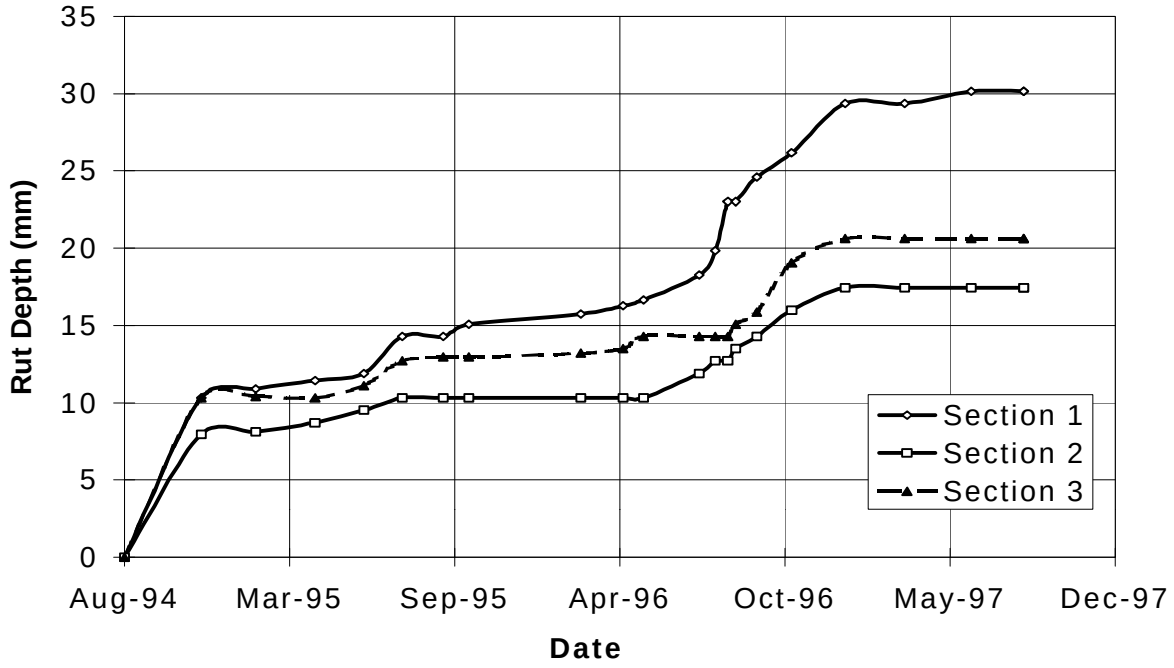

Figure 3.3 Rut depths in sections 1 through

From Figures 3.1, 3.2 and 3.3, it is immediately apparent that the rutting histories of sections 1, 2, and 3 stand apart from those in sections 4 through 9 which are statistically identical. In sections 1, 2 and 3, the magnitude of rutting not only exceeds that in the others, but the rate at which it accumulated is seen increasing. Indeed, it has been observed that since about August 1996, the rutting measured in section 1 exceeded the normal criterion of acceptability (25mm), and the rate at which it is accumulating is accelerating.

The rutting that occurred during the first few months of traffic is mainly due to "normal" initial rutting from compaction under traffic. As can be noted, the rutting observed in the first four months is almost the same for all sections The sharp increase in rutting (in all sections) just before October 1996 is due the application of two weeks of heavy truck loading to accelerate rutting. The relatively low rutting in sections 4 to 6 was due to the greater wander in the area of the intersection.

3.8 GROUND PENETRATING RADAR

Ground penetrating radar (GPR) is a nondestructive technique used in the assessment of civil engineering infrastructure. Some of the applications of the GPR in civil engineering is the location of reinforcement, detection of buried pipes, pavement thickness, location of voids under jointed concrete pavements, determination and detecting deterioration in bridge decks. Its capability to detect under the surface deterioration is very important to maintenance and

rehabilitation scheduling. It operates on the principle of transmitting waves and receiving reflected signals. Reflections occur at interfaces between materials with different dielectric properties.

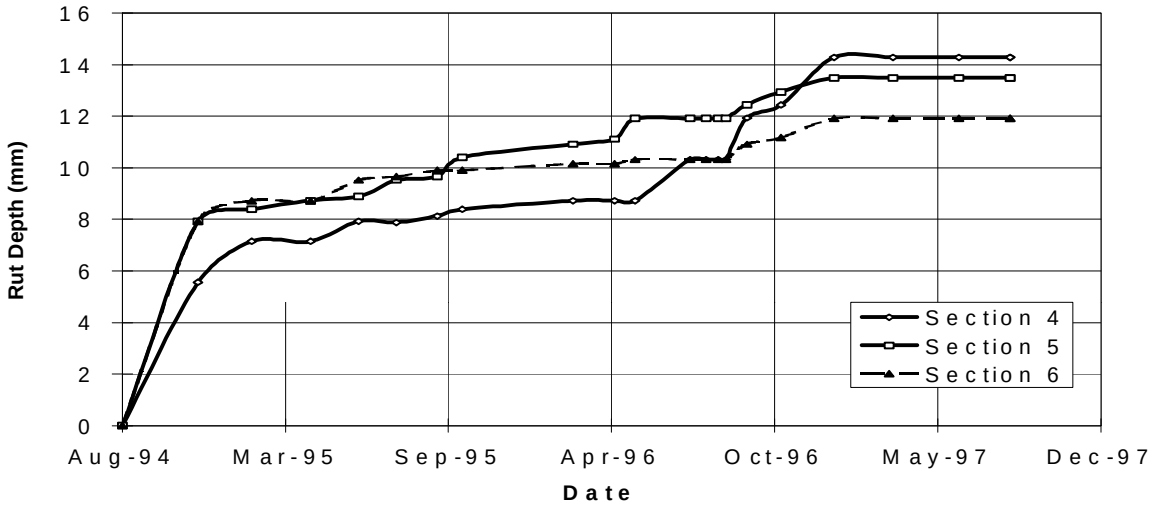

Figure 3.4 Rut depths in sections 4,5, and 6

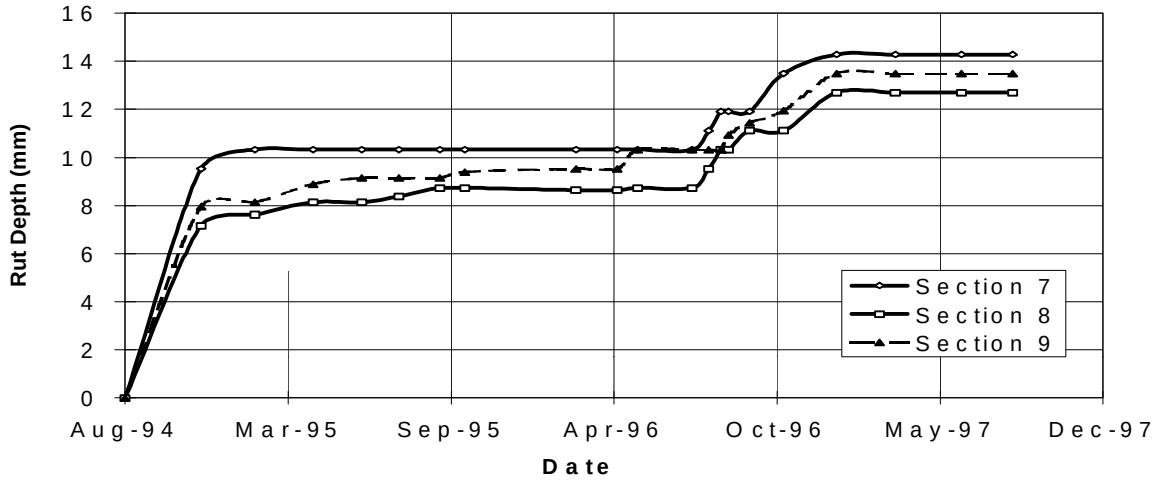

Figure 3.5 Rut depths in sections 7, 8, and 9

Figure 3.6 is a schematic showing the principle of the GPR. A sequence of trigger pulses is generated in the control unit by the radar circuitry. These trigger pulses are sent through a control cable to an antenna where each trigger pulse is transformed into a bipolar transmit pulse. These transmitted pulses encounter different materials in the subsurface with different dielectric properties. In the interface, signals are reflected back to the subsurface where they will be detected by the antenna and are sent to the control unit where they are processed and displayed.

The GPR, used in this research was at 900MHz to detect any variation at base course-subgrade interface on the research site at Bedford County. A determination of the thickness of the soil contaminated base course layer would give an objective evaluation as to the effectiveness of geosynthetics as separators. Figure 3.7 shows the resulting GPR output. The lighter the area, the higher the reflection of electromagnetic waves (Al-Qadi *et al*. 1996). At the base course-subgrade interface, the higher reflection may occur because of higher moisture or subgrade soil migration into the base course. Due to the fact that moisture is the same in the three sections, soil migration is a reasonable assumption in sections 1 and 3.

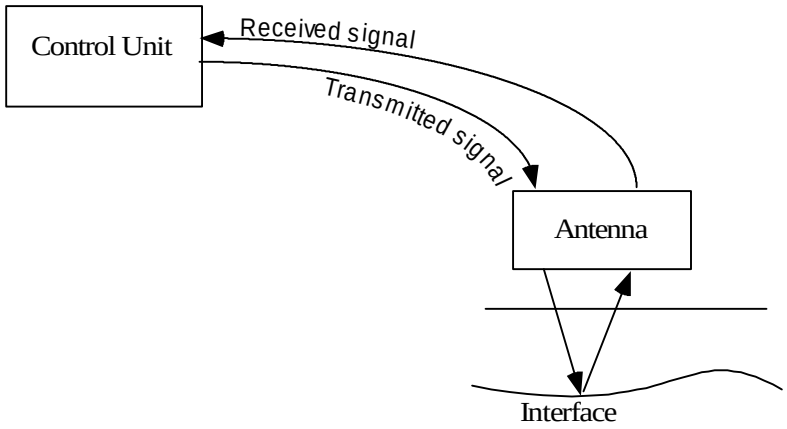

Figure 3.6 GPR Concepts

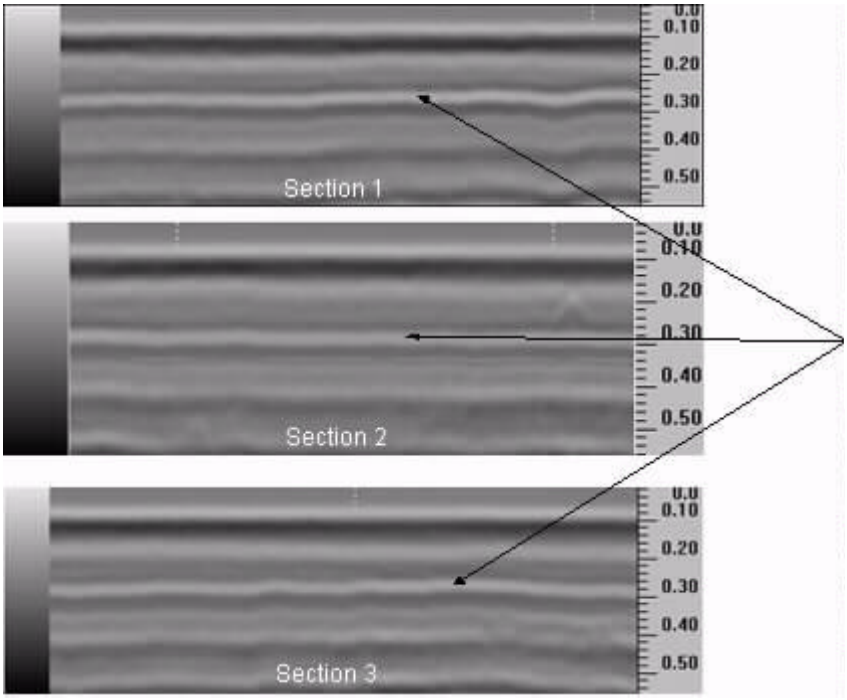

Figure 3.7 Output of GPR for sections 1, 2 and 3

3.9 FALLING WEIGHT DEFLECTOMETER

The monitoring of the geosynthetically stabilized sections and non-stabilized test sections was also accomplished through the use of the Falling Weight Deflectometer (FWD). Falling Weight Deflectometer testing of all nine sections was performed in October 1994, March 1995, April 1996, July 1996, October 1996, January 1997, and April 1997.

All nine sections were subjected to 5 drops each at different nominal load levels of 26.5, 29.4, 39.2, and 49.1 and 54 kN. The response of the pavement sections to the applied loads was measured by 7 geophone sensors located at 0, 304, 457, 608, 910, 1219 and 1324mm from the axis of the loading plate. The deflection data are summarized in Appendix B (Figure B 1 through B 72, Tables B 1 through B 8). Falling Weight Deflectometer picture is shown in Figure 3.6. Details of the analysis of the collected data is presented in Chapter 4.

Figure 3.8 Falling weight deflectometer equipment

CHAPTER 4 - FALLING WEIGHT DEFLECTOMETER ANALYSIS

The data collected by the FWD during the course of this project provide the basis for the quantitative and comparative analysis of section response and estimation of the evolution of the putative transition layer between the subgrade and base course in the control sections. The analysis of the collected deflection data was undertaken in two phases: a simple back-calculation to estimate the effective elastic moduli of the subgrade in each section at each of the periods corresponding to the FWD site visits, followed by a more detailed analysis to estimate the magnitude of any developing transition layer.

4.1 Falling Weight Deflectometer BACKCALCULATION

The initial analysis of the FWD deflection data was performed using the MODULUS Ver 5.0 back-calculation program developed at the Texas Transportation Institute (TTI) for the Texas Department of Transportation (TxDOT). This program has since become an industry "standard" and has been adopted for the analysis of the LTPP data collected nationwide.

Back-calculation is the process of determining material properties of a flexible pavement structure from its response to surface loading. Iteration or optimization schemes are used to calculate theoretical deflections by varying the material properties until a tolerable match of measured deflections is possible. The stiffness producing deflections that match the measured deflections are the back-calculated moduli.

4.1.1 MODULUS Program

MODULUS is a microcomputer program for back-calculating layer moduli (Uzan *et al*., 1988, 1989; Scullion *et al*., 1990). It can be applied to a two-, three-, or four-layer system with or without a rigid bedrock layer. A linear elastic program is used to generate a data base of deflection bowls by assuming different modulus ratios. Once the data base is generated for a particular pavement, the linear elastic program is not called. A pattern search routine is used to match measured and calculated (theoretical) bowls.

The objective function to be minimized is expressed as follows (Huang,1993):

$$\varepsilon^2 = \sum_{i=1}^{s}\left(\frac{w_i^m - w_i^c}{w_i^m}\right)^2 = \sum_{i=1}^{s}\left(1 - \frac{w_i^c}{w_i^m}\right)^2 \qquad (4.1)$$

Where,

ε^2 = squared error;

w^m = measured deflection (mm);

w^c = computed deflection (mm); and

I = sensor number, 1 to s ;

The computed deflection expressed as a function of modulus ratios:

$$w_i = \frac{qa}{E_n} f_i\left(\frac{E_1}{E_n}, \frac{E_2}{E_n}, ..., \frac{E_{n-1}}{E_n}\right) \tag{4.2}$$

Where,

q = contact pressure (kPa);

a = contact radius (mm); and

E_n = elastic modulus of layer n (MPa)

The value of f_i for each sensor i can be obtained from the layer system program and used as a data base. In the back-calculation program, a set of seed moduli is required for the first trial. When E_n and the modulus ratios are known, the modulus of each layer can be determined.

To minimize the error, the value of E_n can be determined by taking derivatives of ε^2 with respect to E_n and setting the result to zero:

$$\frac{\partial e^2}{\partial E_n} = \sum_{i=1}^{s} 2\left(1 - \frac{w_i^c}{w_i^m}\right)\left(\frac{1}{w_i^m}\right)\left(\frac{\partial w_i^c}{\partial E_n}\right) = 0 \tag{4.3}$$

Combining Eq 4.2 and Eq 4.3 yields,

$$\frac{\partial w_i^c}{\partial E_n} = -\frac{qaf_i}{E_n^2} = -\frac{w_i^c}{E_n} \tag{4.4}$$

So 4.3 can be reduced to

$$\sum_{i=1}^{s}\left(1 - \frac{w_i^c}{w_i^m}\right)\left(\frac{w_i^c}{w_i^m}\right) = 0$$

or

$$\sum_{i=1}^{s}\frac{w_i^c}{w_i^m} = \sum_{i=1}^{s}\left(\frac{w_i^c}{w_i^m}\right)^2 \tag{4.5}$$

When both sides are divided by w_1^c with $w_1^c = \frac{qaf_1}{E_n}$ and $\frac{w_i^c}{w_1^c} = \frac{f_i}{f_1}$, Eq 4.5 becomes

$$\sum_{i=1}^{s} \frac{f_i}{f_1 w_i^m} = \sum_{i=1}^{s} \frac{qaf_i^2}{f_1 \left(w_i^m\right)^2 E_n}$$

or

$$E_n = \frac{qaf_i \sum_{i=1}^{s} \left(\frac{f_i}{f_1 w_i^m} \right)^2}{\sum_{i=1}^{s} \left(\frac{f_i}{f_1 w_i^m} \right)} \qquad (4.6)$$

The squared error e^2 is computed using the subgrade modulus from Eq 4.1 and the modulus ratios of the data points. A pattern search routine is used to find the optimum set of modulus ratios such that a minimum e^2 is obtained.

4.1.2 Rigid Bottom Condition

In the mechanistic analysis of nondestructive deflection data, multi-layered, linear elastic pavement models are often used. However, several researchers (Uddin *et al*., 1986; Briggs *et al.*, 1988) have found that a rigid layer below the subgrade influences the measured deflections. It also influences the back-calculation results if analyzed by a multi-layered linear elastic model. Smith *et al*. (1993) presented a method to estimate this depth from deflection data. They adapted the approach suggested by Ullitz (1990). The concept employed in Boussinesq's equations, for deflection from a point load on an infinite half-space, is used in their analysis.

$$D_r = P(1-\nu^2)/\pi r E_r \qquad (4.7)$$

Where,

D_r = Surface deflections at offset r due to load P;

P = Point load ;

ν = Poisson's ratio;

r = Horizontal offset from the load ;

E_r = Representative Young's modulus of the halfspace

For any deflection bowl, Eq 4.7 can be rewritten as :

$$D_r = k[1 / E_r] [1 / r] \qquad (4.8)$$

Where, $k = P (1- \nu^2)/ \pi$

When the deflection measurements from a typical FWD test for a given test load are plotted against the inverse of the distance from the center of the load, the curve shown in Figure 4.1 is obtained. Boussinesq's equation assumes a linear half space, and if the modulus was constant, the curve should be a straight line. The intercept of this line (1/r) axis should represent the distance at

which no deflection occurs. This value should be related to the depth at which no deflection occurs (i.e. is the stiff layer).

Using the method proposed by Smith *et al.* (1993) the depth to rigid layers for all the nine pavement sections were calculated. The results had a similar trend to that obtained from MODULUS Ver 5 program. The following steps explain the procedure used in obtaining the depth to rigid layer proposed by Smith *et al* (1993): (Please note the procedure was developed for British units).

1. A plot of the measured deflection (mils) versus the inverse of the offset of the sensors

(1/r in ft) was made.

2. The steepest part of the curve is extended until it intersects the abscissa (inverse of the

offset). This is found by determing the gradient of the curve.

3. r_o (1/ft units) is put into an equation developed by regression analysis to find the depth to

rigid layer in ft.

For pavement with asphalt surface layers less than 50mm the following equations were found:

$$1/B = 0.0362 + 0.3242r_o - 10.2717\, r_o^2 - 23.6609\, r_o^3 - 0.0037BCI;\ r^2 = 0.94,$$

For pavements with HMA thickness between 100 and 150mm, the inverse of the depth to rigid layer was as follows :

$$1/B = 0.0413 + 0.9929ro - 0.0012SCI + 0.0063BDI - 0.07781\, Log\ (BDI)\ ;\ r^2 = 0.94,$$

For flexible pavements greater than 150mm, the following equation was found:

$$1/B = 0.0409 + 0.5669r_o - 3.0137r_o^2 - 0.0033BDI - 0.0665\, Log\ (BDI);\ r^2 = 0.97.$$

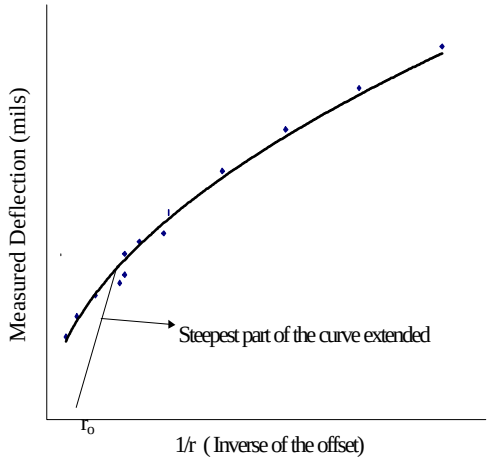

Figure 4.1 Determination of representative depth to rigid layer (after Smith *et al.*, 1993)

Where,

B = Depth to a rigid layer in ft;

r_o = 1/r intercept by extrapolating the steepest section of the 1/r vrs deflection curve;

SCI = D_o - D_1 ;

BDI = D_1 - D_2 ; and

D_i = Surface deflection (mils) normalized to a 9000 Ib. load at an offset i in ft.

The steepest part of the curve was found by finding the gradient of the curve.

The depth to bedrock must be known, especially if the bedrock is within 6 meters from the surface (Uzan *et al*.,1994). Should the depth to this putative layer not be known by direct measurement, then either the built-in routines in MODULUS or the Smith *et al.* (1993*)* method have been shown to yield realistic estimates. The moduli of the subgrade and base are very sensitive to the depth of the relatively shallow bedrock.

The prediction of rigid layer is based on several runs of a linear elastic multi-layered computer program with different pavement and subgrade thicknesses. A correlation between combinations of the surface deflections, parameters of the pavement structure and depth of the bedrock was derived. The correlation works well as long as a true rigid layer exists underneath the subgrade, and the linear elastic behavior is predominant. The correlation would predict a fictitious depth of bedrock (such a bedrock does not really exist) in most cases of a sandy subgrade. This is because the modulus of the sandy subgrade increases with depth (as the overburden increases).

The resilient moduli of all layers in each section were determined using this program. There was a clear pattern of higher resilient modulus values for the subgrade in the geosynthetically stabilized sections as compared to the nonstabilized sections during all the dates FWD measurements were taken. The results of the subgrade resilient modulus values obtained for the 100mm, 150mm and 200mm sections are presented in Appendix C (Tables C1 through C8). The plots of apparent subgrade resilient modulus variation over time is shown in Figure C1 (Appendix C). The higher resilient modulus values for the geosynthetically stabilized sections is shown. The resilient moduli and Poisson's ratios of the HMA and base course determined in the laboratory were used as input for the backcalculation procedure.

FWD measured deflection profiles were recorded and plotted for different periods; October 1994, March 1995, August 1995, April 1996, July 1996, October 1996, January 1997 and June 1997. The purpose of this exercise was to define any inconsistency which might occur in the measurements taken by the geophones. They are presented in Appendix B (Tables B1 through B9) and Figures B1 through B81. Deflection readings from the subgrade and base course layers from some of the pavement sections were taken from different loads drops from the FWD. Loads were dropped and readings from the strain gages were taken. The results are presented in Tables D7 and D8 (Appendix D).

4.2 DATA ANALYSES

Two methods of analysis were used in an attempt to quantify the development of a transition layer (if any) before a more simplified method yielded results that were felt to be realistic. Both methods yielded qualitatively the same pattern of results, however, it became clear that each method had different sensitivities to variability in the field data. Both methods used are described below in brief, followed by a more detailed description of the method finally adopted.

4.2.1 ELSYM5 Analysis

The ELSYM5 program is a linear elastic program that treats up to five-layers above subgrade. The pavement may be loaded with one or more identical uniform circular loads applied vertically to the pavement surface. The program superimposes the effects of the various loads and computes the orthogonal stresses, strains, and displacements, along with the principal stresses and strains, at locations on and within the pavement specified by the user.

Input values required to run the program are the layer thicknesses, resilient moduli and Poisson's ratios of all layers in the system. A load of 40 kN was used with the corresponding tire pressure of 550 kPa . This is generally representative of the greatest percentage of truck traffic on secondary roads and of the FWD loading at 40 kN. The resilient modulus of the asphalt and base course layers (100, 150 and 200mm) were determined in the Materials laboratory at Virginia Tech. It should be stated that the base course resilient moduli were corrected for thicknesses in the analysis. The pavements without geotextiles were modeled as four-layer systems, comprising an HMA, base course, a transition layer (formed as a result of base contamination), and an infinite subgrade layer. For months that FWD data was recorded, the relevant input data was used for the ELSYM5 analysis, i.e the layer thickness, Poisson's ratio and elastic modulus of all the layers. The thickness and elastic modulus of the transition layer was varied for each period in the control and geogrid sections to try and match the stress values obtained from the ELSYM5 program to the stress values recorded in the pavement layers during the calibration runs. The deflection results from the ELSYM5 analysis was also matched to the surface deflection results from the FWD.

In this way, the thickness of the transition layer was estimated for all the periods on which FWD data was taken. The response of the pressure cells in the subgrade layer and base course are tabulated in Appendix D (Tables D1 through D8). ELSYM5 analyses for estimating transition layer are shown in Appendix E (Tables E1a through E10b). The results of the ELSYM5 analysis are summarized in Table E11 (Appendix E). These results were showed an increase in intermixing thickness for sections 1 and 3. There was an increase in intermixing thickness from 12.5mm in March of 1995 to 62.5mm in April 1996 for section 1. There was an increase in intermixing thickness from 2.5mm to 50mm for section 3 during the same period. Intermixing thickness for thicker sections (4 through 9) could not clearly be determined using this Method. The results for these sections were considered inconclusive at this time.

4.2.2 KENLAYER Analysis

The KENLAYER program is a layered program that takes into account the viscoelastic nature of the HMA and its response to dynamic loads. It has the advantage of allowing different material parameters for each seasonal period. The backbone of the layered program is the solution for a multi-layer elastic system under a circular loaded area. The solutions are superimposed for multiple wheels, and collocated at various loading times. With the exception of the HMA layer, all the other layers were assumed to be linearly elastic.

The use of the KENLAYER for the analysis of pavement systems under a moving load involves several steps. A load of 80 kN and tire pressures of 550 kPa were used as input values in the analysis. Laboratory determined creep compliance results of HMA were used as input;. HMA layer was considered linear viscoelastic Solutions due to either moving or stationary loads can be obtained. Since the load–time pulse imparted by the FWD is similar to that of a truck wheel moving at 64 km/hr, this speed was used in the viscoelastic analysis.

As in the ELSYM5 program, the thickness, Poisson's ratio, and resilient modulus of the four layer model were used as input data in the program. By varying the thickness and elastic moduli of the transition layer, deflection and stress at any specified depth in the subgrade for each section (control and geogrid) were obtained. This was done for all FWD measurements.

The stress and deflection values obtained from KENLAYER were compared to those obtained from the calibration runs and FWD deflection basin data. In this way the thickness for the transition layer could be estimated. Computed deflections from the KENLAYER analysis gave higher deflections than measured deflection values from the FWD analysis. The stresses, however, were lower. The higher predicted deflection may be attributed to the viscoelastic treatment of the HMA layer in the analysis. That also results in less predicted stresses at the base course-subgrade interface. Results are shown in Appendix F (Tables F1.through F5.).

4.2.3 Determination of Base Course Contamination from The Thickness Addition Method Using The Modulus Program

For most of the months for which FWD tests were performed, subgrade resilient moduli for the geotextile stabilized sections were greater than those observed in the control and geogrid sections of the same base thickness. This indicated weakened control and geogrid base courses, which is consistent with the hypothesis of fine pumping from the subgrade to the base course layer. To determine the transition layer thickness that may be developed in control and geogrid stabilized sections, an independent layer of resilient modulus value between the base and subgrade was added to the geotextile section. After adding the transition layer with known properties as a partial replacement of base material, a back-calculation configuration procedure was adopted to determine the subgrade resilient modulus. This is an iterative process where the thickness of the transition layer is modified gradually, to yield a subgrade resilient modulus in close proximity to the control or geogrid stabilized sections. In this way the transition layer or extent of base contamination is estimated.

For the data collected in August 1995, subgrade resilient modulus for section 1 (100mm base thickness) is 105 MPa. Section 2 (with geotextile) had a subgrade resilient modulus of 110 MPa. Transition thickness of 13mm and resilient modulus of 138 MPa was added to the base course of the geotextile section until the subgrade resilient modulus dropped to 105 MPa, see Table 4.1. For April 1996, a transition layer thickness of 64mm and a resilient modulus of 172.5 MPa was obtained from the MODULUS back-calculation program for the control section. This indicates that the transition layer thickness had increased over a span of 8 months. The base contamination in section 3 (with geogrid) during the same period was 48mm. In July 1996, the extent of base contamination for the 100mm control section was found to be 64mm, which is the same as that calculated in April 1996. The transition layer thickness increased to 69mm in October 1996 indicating asymptotic stabilization of transition layer versus time. In January 1997, the resilient modulus of the subgrade in section 2 was determined as 73 MPa, where the control section had a resilient modulus value of 54 MPa. Transition layer thickness of over 100mm was needed to have the resilient modulus drop from 73 MPa to 54 MPa. This is interpreted to mean that the extent of base contamination had reached a point where it is no longer sensitive to small changes in thickness. This indicates a clear asymptotic behavior. The resilient modulus is lower than what it was assumed, or the subgrade resilient modulus was decreased due to the fine migration. However, for the thicker base course sections (150mm and 200mm), the MODULUS program was insensitive at this time. A flowchart showing an iterative procedure using MODULUS program to determine the transition layer thickness is presented in Figure 4.2. The development of the transition layer with time is shown in Figure 4.3.

Table 4.1 Transition Layer thickness

	Transition Layer thickness (mm)				
Section	**Aug-95**	**Apr-96**	**Jul-96**	**Oct-96**	**Jan-97**
1	13	64	65	69	69
3	0	48	64	64	64

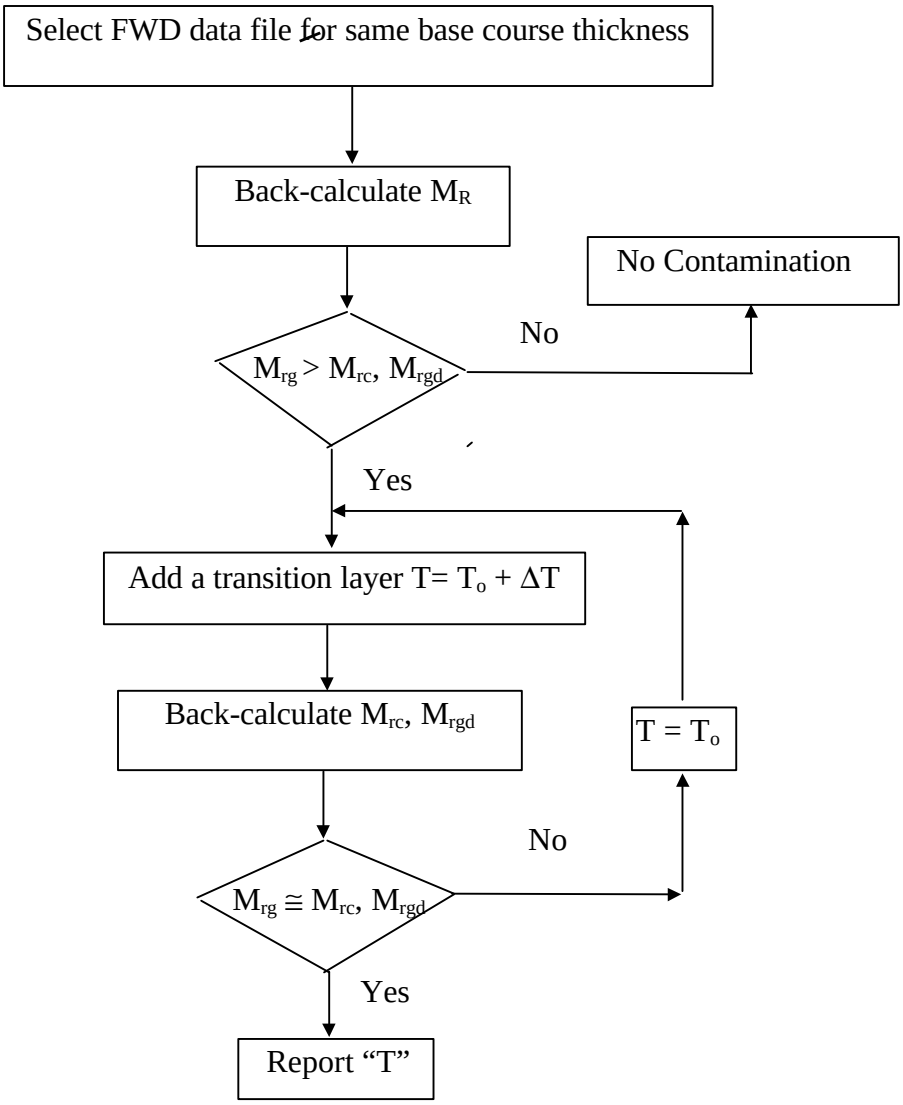

T= Thickness of the transition layer;
T_o= Initial thickness of transition layer, equal to zero in the first step;
ΔT= Increment in thickness of the transition layer = 5mm;
M_{rg} = Subgrade resilient modulus of geotextile stabilized section;
M_{rc} = Subgrade resilient modulus of control section; and
M_{rgd} = Subgrade resilient modulus of geogrid stabilized section.

Figure 4.2 Flow Chart of the iterative procedure.

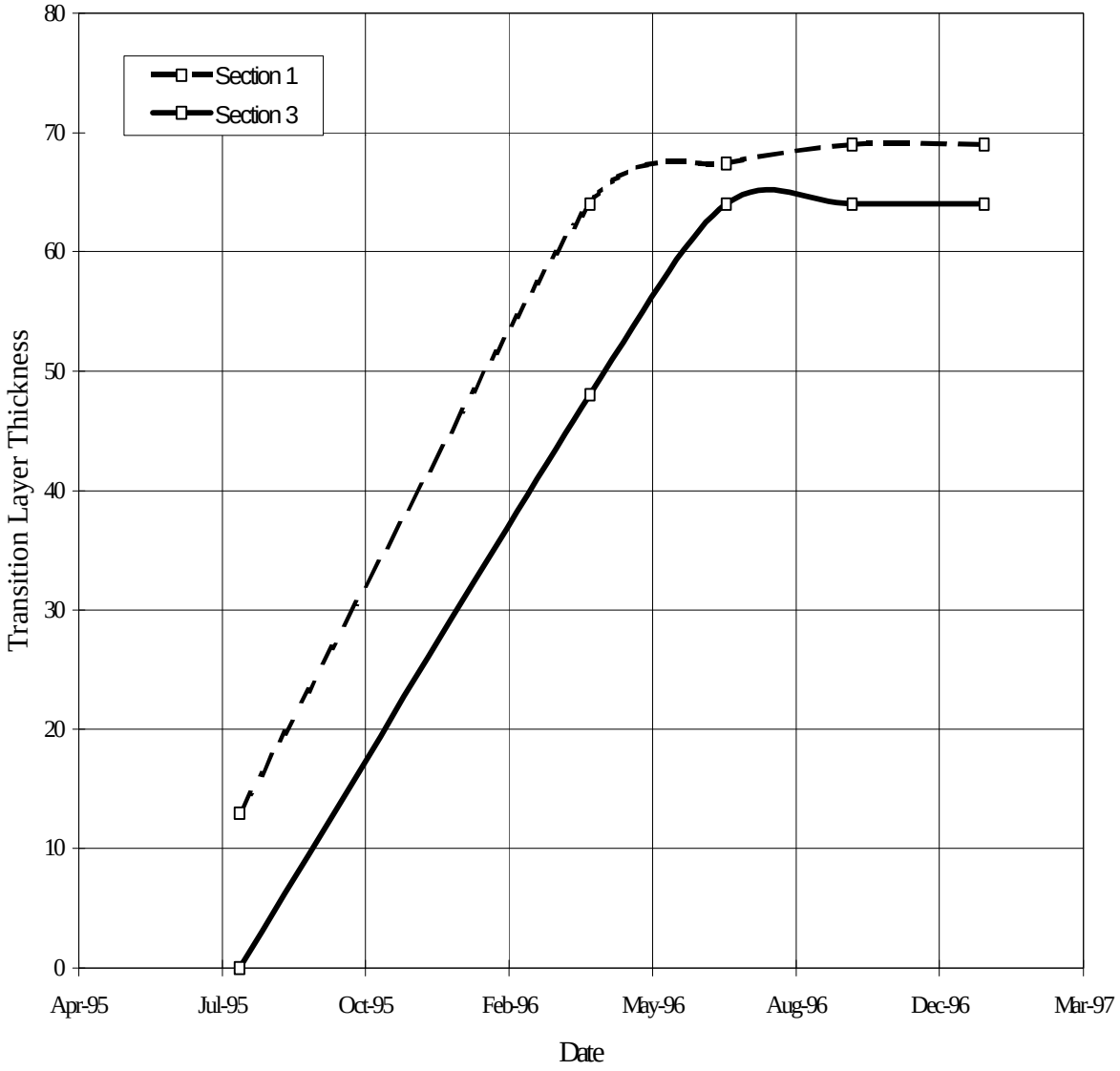

Figure 4.3 Transition layer development with time

Table 4.2 Summary of iterative process for March 1995

Section	**Initial Base thickness (mm)**	**Contamination thickness (mm)**	**Apparent Subgrade M_R (MPa)**
1	100	0	98
2	100	_	115
3	100	0	116
4	150	0	66
5	150	_	57
6	150	0	50
7	200	0	40
8	200	_	42
9	200	0	118

HMA layer resilient modulus = 2898 MPa
Base layer resilient modulus = 255.3 MPa
Assumed transition layer modulus = 138 MPa

Table 4.3 Summary of iterative process for August 1995

Section	**Initial Base thickness (mm)**	**Contamination thickness (mm)**	**Apparent Subgrade M_R (MPa)**
1	100	13	92
2	100	0	110
3	100	0	105
4	150	I *	60
5	150	0	75
6	150	I *	63
7	200	I *	57
8	200	0	73
9	200	I *	103

HMA layer resilient Modulus = 2829 MPa
Base layer resilient Modulus = 276 MPa
Assumed transition layer modulus = 138 MPa
* I = Insensitive to back-calculation

Table 4.4 Summary of iterative process for April 1996

Section	Initial Base thickness (mm)	Contamination thickness (mm)	Apparent Subgrade M_R (MPa)
1	100	64	35
2	100	0	58
3	100	48	45
4	150	I*	31
5	150	0	41
6	150	I*	31
7	200	I*	28
8	200	0	39
9	200	I*	38

HMA layer resilient Modulus = 2863.5 MPa
Base layer resilient Modulus = 255.3 MPa
Assumed transition layer modulus = 124.2 MPa
* I = Insensitive to back-calculation

Table 4.5 Summary of iterative process for July 1996

Section	Initial Base thickness (mm)	Contamination thickness (mm)	Apparent Subgrade M_R (MPa)
1	100	65	37
2	100	0	63
3	100	64	42
4	150	I*	23
5	150	0	32
6	150	I*	26
7	200	I*	27
8	200	0	30
9	200	I*	33

HMA layer Resilient Modulus = 2898 MPa
Base layer Resilient Modulus = 269.1 MPa
Assumed transition layer modulus = 138 MPa
*I = Insensitive to back-calculation

Table 4.6 Summary of Iterative process for OCTOBER 1996

Section	Initial Base thickness (mm)	Contamination thickness (mm)	Apparent Subgrade M_R (MPa)
1	100	70	57
2	100	0	103
3	100	64	88
4	150	I*	39
5	150	0	51
6	150	I*	37
7	200	I*	27
8	200	0	30
9	200	I*	84

HMA layer Resilient Modulus = 2829 MPa
Base layer Resilient Modulus = 255.3 MPa
Assumed transition layer modulus = 138 MPa
* I = Insensitive to back-calculation

Table 4.7 Summary of Iterative process for January 1997

Section	Initial Base thickness (mm)	Contamination thickness (mm)	Apparent Subgrade M_R (MPa)
1	100	70	54
2	100	0	83
3	100	64	78
4	150	I*	39
5	150	0	47
6	150	I*	35
7	200	I*	28
8	200	0	40
9	200	I*	42

HMA layer Resilient Modulus = 2808.3 MPa
Base layer Resilient Modulus = 269.1 MPa
Assumed transition layer modulus = 138 MPa
*I = Insensitive to back-calculation

CHAPTER 5 SUMMARY, CONCLUSIONS AND RECOMMENDATIONS

5.1 SUMMARY AND CONCLUSIONS

As part of a field study on the performance of an instrumented geosynthetically stabilized flexible pavement, the development of a contaminated layer "transition layer" between base course layer and subgrade was hypothesized. The objective of the research was to investigate the occurrence of a base contamination in sections without geotextiles and quantify its progress over time. To achieve that, in situ stresses were measured as well as pavement responses to pulse loading, falling weight deflectometer (FWD). Comparing measured stresses to calculated stresses using elastic and viscoelastic methods were inclusive. The study used an iterative method to backcalculate the extent of contamination of the base layer over time. It was concluded that for under design sections with 100mm (4in) base course, 70% of the base course was contaminated in the first 2.5 years for the control section and 65% for the section stabilized with geogrid. Although this number may be considered high, it is in good agreement with rut measurements for the control which already failed. The contamination is expected to be very low (at this stage) in the other sections and this procedure (back-calculation) is insensitive to changes at this time. The short duration of the project prevents clear distinctions from being made in the thicker base sections (4 through 9). It may be concluded that in the 100mm base course sections, the geotextiles provide adequate protection against subgrade intrusion, while the geogrid provides a partial one.

5.2 RECOMMENDATIONS

Based on the findings of this study, the following recommendations may be made:

The continual monitoring is needed of test sections 4 through 9 for rut depth development and FWD testing to determine existence of base contamination over a longer period of time. It is recommended that in future research projects, such as the one in Bedford, geotechnical studies be performed at the beginning of the project to determine the presence of a rigid layer. This would enhance the accuracy of results from the back-calculation procedure, which is very sensitive to rigid layers depth. A rigid layer, as recognized by FWD does not necessarily imply a rock layer. It can be any stiff material or a subgrade in which the effective stiffness increases with depth.

Upon completion of the field study at Bedford County it is recommended that excavation of all the test sections 1 through 9 be conducted. A relationship could be developed between the calculated base contamination and the contamination observed in the field sections.

The author finally recommends additional studies to determine the following (as part of the development of a pavement design procedure incorporating geosynthetics as):

(a) The amount of additional aggregate base needed in the original design when geotextiles are not used.

(b) The depth of a asphaltic concrete overlay needed after base contamination occurs.

6. REFERENCES

Al-Qadi, I. L., T. L. Brandon, R. J. Valentine, and T. E. Smith. (1994). "Laboratory Evaluation of Geosynthetic Reinforced Pavement Sections." Transportation Research Board, No. 1439, 73rd Annual Meeting, Washington, DC, pp.25-31

Al-Qadi, I. L., Brandon T. L., Lacina, B.A., and Bhutta S. A. (1996). "Construction and Instrumentation of Geosynthetically Stabilized Secondary Road Test Sections." Transportation Research Board, No 1534, Washington D.C., pp.55-57

Al-Qadi, I. L., Brandon, T. L., Bhutta, S. A., Appea, A., and Lacina, B. A. (1996). "Field Testing of Geosynthetically Stabilized Pavement Sections." Second Progress Report, Dept of Civil Eng, Virginia Polytechnic Institute and State University, Blacksburg, VA.

Annual Book of ASTM Standards Soil and Rock; Geosynthetics, Vol. 04.08, 1997.

Annual Book of ASTM Standards Road and Paving Materials, Vol 04.03, 1995.

Austin, D. N. and Coleman, D. M. (1993). "A Field Evaluation of Geosynthetic-Reinforced Haul Roads over Soft Foundation Soils." Geosynthetics 93, Vancouver, Canada, pp. 65-80.

Barrett, R. J. (1966). "Use of Plastic Filter in Coastal Structure." Proceedings of the 16th International Conference Coastal Engineering, Tokyo, Japan pp.1048-1067.

Barsvary, A.K. and P. Korgemagi. (1979). The Geotextile Use of Filter Fabrics in Highway Construction. Rep. EM-13, Ministry of Transport and Communications, Engineeering. Materials Office, Ontario, Canada.

Bell, J. R. (1980). "Geotextile for Soil Improvement." Proceedings of the American Society of Civil Engineers National Convention, Portland, OR, pp.1-30.

Bell, A. L., McCullough, M. L., and Snaith, M. S. (1982). "An Experimental Investigation of Sub-Base Protection Using Geotextiles." Proceedings of the Second International Conference on Geotextiles, Vol 2, Las Vegas, NV pp. 435-440.

Becham, W.K.,and Mills, W. H. Mills. (1935). "Cotton-Fabric Reinforced Roads." Engineering News Record, Oct. 3, pp. 453-455.

Briggs R. C. and Nazarian S. (1989). "Effects of Unknown Rigid Subgrade Layers on Backcalculation of Pavement Moduli and Projections of Pavement Performance." 68th Annual TRB Meeting, Washington D.C.,

Barksdale, R. D., Brown, S. F., and Chan, F. (1989). Potential Benefits of Geosynthetics in Flexible Pavement Systems, National Cooperative Highway Research Program Report 315, Transportation Research Board, Washington, D.C.

Jorenby, B. N., and Hicks, R .G., (1986). "Base Contamination Limits." Transportation Research Record, No. 1095, Washington D.C. pp. 86-102.

Bush, A. (1980). Nondestructive Testing for Lighter Aircraft Pavements; Phase II, Development of the Nondestructive Evaluation Methodology. Report No. FAA-RD-80-9-II, US Department of Transportation, Washington, D.C.

Carroll, R. G. Jr., Wall, J. C., and Hass, R. (1987). "Granular Base Reinforcement of Flexible Pavements Using Geogrids." Geosynthetic Conference, New Orleans, LA, pp. 46-57.

Chan, F., Barksdale, R. D. and Brown S. F. (1989). "Aggregate Base Reinforcement of Surfaced Pavements." Geotextiles and Geomembranes, Vol. 8, No. 3, 165-189.

Christopher, B. R. and R.D Holtz. (1985). Geotextile Engineering Manual. Report FHWA-TS-86/203 STS Consultants, Ltd, Northbrook, IL, for Federal Highway Administration, Washington, D.C.

Dewar, S. (1962). "The Oldest Roads in Britain." The Countryman, Vol. 59, No.3, pp. 547-555.

De Groat, M., Janse, E., Maagdenberg, T. A .C., and Van Den Berg, C. (1986). "Design Methods and Guidelines for Geotextile Applications in Road Construction." Proceedings Of the Third International Conference on Geotextiles. Vienna, Austria, Austria.

Giroud, J. P., and Noiray, L. (1980). "Geotextile Reinforced Unpaved Road Design." Journal of. Geotechnical Engineering, ASCE, Vol. GT 9, No. 1107, pp. 1233-1254.

Guram, D., Marienfeld, M., and Hayes, C. (1994). "Evaluation of Nonwoven Geotextile versus Lime-Treated Subgrade in Atoka County, Oklahoma." Transportation Research Record, No 1439, Washington, D.C.,pp.7-12

Hausmann, M. R. (1987). "Geotextile for Unpaved Roads- Review of Design Procedures." Geotextiles and Geomembranes, 1987, Vol. 5, No. 3, pp 201-233.

Haliburton, T. A., and J. V. Barron. (1983). "Optimum Method for Design of Fabric-Reinforced Unsurfaced Roads." Transportation Research Record No. 916, No 26-32, tWashington, D.C., pp. 26-32

Hoare, D. J., (1982). "A Laboratory Study into Pumping Clay Through Geotextiles under Dynamic Loading." Proceedings of the Second International Conference on Geotextiles, Vol. 2, Las Vegas, NV pp. 423-428

Holtz, R. D. and Harr, M .E. (1983). "Analytical and Experimental Investigation of Soil Reinforcing," Report No. ESL-TR-82-31, Purdue University, West Lafayette, IN for Tyndall AFB, FL.

Huang, Y. H. (1993). "*Pavement Analysis and Design*, Prentice Hall, Englewood Cliffs, New Jersey.

Jagielski, K. (1995). "Lining Systems Show Growth." Geotech Fabrics Report, Vol. 9, No. 6, pp 26-28.

Le, T.T. (1982) "The Effects of Engineering Fabric in Street Pavement On Low Bearing Capacity Soil in New Orleans", Ph.D Thesis, Tulane University, pp.431

Kennepohl, G., Kamel, N., Walls, J. and Hass, R., (1985). "Geogrid Reinforcement of Flexible Pavements." Proceedings of the Association of Asphalt Paving Technologists, San Antonio, Texas, February, Vol. 54, pp. 45-70.

Koerner, M. R. (1985). *Designing with Geosynthetics*. Prenctice Hall, Rotterdam, The Netherlands.

Lytton R. L. (1989). "Back-calculation of Pavement Layer Properties. Non destructive Testing of Pavement and Back-calculation of Moduli." ASTM STP 1026, American Society for Testing and Materials, Philadelphia, pp 7-38.

Milligan, G. W. E., Jewell, R. A., Houlsby G. T. and Burh H. J. (1989). "A New Approach to the Design of Unpaved roads." Ground Engineering, Vol. 22, No. 3, pp.25-29.

Potter, J. F. and Currer, E. W.H. (1981). "The Effect of a Fabric Membrane on the Structural Behaviour of a Granular Road Pavement." Report No. LR996, TRRL, Crowthorne, UK,

Robnett, Q., and Lai, J. (1982a). "Effects of Fabric Properties on the Performance and Design of Aggregate-Fabric-Soil-Systems." The Second International Conference on Geotextiles, Vol 2, Las Vegas, NV, pp. 381-386

Robnett, Q., and Lai, J. (1982b). "Fabric-Reinforced Aggregate Roads-Overview," Transportation Research Record, No. 875, Washington D.C.,pp. 42-50

Sellmeijer, J. B. (1990). “Design of Geotextile Reinforced Paved Roads and Parking Areas.” The Fourth International Conference on Geotextiles, Geomembranes and Related Products, Vol. 1, Hague, pp. 177-182.

Smith R. E., Yang W., and Rhode, G.(1993). “Inclusion of Depth to Rigid Layer in Determining Pavement Layer Properties.” Texas A&M University, College Station, TX.

Snaith M. S., and Bell A. L. (1978). “The Filtration Behavior of Constructed Fabrics Under Conditions of Dynamic Loading.” Geotechnique, Vol. 28, No. 4, pp. 466-469.

Webster, S. L. (1991). Geogrid Reinforced Base Courses for Flexible Pavements for Light Aircraft, Report No. GL-93-6, Report for the U.S Department of Transportation/ Federal Aviation Administration/ Department of Army Geotechical Laboratory, Vicksburg, MS

White, D. W.(1991). “Literature Review on Geotextiles to Improve Pavements For General Aviation Airports”, Paper GL-91-3, USAE Waterways Experiment Station.

Ullitz P. (1990) “Discussions at the Annual Meeting of Committee A2b05, Committee on Strength and Deformation Characteristics of Pavement Section. ’’ 69th Annual TRB Meeting, Washington, D.C.

Uzan J., Rhode G. T., Smith, R. E and Lytton, R. L., (1989) “Development of the New Mechanistic-empirical Design Program for Texas.” Draft Research Report 2455, Texas Transportation Institute, College Station, TX.

Vita

Alexander Kwasi Appea

Alexander Kwasi Appea was born on October 9th, 1966 in Tamale, Republic of Ghana. He graduated from Saint Peter's Secondary School in June of 1985. In October 1990, he received his Bachelor degree in Civil Engineering from the Kwame Nkrumah University of Science and Technology in Kumasi, Republic of Ghana. He worked for two years as a transportation engineer with the Ghana Highway Authority. In 1995, he joined the Master of Science Program in the Materials Division of Virginia Tech. During his graduate studies, he worked as a research assistant at the Structures and Materials Laboratory.

LIST OF APPENDICES

APPENDIX A

Table A 1 Results of Atterberg limits on subgrade soil

Sample No	Color	LL	PL	PI	USCS
T1B3	Yell-Brn	40.3	36.7	3.6	ML
T3B1	Yell-Brn	41.0	37.0	4.0	ML
T3B3	Yell-Brn	41.6	36.0	5.6	ML
T2B3	Red-Brn	68.3	31.0	37.3	CH
T1B2	Red-Brn	55.8	28.3	27.5	CH
T1B1	Red-Brn	58.4	29.1	29.3	CH

Table A 2 Specific gravity tests results

Material	Sample No	G_S	Average G_s
Base Course, (GW)	All	2.78	2.78
Subgrade, ML	T1B1	2.75	2.74
Subgrade, ML	T3B3	2.74	2.74
Subgrade, ML	T3B2	2.74	2.74
Subgrade,CH	T1B2	2.78	2.77
Subgrade,CH	T1B1	2.78	2.77
Subgrade,CH	T2B2	2.76	2.77

Table A 3 Average field dry densities and water contents of subgrade soil by nuclear methods (ASTM D 3017-96)

Section No.	Dry Density (kN/m^3)	Dry Density (kN/m^3)	Water Content (%)
1	18.1	14.1	28.7
2	18.0	13.8	30.3
3	17.9	14.4	24.0
4	17.2	13.4	28.4
5	17.2	13.9	23.8
6	17.8	14.1	26.3
7	18.6	14.3	29.9
8	18.9	14.6	29.0
9	17.7	13.5	31.1

Table A 4 Base course resilient modulus (laboratory tests)

Calibration Number 1

Base Thickness (mm)	Measured Vertical Stress s_V (kPa)	Horizontal Stress s_H (kPa)	Bulk Stress (kPa)	Resilient Modulus (MPa)
100	144.3	51.9	248.2	276
150	138.3	49.8	237.8	268
200	126.6	45.6	217.7	253

Calibration Number 2

Base Thickness (mm)	Measured Vertical Stress s_V (kPa)	Horizontal Stress s_H (kPa)	Bulk Stress (kPa)	Resilient Modulus (MPa)
100	152.3	54.8	262.0	286
150	142.2	51.2	244.6	273
200	134.2	48.3	230.9	263

Table A 5 Geotextile properties (after Amoco Fabrics and Fibers Company, 1994)

Property	Grab Tensile (N)	Grab Elongation (%)	Mullen Burst (MPa)	Puncture (N)	Trapezoidal Tear (N)	UV Resistance (%)**
ASTM Test No.	D 4632	D 4632	D 3786	D 4833	D 4533	D 4355*
2002	889.6	15	2.8	400.32	333.6	70

* Fabrics conditioned as per ASTM D 4355

** Percent of minimum grab tensile after conditioning

Table A 6 Geogrid properties (after Industrial Fabrics Association International, 1994)

Property	Mass/Unit Area ($kg/m^{3)}$	Aperture Size MD/XD (mm)	Thickness at Rib/Junction (mm)	Wide Width Strip Tensile Test kg/m		
				Strain (2%)	Strain (5%)	Ultimate
ASTM Test No.	D 3776-84		D 1777-64	D 4595-86		
BX1200	34.8	25/33	1.0/3.8	369	697	1169

Table A 7 Bulk specific gravity (saturated surface dry method)

Sample Number		1-9	1-10	2-9	2-10	3-9
Dry wt in air, g	A	1183.5	1215.4	1191.6	1165.9	1172.3
Submerged wt, g	B	685.5	7.4.6	674.7	662	670.5
SSD wt, g	C	1184.3	1215.9	1202.8	1180.8	1185.4
Bulk Specific Gravity, G_{mb}	A/(C-B)	2.373	2.377	2.256	2.247	2.277

Table A 8 VMA, VFA, VTM for the laboratory specimens (October, 1994 and November, 1996).

Specimen No	October, 1994			
	VTM (%)	**VMA (%)**	**VFA (%)**	**Density (kN/m^3)**
Lot 1	3.38	14.70	77.00	22.83
Lot 2	5.74	19.70	70.66	21.69
Lot 3	4.75	19.27	75.33	22.09

Specimen No	November, 1996			
	VTM (%)	**VMA (%)**	**VFA (%)**	**Density (kN/m^3)**
1	2.89	18.35	84.23	23.02
4	2.90	18.68	84.45	22.92
8	3.70	18.01	79.43	22.92

Table A 9 Marshall test results for laboratory specimens

Specimen No.	**Stability (kN)**	**Flow (mm)**
Section 9 (A)	13	14
Section 9 (B)	13	11
Section 2 (A)	12	8
Section 2 (B)	11	9
Section 5 (A)	11	8
Section 5 (B)	14	12

Table A 10 Asphalt content lot No. 1 (ashing method).

LINE	ITEM		SAMPLE 1 (1-1)	SAMPLE 2 (1-2)
A	Wt of original sample and cone and filter, g		1839.3	1844.7
B	Wt of cone, g		469.9	468.1
C	Wt of original sample, g	A-B-G	1361.2	1368.3
D	Wt of clean aggregate and container, g		1438.6	1445.7
E	Wt of container, g		168	168.4
F	Wt of clean aggregate, g	D-E	1270.6	1277.3
G	Initial wt of filter paper, g		8.2	8.3
H	Final wt of filter paper, g		8.6	8.6
I	Wt of filler in filter paper. g	H-G	0.4	0.3
J	Total volume of solvent, cm^3		880	860
K	Wt of solvent, g		1148.2	1123.2
L	Final wt of AC and fines in solvent, g	C-F	90.6	91
M	Volume of AC and fines in solvent, cm^3	J-(K-L)/1.329	84.2	83.3
O	Amount of filler in total solvent, g	1.656(L-1.03M)	6.4	8.6
P	Total wt of aggregate in sample, g	F+I+O	1277.4	1286.2
Q	Percentage of asphalt, %	(C-F-O)100/C	6.20%	6.00%
	Average Asphalt Content = 6.1%			

Table A 11 Asphalt content lot No. 2 (ashing method).

LINE	ITEM		SAMPLE 1 (2-1)	SAMPLE 2 (2-2)
A	Wt of original sample and cone and filter, g		1867.4	1702.3
B	Wt of cone, g		468	468.1
C	Wt of original sample, g	A-B-G	1391.1	1226
D	Wt of clean aggregate and container, g		1568.3	1426.3
E	Wt of container, g		275.2	276.9
F	Wt of clean aggregate, g	D-E	1293.1	1149.4
G	Initial wt of filter paper, g		8.3	8.2
H	Final wt of filter paper, g		8.7	8.4
I	Wt of filler in filter paper. g	H-G	0.4	0.2
J	Total volume of solvent, cm^3		1475	940
K	Wt of solvent, g		1937.7	1228.9
L	Final wt of AC and fines in solvent, g	C-F	98	76.6
M	Volume of AC and fines in solvent, cm^3	J-(K-L)/1.329	90.7	73
O	Amount of filler in total solvent, g	1.656(L-1.03M)	7.6	2.3
P	Total wt of aggregate in sample, g	F+I+O	1301.1	1151.9
Q	Percentage of asphalt, %	(C-F-O)100/C	6.50%	6.10%
	Average Asphalt Content = 6.3%			

Table A 12 Asphalt content lot No. 3 (ashing method).

LINE	ITEM		SAMPLE 1 (3-1)	SAMPLE 2 (3-2)
A	Wt of original sample and cone and filter, g		1766.9	1662.8
B	Wt of cone, g		470.1	467.6
C	Wt of original sample, g	A-B-G	1288.2	1186.6
D	Wt of clean aggregate and container, g		1375.8	1276.1
E	Wt of container, g		168.7	167.5
F	Wt of clean aggregate, g	D-E	1207.1	1108.6
G	Initial wt of filter paper, g		8.6	8.5
H	Final wt of filter paper, g		9.2	8.9
I	Wt of filler in filter paper. g	H-G	0.6	0.4
J	Total volume of solvent, cm^3		890	885.6
K	Wt of solvent, g		1161.3	1156.7
L	Final wt of AC and fines in solvent, g	C-F	81.1	78
M	Volume of AC and fines in solvent, cm^3	J-(K-L)/1.329	77.2	73.9
O	Amount of filler in total solvent, g	1.656(L-1.03M)	2.6	3.1
P	Total wt of aggregate in sample, g	F+I+O	1210.3	1112.1
Q	Percentage of asphalt, %	(C-F-O)100/C	6.10%	6.30%
	Average Asphalt Content = 6.2%			

Table A 13 HMA resilient modulus test results for various sections.

November, 1996			
Section No	5°C (MPa)	25°C (MPa)	40°C (MPa)
1	3222	2950	2832
2	3206	2963	2841
3	3236	2957	2838
4	3143	2960	2847
5	3199	2957	2862
6	3279	2996	2842
7	3217	3025	2885
8	3257	2962	2875
9	3325	3018	2846
Average	3232	2976	2852

October 1994,			
Section No	5°C (MPa)	25°C (MPa)	40°C (MPa)
C-3	3205	2720	2583
C1-A	3138	2811	2630
C1-B	3250	2845	2570
C4-A	3140	2708	2651
C5-A	3073	2737	2659
C9-A	3202	2769	2622
Average	3168	2765	2619

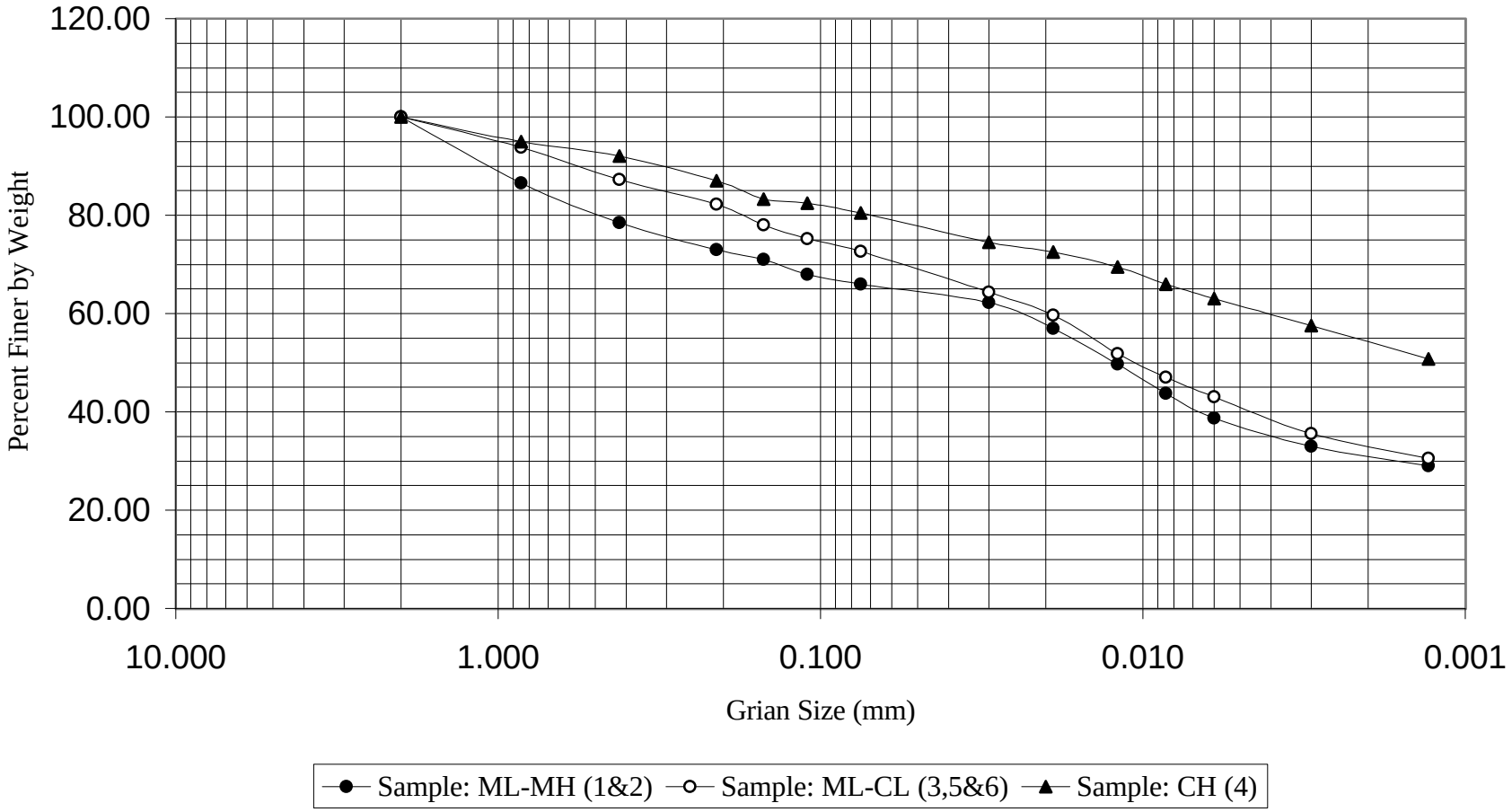

Figure A 1 Gradation analysis of subgrade soil

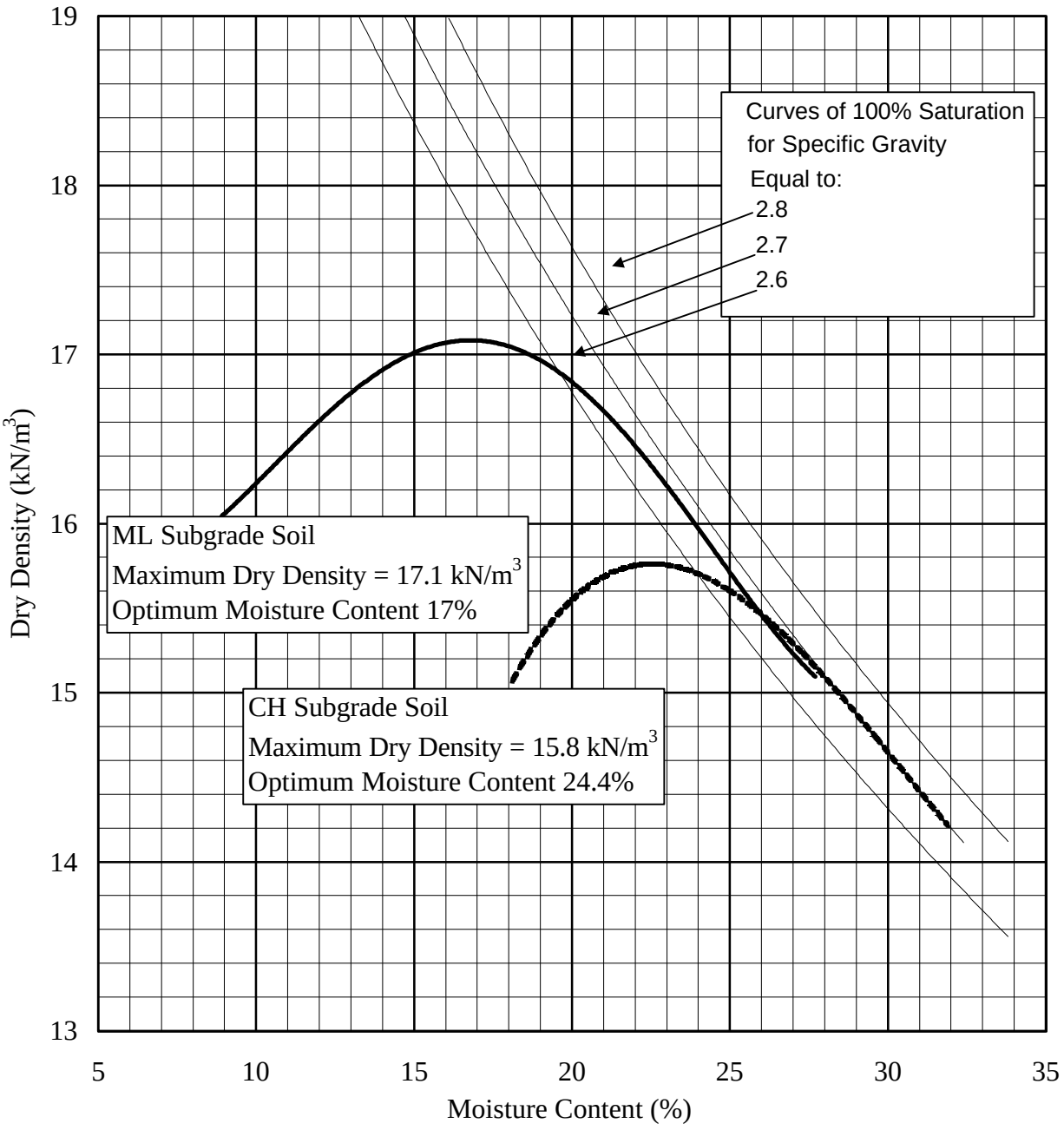

Figure A 2 Dry density versus water content for subgrade soil at a modified Proctor effort of 2700 kN-m/m^3

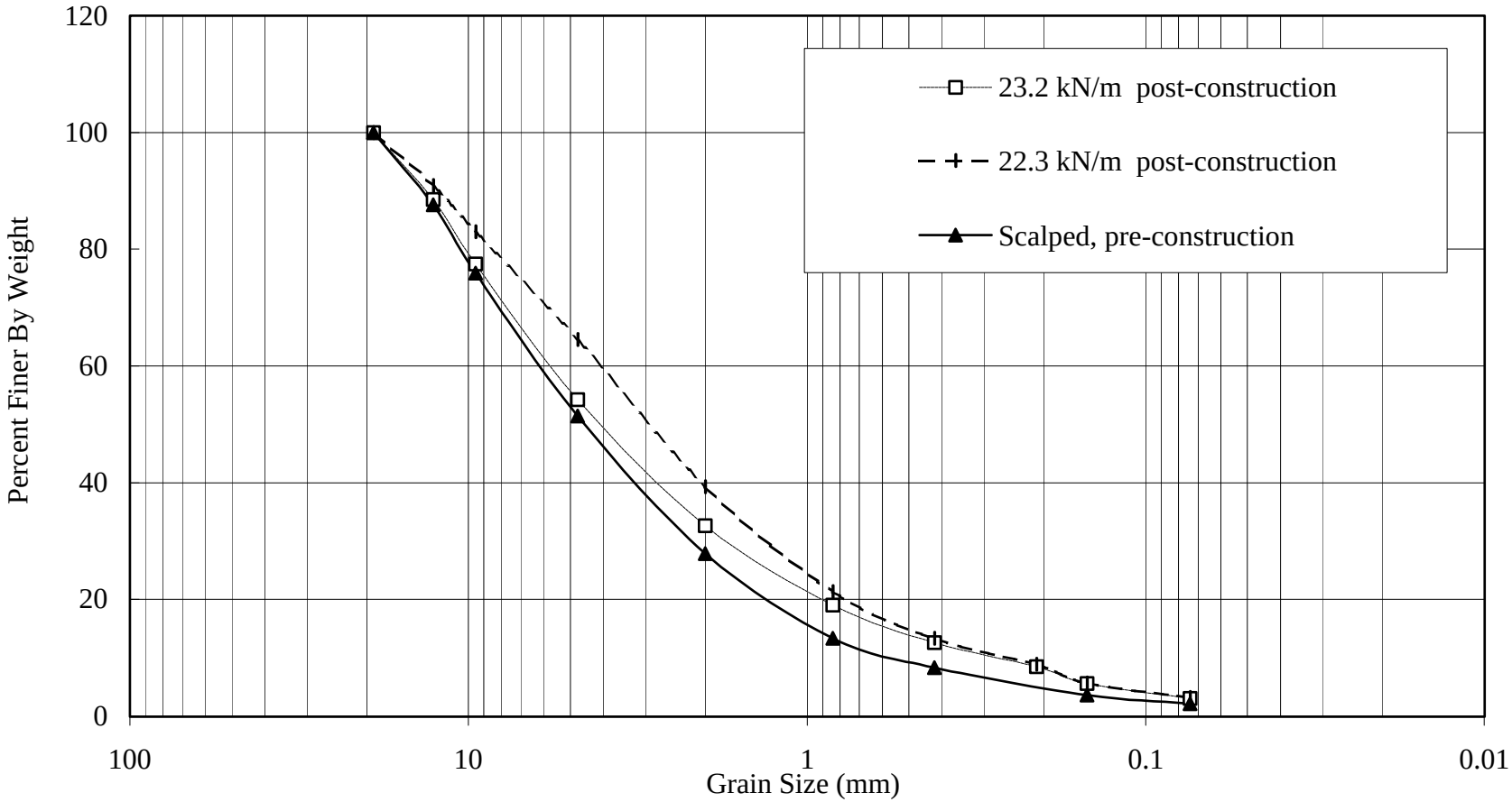

Figure A 3 Gradation Curve for pre- and post- construction base course samples

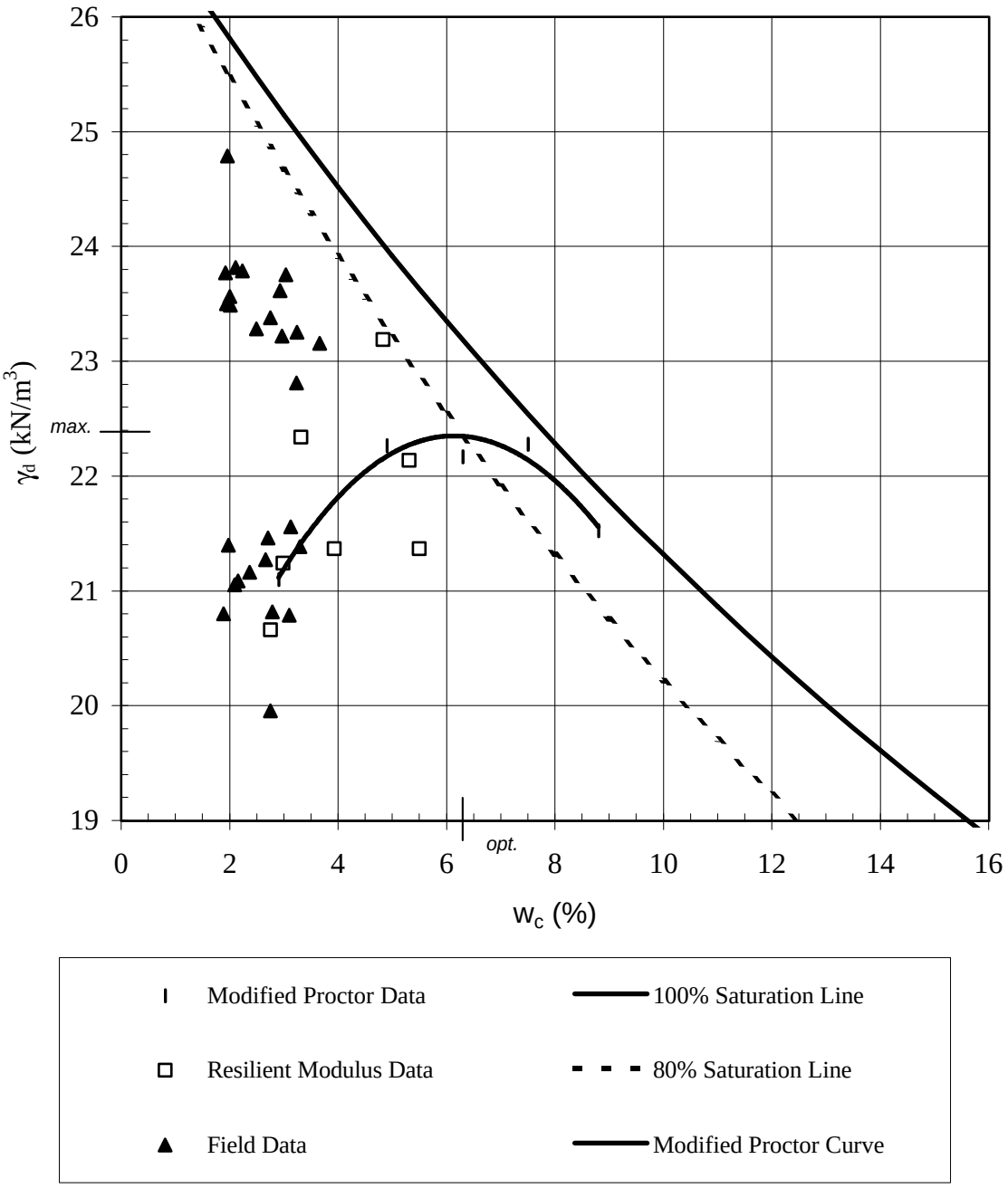

Figure A 4 Dry density vs. water content for the base course material

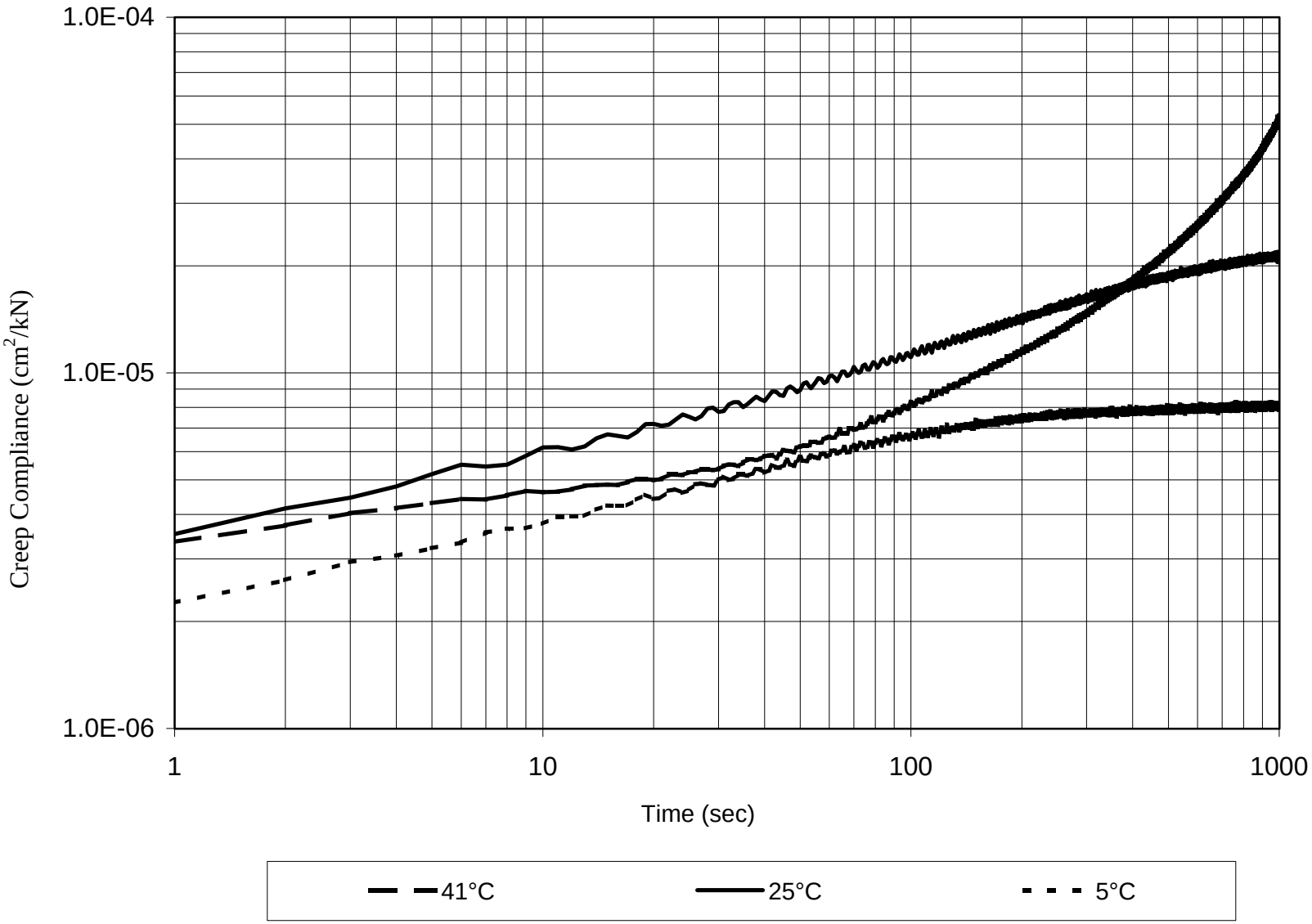

Figure A 5 Creep Compliance, section 1 (1000 sec)

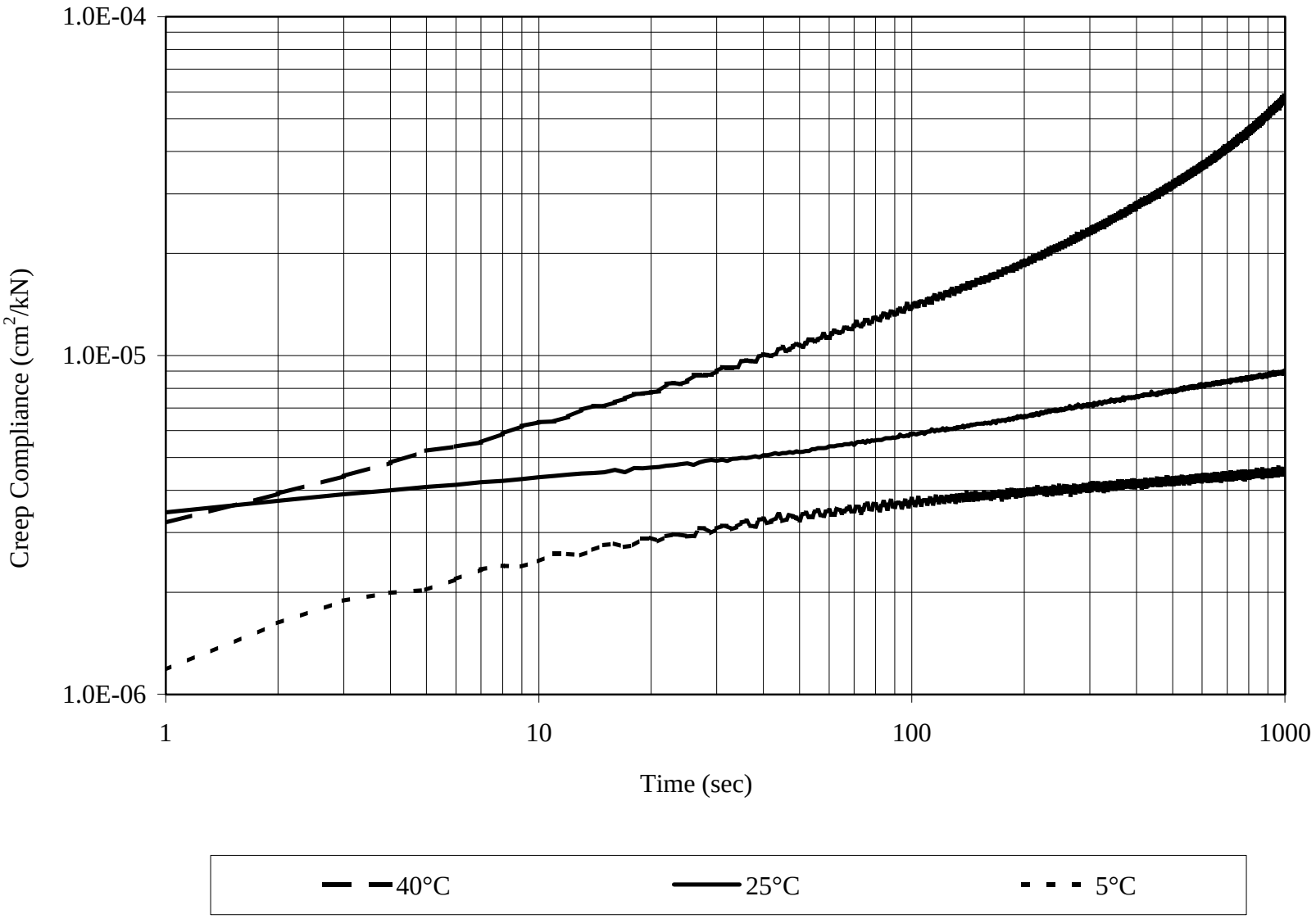

Figure A 6 Creep Compliance, section 2 (1000 sec)

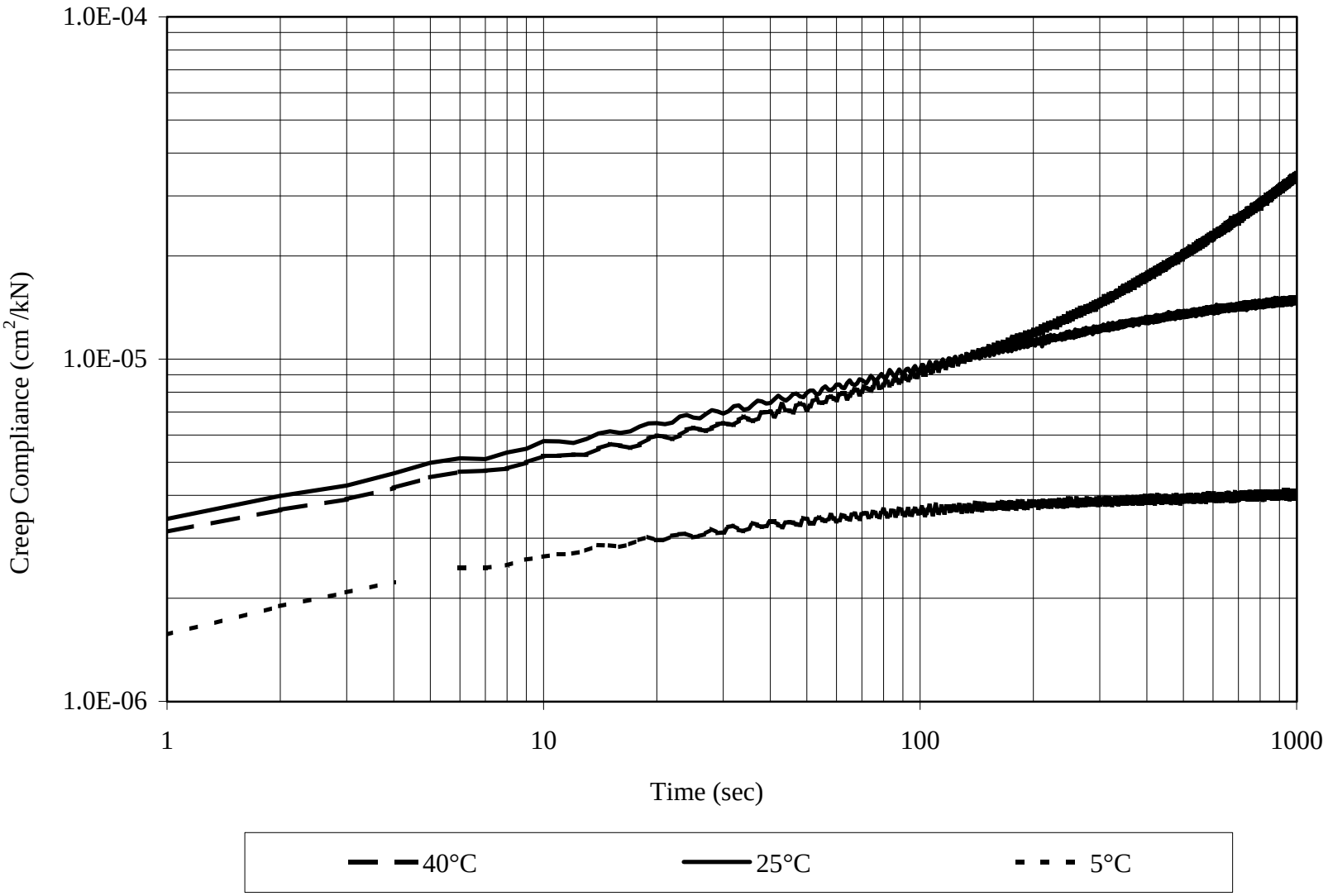

Figure A 7 Creep Compliance, section 3 (1000 sec)

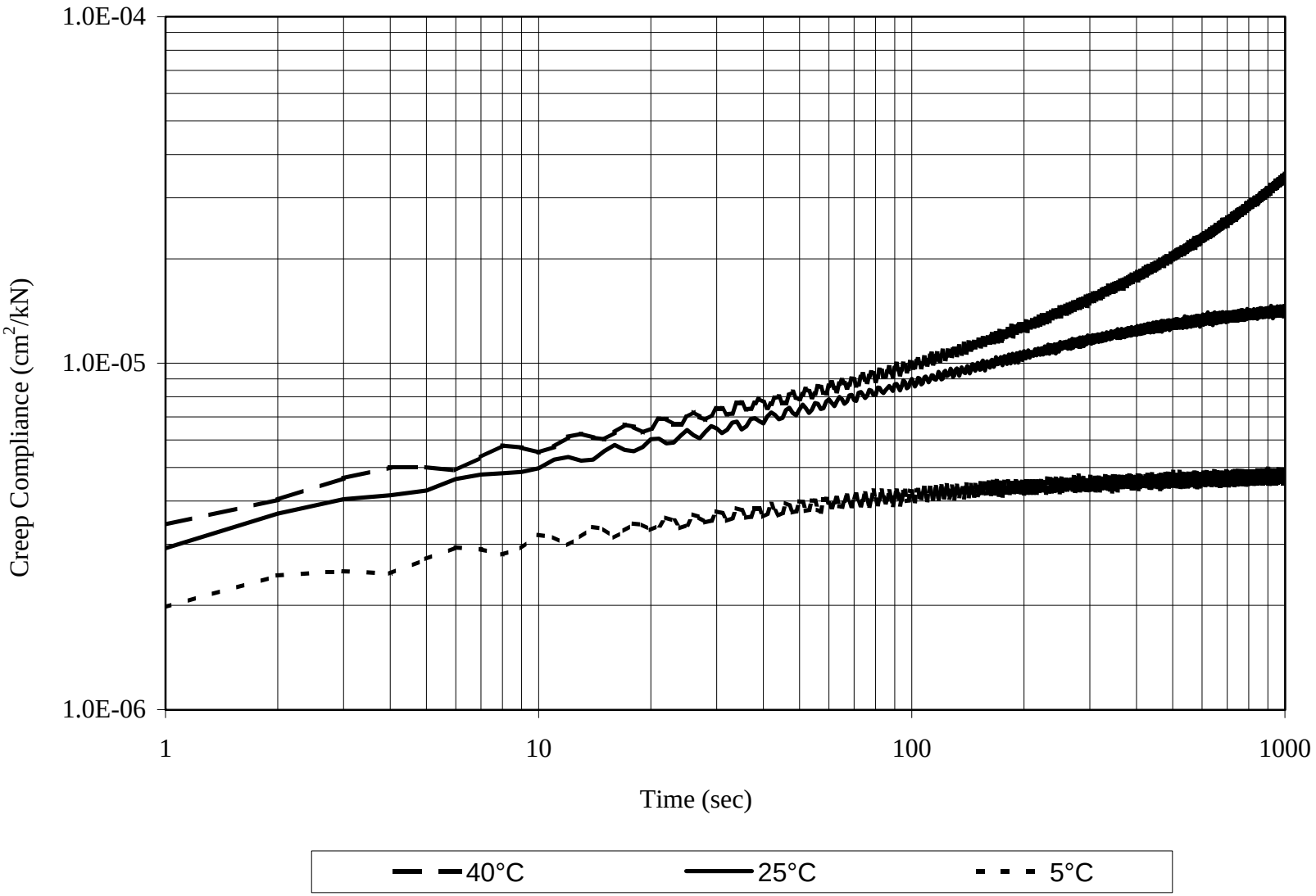

Figure A 8 Creep Compliance, section 4 (1000 sec)

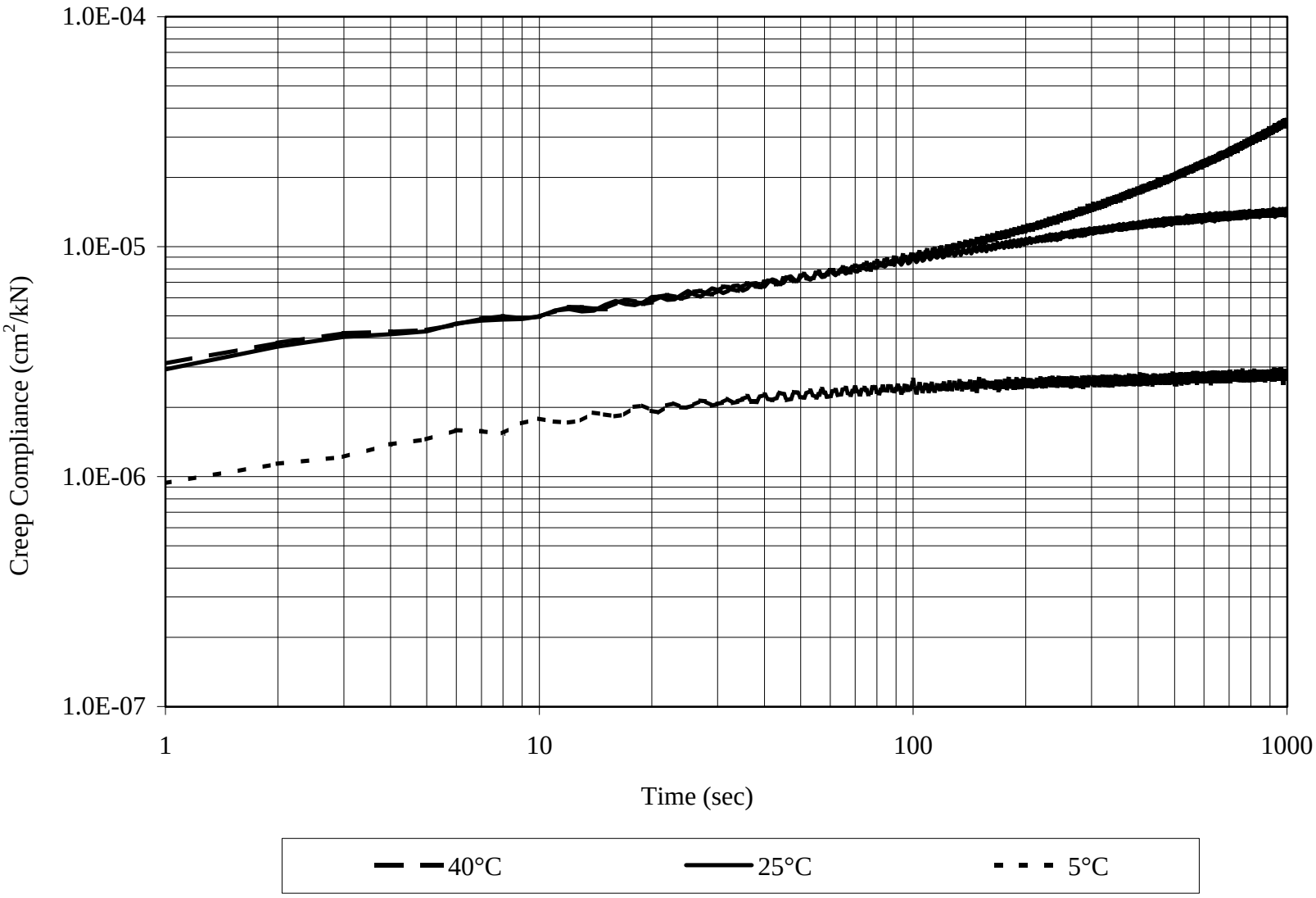

Figure A 9 Creep Compliance, section 5 (1000 seconds)

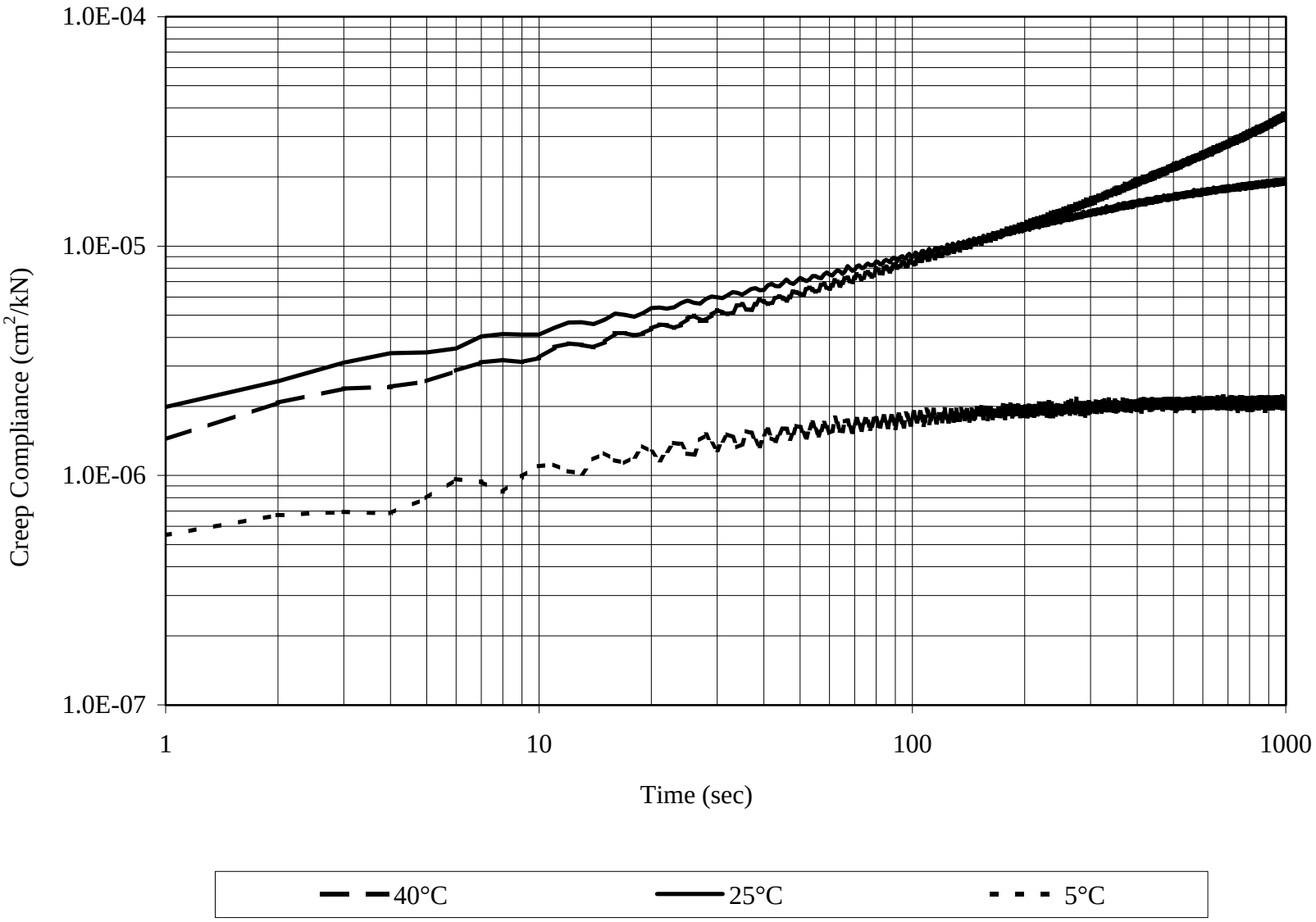

Figure A 10 Creep Compliance, section 6 (1000 seconds)

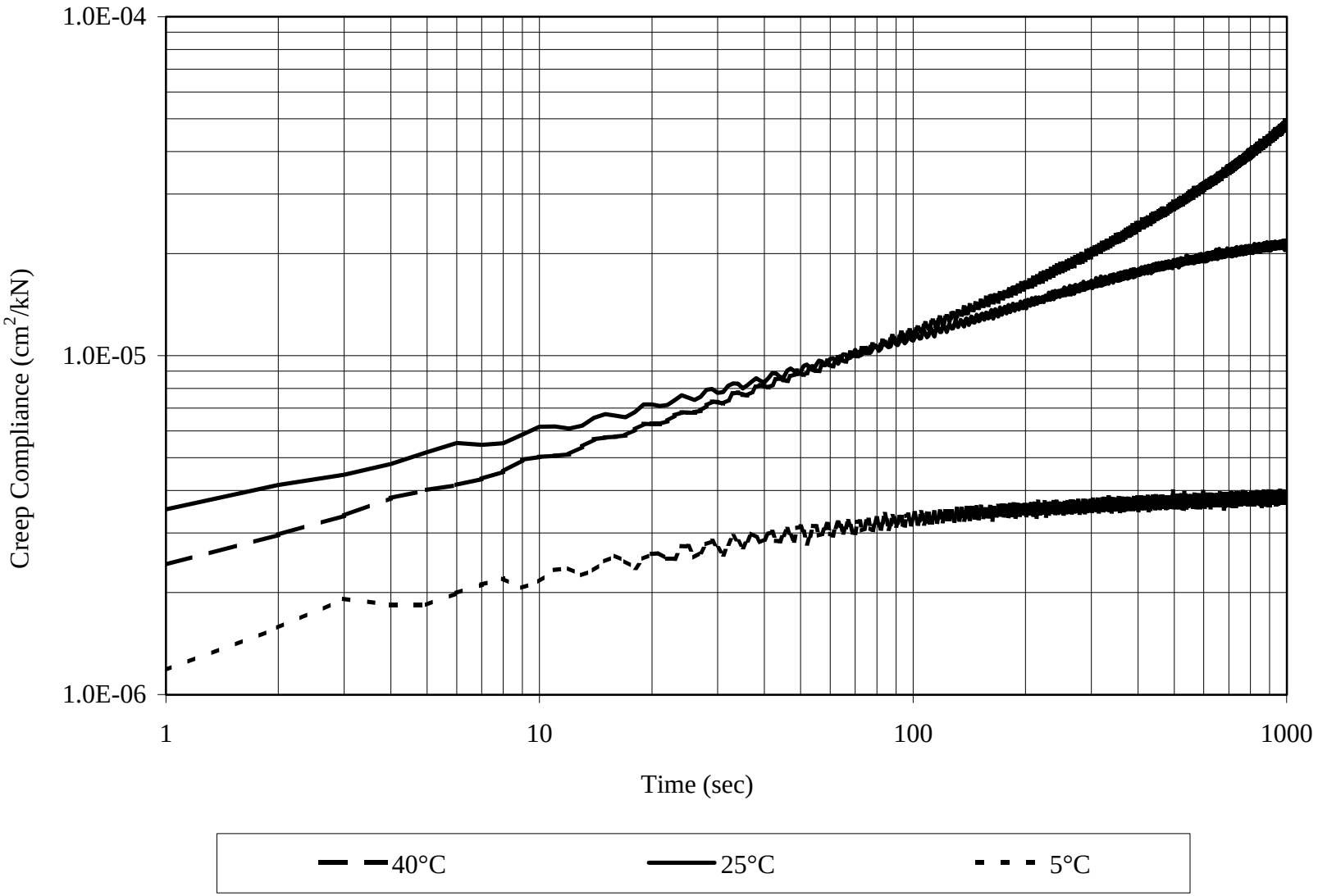

Figure A 11 Creep Compliance, section 7 (1000 sec)

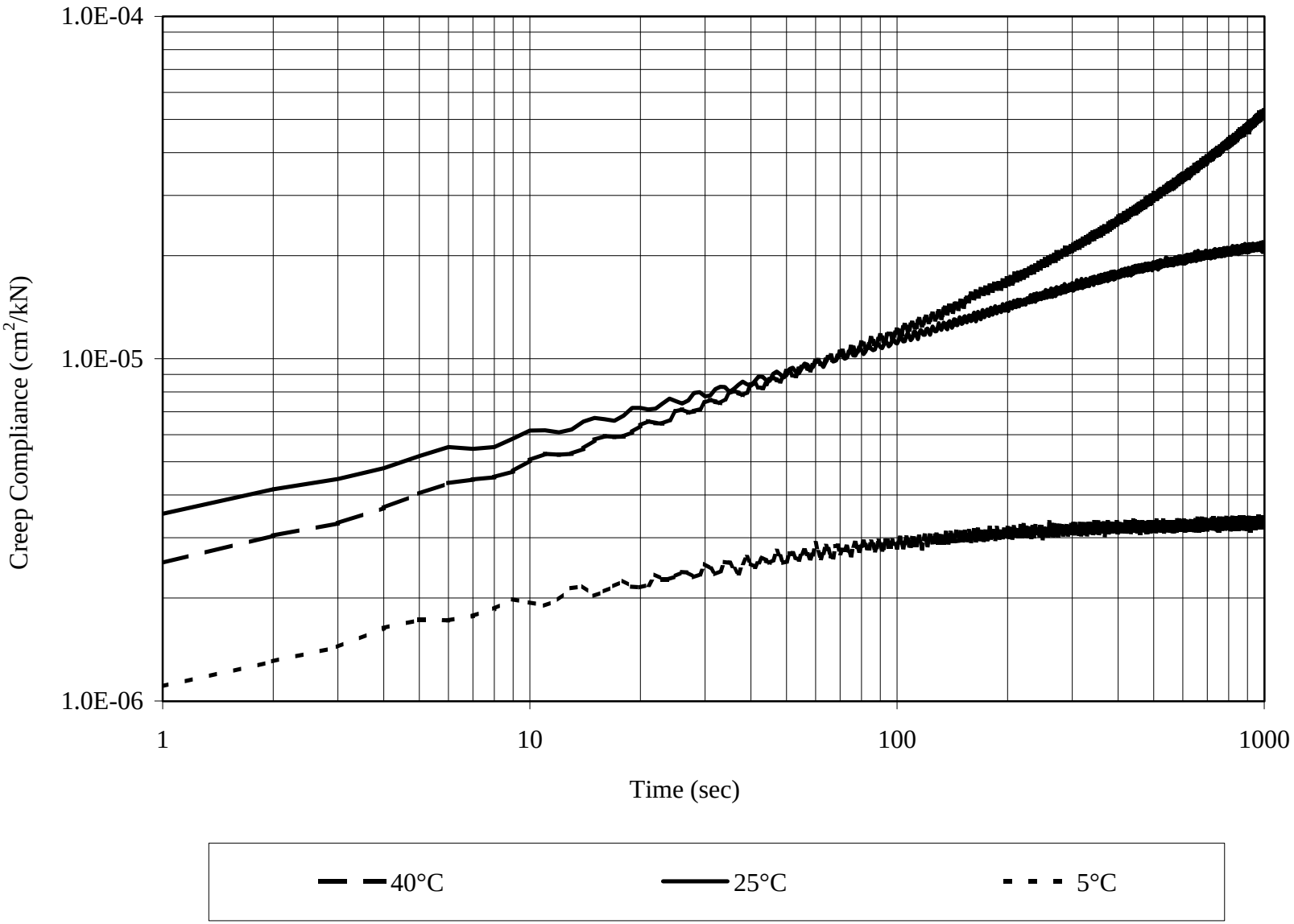

Figure A 12 Creep Compliance, section 8 (1000 sec)

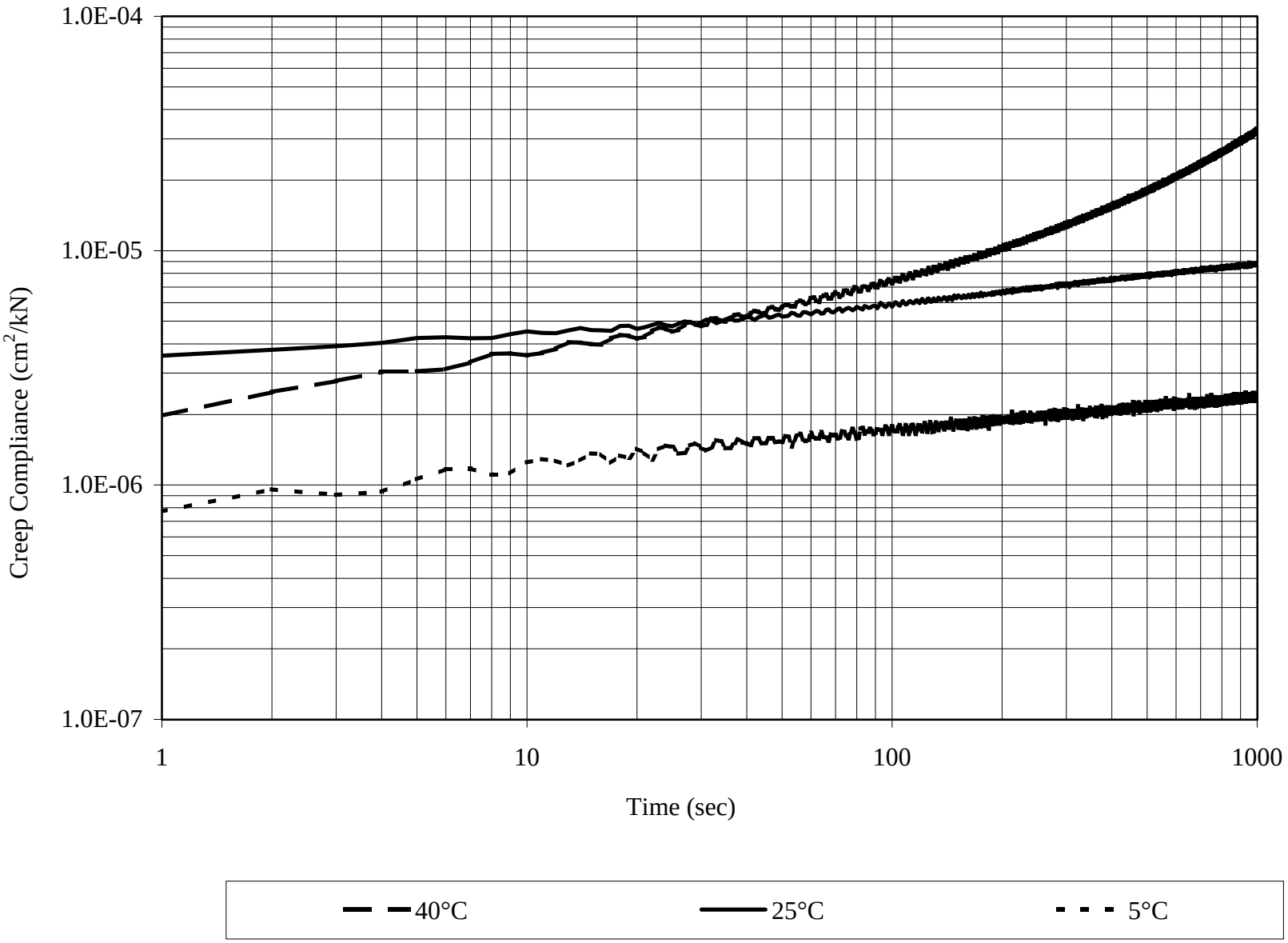

Figure A 13 Creep Compliance, section 9 (1000 seconds)

APPENDIX B

Table B 1 FWD Deflection Data - October 1994

Section	Load kN	Geophone Radial Offset (mm)						
		0.000	0.305	0.610	0.914	1.219	1.524	1.829
1	24.5	0.350	0.151	0.035	0.015	0.010	0.009	0.008
1	33.5	0.464	0.191	0.041	0.018	0.017	0.013	0.010
1	39.5	0.518	0.224	0.055	0.021	0.017	0.016	0.013
1	47.8	0.654	0.309	0.077	0.026	0.021	0.019	0.015
2	24.4	0.287	0.148	0.053	0.028	0.019	0.016	0.014
2	32.9	0.394	0.214	0.086	0.039	0.028	0.023	0.019
2	39.1	0.435	0.235	0.093	0.047	0.029	0.028	0.024
2	46.5	0.491	0.285	0.123	0.060	0.038	0.033	0.026
3	24.0	0.280	0.152	0.063	0.032	0.019	0.014	0.011
3	32.6	0.401	0.233	0.098	0.046	0.025	0.019	0.015
3	38.6	0.497	0.284	0.119	0.052	0.027	0.021	0.017
3	46.3	0.536	0.318	0.140	0.066	0.035	0.027	0.020
4	23.1	0.493	0.319	0.163	0.089	0.055	0.047	0.035
4	30.7	0.707	0.472	0.243	0.137	0.084	0.066	0.050
4	37.3	0.856	0.569	0.302	0.170	0.104	0.082	0.058
4	44.4	0.964	0.664	0.368	0.207	0.125	0.091	0.076
5	23.6	0.460	0.274	0.128	0.070	0.043	0.035	0.030
5	31.5	0.624	0.381	0.189	0.110	0.076	0.064	0.052
5	39.3	0.796	0.495	0.242	0.136	0.089	0.076	0.062
5	45.0	0.906	0.565	0.279	0.156	0.103	0.086	0.072
6	23.2	0.490	0.310	0.170	0.110	0.070	0.060	0.040
6	30.7	0.820	0.540	0.290	0.170	0.110	0.090	0.070
6	44.3	1.000	0.670	0.390	0.240	0.150	0.120	0.090
7	23.2	0.465	0.297	0.151	0.083	0.053	0.041	0.031
7	31.1	0.669	0.433	0.225	0.122	0.072	0.057	0.046
7	38.8	0.872	0.573	0.300	0.167	0.099	0.077	0.063
7	44.3	0.958	0.638	0.343	0.190	0.113	0.088	0.067
8	23.3	0.541	0.295	0.123	0.065	0.044	0.033	0.026
8	31.0	0.727	0.418	0.182	0.094	0.058	0.049	0.040
8	38.9	0.947	0.560	0.244	0.129	0.080	0.065	0.052
8	44.5	1.017	0.604	0.285	0.149	0.093	0.071	0.059
9	24.0	0.283	0.141	0.054	0.033	0.026	0.024	0.020
9	32.7	0.380	0.197	0.077	0.046	0.036	0.033	0.027
9	40.7	0.472	0.260	0.115	0.067	0.049	0.041	0.039
9	46.1	0.491	0.273	0.126	0.075	0.053	0.047	0.041

Table B 2 FWD Deflection Data - March 1995

Section	Load kN	Geophone Radial Offset (mm)						
		0.000	0.305	0.610	0.914	1.219	1.524	1.829
1	24.5	0.350	0.151	0.035	0.015	0.010	0.009	0.008
1	33.5	0.464	0.191	0.041	0.018	0.017	0.013	0.010
1	39.4	0.518	0.226	0.054	0.021	0.017	0.015	0.013
1	47.8	0.654	0.309	0.077	0.026	0.021	0.019	0.015
2	24.4	0.287	0.148	0.053	0.028	0.019	0.016	0.014
2	32.9	0.394	0.214	0.086	0.039	0.028	0.023	0.019
2	46.5	0.491	0.285	0.123	0.060	0.038	0.033	0.026
3	24.0	0.280	0.152	0.063	0.032	0.019	0.014	0.011
3	32.6	0.401	0.233	0.098	0.046	0.025	0.019	0.015
3	39.1	0.435	0.235	0.093	0.047	0.029	0.028	0.024
3	46.3	0.536	0.318	0.140	0.066	0.035	0.027	0.020
4	23.1	0.493	0.319	0.163	0.089	0.055	0.047	0.035
4	30.7	0.707	0.472	0.243	0.137	0.084	0.066	0.050
4	44.4	0.964	0.664	0.368	0.207	0.125	0.091	0.076
5	23.4	0.460	0.274	0.128	0.070	0.043	0.035	0.030
5	31.5	0.624	0.381	0.189	0.110	0.076	0.064	0.052
5	37.3	0.856	0.569	0.302	0.170	0.104	0.082	0.058
5	45.0	0.906	0.565	0.279	0.156	0.103	0.086	0.072
6	23.2	0.495	0.313	0.169	0.105	0.068	0.057	0.043
6	30.7	0.823	0.536	0.290	0.171	0.110	0.087	0.066
6	44.3	0.998	0.672	0.393	0.241	0.153	0.119	0.093
7	23.2	0.465	0.297	0.151	0.083	0.053	0.041	0.031
7	31.1	0.669	0.433	0.225	0.122	0.072	0.057	0.046
7	44.3	0.958	0.638	0.343	0.190	0.113	0.088	0.067
8	23.0	0.541	0.295	0.123	0.065	0.044	0.063	0.026
8	31.0	0.727	0.418	0.182	0.094	0.058	0.049	0.040
8	44.5	1.017	0.604	0.285	0.149	0.093	0.071	0.059
9	24.4	0.283	0.141	0.054	0.033	0.026	0.024	0.020
9	32.7	0.380	0.197	0.077	0.046	0.036	0.033	0.027
9	46.1	0.491	0.273	0.126	0.075	0.053	0.047	0.041

Table B 3 FWD Deflection Data - August 1995

Section	Load kN	Geophone Radial Offset (mm)						
		0.000	0.305	0.610	0.914	1.219	1.524	1.829
1	23.5	0.377	0.110	0.023	0.014	0.011	0.010	0.008
1	26.7	0.470	0.138	0.029	0.017	0.013	0.012	0.009
1	32.4	0.583	0.172	0.032	0.019	0.017	0.013	0.010
1	39.9	0.710	0.221	0.041	0.022	0.020	0.016	0.014
1	51.2	0.945	0.270	0.045	0.023	0.023	0.020	0.016
2	23.8	0.330	0.124	0.046	0.027	0.021	0.018	0.015
2	26.3	0.410	0.153	0.056	0.031	0.022	0.020	0.019
2	32.5	0.465	0.176	0.067	0.037	0.029	0.024	0.023
2	39.5	0.608	0.219	0.081	0.043	0.034	0.029	0.025
2	48.7	0.722	0.265	0.097	0.053	0.041	0.035	0.030
2	46.3	0.536	0.318	0.140	0.066	0.035	0.027	0.020
3	23.5	0.352	0.142	0.054	0.028	0.018	0.015	0.012
3	26.5	0.418	0.171	0.065	0.031	0.021	0.016	0.013
3	32.7	0.539	0.214	0.080	0.037	0.024	0.019	0.015
3	40.5	0.697	0.289	0.107	0.049	0.031	0.025	0.020
3	49.1	0.888	0.361	0.132	0.059	0.037	0.028	0.023
4	23.6	0.542	0.274	0.131	0.080	0.055	0.047	0.040
4	26.9	0.654	0.346	0.170	0.096	0.065	0.053	0.045
4	32.9	0.797	0.415	0.206	0.114	0.077	0.064	0.054
4	41.1	1.093	0.589	0.297	0.163	0.110	0.086	0.072
4	49.2	1.343	0.732	0.372	0.204	0.134	0.107	0.085
5	23.1	0.473	0.238	0.122	0.070	0.048	0.040	0.034
5	26.3	0.543	0.281	0.146	0.082	0.059	0.049	0.043
5	32.6	0.719	0.370	0.189	0.108	0.073	0.060	0.052
5	41.1	0.937	0.491	0.250	0.139	0.097	0.077	0.064
5	48.9	1.148	0.606	0.310	0.172	0.115	0.095	0.079
6	23.8	0.476	0.265	0.157	0.100	0.068	0.053	0.048
6	27.1	0.554	0.311	0.183	0.116	0.076	0.060	0.049
6	32.9	0.757	0.440	0.259	0.160	0.105	0.082	0.067
6	41.4	0.965	0.567	0.335	0.208	0.135	0.105	0.084
6	48.8	1.392	0.829	0.492	0.293	0.184	0.138	0.113
7	23.4	0.586	0.301	0.145	0.077	0.048	0.038	0.031
7	26.8	0.699	0.364	0.171	0.093	0.057	0.047	0.040
7	32.4	0.901	0.477	0.229	0.117	0.074	0.058	0.051
7	40.9	1.149	0.625	0.306	0.157	0.096	0.074	0.059
7	48.8	1.428	0.796	0.394	0.202	0.122	0.096	0.076
8	22.8	0.634	0.280	0.110	0.057	0.042	0.033	0.031
8	26.2	0.740	0.326	0.128	0.068	0.050	0.040	0.034
8	32.5	0.933	0.421	0.172	0.088	0.064	0.053	0.045
8	40.6	1.179	0.576	0.235	0.118	0.084	0.069	0.058
8	48.8	1.469	0.696	0.284	0.141	0.100	0.083	0.068
9	23.6	0.286	0.110	0.051	0.033	0.026	0.024	0.023
9	26.5	0.320	0.133	0.060	0.040	0.032	0.027	0.026
9	32.8	0.410	0.171	0.080	0.051	0.039	0.035	0.032
9	40.7	0.518	0.214	0.099	0.063	0.051	0.045	0.041
9	48.6	0.631	0.272	0.126	0.077	0.062	0.055	0.049

Table B 4 FWD Deflection Data - April 1996

	Load	Geophone Radial Offset (mm)						
Section	kN	0.000	0.305	0.457	0.610	0.914	1.219	1.524
1	25.9	0.798	0.542	0.414	0.321	0.198	0.150	0.116
1	31.7	0.951	0.616	0.468	0.364	0.213	0.156	0.140
1	42.6	1.280	0.847	0.654	0.507	0.322	0.242	0.197
1	49.6	1.495	0.968	0.758	0.561	0.360	0.269	0.223
1	59.5	1.820	1.195	0.901	0.696	0.478	0.348	0.276
2	26.0	0.562	0.343	0.243	0.193	0.109	0.094	0.075
2	31.5	0.681	0.394	0.288	0.204	0.129	0.106	0.077
2	42.1	0.899	0.544	0.395	0.282	0.188	0.147	0.113
2	49.1	1.049	0.628	0.439	0.340	0.210	0.159	0.143
2	58.4	1.278	0.770	0.551	0.412	0.265	0.201	0.176
3	25.6	0.620	0.424	0.327	0.243	0.169	0.121	0.096
3	31.1	0.735	0.488	0.379	0.281	0.195	0.134	0.125
3	41.7	1.010	0.678	0.514	0.389	0.267	0.179	0.133
3	48.3	1.158	0.775	0.598	0.478	0.297	0.218	0.161
3	57.6	1.407	0.945	0.714	0.567	0.366	0.266	0.218
4	24.4	0.690	0.488	0.397	0.311	0.223	0.173	0.141
4	30.1	0.803	0.597	0.465	0.364	0.266	0.191	0.163
4	40.1	1.096	0.801	0.653	0.521	0.371	0.260	0.224
4	46.5	1.287	0.924	0.748	0.592	0.409	0.312	0.248
4	55.5	1.567	1.134	0.901	0.751	0.526	0.376	0.288
5	28.0	0.579	0.386	0.311	0.245	0.185	0.092	0.068
5	30.7	0.674	0.442	0.358	0.277	0.211	0.118	0.078
5	40.5	0.896	0.601	0.504	0.386	0.291	0.133	0.106
5	47.1	1.060	0.712	0.598	0.462	0.322	0.170	0.125
5	56.2	1.201	0.878	0.732	0.566	0.377	0.217	0.149
6	28.5	0.722	0.538	0.432	0.361	0.196	0.173	0.143
6	30.4	0.839	0.619	0.525	0.417	0.295	0.214	0.174
6	40.3	1.168	0.855	0.703	0.567	0.381	0.295	0.205
6	47.1	1.351	1.010	0.840	0.649	0.469	0.332	0.273
6	55.6	1.623	1.199	0.969	0.807	0.560	0.409	0.322
7	27.4	0.667	0.482	0.420	0.340	0.270	0.180	0.128
7	29.8	0.772	0.536	0.466	0.377	0.301	0.225	0.163
7	39.8	1.054	0.765	0.665	0.543	0.383	0.289	0.239
7	46.1	1.231	0.919	0.800	0.650	0.445	0.347	0.268
7	54.8	1.512	1.122	0.976	0.799	0.542	0.428	0.307
8	27.7	0.556	0.388	0.311	0.238	0.161	0.122	0.105
8	30.1	0.620	0.457	0.378	0.295	0.208	0.118	0.138
8	40.2	0.858	0.674	0.502	0.384	0.264	0.206	0.161
8	46.7	0.907	0.906	0.575	0.457	0.315	0.244	0.200
8	55.5	1.109	1.111	0.708	0.579	0.385	0.281	0.235
9	29.0	0.599	0.415	0.321	0.288	0.213	0.154	0.110
9	31.6	0.705	0.499	0.427	0.337	0.218	0.181	0.138
9	42.0	0.950	0.629	0.546	0.463	0.320	0.244	0.194
9	48.5	1.101	0.702	0.637	0.502	0.375	0.292	0.212
9	57.7	1.351	0.838	0.755	0.637	0.456	0.361	0.248

Table B 5 FWD Deflection Data - July 1996

Section	Load kN	Geophone Radial Offset (mm)						
		0.000	0.305	0.457	0.610	0.914	1.219	1.524
1	23.7	0.674	0.481	0.357	0.283	0.181	0.137	0.111
1	28.1	0.805	0.549	0.444	0.354	0.215	0.148	0.090
1	42.5	1.155	0.803	0.621	0.478	0.320	0.244	0.197
1	50.9	1.350	0.951	0.725	0.564	0.379	0.268	0.207
2	23.7	0.546	0.373	0.289	0.212	0.141	0.080	0.072
2	27.8	0.643	0.442	0.339	0.258	0.161	0.109	0.100
2	41.7	0.953	0.652	0.462	0.371	0.240	0.169	0.111
2	50.1	1.106	0.738	0.551	0.411	0.289	0.186	0.170
3	23.1	0.621	0.428	0.310	0.242	0.166	0.110	0.092
3	27.2	0.723	0.493	0.359	0.298	0.183	0.132	0.120
3	41.3	1.050	0.720	0.543	0.408	0.260	0.178	0.157
3	49.9	1.236	0.818	0.614	0.505	0.310	0.234	0.185
4	22.4	0.807	0.600	0.487	0.413	0.281	0.227	0.164
4	26.7	0.917	0.691	0.576	0.471	0.337	0.249	0.181
4	40.8	1.361	1.026	0.855	0.710	0.499	0.374	0.303
4	48.3	1.564	1.162	0.937	0.818	0.564	0.414	0.309
5	22.7	0.639	0.464	0.357	0.298	0.226	0.150	0.124
5	26.9	0.747	0.544	0.449	0.372	0.236	0.196	0.141
5	41.0	1.106	0.798	0.652	0.513	0.364	0.256	0.211
5	49.6	1.282	0.927	0.759	0.593	0.437	0.320	0.235
6	22.5	0.727	0.541	0.423	0.367	0.263	0.184	0.138
6	26.9	0.853	0.644	0.531	0.427	0.287	0.221	0.158
6	40.6	1.264	0.919	0.776	0.618	0.476	0.283	0.231
6	48.0	1.475	1.073	0.875	0.715	0.539	0.376	0.287
7	22.5	0.606	0.441	0.350	0.243	0.209	0.154	0.151
7	26.6	0.756	0.551	0.439	0.385	0.270	0.224	0.164
7	40.2	1.102	0.810	0.677	0.564	0.420	0.322	0.233
7	50.6	1.248	0.922	0.777	0.646	0.433	0.336	0.259
8	22.5	0.630	0.435	0.403	0.317	0.231	0.166	0.122
8	26.9	0.698	0.526	0.442	0.338	0.238	0.179	0.129
8	40.7	1.006	0.731	0.592	0.503	0.343	0.279	0.216
8	50.4	1.187	0.927	0.697	0.570	0.428	0.313	0.233
9	23.7	0.595	0.417	0.351	0.282	0.212	0.160	0.103
9	27.8	0.690	0.498	0.418	0.334	0.230	0.193	0.135
9	41.4	0.997	0.702	0.568	0.451	0.323	0.245	0.185
9	49.6	1.162	0.912	0.676	0.554	0.395	0.284	0.219

Table B 6 FWD Deflection Data - October 1996

	Load	Geophone Radial Offset (mm)						
Section	kN	0.000	0.305	0.457	0.610	0.914	1.219	1.524
1	27.1	0.533	0.243	0.102	0.046	0.013	0.012	0.012
1	31.2	0.622	0.290	0.124	0.056	0.015	0.015	0.014
1	51.3	0.915	0.420	0.181	0.078	0.017	0.021	0.022
1	56.3	0.998	0.453	0.191	0.083	0.017	0.021	0.023
2	27.3	0.395	0.219	0.124	0.078	0.036	0.024	0.022
2	31.0	0.454	0.253	0.145	0.093	0.042	0.029	0.024
2	50.4	0.692	0.391	0.229	0.148	0.068	0.044	0.040
2	55.2	0.690	0.394	0.234	0.156	0.075	0.049	0.041
3	26.6	0.416	0.232	0.129	0.079	0.031	0.020	0.014
3	30.4	0.485	0.276	0.159	0.098	0.039	0.024	0.016
3	49.8	0.774	0.456	0.268	0.170	0.067	0.036	0.028
3	54.2	0.821	0.496	0.302	0.198	0.080	0.042	0.029
4	25.9	0.669	0.442	0.299	0.223	0.126	0.082	0.063
4	29.7	0.815	0.554	0.381	0.282	0.157	0.100	0.073
4	47.7	1.305	0.916	0.645	0.489	0.281	0.176	0.126
4	51.9	1.432	1.026	0.724	0.552	0.317	0.197	0.138
5	26.2	0.532	0.343	0.228	0.169	0.101	0.071	0.056
5	30.0	0.589	0.386	0.264	0.200	0.118	0.081	0.066
5	48.6	0.985	0.668	0.461	0.353	0.213	0.144	0.110
5	53.3	1.061	0.716	0.503	0.382	0.232	0.157	0.120
6	26.0	0.668	0.465	0.333	0.261	0.160	0.104	0.073
6	29.8	0.792	0.573	0.414	0.326	0.203	0.135	0.097
6	47.7	1.309	0.980	0.732	0.585	0.371	0.240	0.166
6	51.7	1.421	1.057	0.793	0.631	0.401	0.258	0.183
7	26.1	0.639	0.411	0.261	0.185	0.098	0.066	0.051
7	29.8	0.736	0.496	0.328	0.237	0.123	0.080	0.062
7	47.6	1.198	0.839	0.577	0.425	0.228	0.139	0.102
7	52.0	1.298	0.906	0.627	0.461	0.253	0.156	0.115
8	26.0	0.663	0.390	0.234	0.156	0.078	0.052	0.043
8	29.9	0.785	0.469	0.283	0.192	0.097	0.064	0.052
8	48.2	1.239	0.777	0.484	0.331	0.169	0.110	0.085
8	52.5	1.313	0.824	0.517	0.362	0.186	0.120	0.092
9	27.5	0.375	0.202	0.113	0.076	0.043	0.033	0.028
9	30.9	0.437	0.235	0.136	0.089	0.051	0.038	0.033
9	41.0	0.557	0.315	0.190	0.130	0.075	0.057	0.049
9	49.8	0.654	0.373	0.223	0.152	0.088	0.067	0.057
9	54.17	0.703	0.4	0.24	0.165	0.096	0.072	0.061

Table B 7 FWD Deflection Data - January 1997

	Load	Geophone Radial Offset (mm)						
Section	kN	0.000	0.305	0.457	0.610	0.914	1.219	1.524
1	27.1	0.533	0.362	0.254	0.224	0.140	0.088	0.063
1	31.2	0.622	0.417	0.327	0.234	0.167	0.117	0.090
1	41.9	0.815	0.555	0.378	0.289	0.194	0.145	0.121
1	51.3	0.983	0.648	0.485	0.383	0.246	0.173	0.149
1	55.1	1.056	0.712	0.531	0.406	0.264	0.193	0.150
2	27.3	0.420	0.245	0.192	0.129	0.087	0.074	0.047
2	31.0	0.454	0.287	0.221	0.169	0.093	0.054	0.049
2	41.4	0.595	0.331	0.273	0.200	0.131	0.090	0.056
2	50.5	0.743	0.441	0.322	0.249	0.169	0.120	0.090
2	54.1	0.781	0.483	0.347	0.256	0.175	0.124	0.091
3	27.3	0.420	0.245	0.192	0.129	0.087	0.074	0.047
3	31.0	0.454	0.287	0.221	0.169	0.093	0.054	0.049
3	41.4	0.595	0.331	0.273	0.200	0.131	0.090	0.056
3	50.5	0.743	0.441	0.322	0.249	0.169	0.120	0.090
3	54.1	0.781	0.483	0.347	0.256	0.175	0.124	0.091
4	25.9	0.567	0.442	0.299	0.273	0.177	0.132	0.088
4	29.8	0.679	0.478	0.381	0.282	0.208	0.151	0.123
4	39.5	0.882	0.626	0.531	0.395	0.277	0.193	0.134
4	47.7	1.051	0.755	0.594	0.463	0.315	0.243	0.186
4	50.9	1.130	0.803	0.635	0.511	0.339	0.267	0.186
5	26.2	0.532	0.343	0.296	0.220	0.177	0.121	0.081
5	30.0	0.615	0.386	0.332	0.251	0.194	0.132	0.091
5	39.9	0.808	0.559	0.387	0.344	0.251	0.168	0.139
5	48.6	0.976	0.668	0.495	0.429	0.289	0.195	0.161
5	52.2	1.032	0.705	0.563	0.445	0.303	0.205	0.168
6	26.0	0.668	0.465	0.333	0.261	0.210	0.104	0.098
6	29.9	0.741	0.573	0.414	0.326	0.229	0.161	0.148
6	39.6	0.958	0.704	0.547	0.466	0.299	0.195	0.138
6	47.7	1.149	0.853	0.673	0.543	0.371	0.240	0.217
6	50.8	1.247	0.904	0.739	0.588	0.412	0.273	0.229
7	26.2	0.639	0.487	0.388	0.337	0.251	0.193	0.136
7	29.8	0.736	0.547	0.480	0.390	0.301	0.207	0.163
7	39.4	1.005	0.691	0.598	0.518	0.359	0.264	0.211
7	47.6	1.198	0.839	0.678	0.628	0.439	0.342	0.271
7	51.0	1.273	0.946	0.773	0.655	0.476	0.355	0.289
8	26.0	0.519	0.365	0.285	0.232	0.154	0.128	0.093
8	29.9	0.624	0.469	0.334	0.294	0.224	0.14	0.103
8	40.0	0.803	0.574	0.447	0.372	0.264	0.189	0.147
8	48.2	0.977	0.701	0.543	0.441	0.321	0.237	0.187
8	51.5	1.039	0.736	0.579	0.475	0.334	0.264	0.192
9	27.4	0.447	0.29	0.216	0.164	0.115	0.084	0.062
9	31.2	0.494	0.329	0.267	0.217	0.136	0.112	0.089
9	41.0	0.649	0.414	0.345	0.262	0.199	0.141	0.116
9	49.7	0.798	0.52	0.418	0.318	0.213	0.168	0.136
9	53.9	0.875	0.568	0.445	0.372	0.242	0.191	0.139

Table B 8 FWD Deflection Data - April 1997

Section	Load kN	Geophone Radial Offset (mm)						
		0.000	0.305	0.457	0.610	0.914	1.219	1.524
1	28.3	0.546	0.261	0.114	0.055	0.012	0.012	0.011
1	41.6	0.795	0.362	0.150	0.062	0.012	0.016	0.020
1	52.0	1.011	0.460	0.186	0.077	0.012	0.018	0.023
1	56.8	1.147	0.510	0.207	0.080	0.008	0.020	0.023
2	27.9	0.398	0.220	0.126	0.079	0.035	0.024	0.019
2	50.8	0.763	0.405	0.226	0.138	0.062	0.043	0.037
2	55.6	0.851	0.455	0.255	0.154	0.066	0.046	0.040
3	27.4	0.401	0.239	0.140	0.090	0.036	0.021	0.015
3	40.5	0.619	0.368	0.216	0.138	0.054	0.029	0.023
3	50.6	0.818	0.481	0.283	0.181	0.068	0.036	0.028
3	55.1	0.949	0.545	0.311	0.194	0.072	0.037	0.031
4	26.3	0.759	0.529	0.368	0.275	0.150	0.094	0.067
4	38.8	1.163	0.815	0.569	0.422	0.232	0.143	0.100
4	48.4	1.488	1.040	0.727	0.548	0.301	0.184	0.131
4	52.7	1.707	1.187	0.822	0.613	0.339	0.209	0.146
5	26.8	0.551	0.363	0.250	0.187	0.108	0.075	0.061
5	39.4	0.863	0.572	0.393	0.299	0.173	0.118	0.092
5	49.4	1.135	0.755	0.515	0.387	0.222	0.151	0.117
5	53.9	1.262	0.829	0.565	0.426	0.246	0.167	0.129
6	26.2	0.756	0.556	0.408	0.318	0.189	0.123	0.086
6	38.4	1.257	0.938	0.695	0.543	0.330	0.211	0.150
6	48.0	1.584	1.165	0.860	0.675	0.408	0.262	0.179
6	52.4	1.774	1.305	0.953	0.754	0.456	0.293	0.204
7	26.4	0.626	0.430	0.296	0.217	0.112	0.069	0.048
7	38.5	1.047	0.708	0.478	0.351	0.182	0.105	0.087
7	48.1	1.380	0.925	0.624	0.452	0.234	0.143	0.106
7	52.6	1.538	1.039	0.701	0.514	0.263	0.160	0.115
8	26.5	0.699	0.428	0.261	0.177	0.087	0.061	0.049
8	39.2	1.101	0.670	0.409	0.280	0.136	0.095	0.077
8	48.8	1.437	0.858	0.524	0.348	0.168	0.116	0.093
8	53.7	1.511	0.913	0.551	0.369	0.184	0.128	0.105
9	27.4	0.434	0.255	0.150	0.099	0.050	0.038	0.031
9	40.1	0.624	0.367	0.218	0.147	0.078	0.059	0.051
9	50.3	0.818	0.472	0.278	0.185	0.095	0.073	0.063
9	54.9	0.874	0.503	0.300	0.204	0.111	0.084	0.071

Table B 9 FWD Deflection Data - June 1997

	Load	Geophone Radial Offset (mm)						
Section	kN	0	305	457	610	914	1219	1524
1	31.9	1.190	0.474	0.167	0.058	0.018	0.024	0.021
1	39.4	1.394	0.585	0.209	0.079	0.022	0.030	0.027
1	48.5	1.661	0.711	0.262	0.093	0.019	0.033	0.031
1	55.8	1.795	0.758	0.267	0.089	0.016	0.037	0.034
2	31.7	0.896	0.428	0.210	0.125	0.060	0.047	0.042
2	39.0	1.021	0.489	0.250	0.155	0.074	0.058	0.052
2	47.8	1.235	0.631	0.320	0.197	0.089	0.068	0.061
2	54.7	1.354	0.693	0.367	0.225	0.102	0.075	0.067
3	30.9	0.899	0.464	0.241	0.144	0.057	0.035	0.028
3	38.0	1.117	0.586	0.314	0.186	0.069	0.044	0.035
3	47.0	1.345	0.710	0.383	0.234	0.087	0.052	0.040
3	53.9	1.516	0.835	0.468	0.285	0.104	0.059	0.045
4	30.4	1.468	0.940	0.607	0.448	0.241	0.158	0.116
4	37.3	1.800	1.171	0.774	0.578	0.313	0.201	0.145
4	45.3	2.182	1.429	0.960	0.719	0.394	0.251	0.181
4	51.6	2.493	1.698	1.147	0.868	0.477	0.301	0.213
5	30.5	1.180	0.695	0.436	0.320	0.181	0.131	0.106
5	37.6	1.450	0.867	0.559	0.410	0.232	0.164	0.133
5	46.1	1.713	1.060	0.692	0.508	0.291	0.205	0.165
5	52.6	1.893	1.187	0.791	0.584	0.340	0.239	0.190
6	30.5	1.468	0.996	0.688	0.536	0.320	0.213	0.151
6	37.2	1.804	1.254	0.888	0.698	0.417	0.280	0.203
6	44.8	2.361	1.636	1.154	0.895	0.535	0.349	0.245
6	50.9	2.451	1.766	1.284	1.015	0.619	0.406	0.286
7	30.3	1.365	0.841	0.522	0.367	0.185	0.122	0.092
7	37.3	1.657	1.052	0.668	0.476	0.240	0.152	0.116
7	44.9	2.083	1.337	0.862	0.626	0.320	0.201	0.150
7	51.2	2.251	1.449	0.955	0.692	0.356	0.231	0.165
8	30.7	1.343	0.729	0.403	0.270	0.137	0.101	0.078
8	37.3	1.720	0.944	0.543	0.368	0.180	0.128	0.105
8	45.5	1.946	1.115	0.658	0.439	0.224	0.156	0.123
8	51.8	2.209	1.280	0.762	0.518	0.258	0.179	0.143
9	31.4	0.761	0.397	0.213	0.142	0.082	0.067	0.056
9	38.1	0.916	0.488	0.272	0.183	0.105	0.085	0.073
9	46.7	1.071	0.590	0.338	0.231	0.131	0.103	0.088
9	53.2	1.193	0.667	0.392	0.267	0.150	0.116	0.097

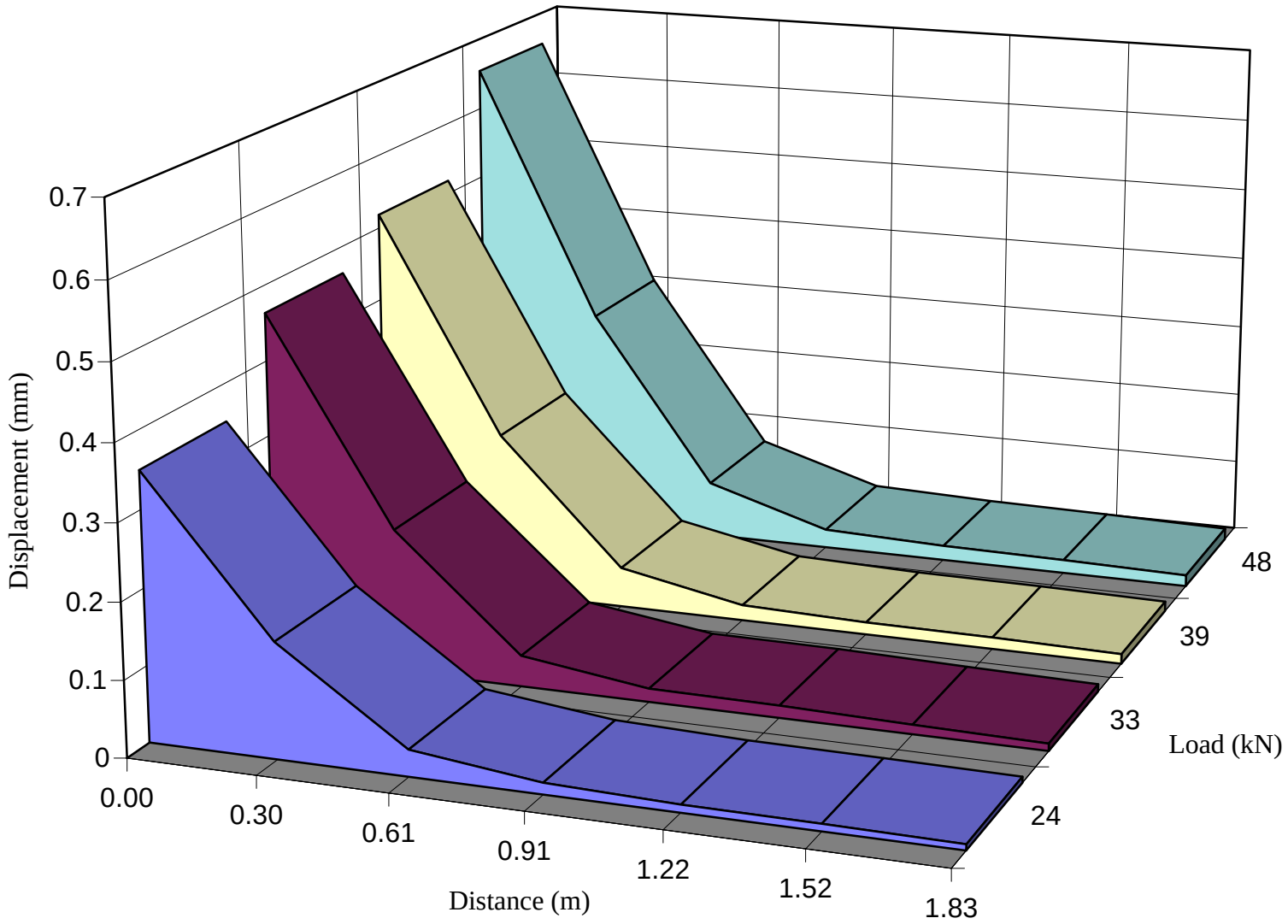

Figure B1 Displacement as a function of distance for different FWD load levels (October 1994, section 1).

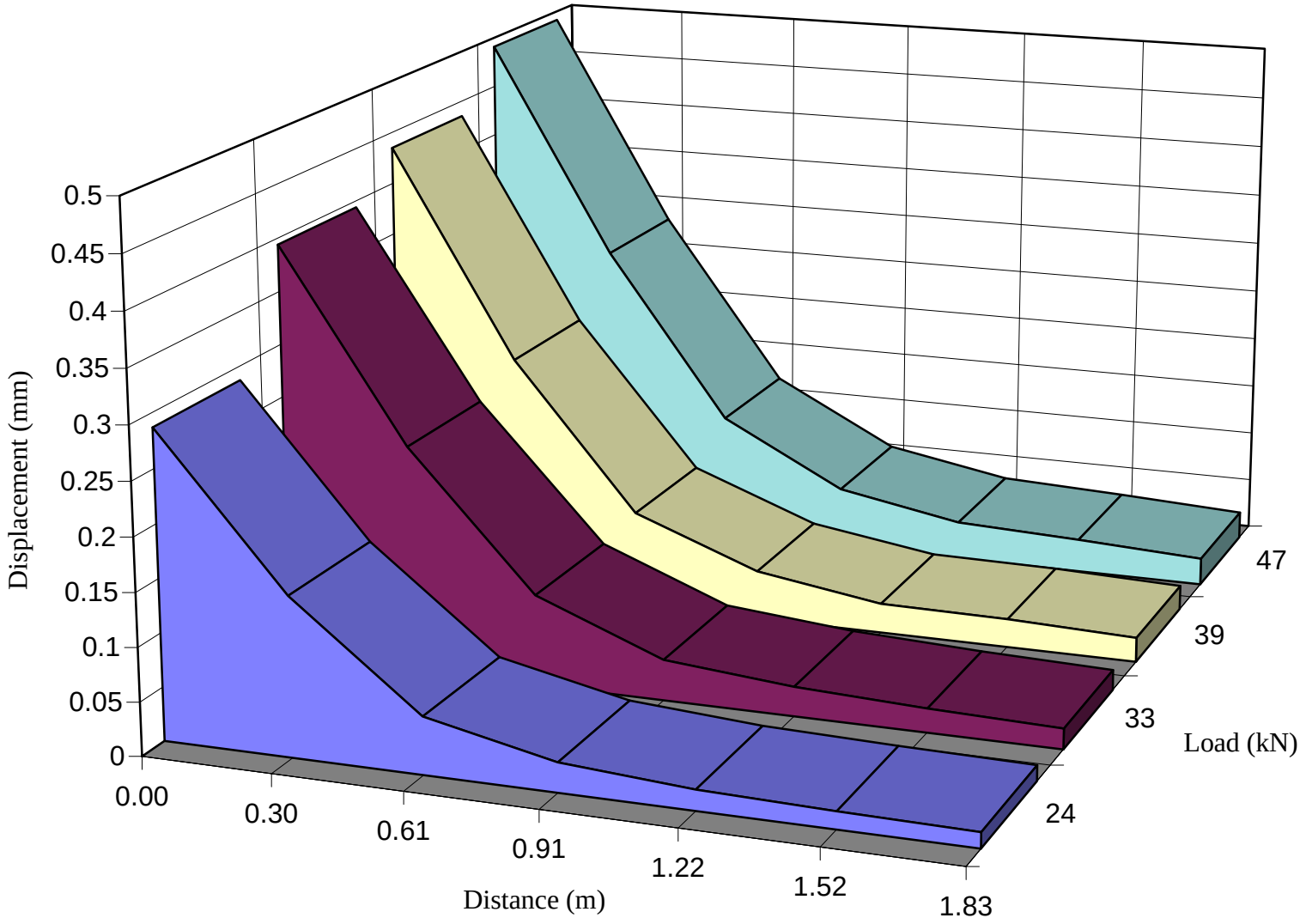

Figure B 2 Displacement as a function of distance for different FWD load levels (October 1994, section 2).

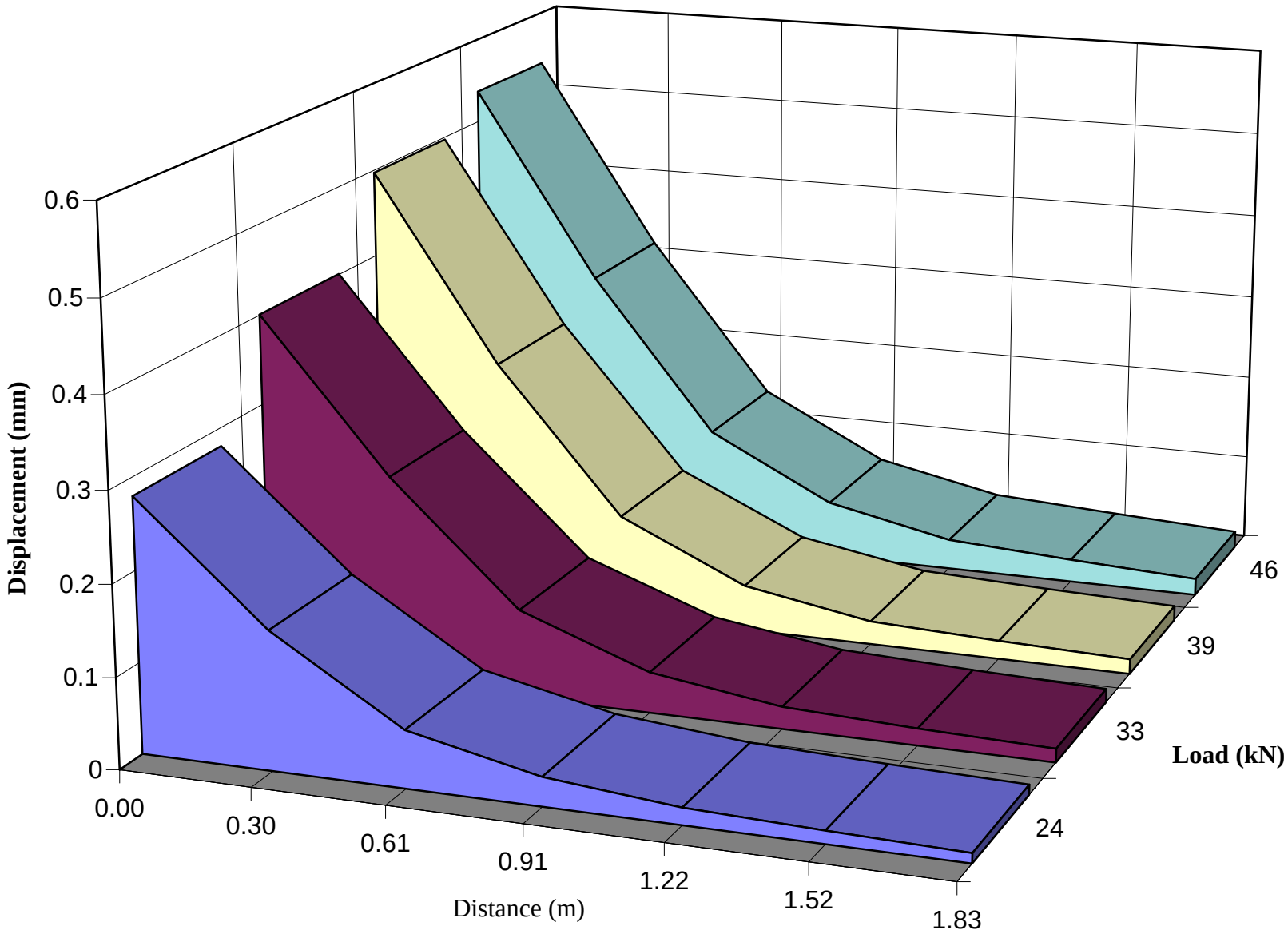

Figure B 3 Displacement as a function of distance for different FWD load levels (October 1994, section 3).

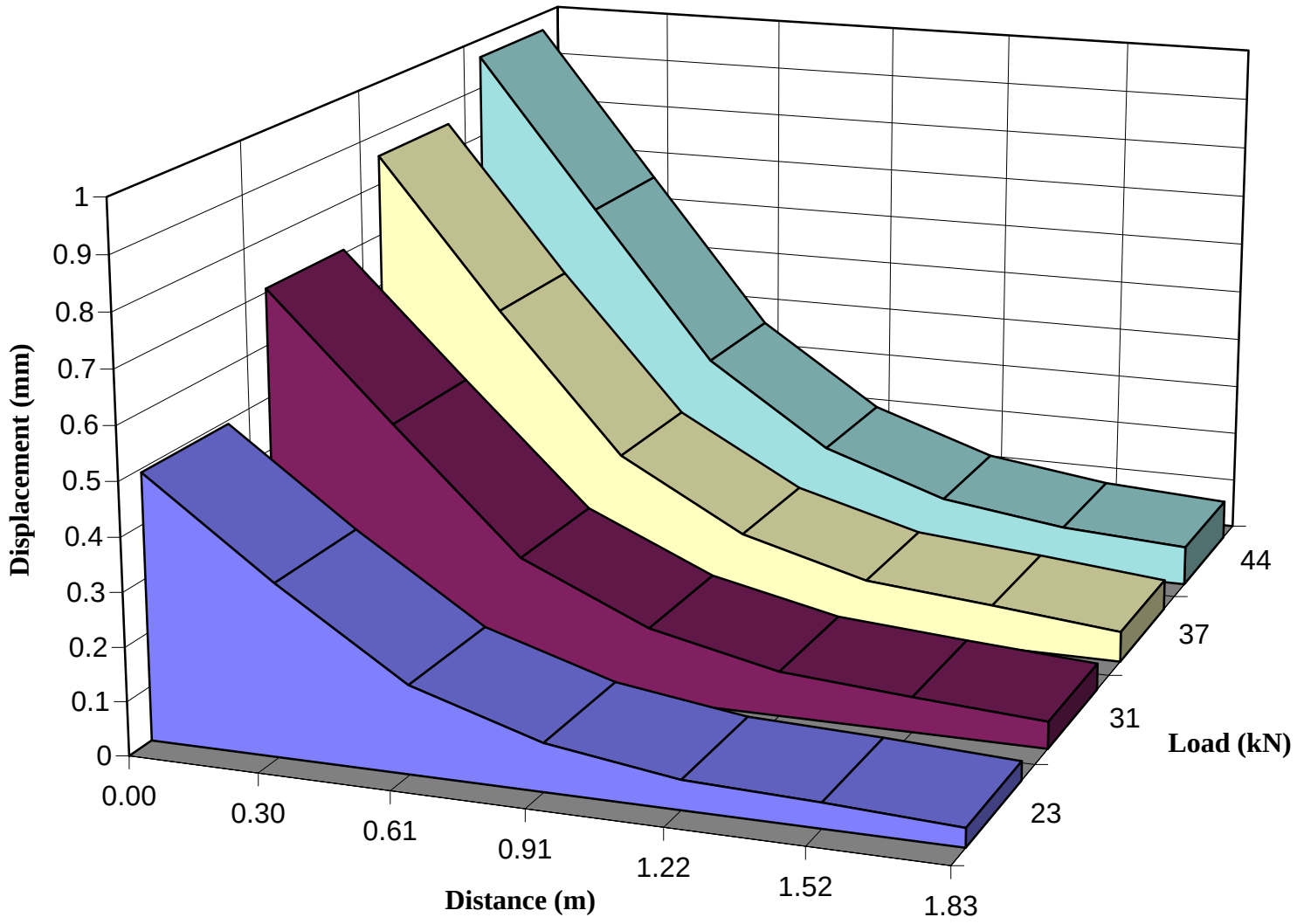

Figure B 4 Displacement as a function of distance for different FWD load levels (October 1994, section 4).

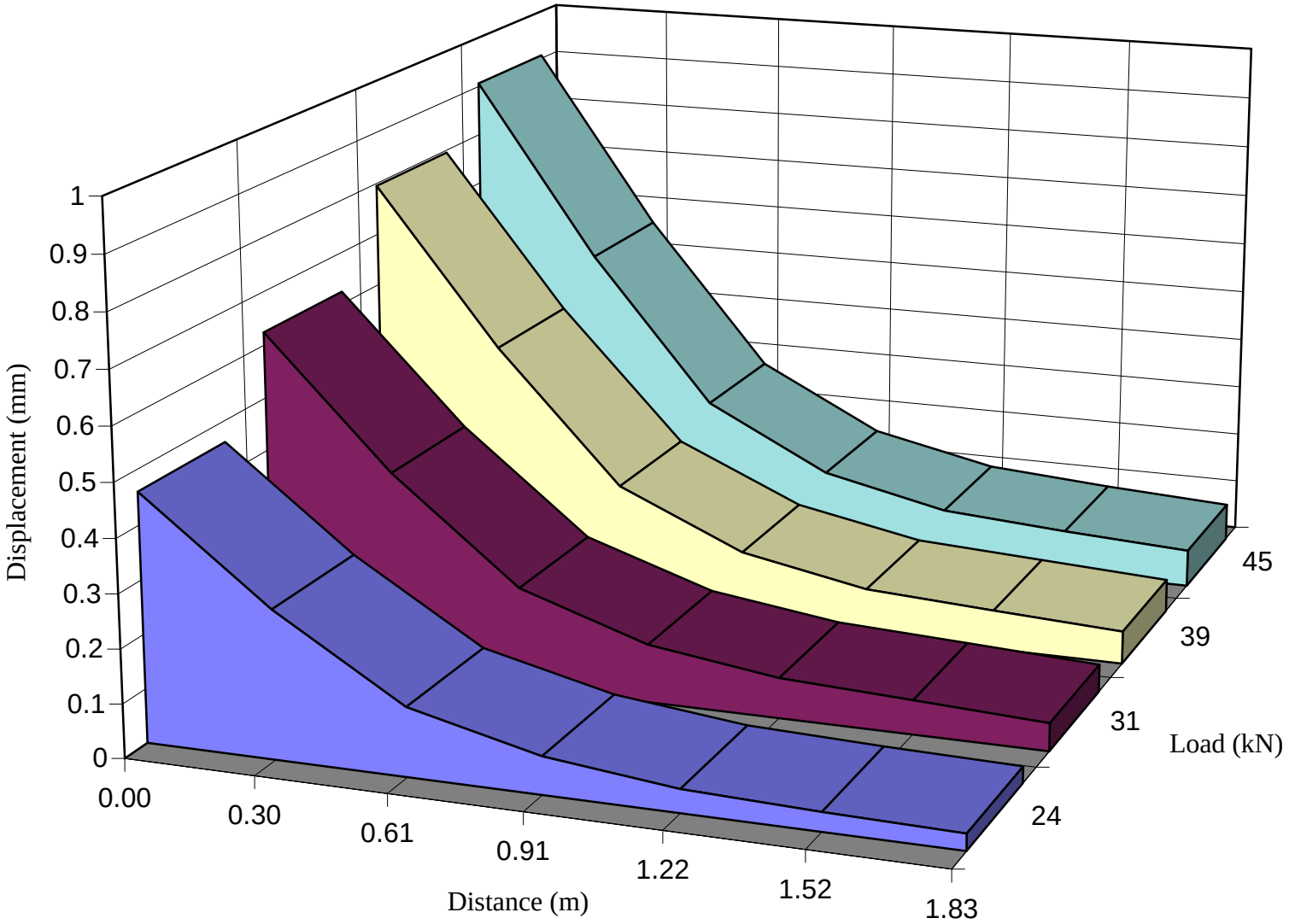

Figure B 5 Displacement as a function of distance for different FWD load levels (October 1994, section 5).

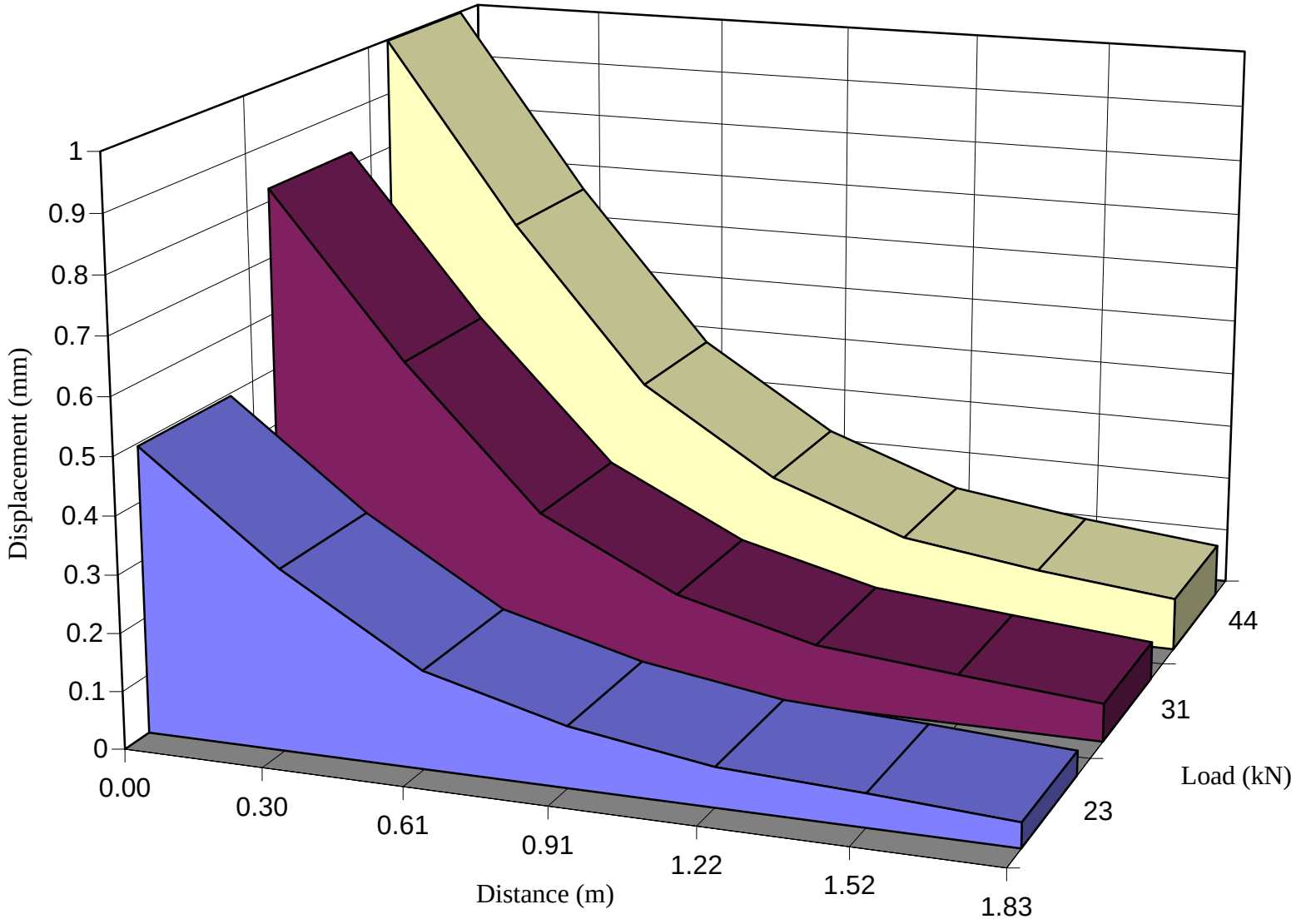

Figure B 6 Displacement as a function of distance for different FWD load levels (October 1994, section 6).

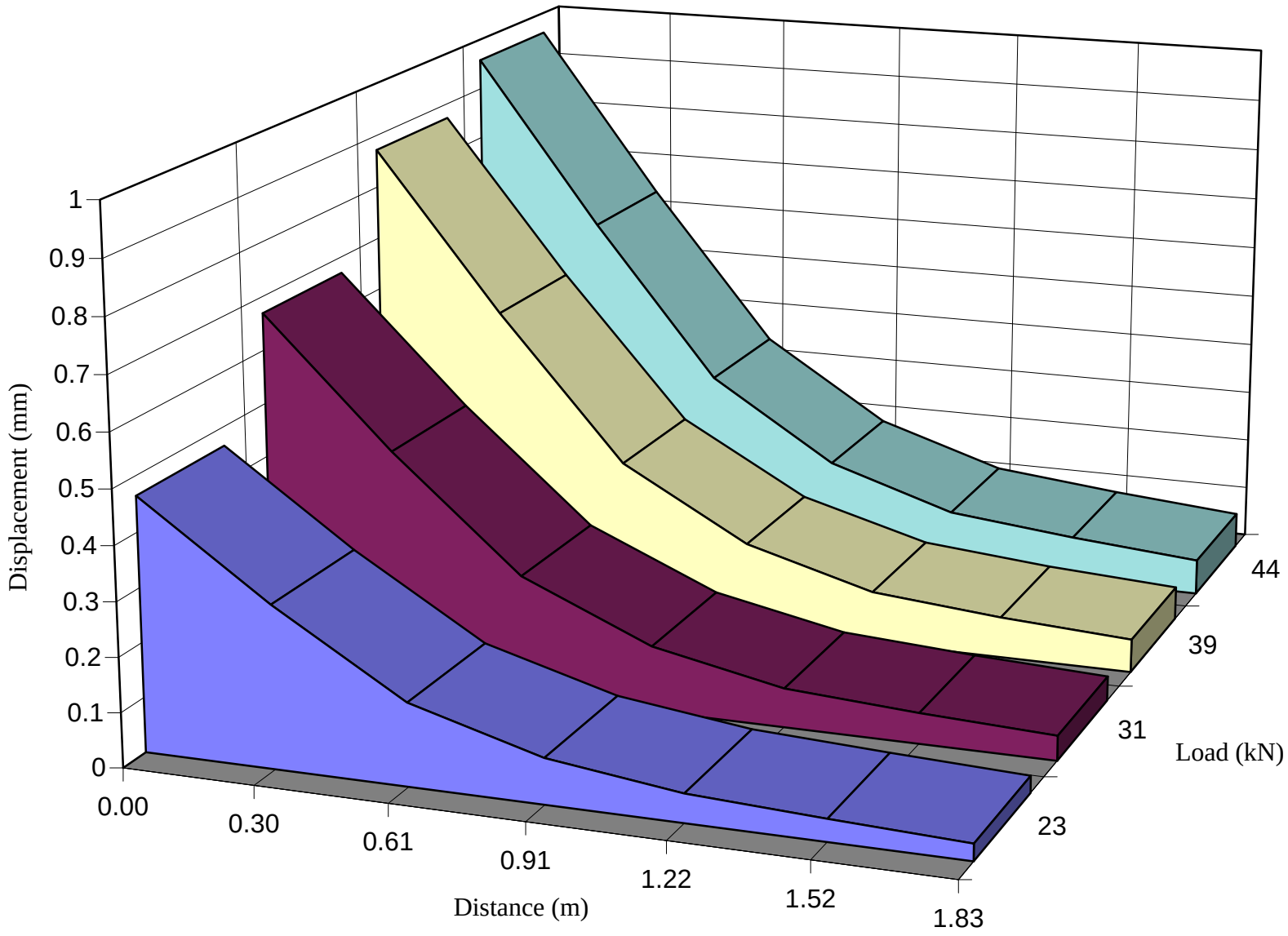

Figure B 7 Displacement as a function of distance for different FWD load levels (October 1994, section 7).

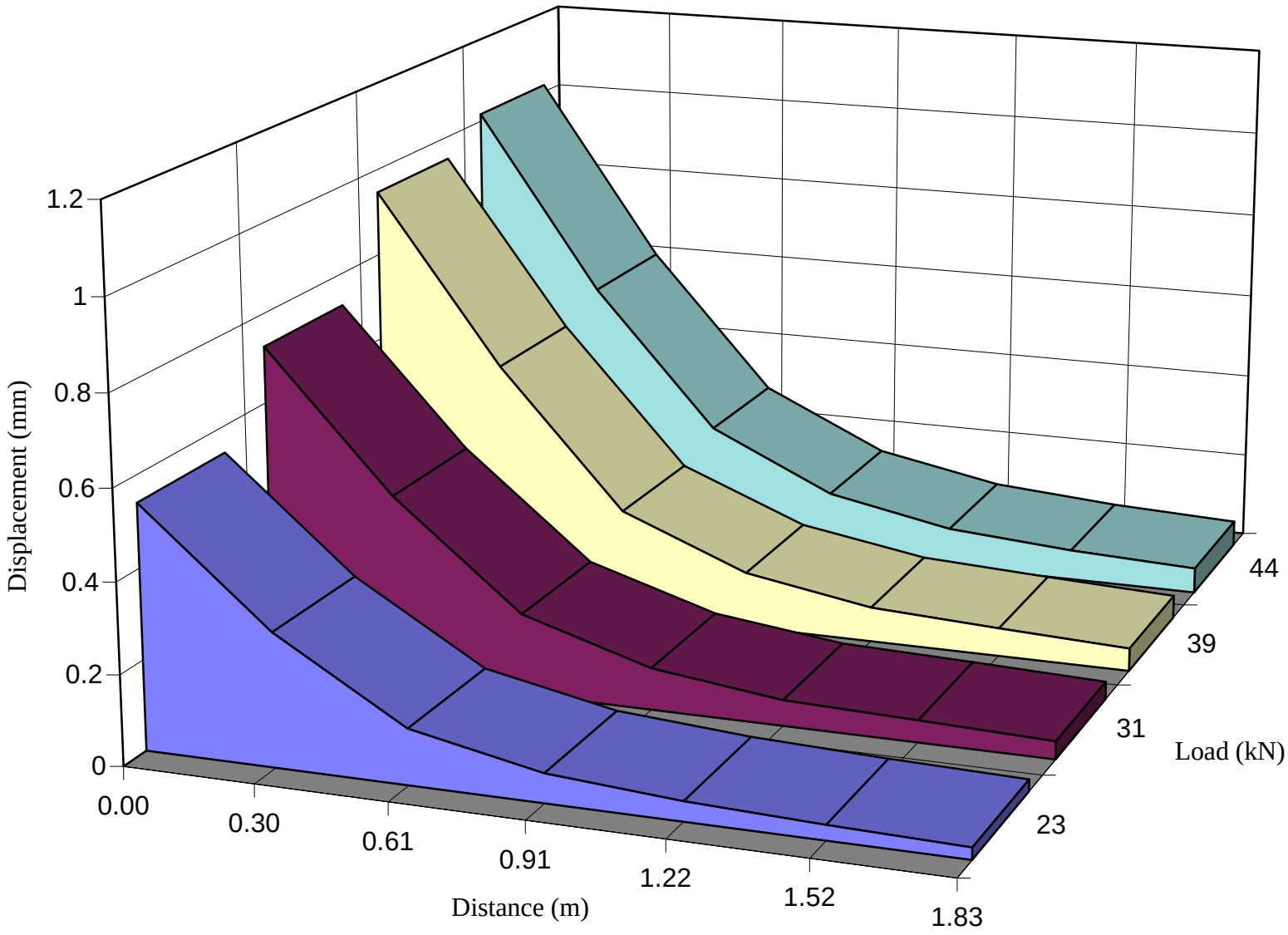

Figure B 8 Displacement as a function of distance for different FWD load levels (October 1994, section 8).

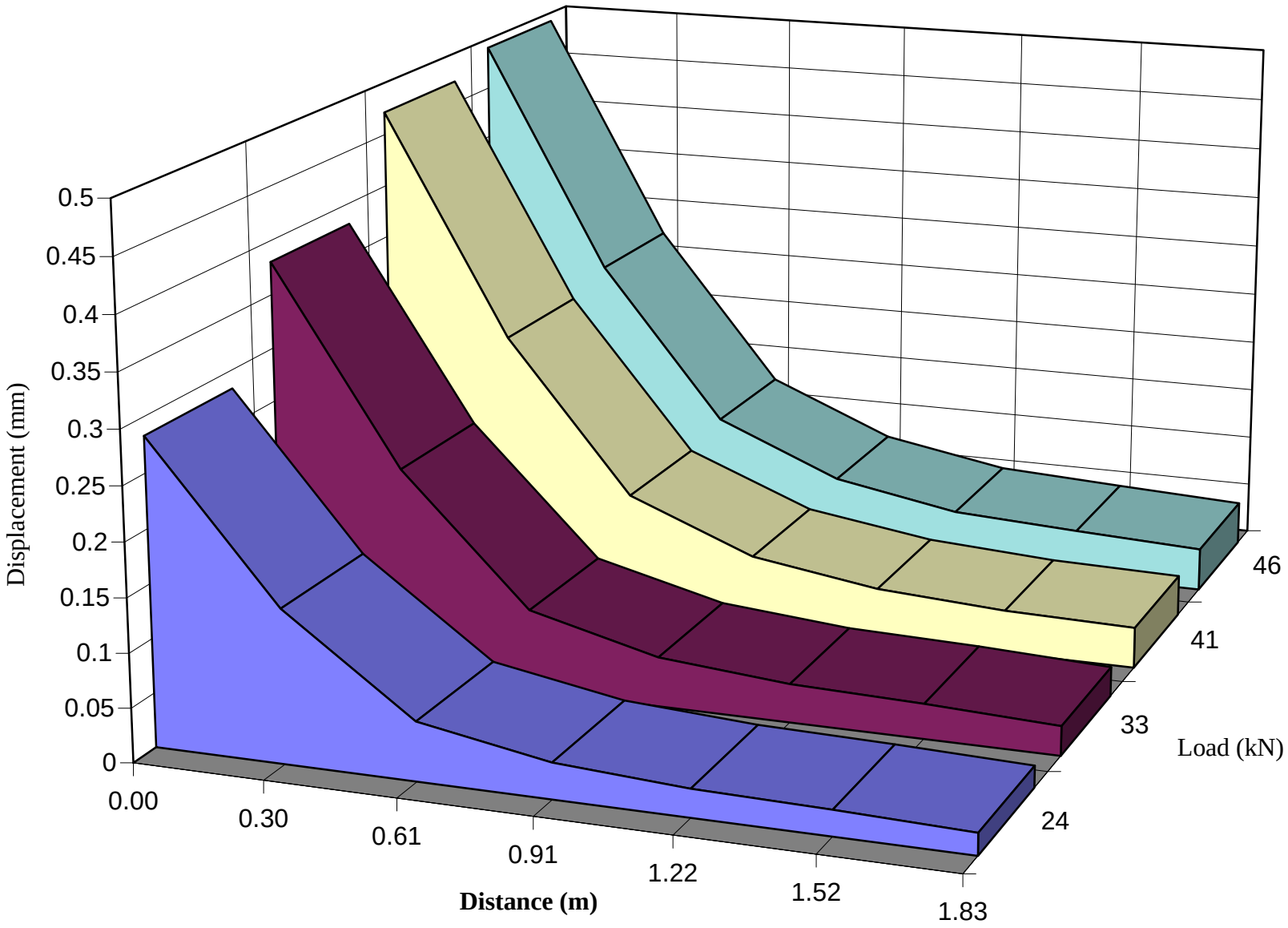

Figure B 9 Displacement as a function of distance for different FWD load levels (October 1994, section 9).

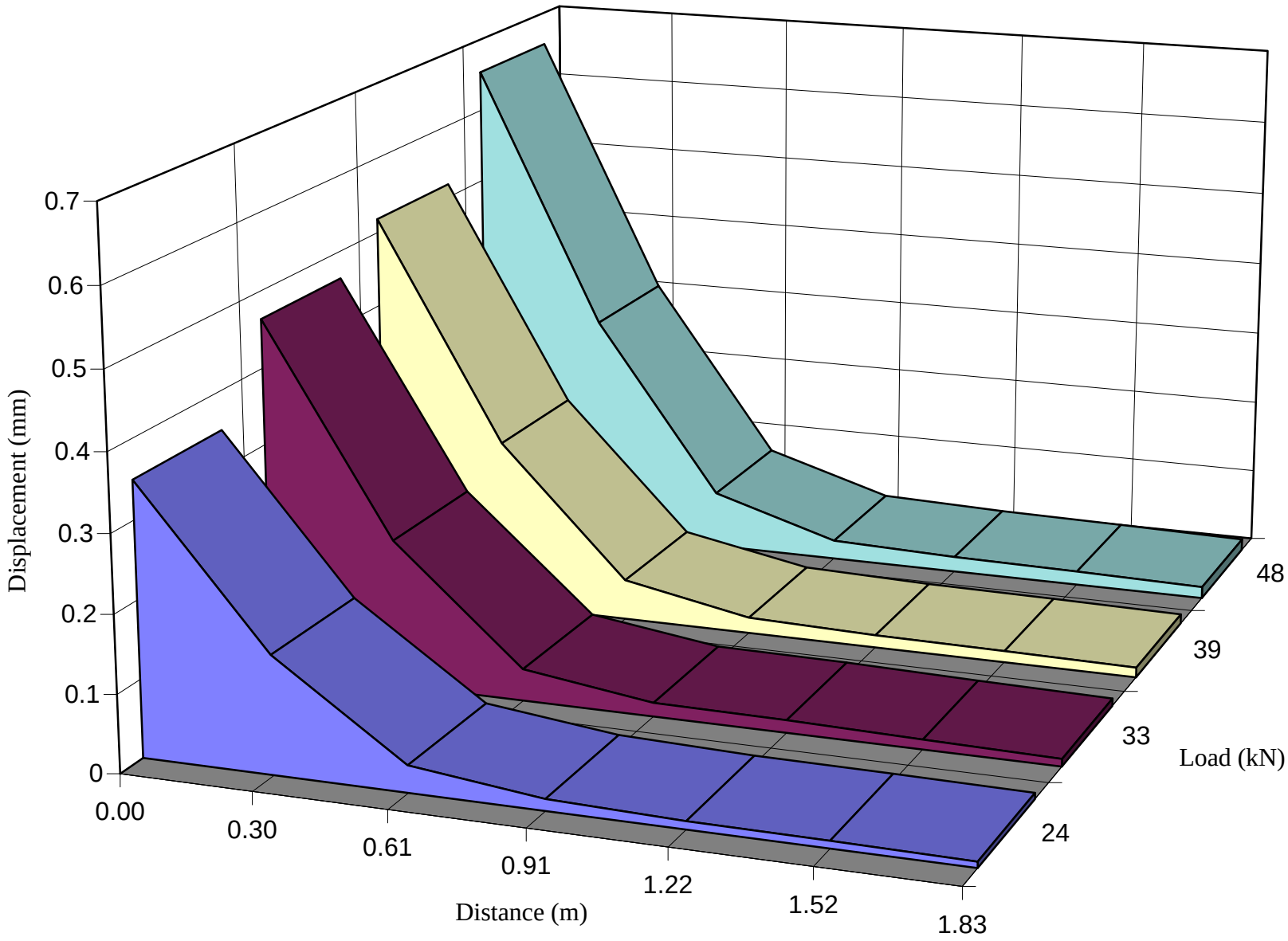

Figure B 10 Displacement as a function of distance for different FWD load levels (March 1995, section 1).

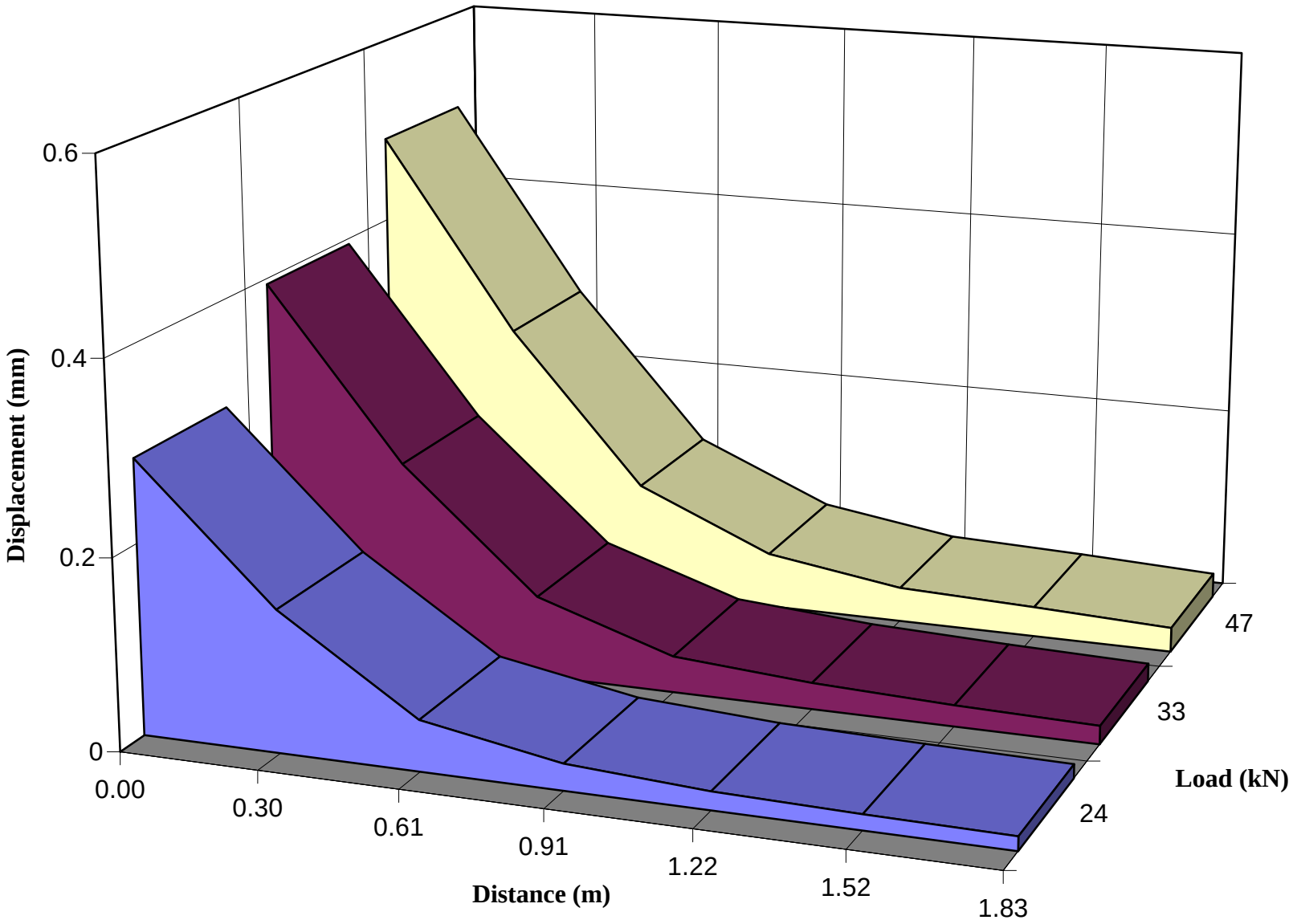

Figure B 11 Displacement as a function of distance for different FWD load levels (March 1995, section 2).

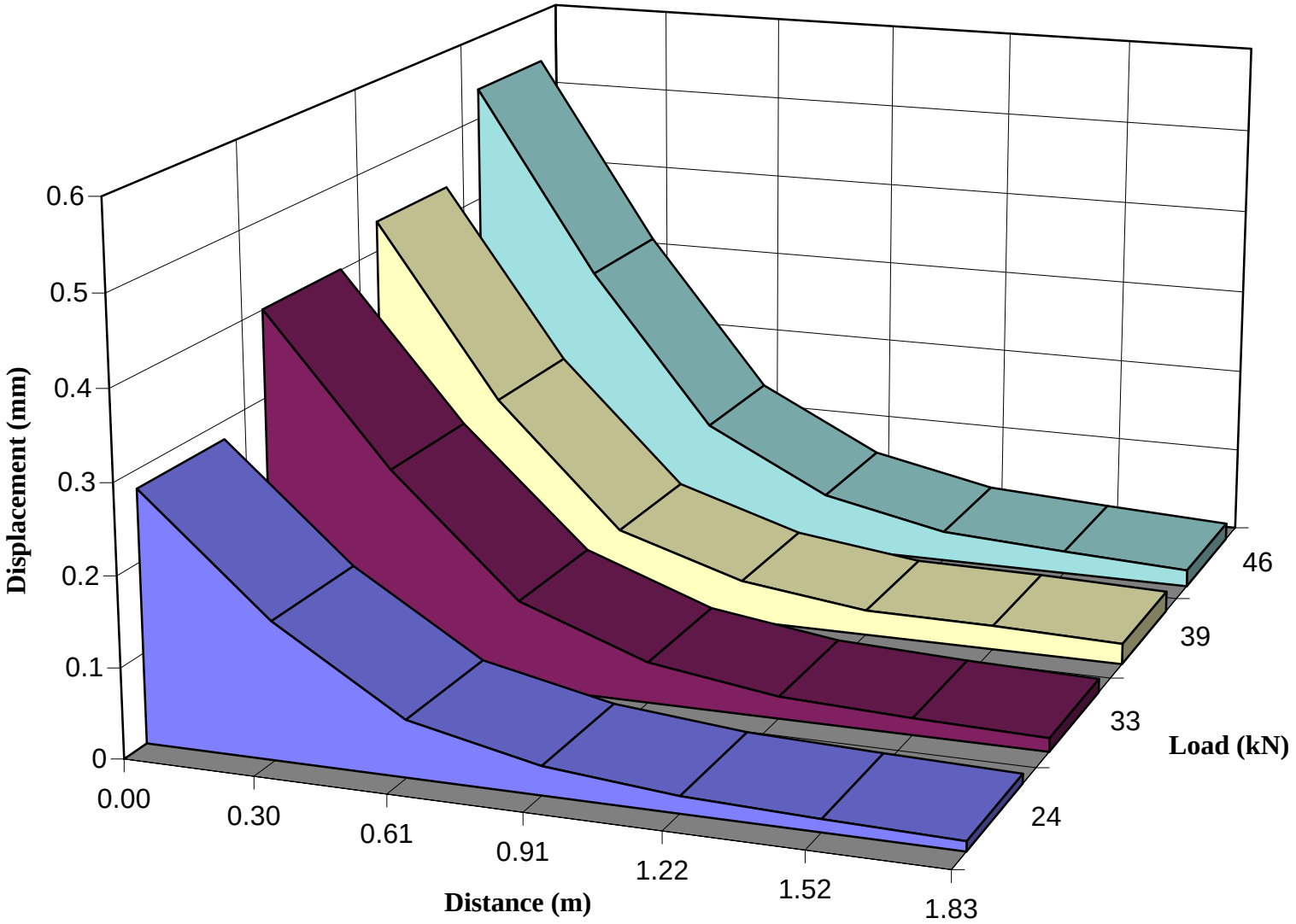

Figure B 12 Displacement as a function of distance for different FWD load levels (March 1995, section 3).

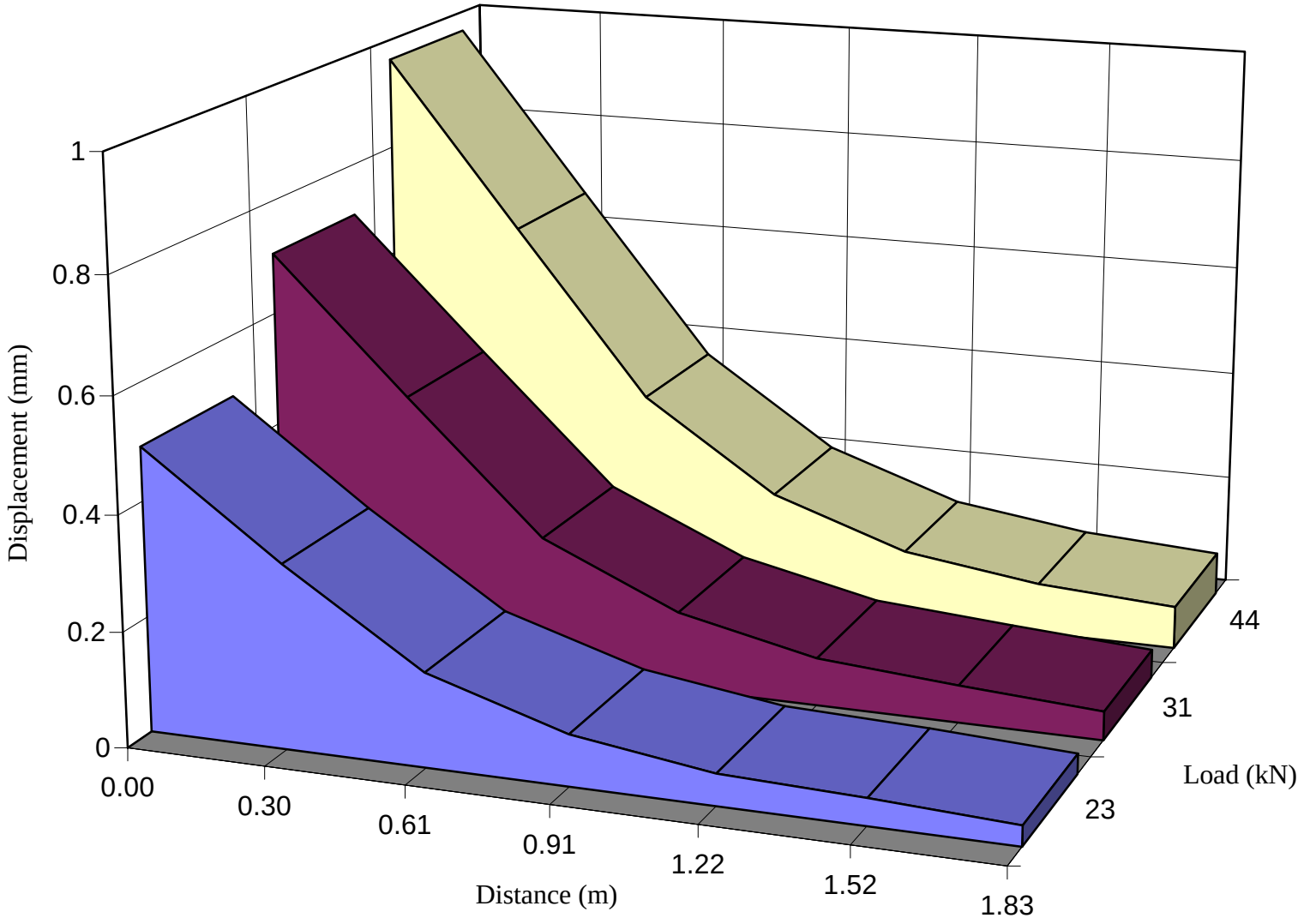

Figure B 13 Displacement as a function of distance for different FWD load levels (March 1995, section 4).

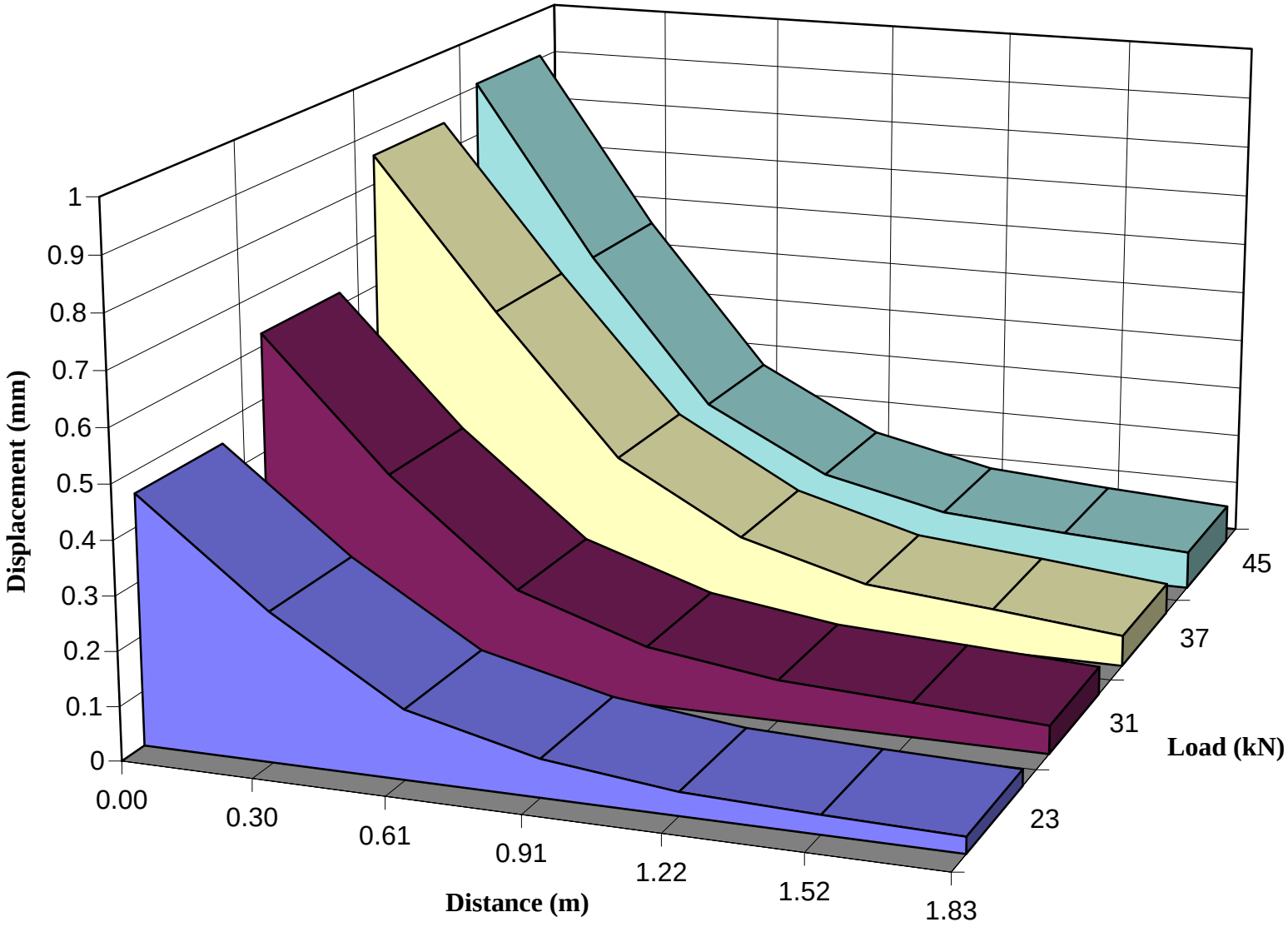

Figure B 14 Displacement as a function of distance for different FWD load levels (March 1995, section 5).

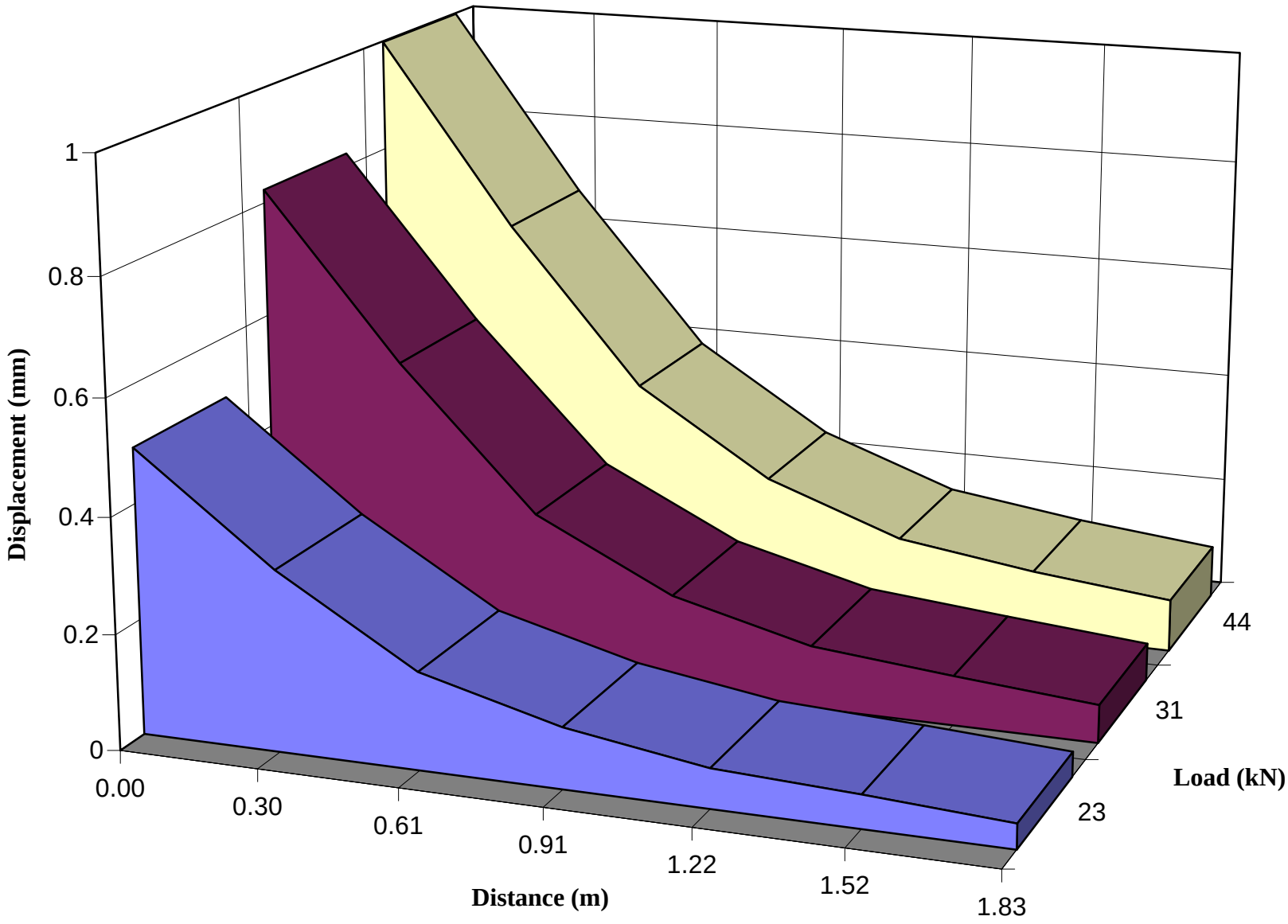

Figure B 15 Displacement as a function of distance for different FWD load levels (March 1995, section 6).

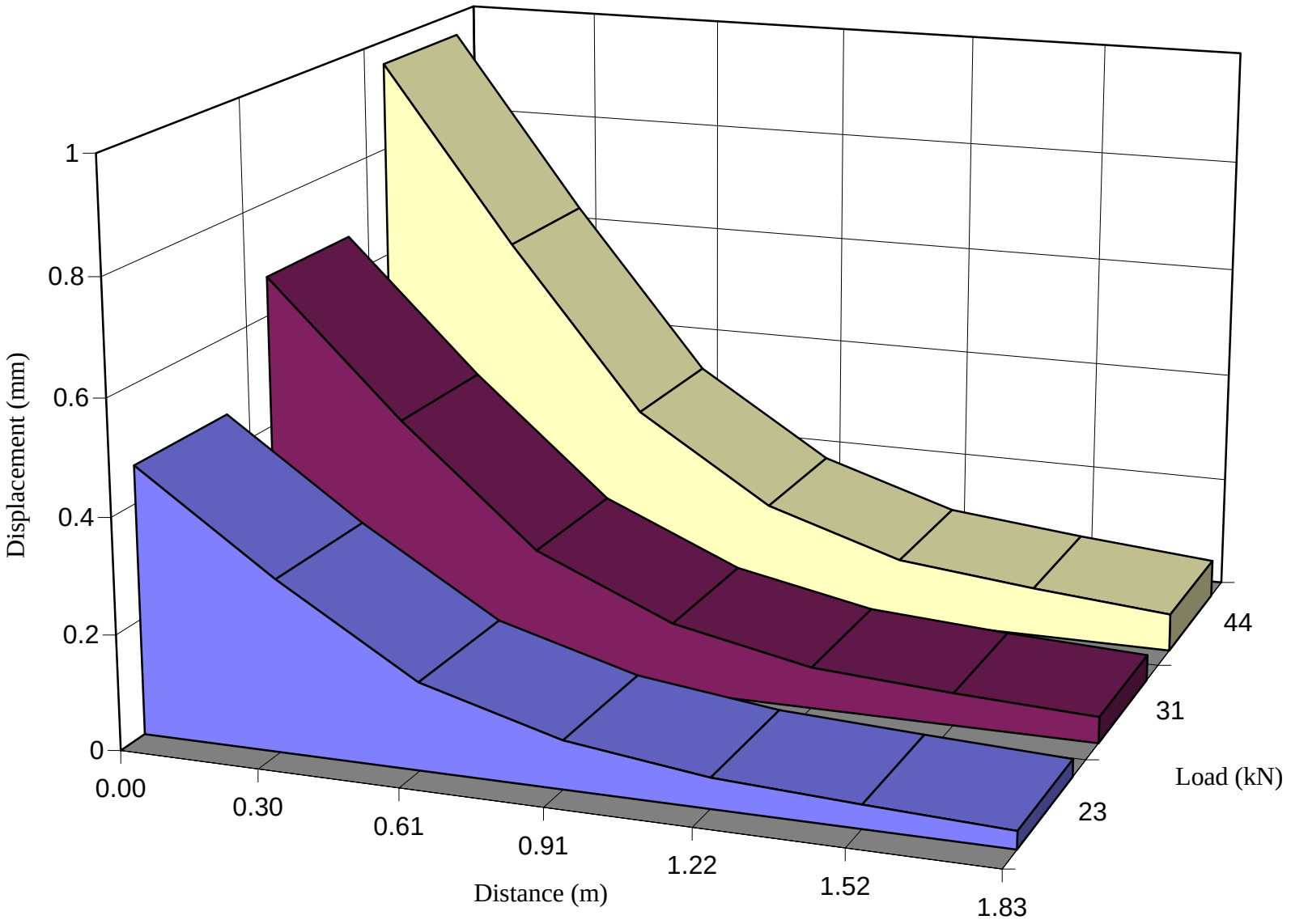

Figure B 16 Displacement as a function of distance for different FWD load levels (March 1995, section 7).

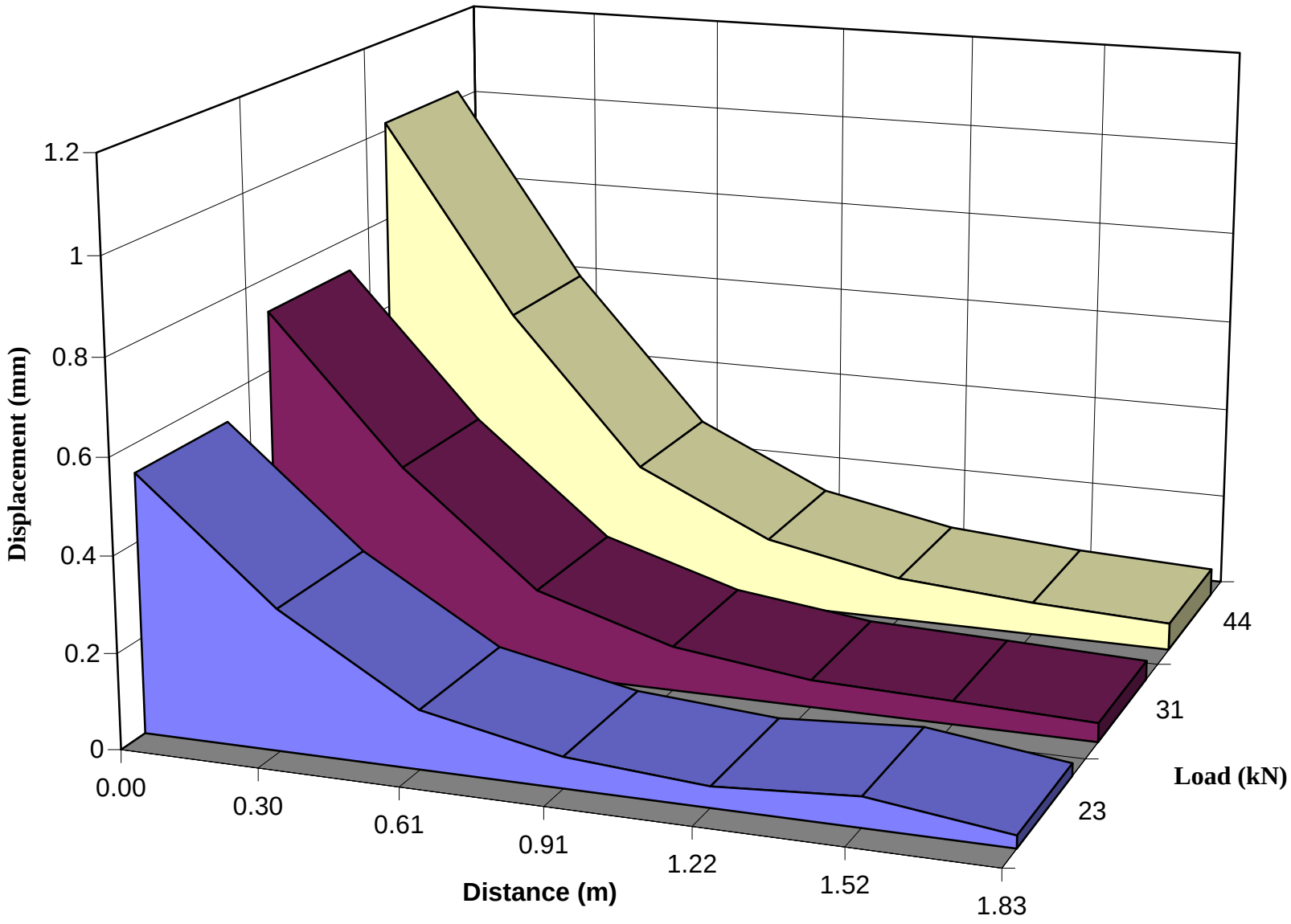

Figure B 17 Displacement as a function of distance for different FWD load levels (March 1995, section 8).

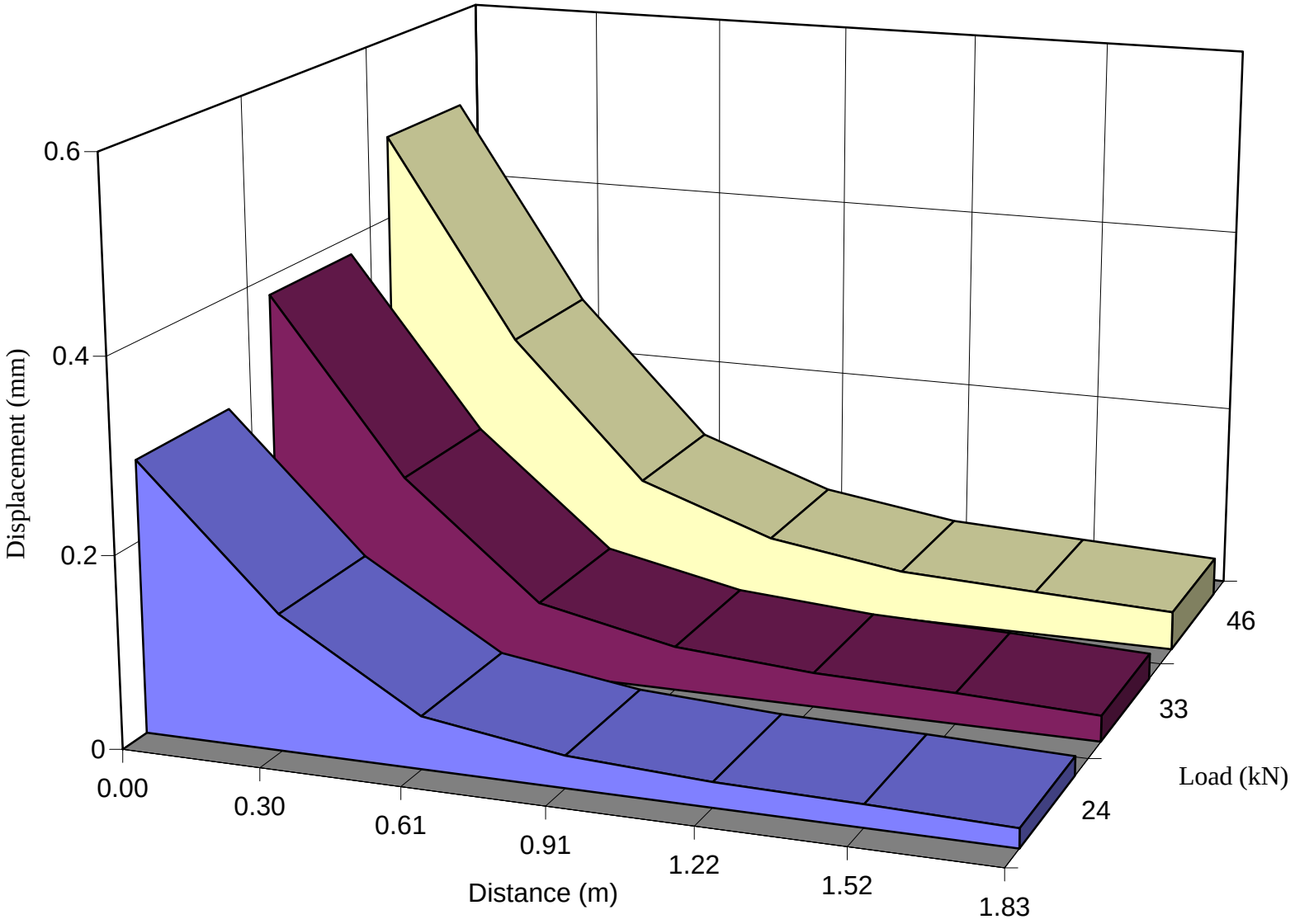

Figure B 18 Displacement as a function of distance for different FWD load levels (March 1995, section 9).

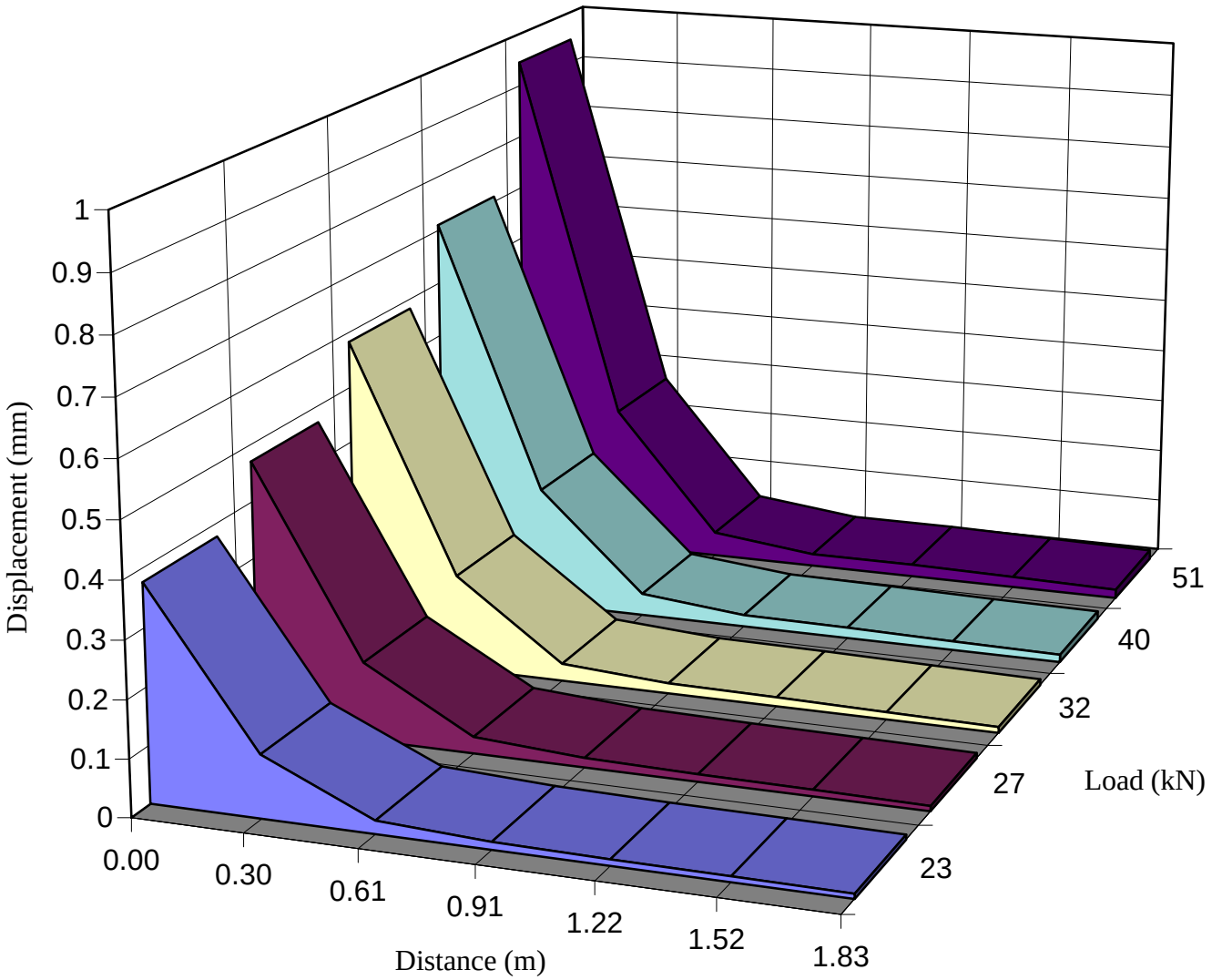

Figure B 19 Displacement as a function of distance for different FWD load levels (August 1995, section 1).

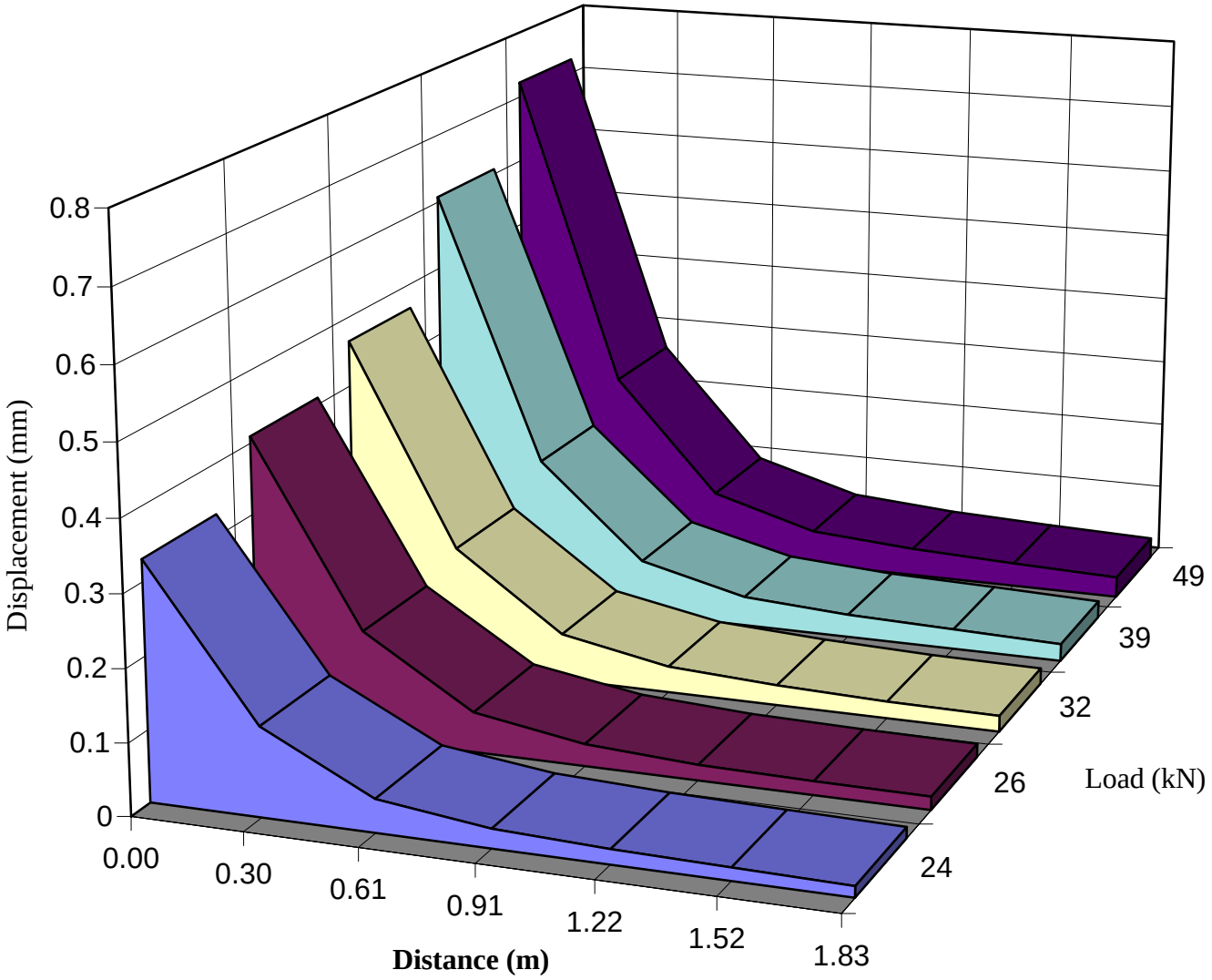

Figure B 20 Displacement as a function of distance for different FWD load levels (August 1995, section 2).

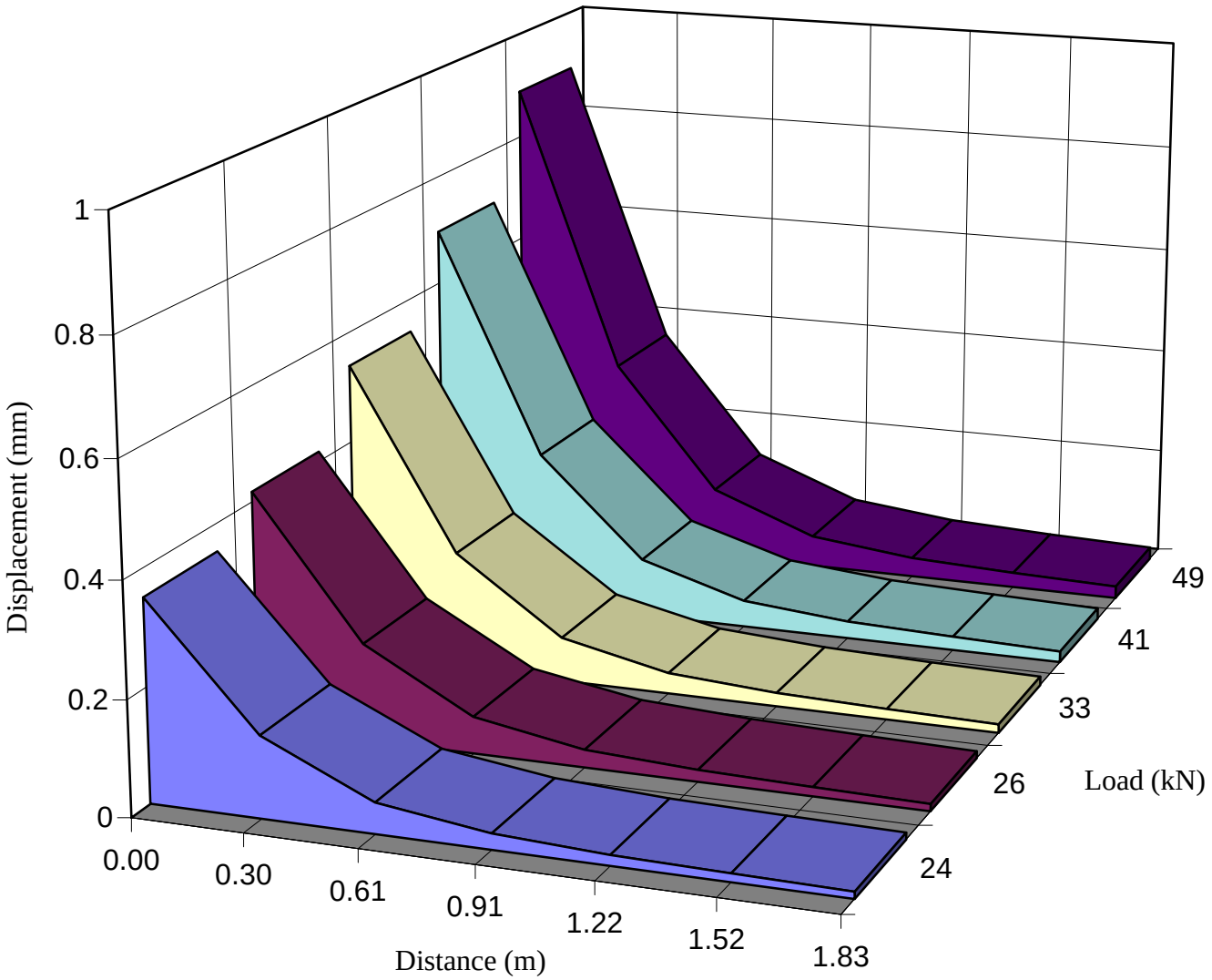

Figure B 21 Displacement as a function of distance for different FWD load levels (August 1995, section 3).

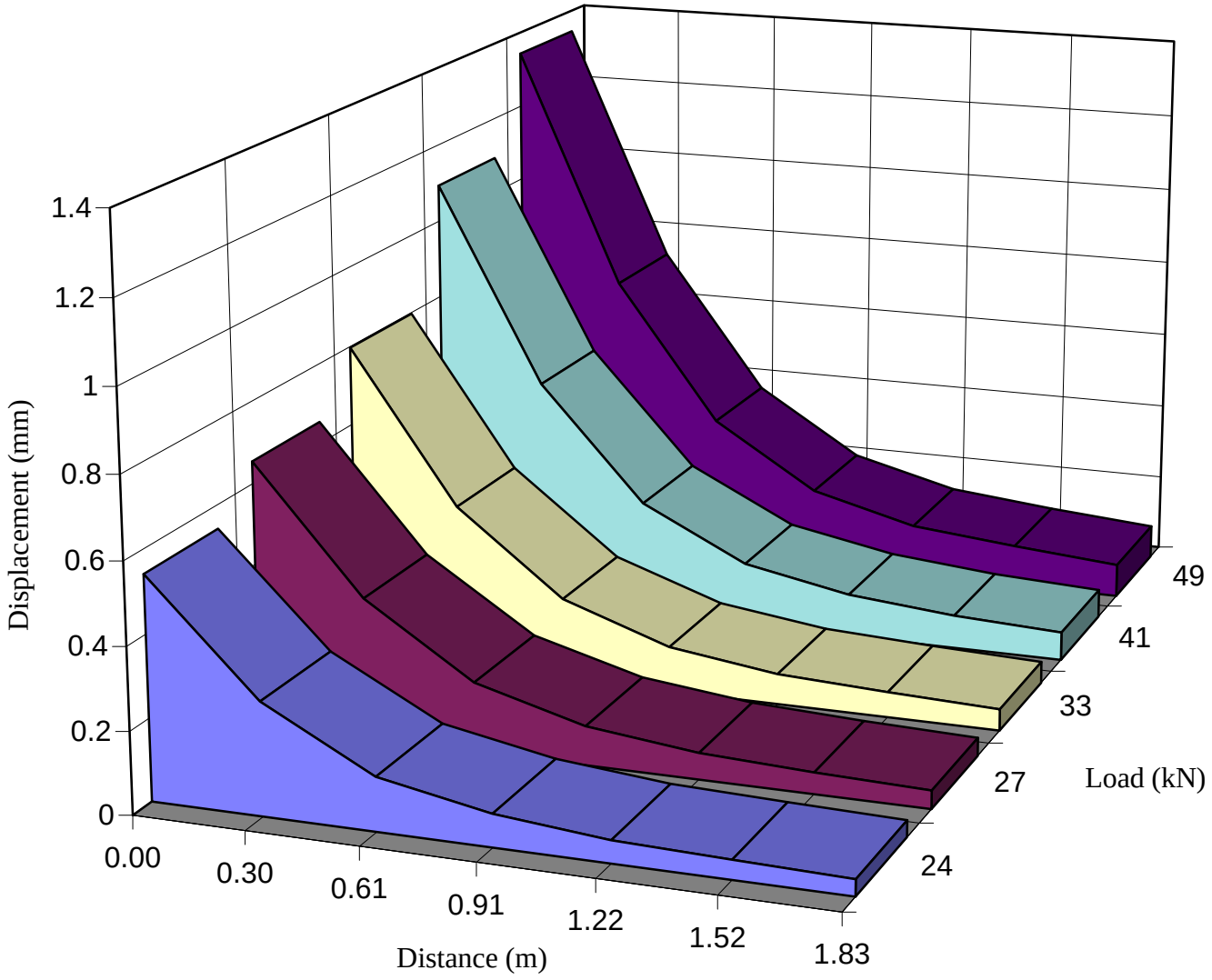

Figure B 22 Displacement as a function of distance for different FWD load levels (August 1995, section 4).

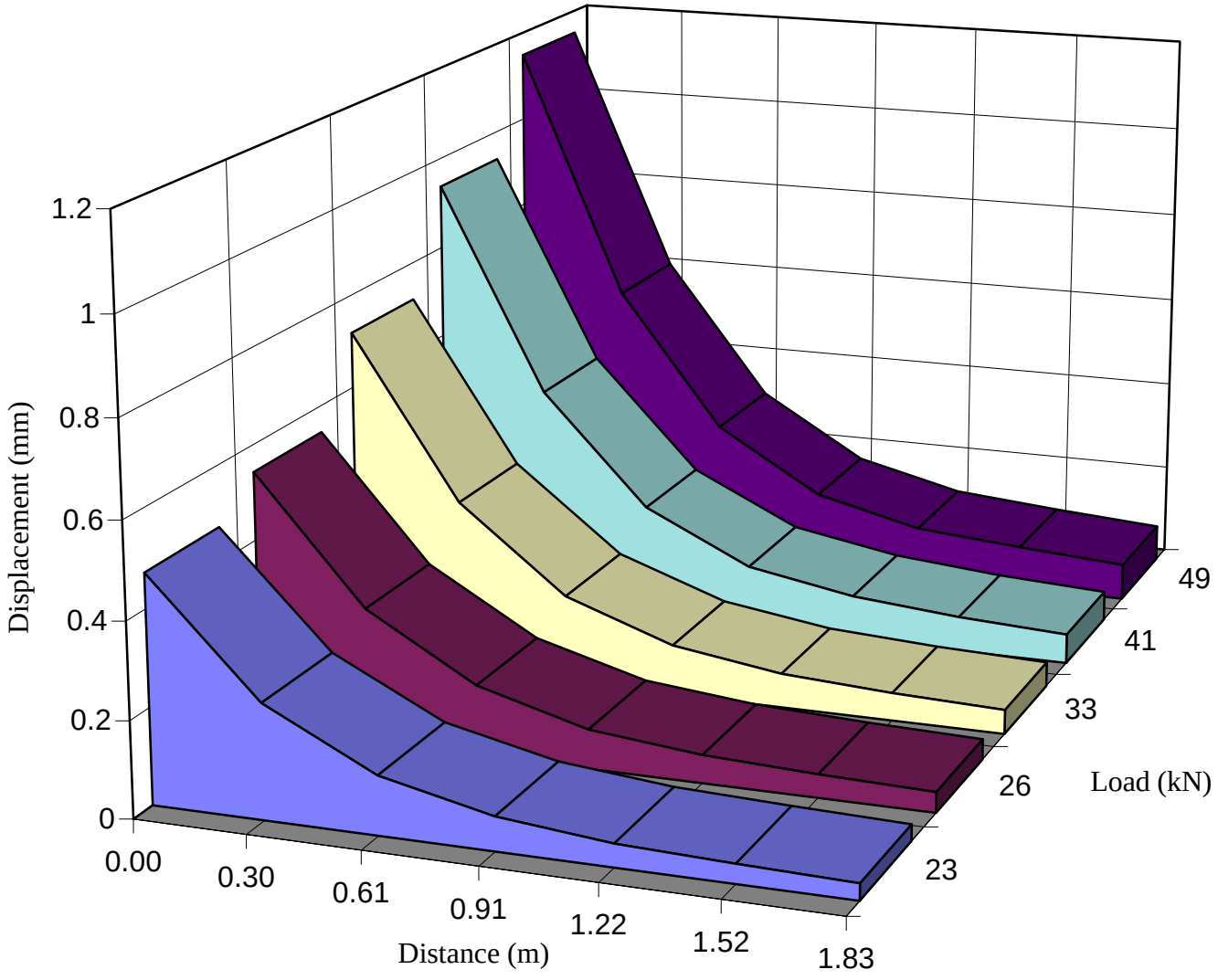

Figure B 23 Displacement as a function of distance for different FWD load levels (August 1995, section 5).

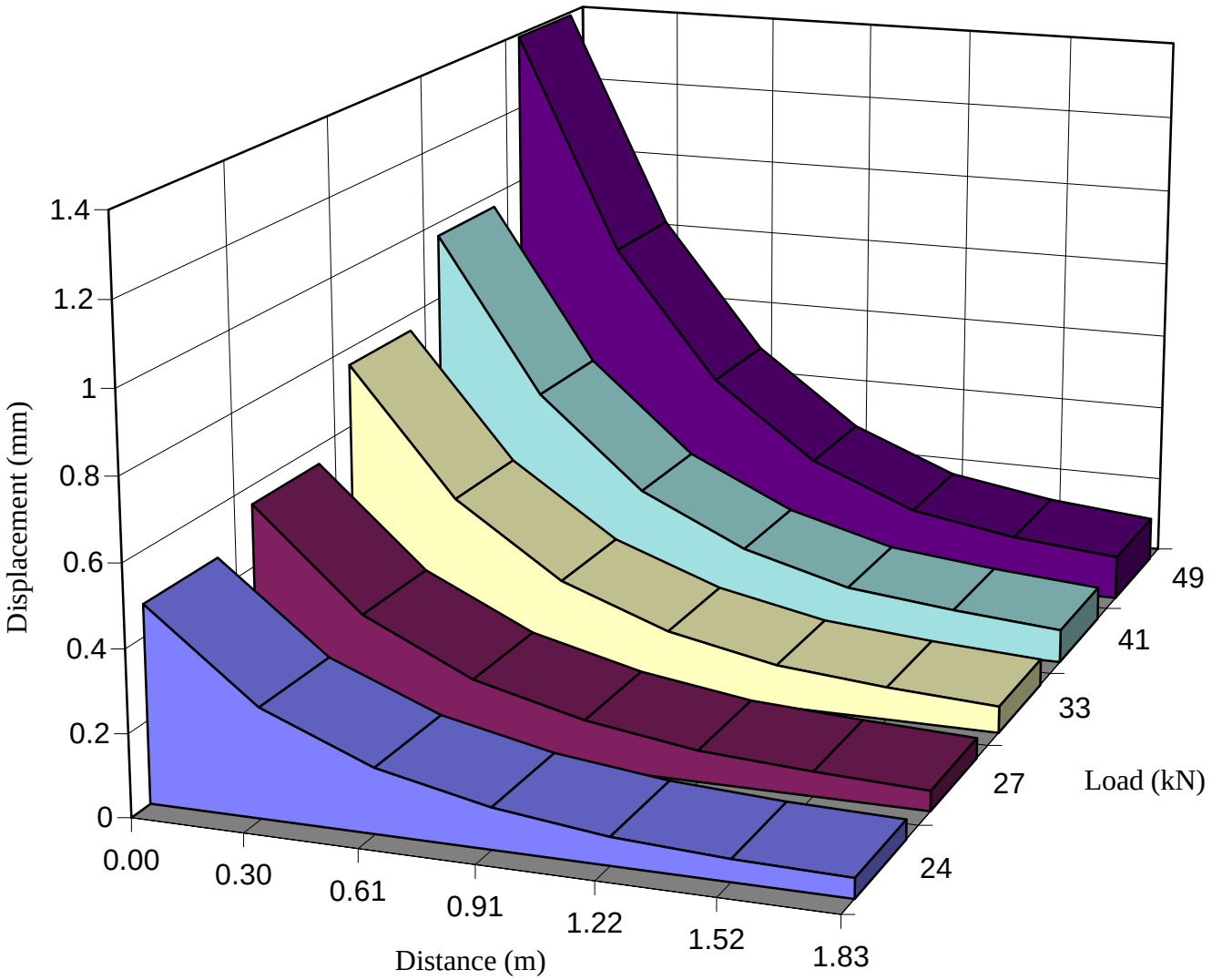

Figure B 24 Displacement as a function of distance for different FWD load levels (August 1995, section 6).

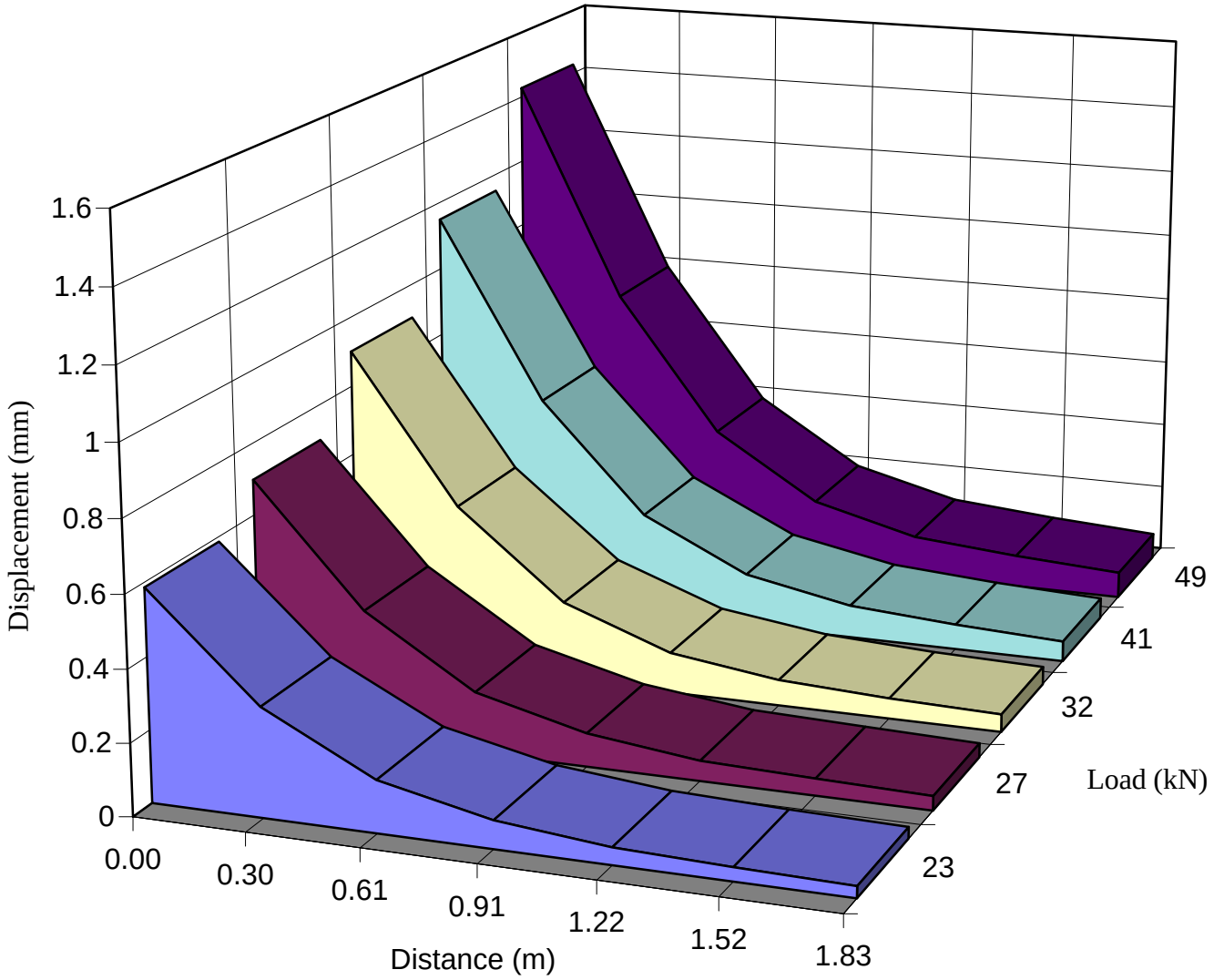

Figure B 25 Displacement as a function of distance for different FWD load levels (August 1995, section 7).

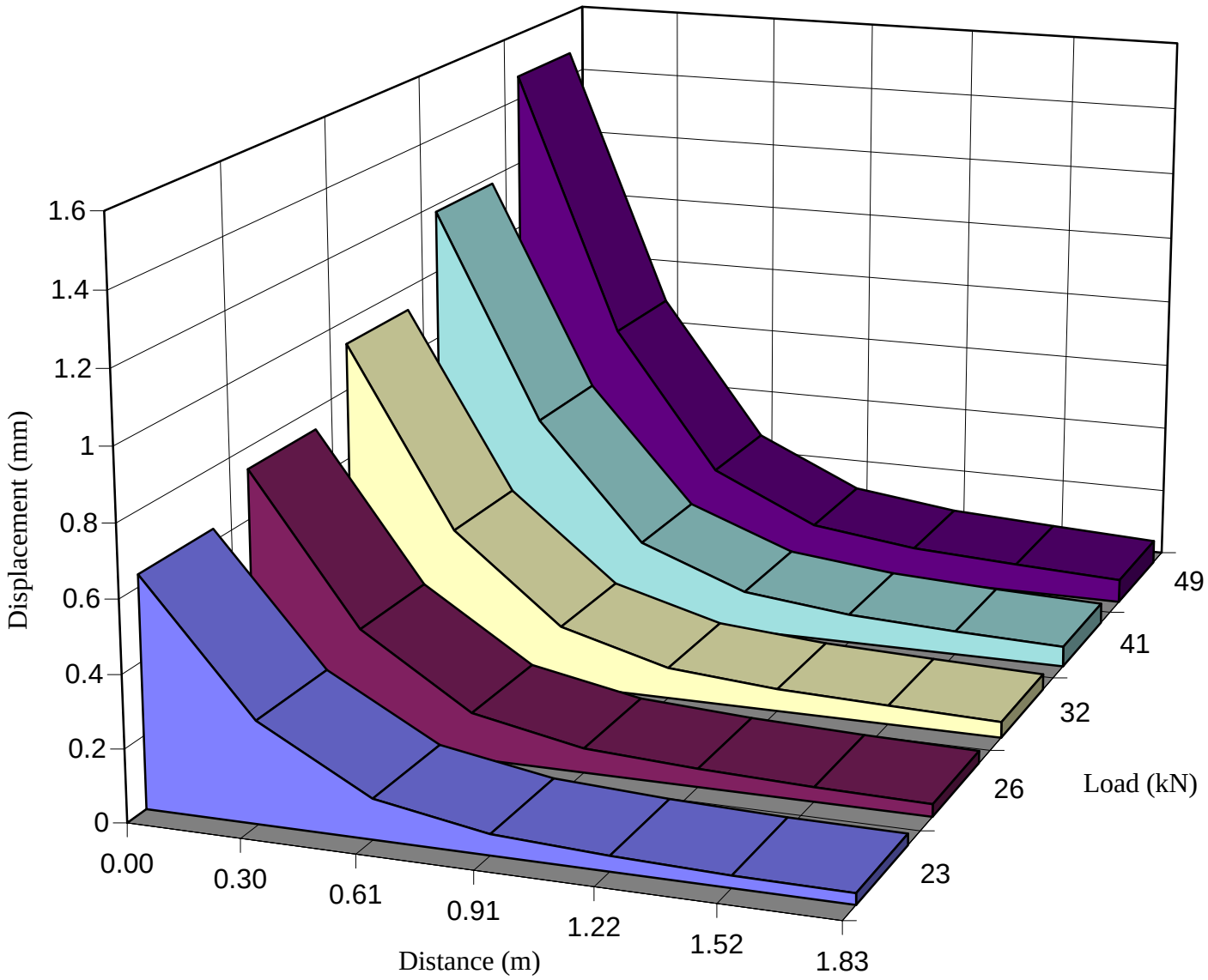

Figure B 26 Displacement as a function of distance for different FWD load levels (August 1995, section 8).

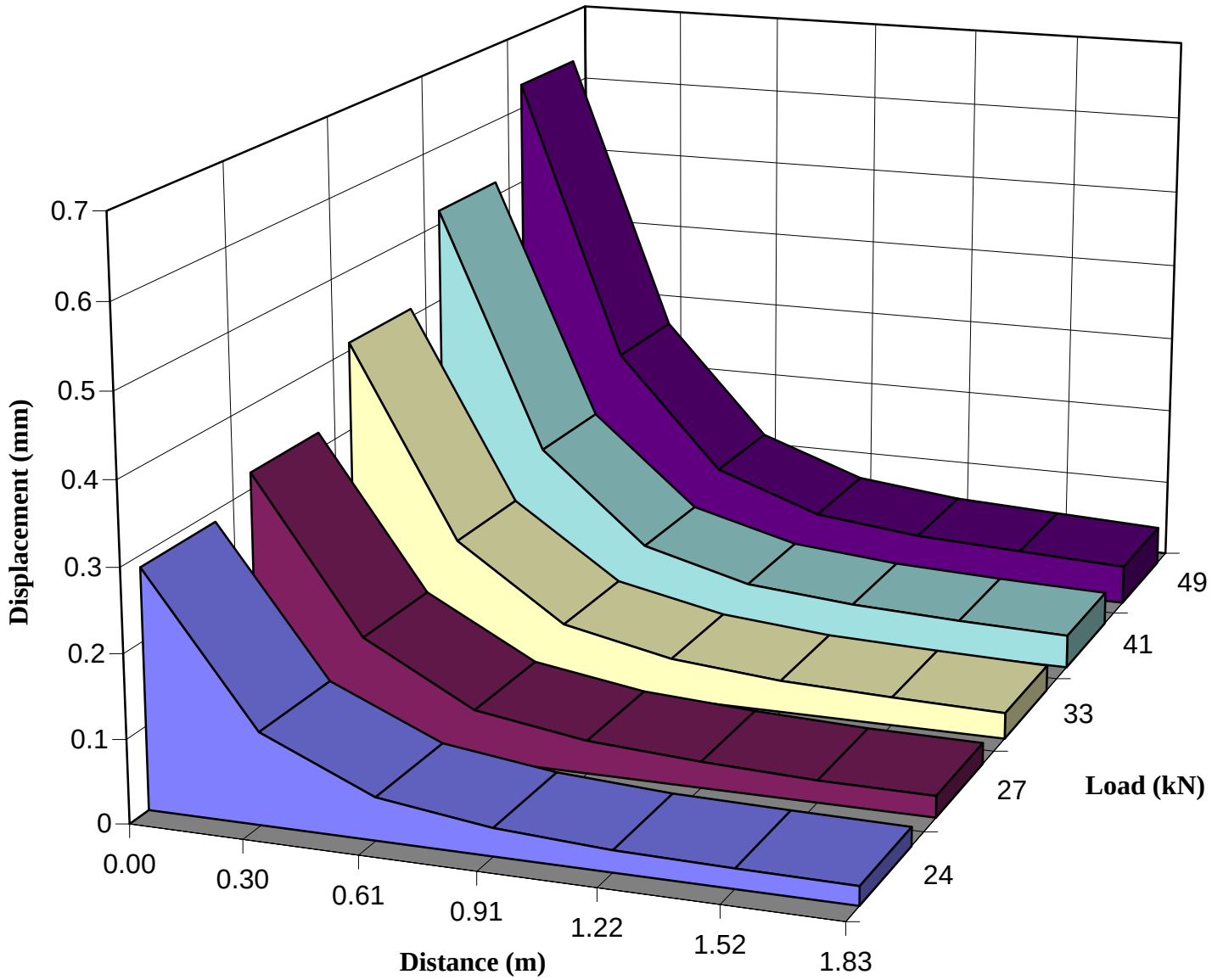

Figure B 27 Displacement as a function of distance for different FWD load levels (August 1995, section 9).

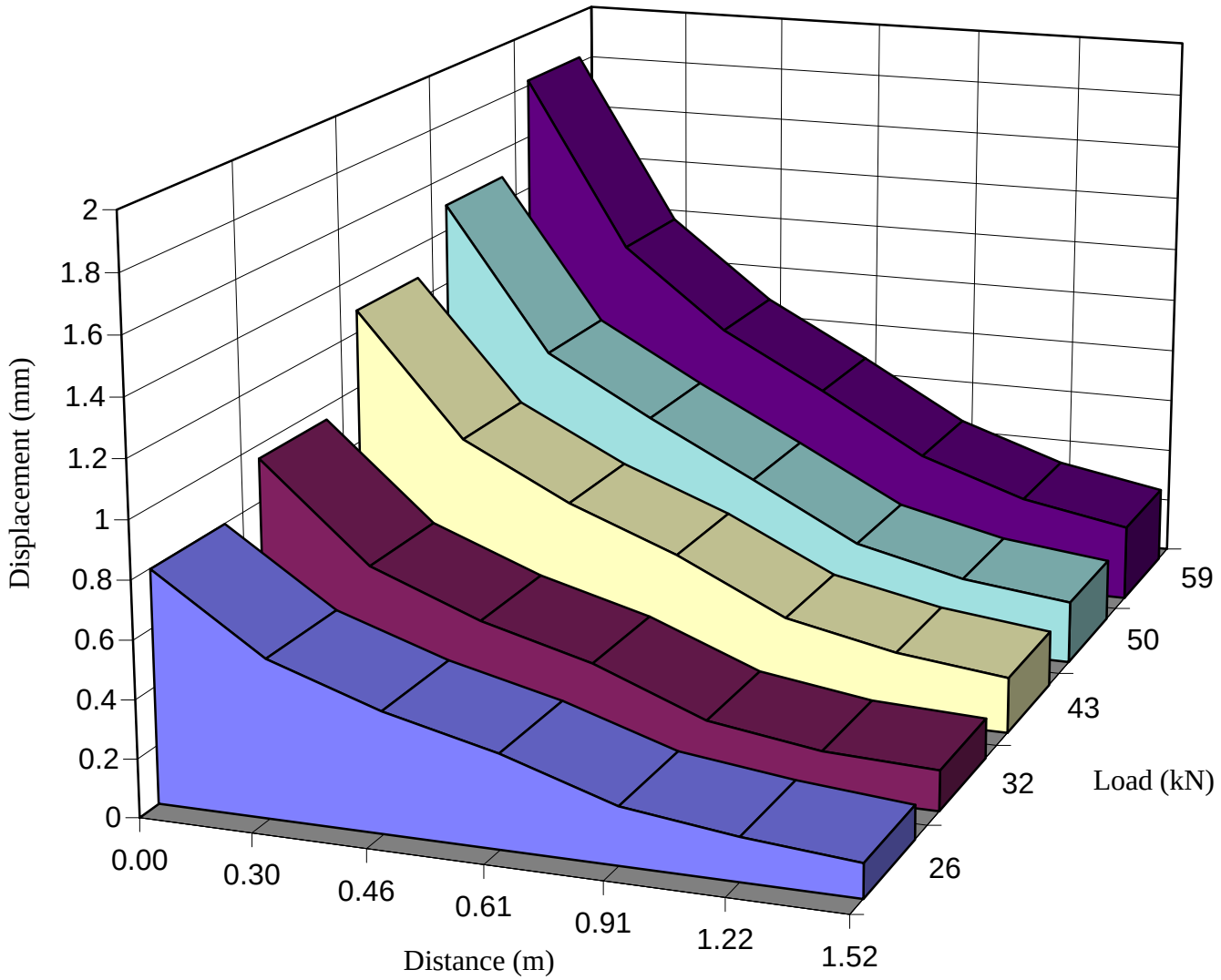

Figure B 28 Displacement as a function of distance for different FWD load levels (April 1996, section 1).

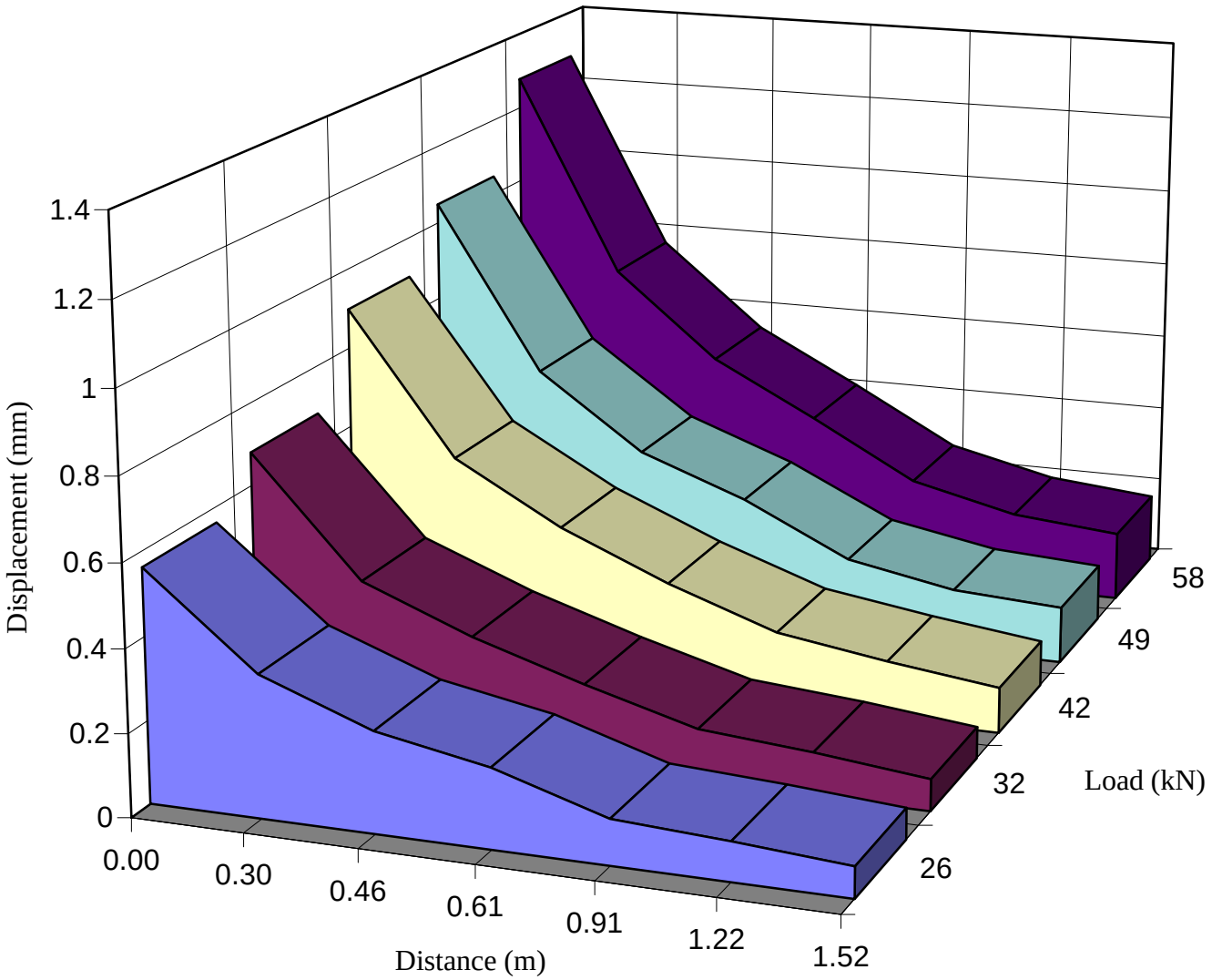

Figure B 29 Displacement as a function of distance for different FWD load levels (April 1996, section 2).

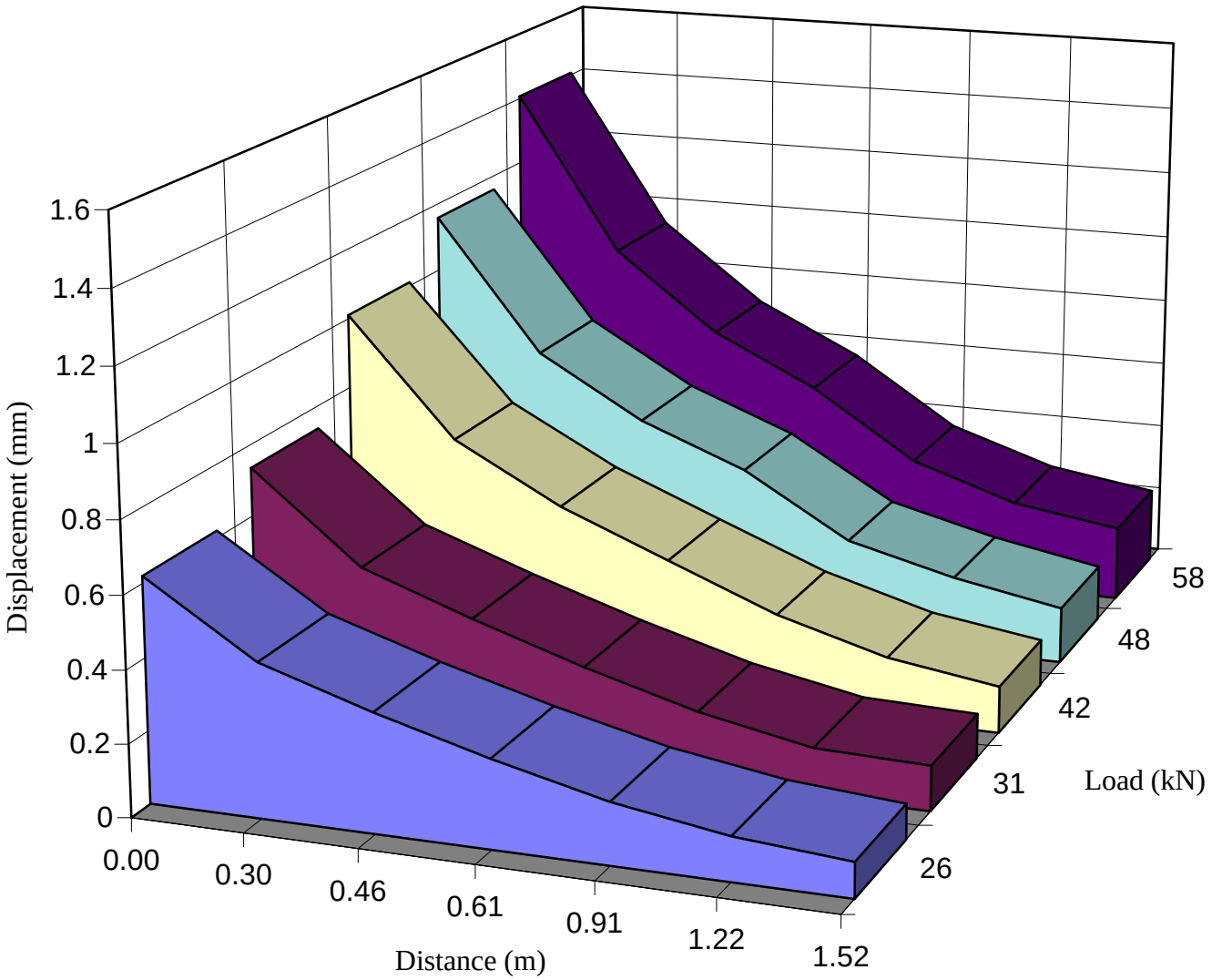

Figure B 30 Displacement as a function of distance for different FWD load levels (April 1996, section 3).

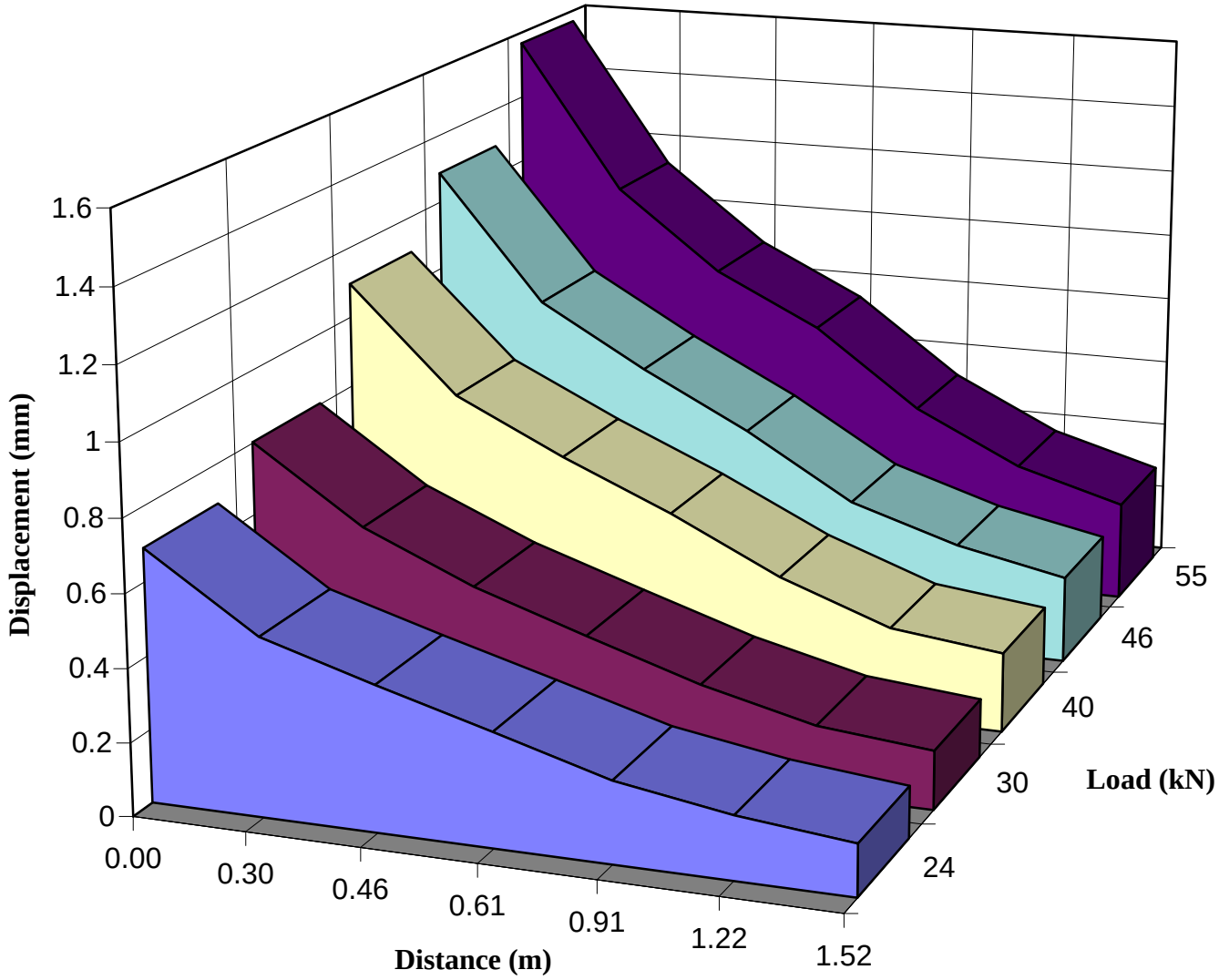

Figure B 31 Displacement as a function of distance for different FWD load levels (April 1996, section 4).

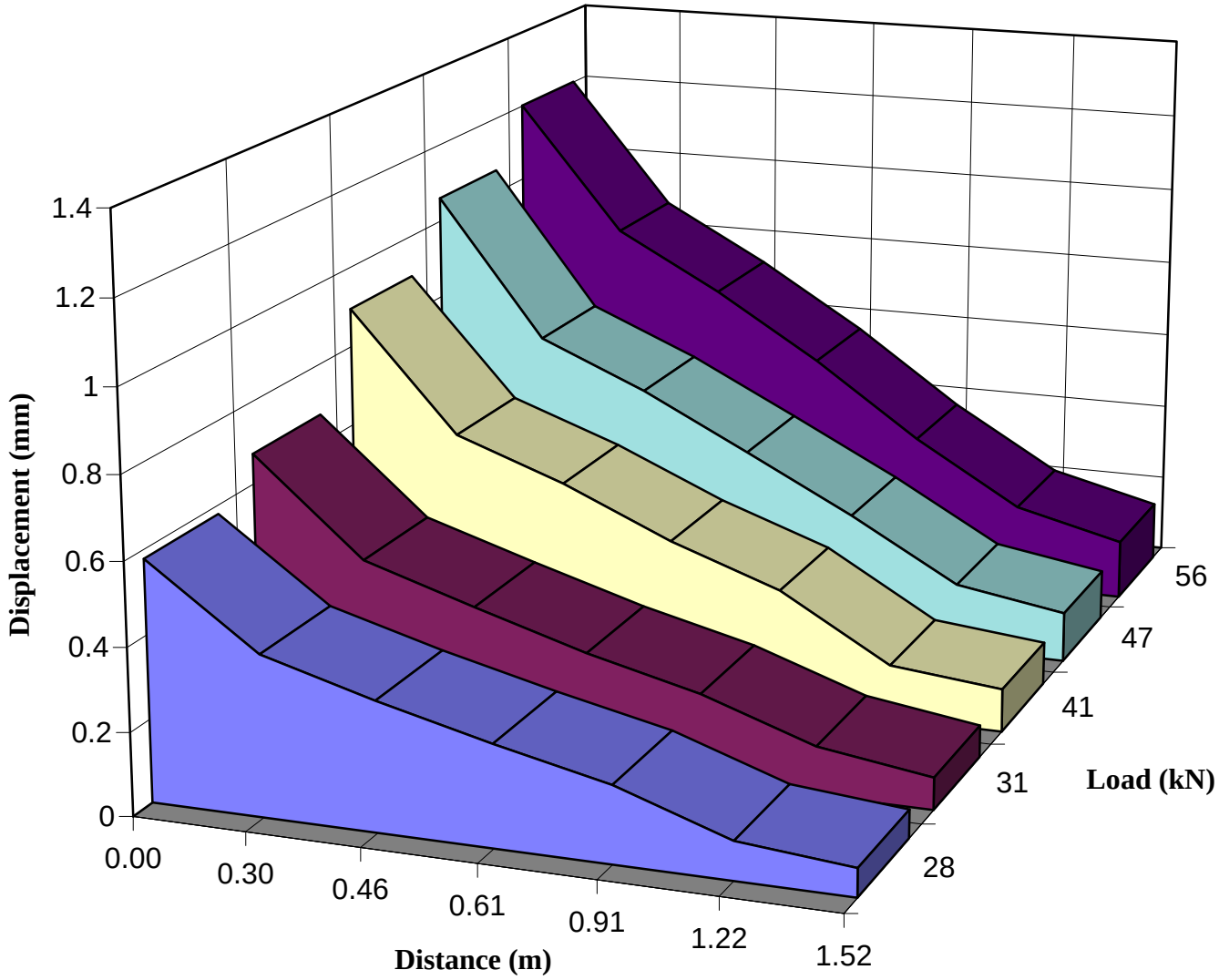

Figure B 32 Displacement as a function of distance for different FWD load levels (April 1996, section 5).

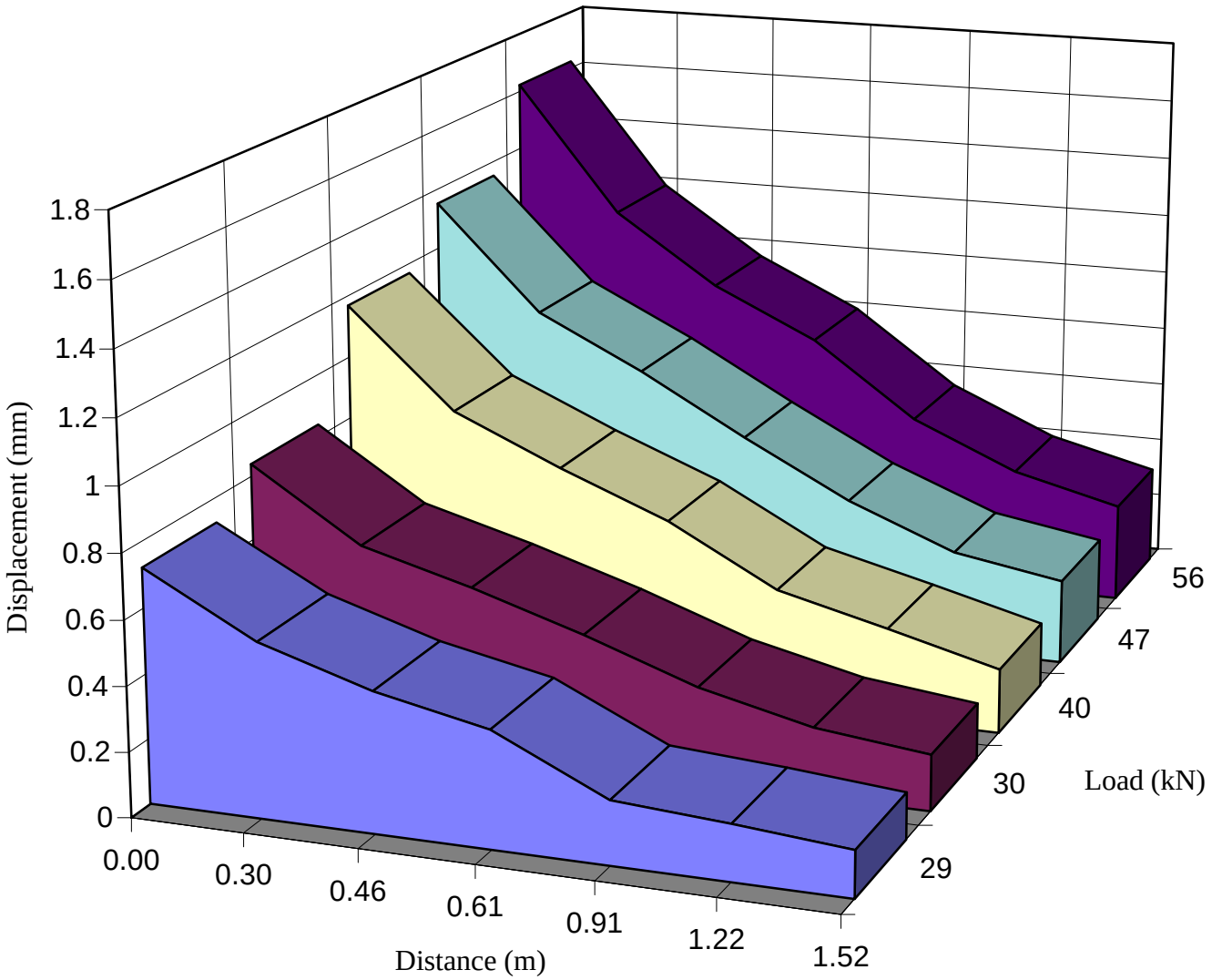

Figure B 33 Displacement as a function of distance for different FWD load levels (April 1996, section 6).

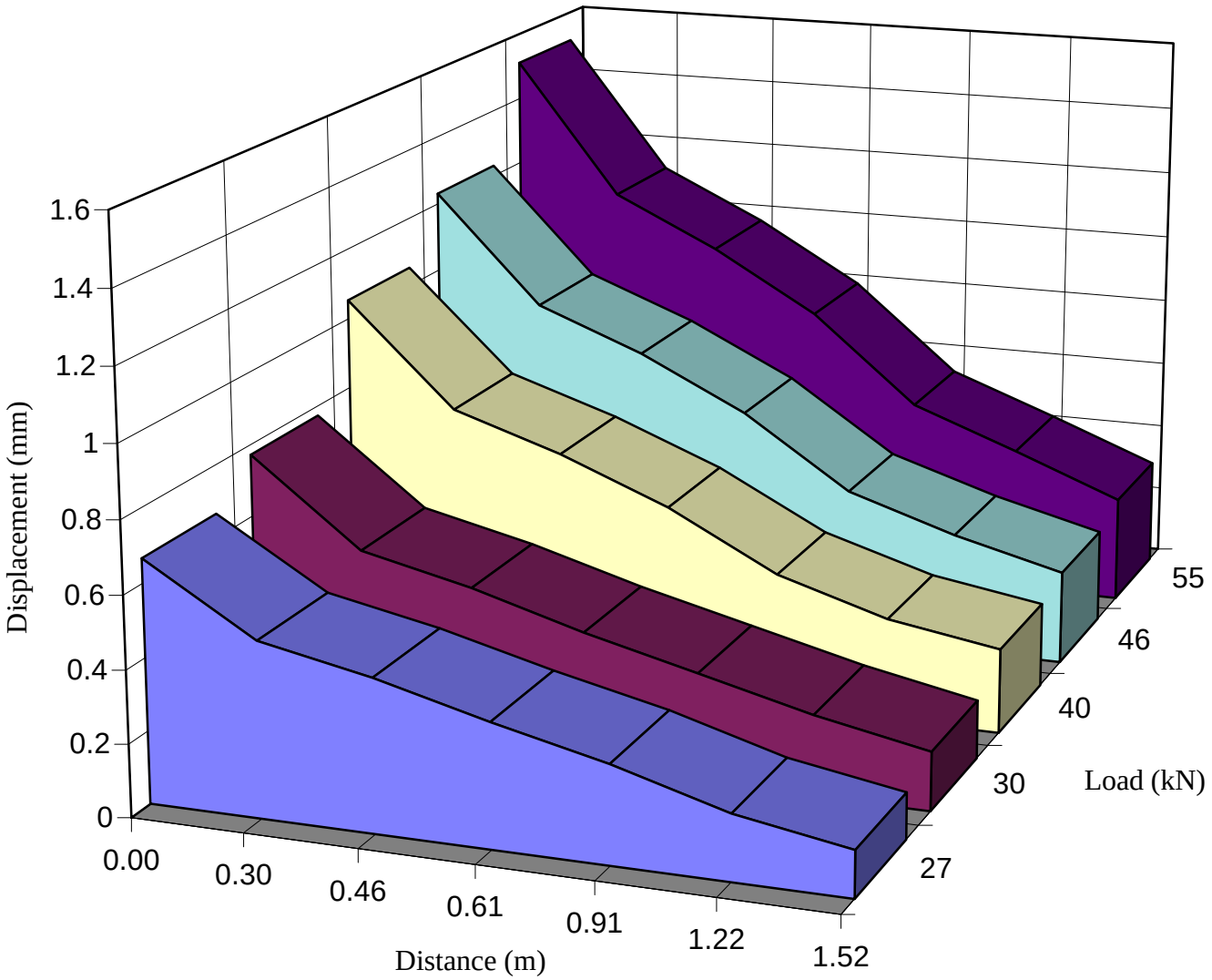

Figure B 34 Displacement as a function of distance for different FWD load levels (April 1996, section 7).

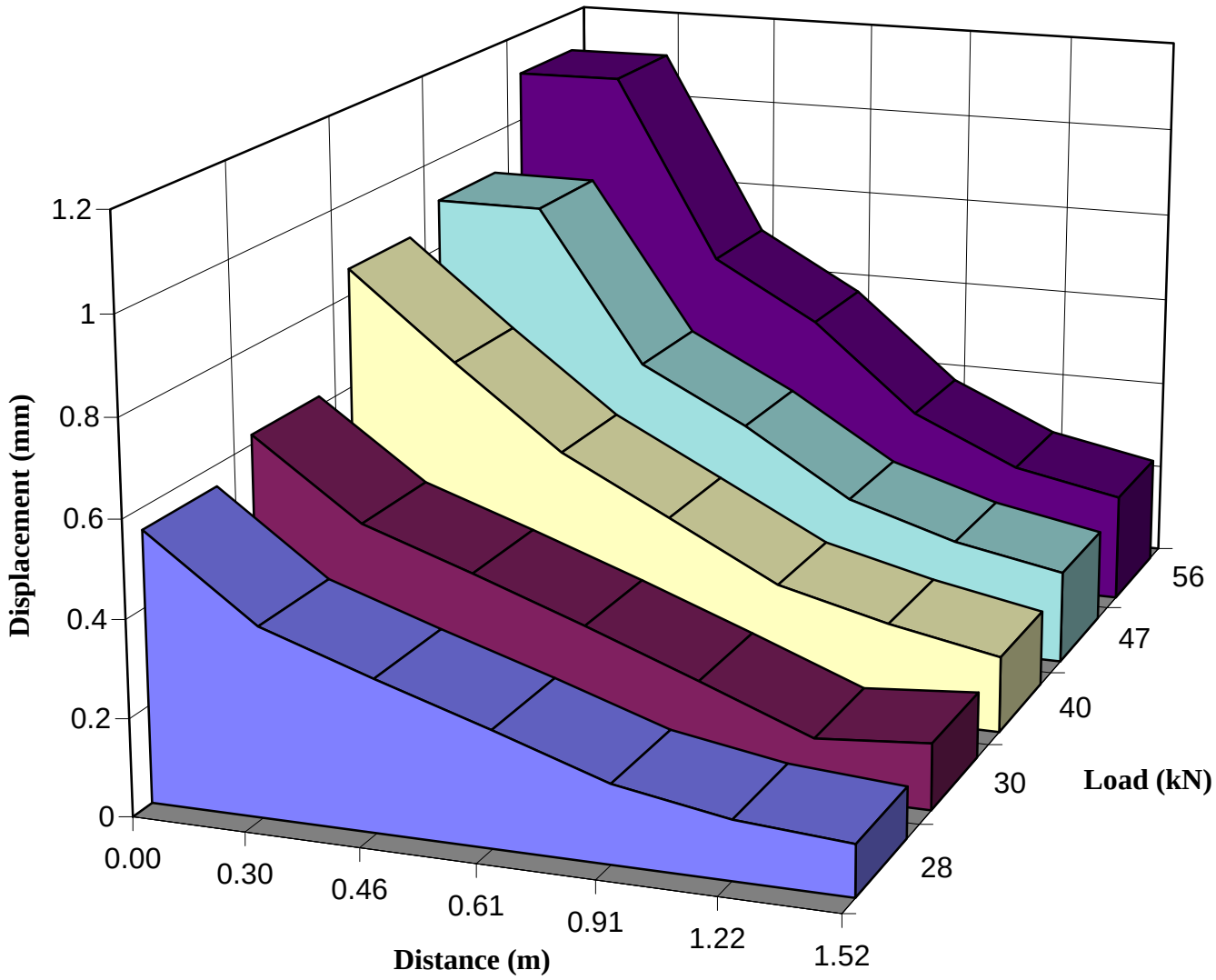

Figure B 35 Displacement as a function of distance for different FWD load levels (April 1996, section 8).

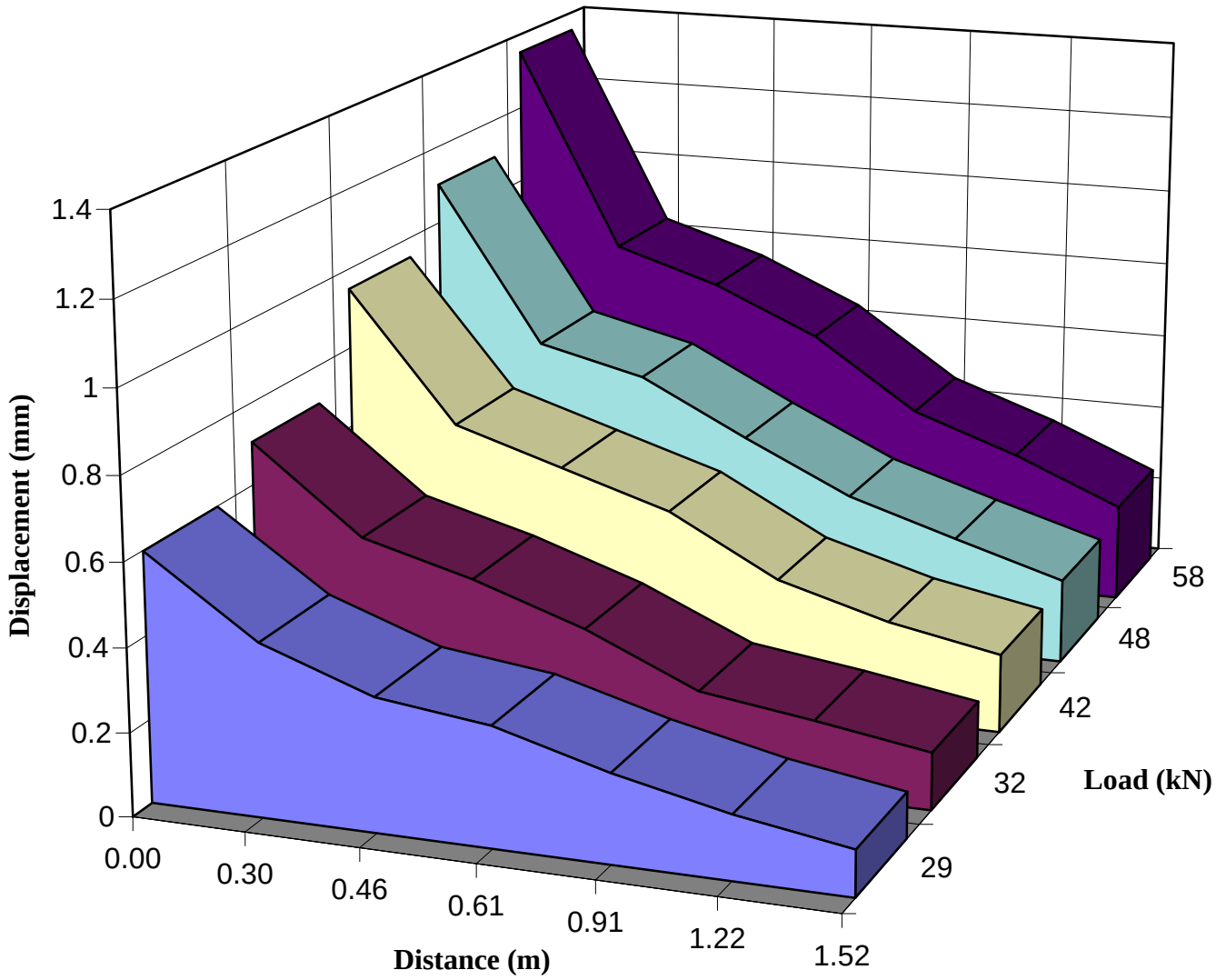

Figure B 36 Displacement as a function of distance for different FWD load levels (April 1996, section 9).

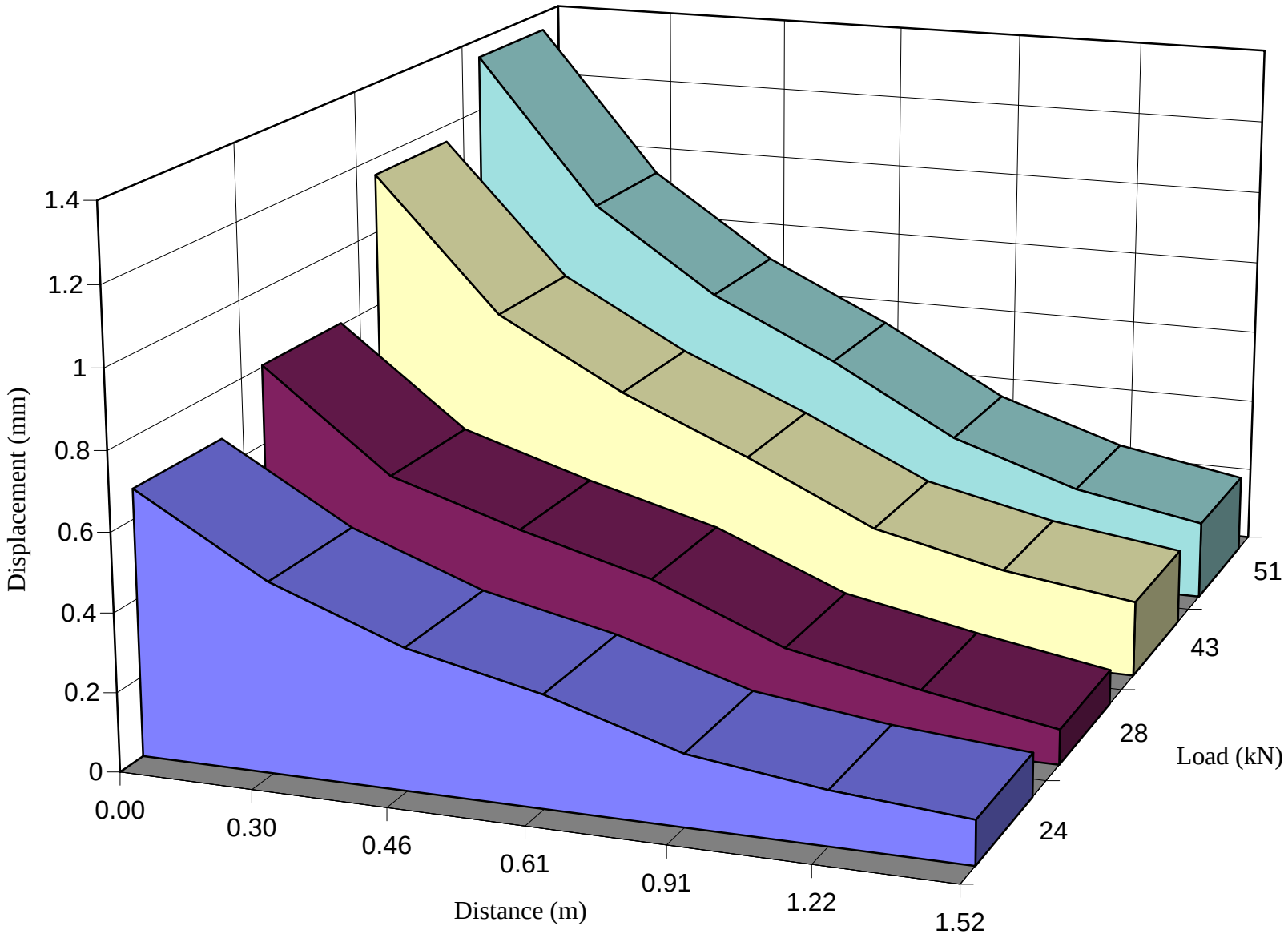

Figure B 37 Displacement as a function of distance for different FWD load levels (July 1996, section 1).

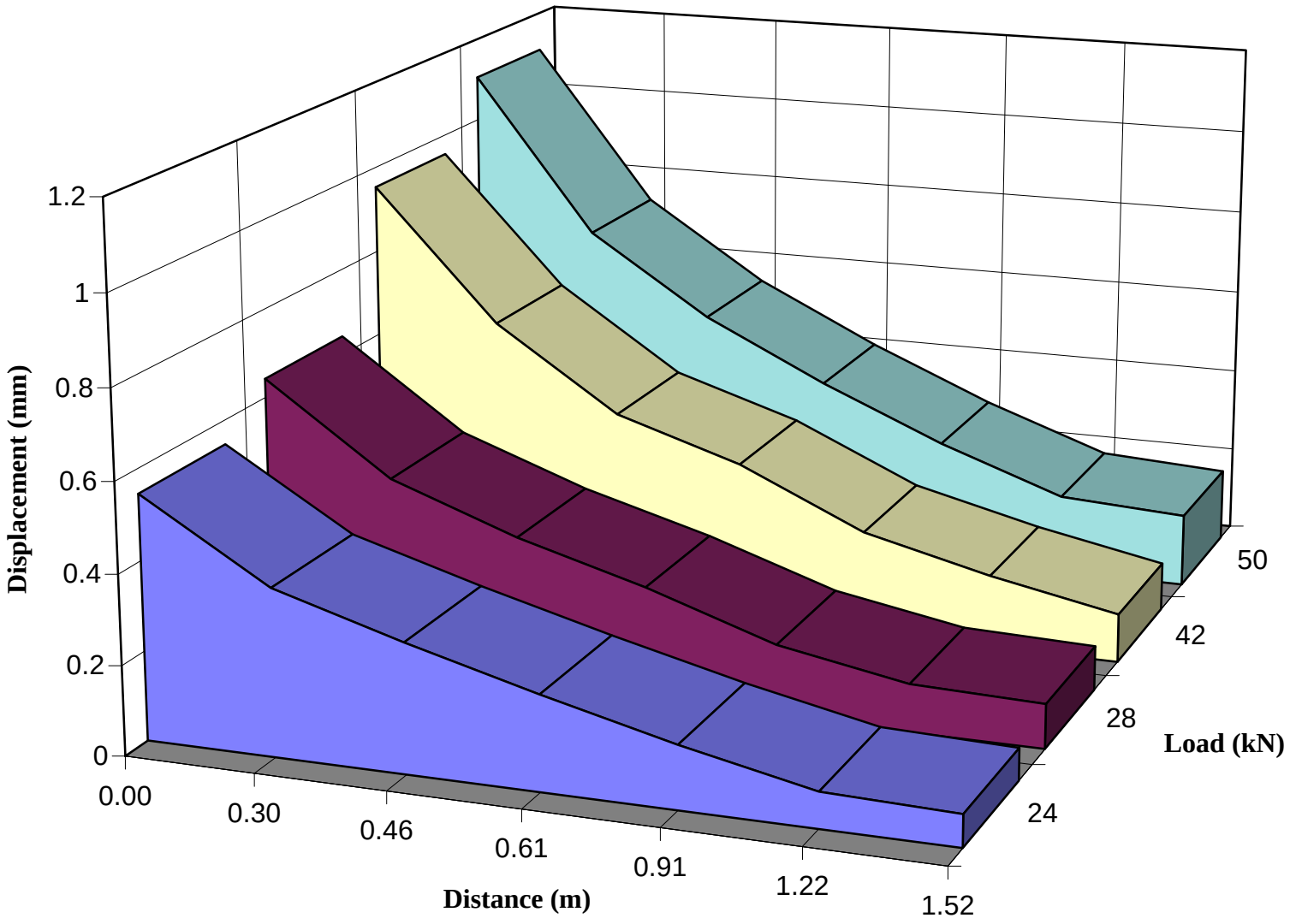

Figure B 38 Displacement as a function of distance for different FWD load levels (July 1996, section 2).

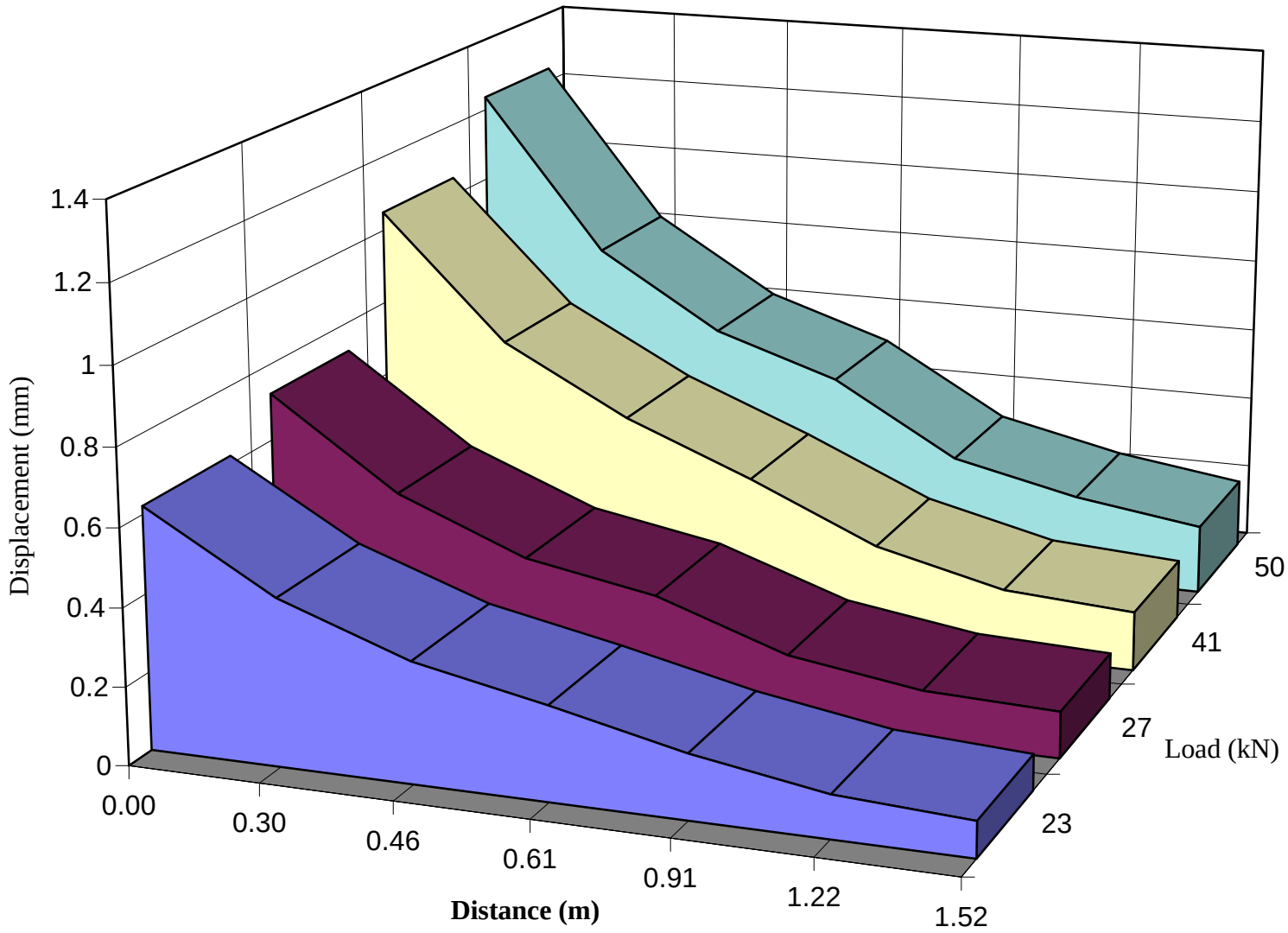

Figure B 39 Displacement as a function of distance for different FWD load levels (July 1996, section 3).

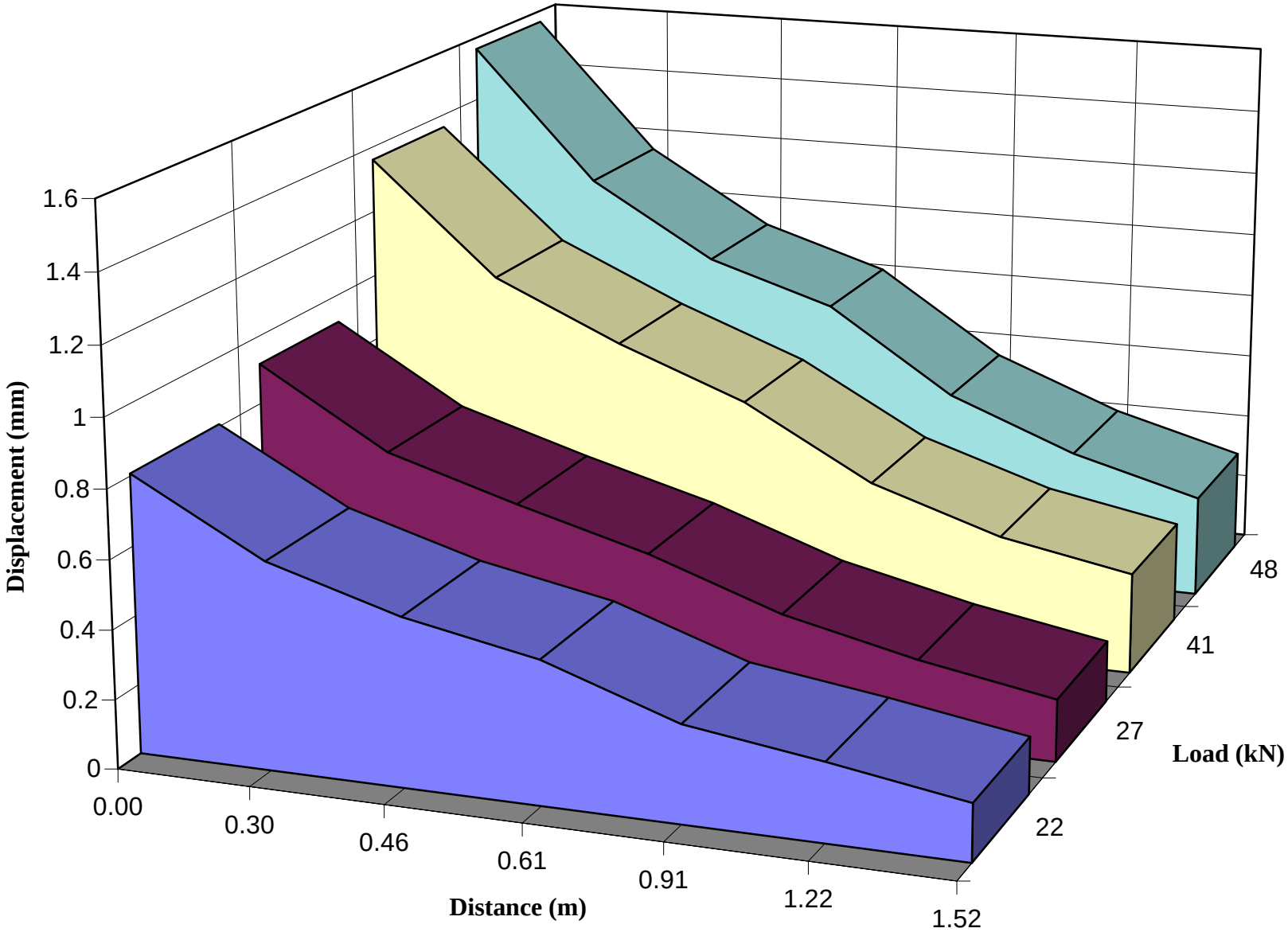

Figure B 40 Displacement as a function of distance for different FWD load levels (July 1996, section 4).

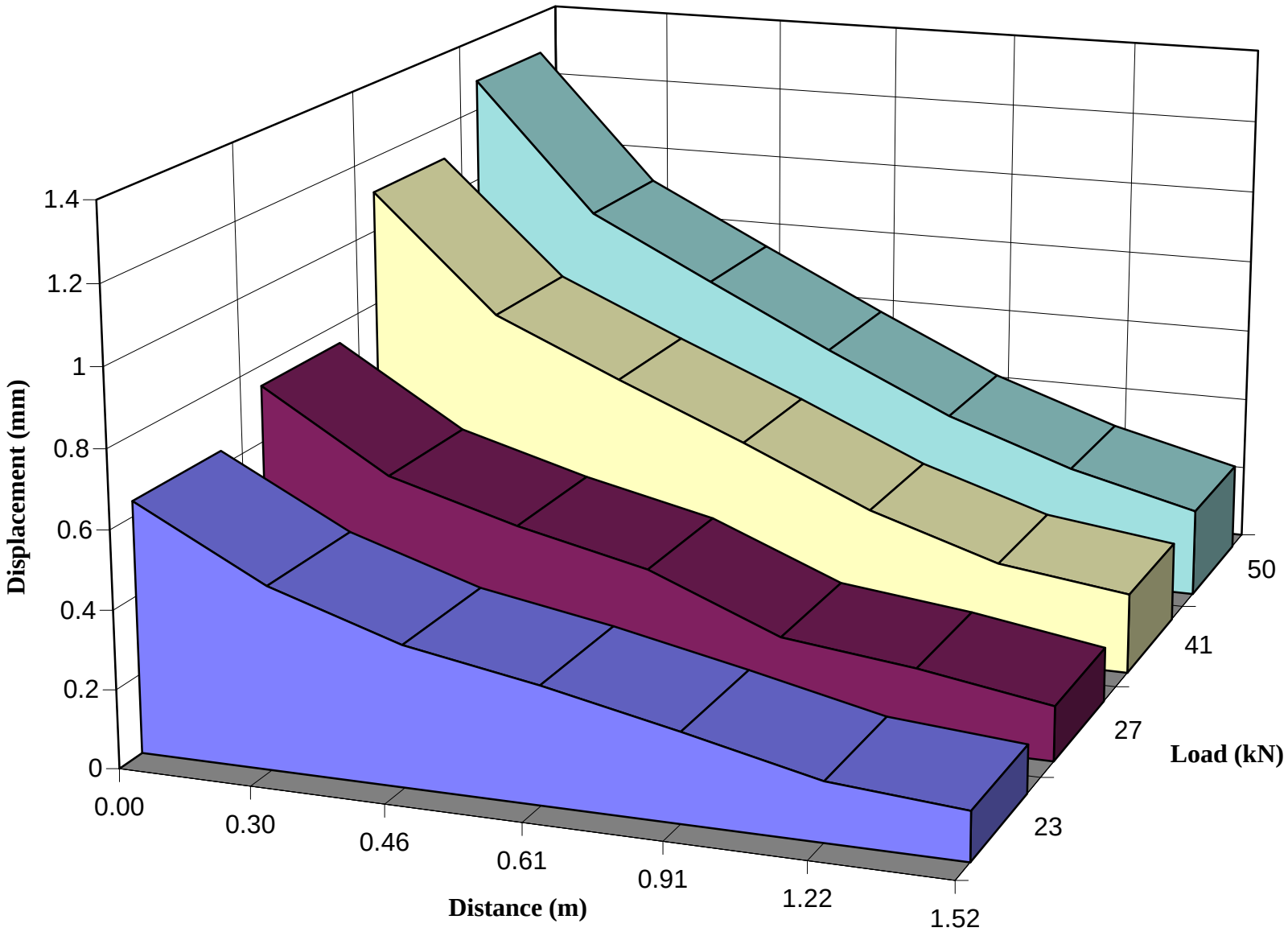

Figure B 41 Displacement as a function of distance for different FWD load levels (July 1996, section 5).

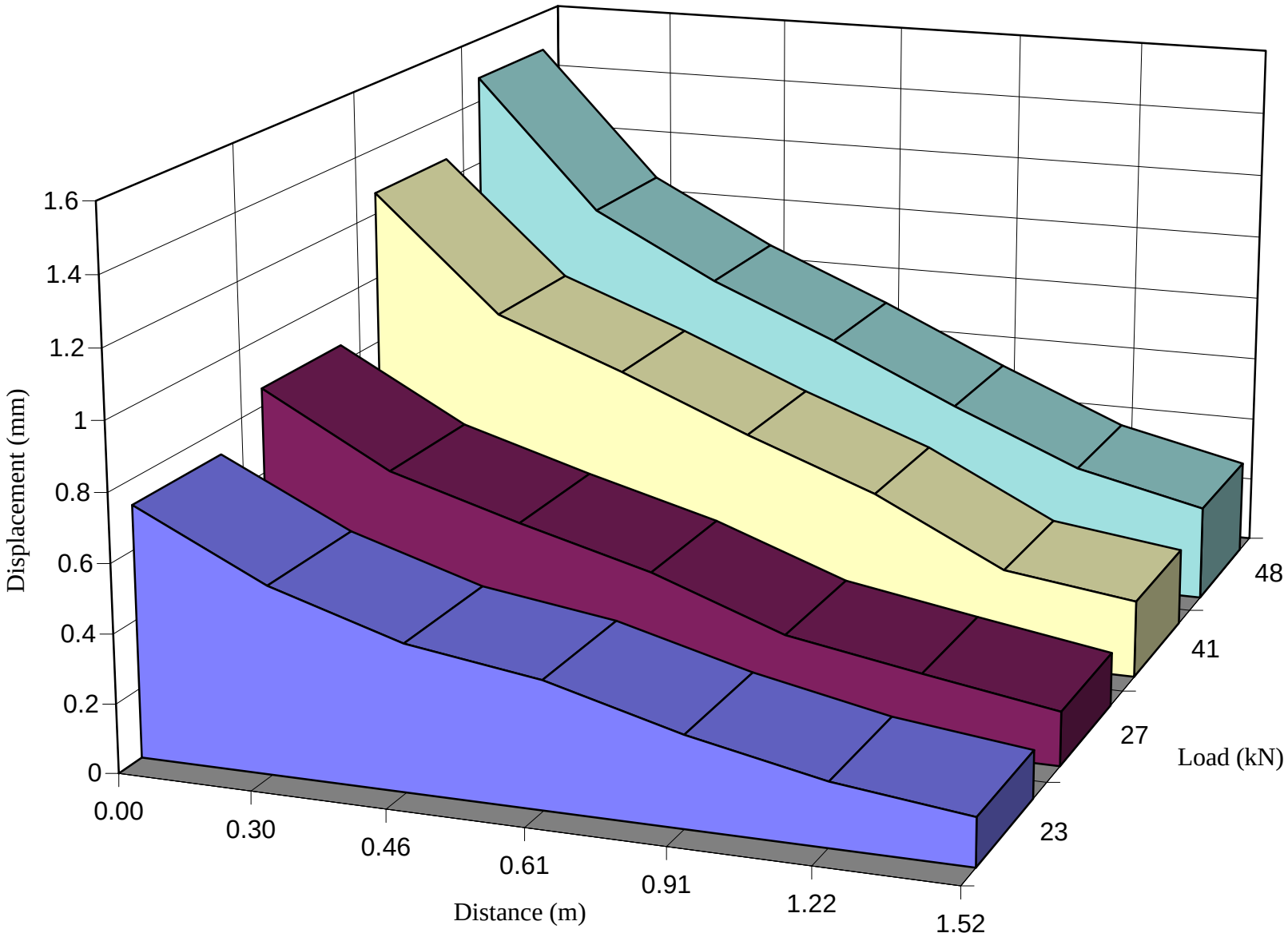

Figure B 42 Displacement as a function of distance for different FWD load levels (July 1996, section 6).

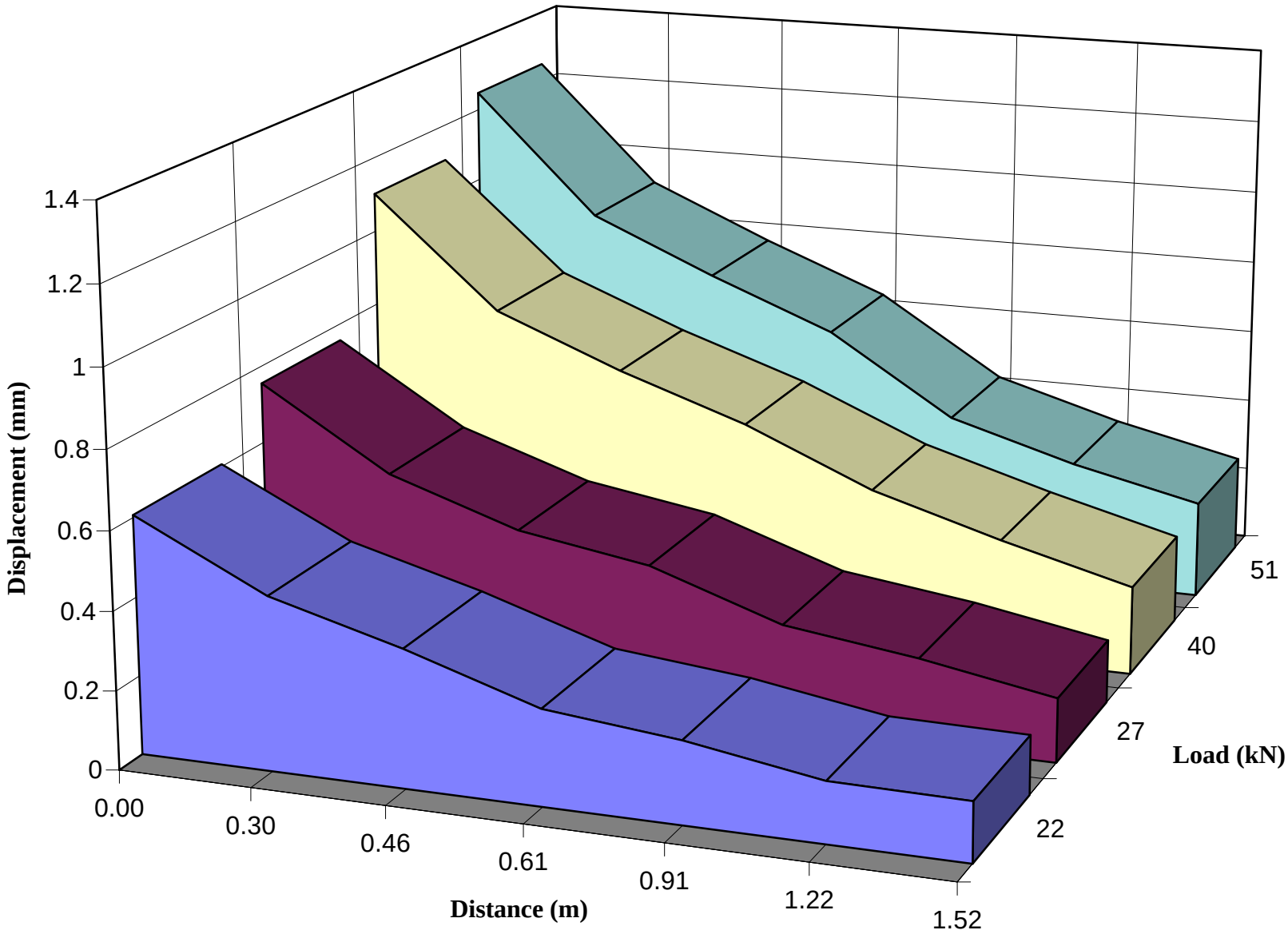

Figure B 43 Displacement as a function of distance for different FWD load levels (July 1996, section 7).

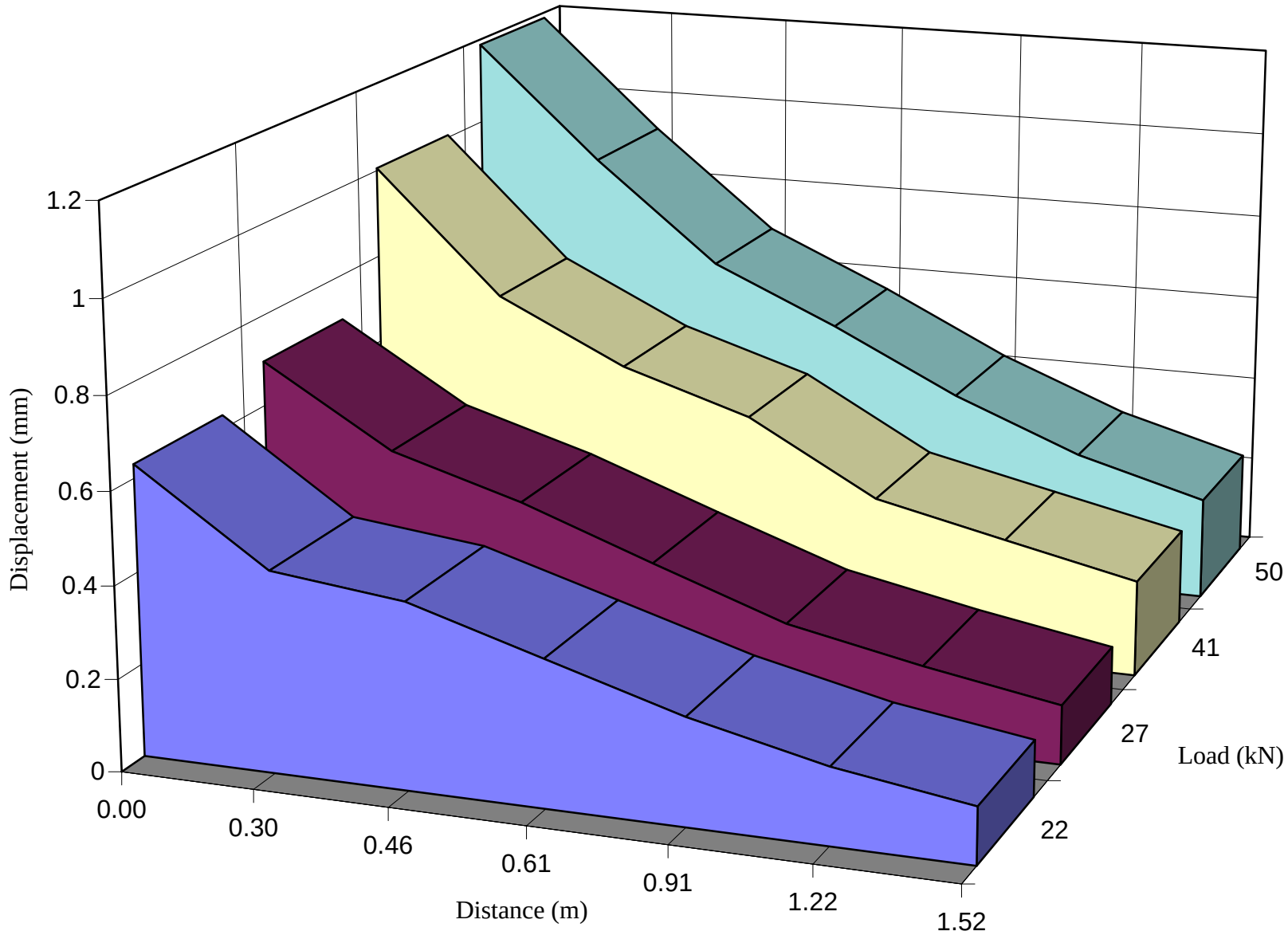

Figure B 44 Displacement as a function of distance for different FWD load levels (July 1996, section 8).

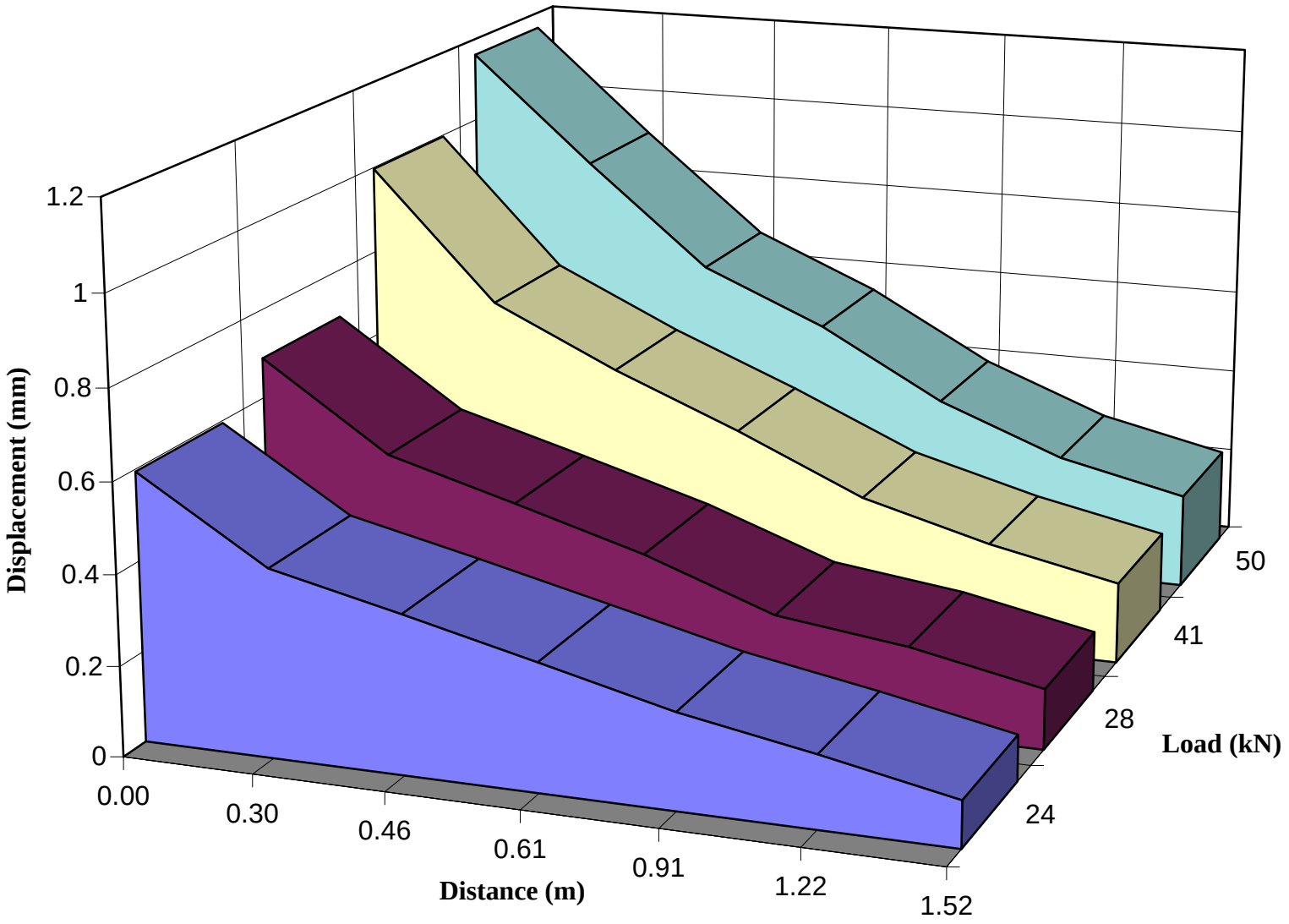

Figure B 45 Displacement as a function of distance for different FWD load levels (July 1996, section 9).

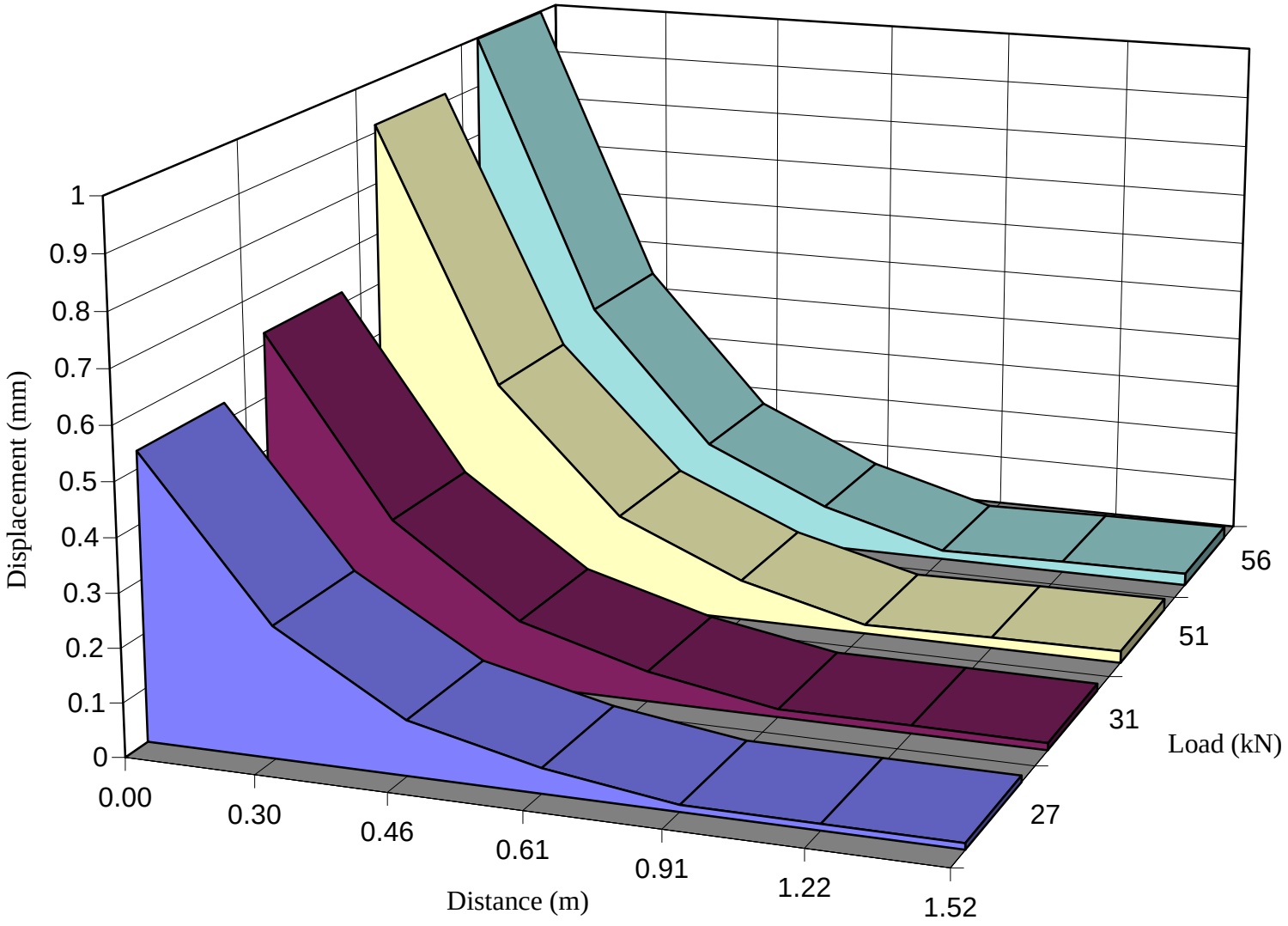

Figure B 46 Displacement as a function of distance for different FWD load levels (October 1996, section 1).

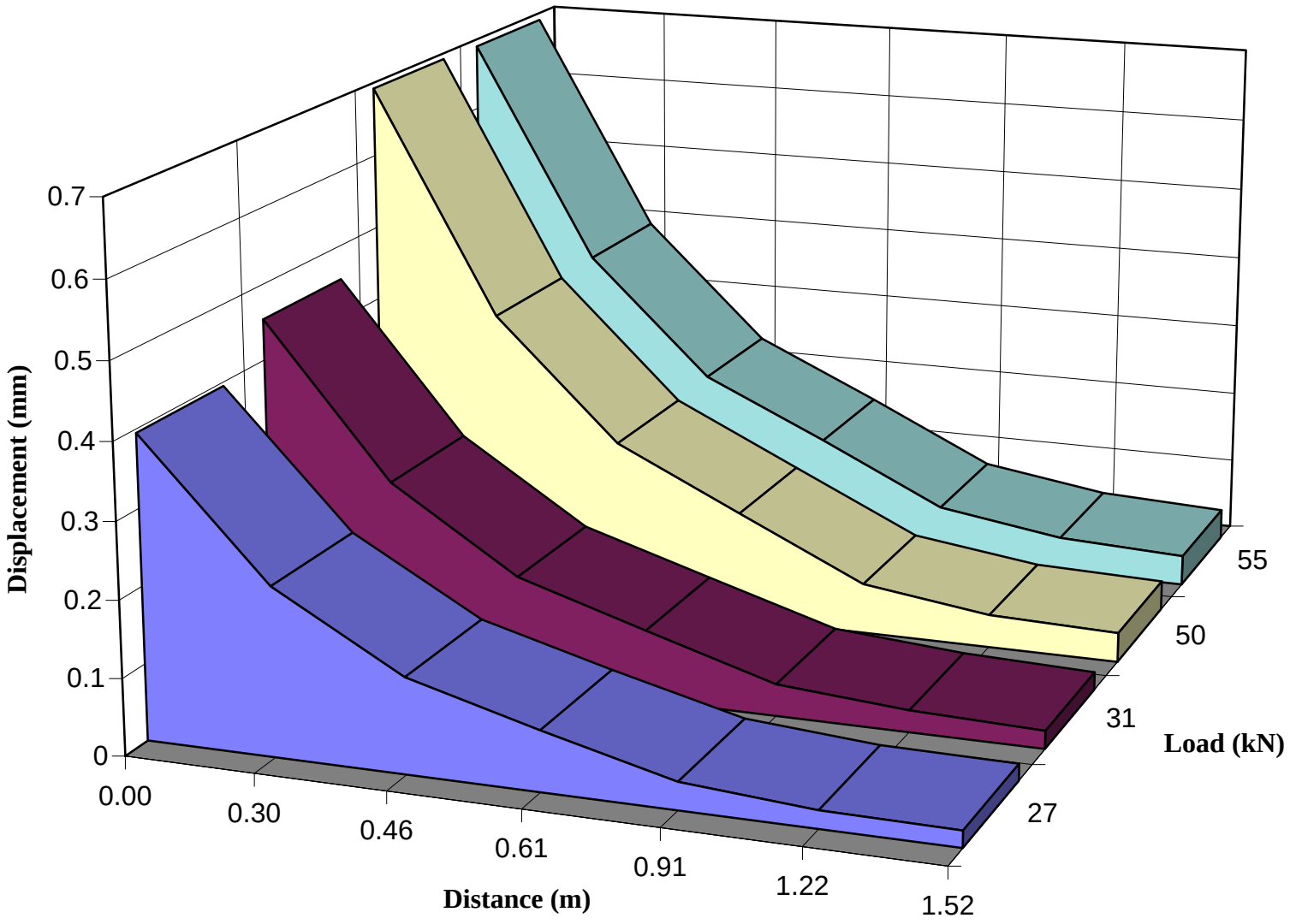

Figure B 47 Displacement as a function of distance for different FWD load levels (October 1996, section 2).

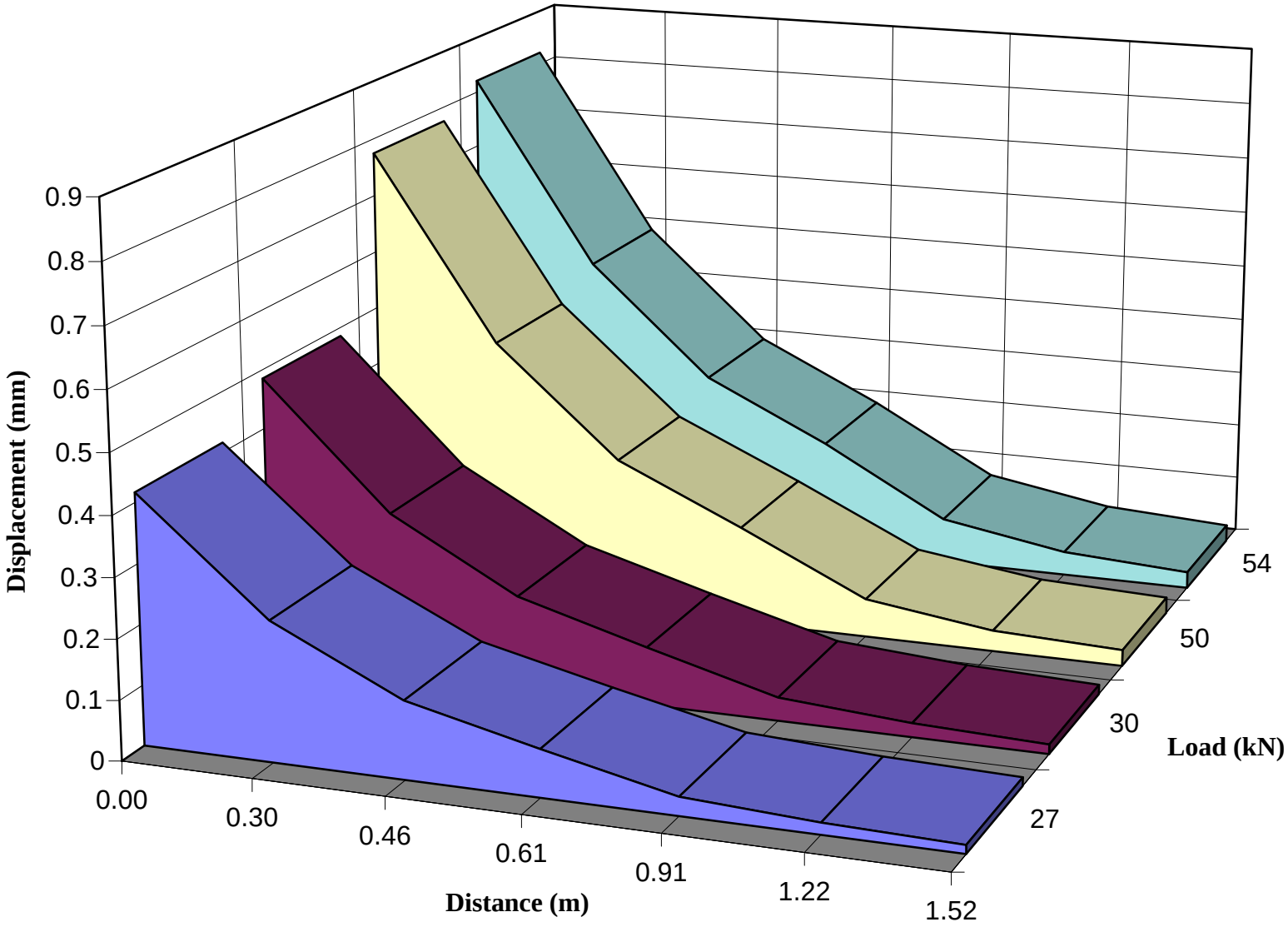

Figure B 48 Displacement as a function of distance for different FWD load levels (October 1996, section 3).

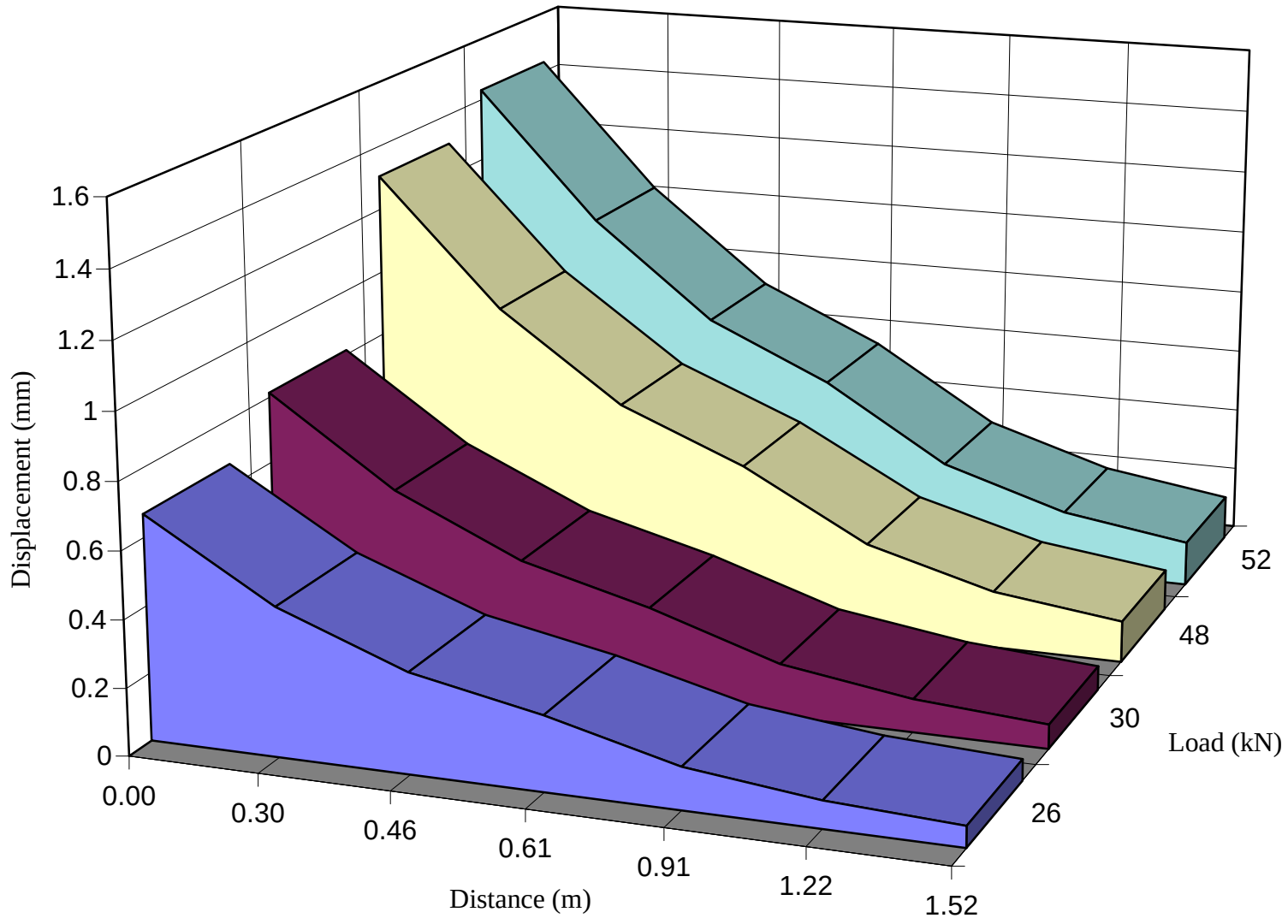

Figure B 49 Displacement as a function of distance for different FWD load levels (October 1996, section 4).

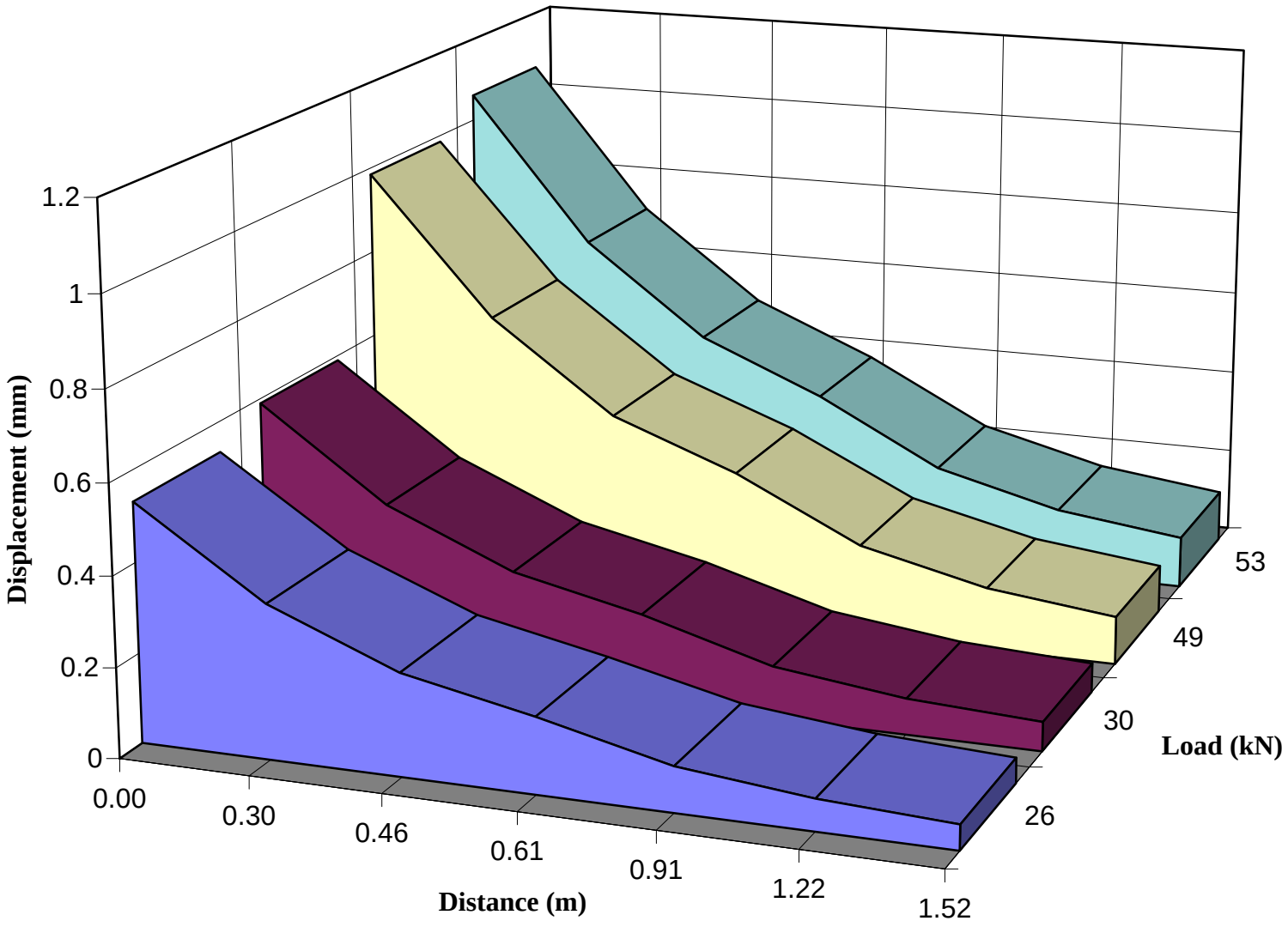

Figure B 50 Displacement as a function of distance for different FWD load levels (October 1996, section 5).

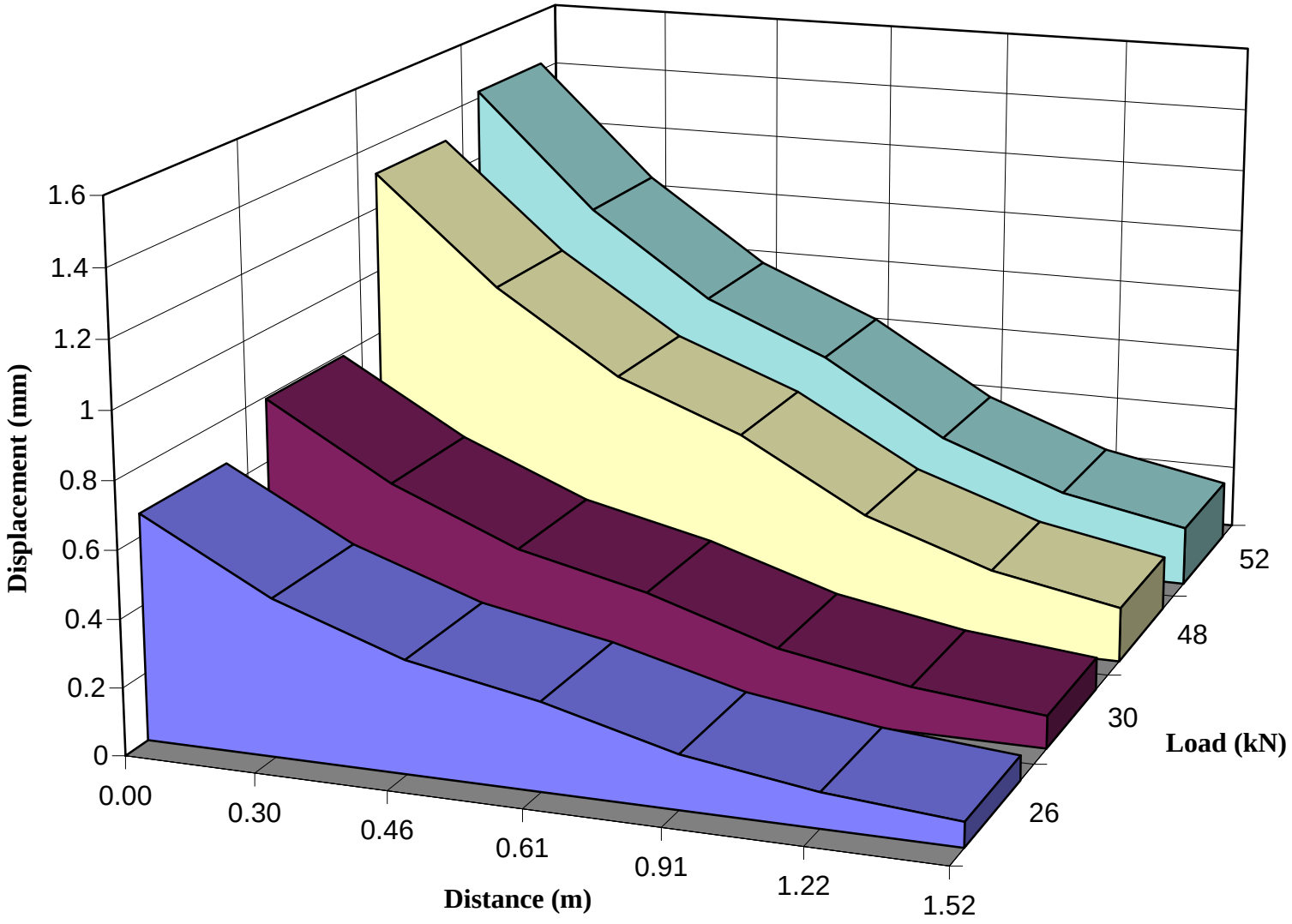

Figure B 51 Displacement as a function of distance for different FWD load levels (October 1996, section 6).

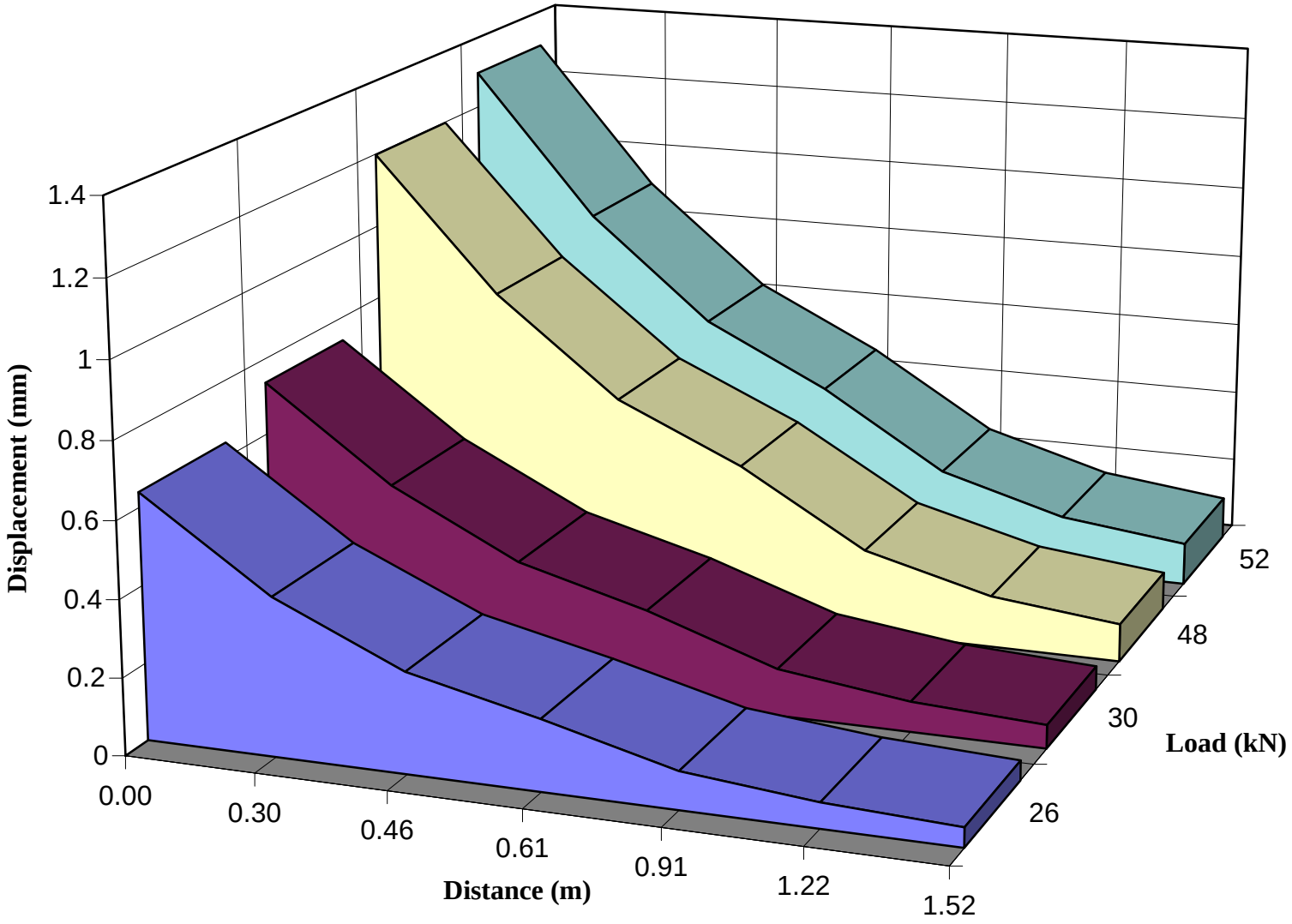

Figure B 52 Displacement as a function of distance for different FWD load levels (October 1996, section 7).

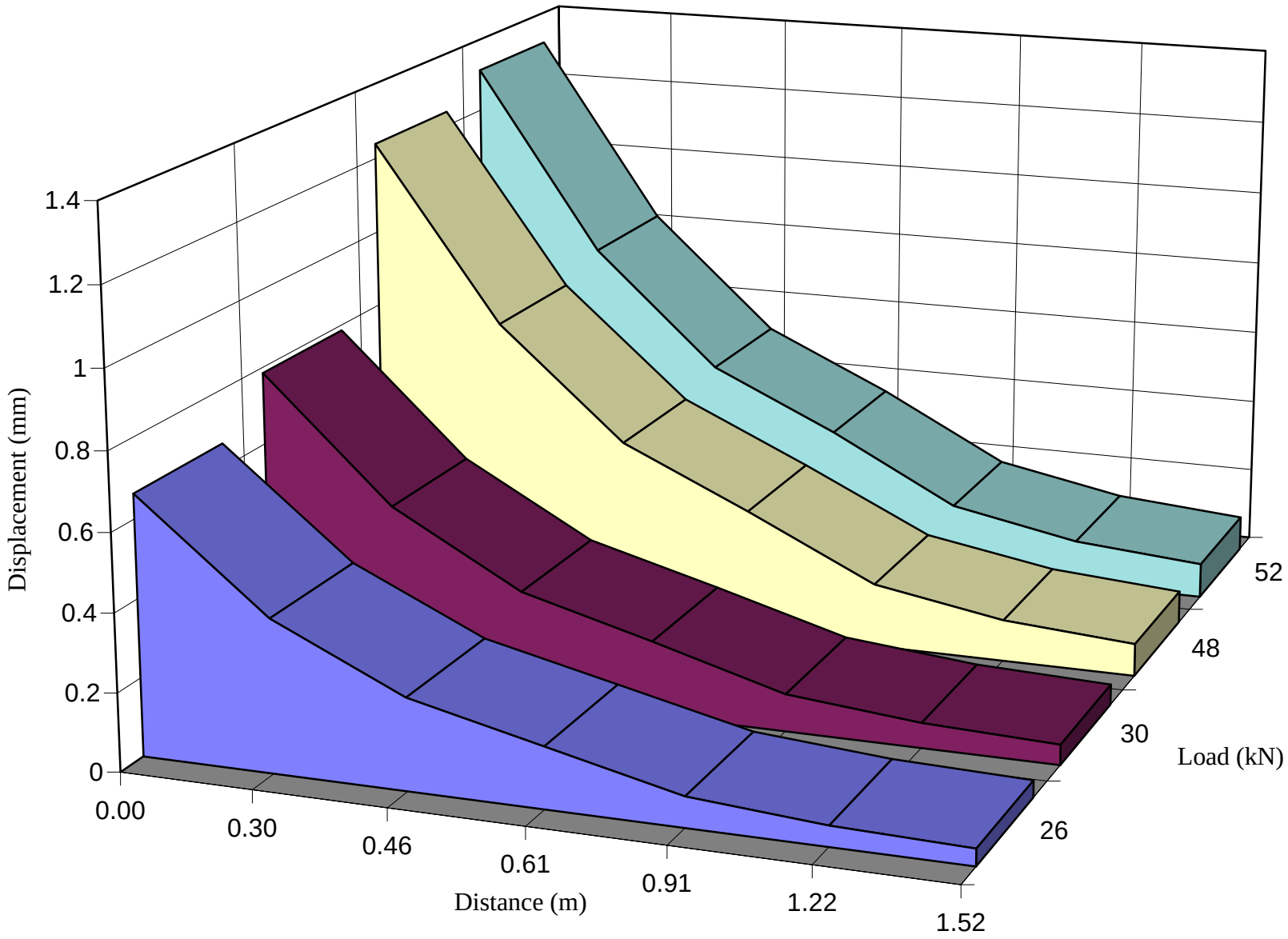

Figure B 53 Displacement as a function of distance for different FWD load levels (October 1996, section 8).

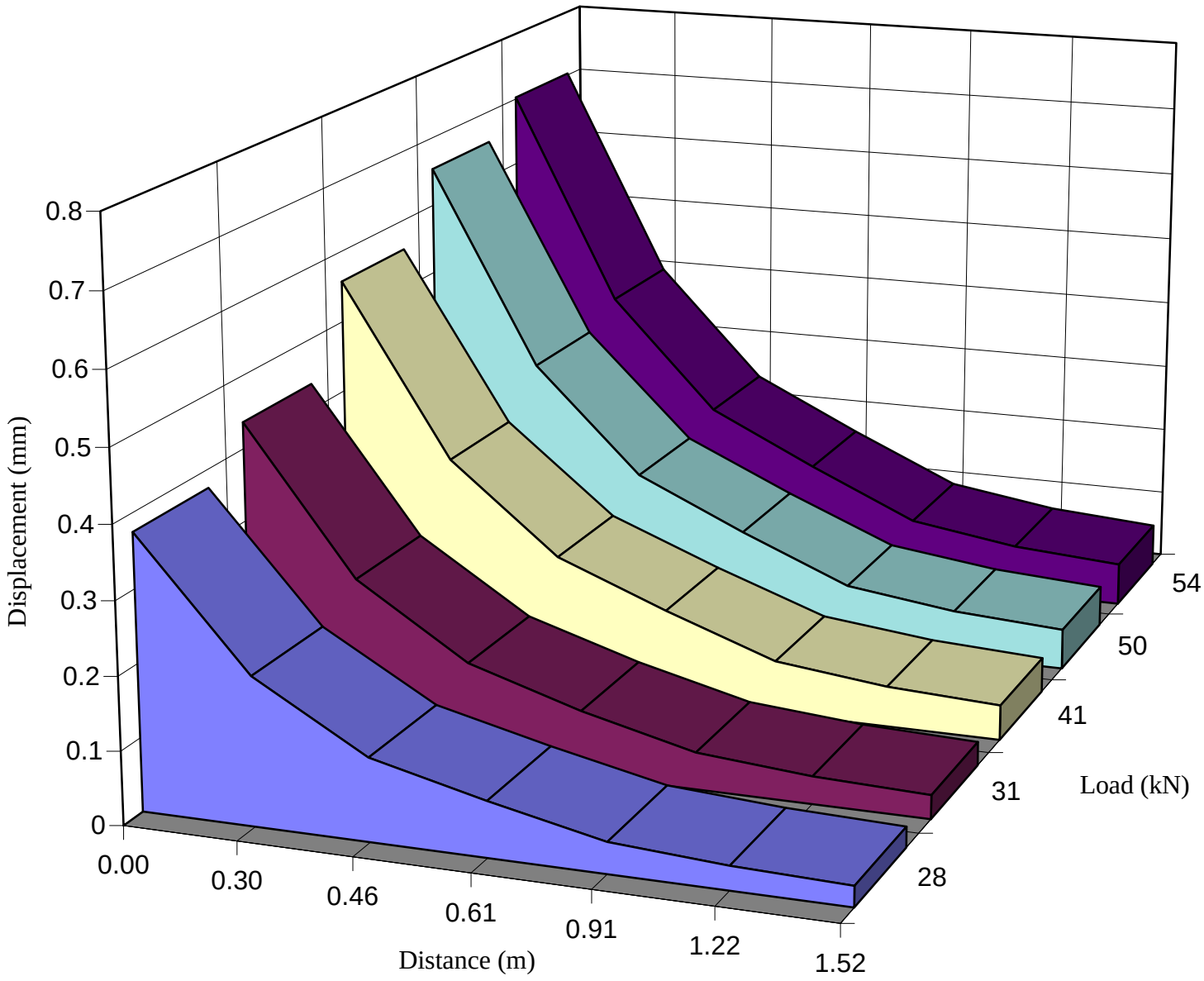

Figure B 54 Displacement as a function of distance for different FWD load levels (October 1996, section 9).

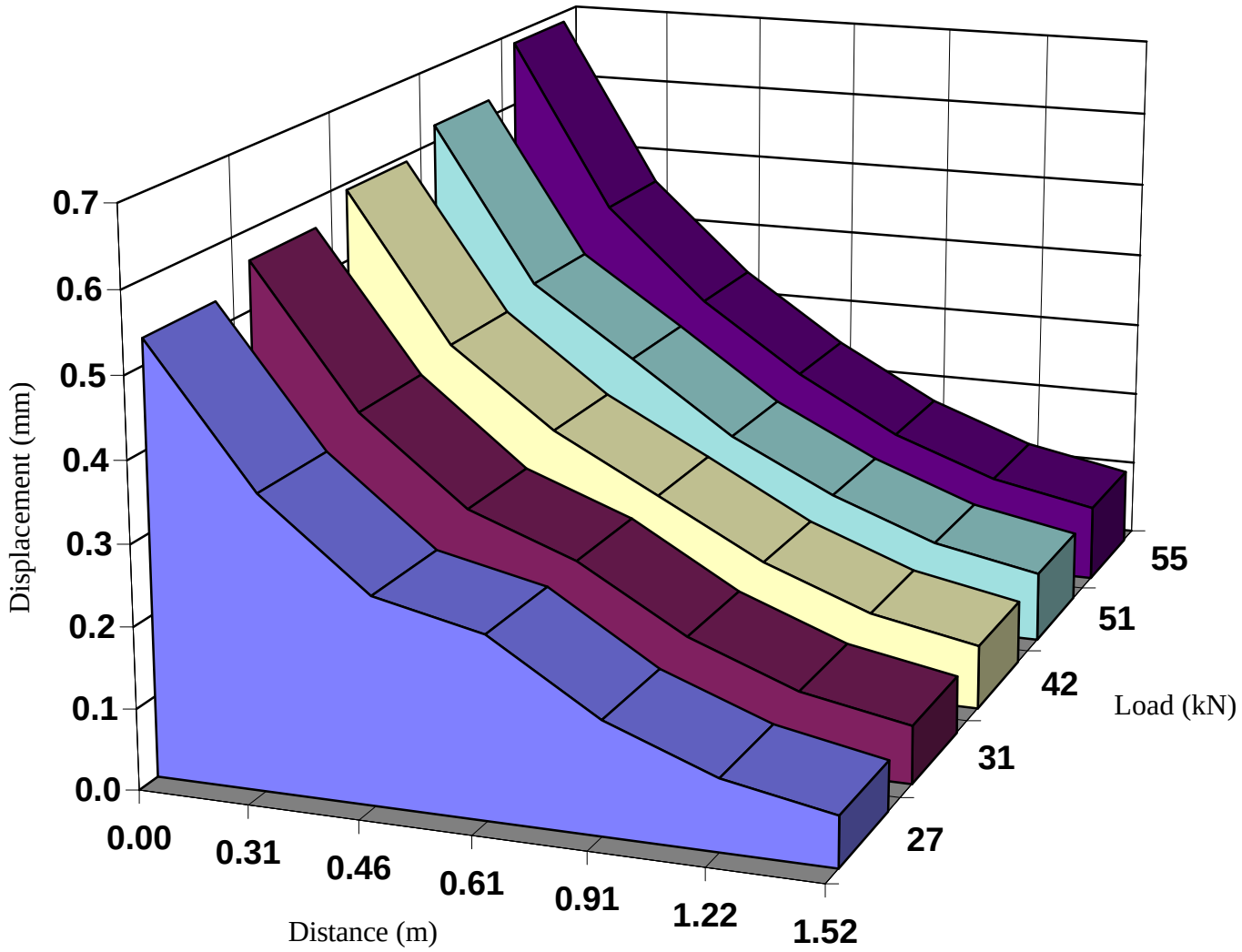

Figure B 55 Displacement as a function of distance for different FWD load levels (January 1997, section 1).

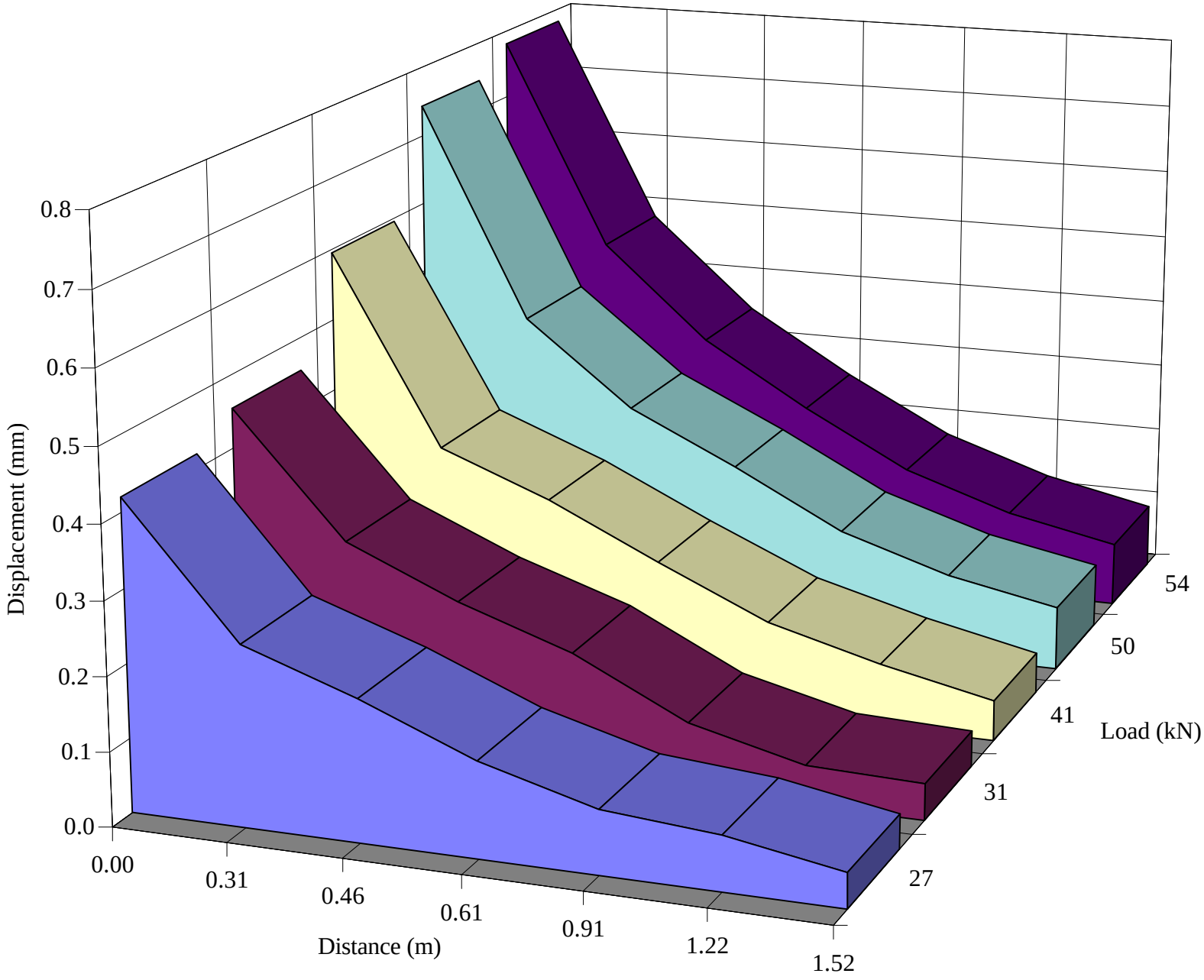

Figure B 56 Displacement as a function of distance for different FWD load levels (January 1997, section 2)

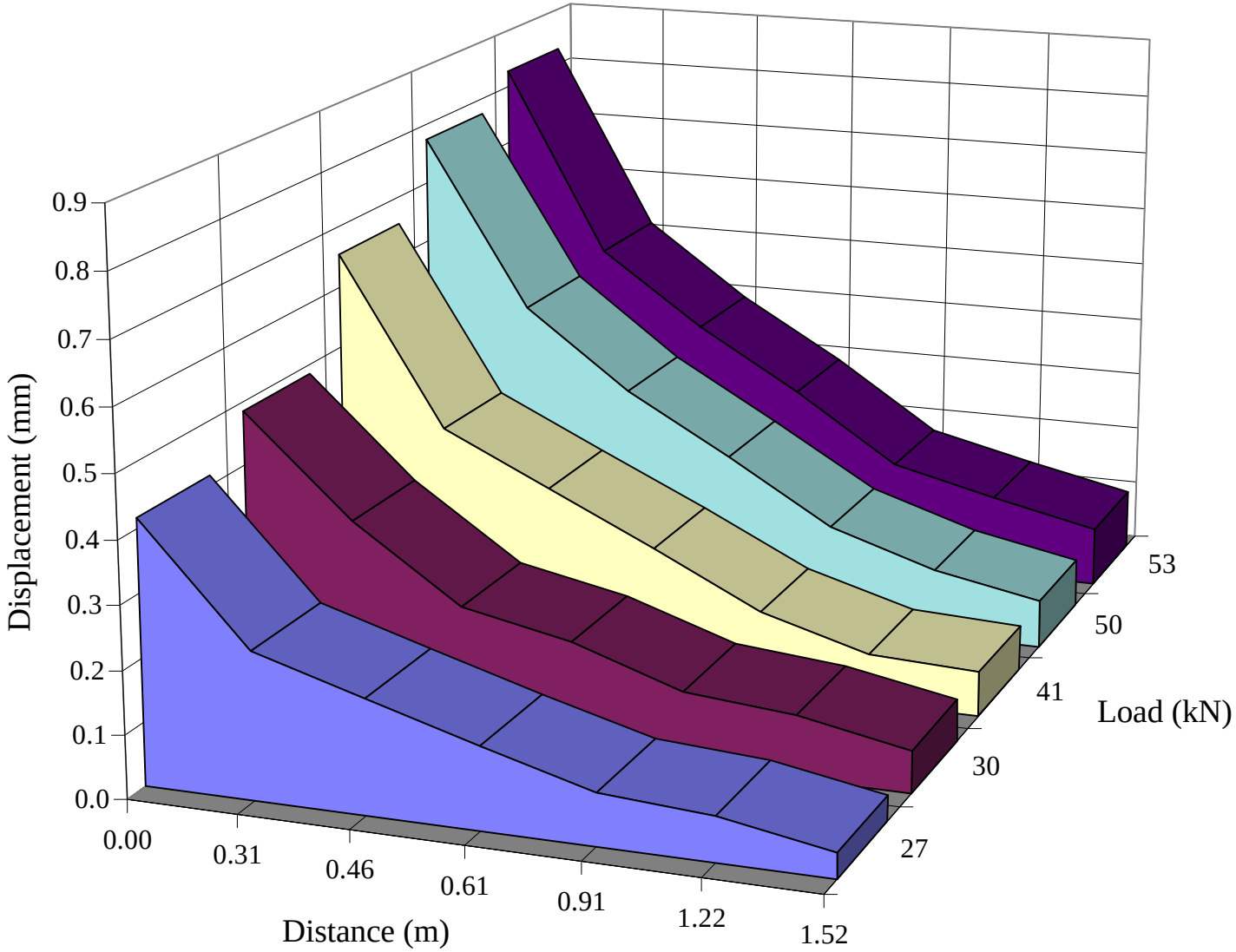

Figure B 57 Displacement as a function of distance for different FWD load levels (January 1997, section 3)

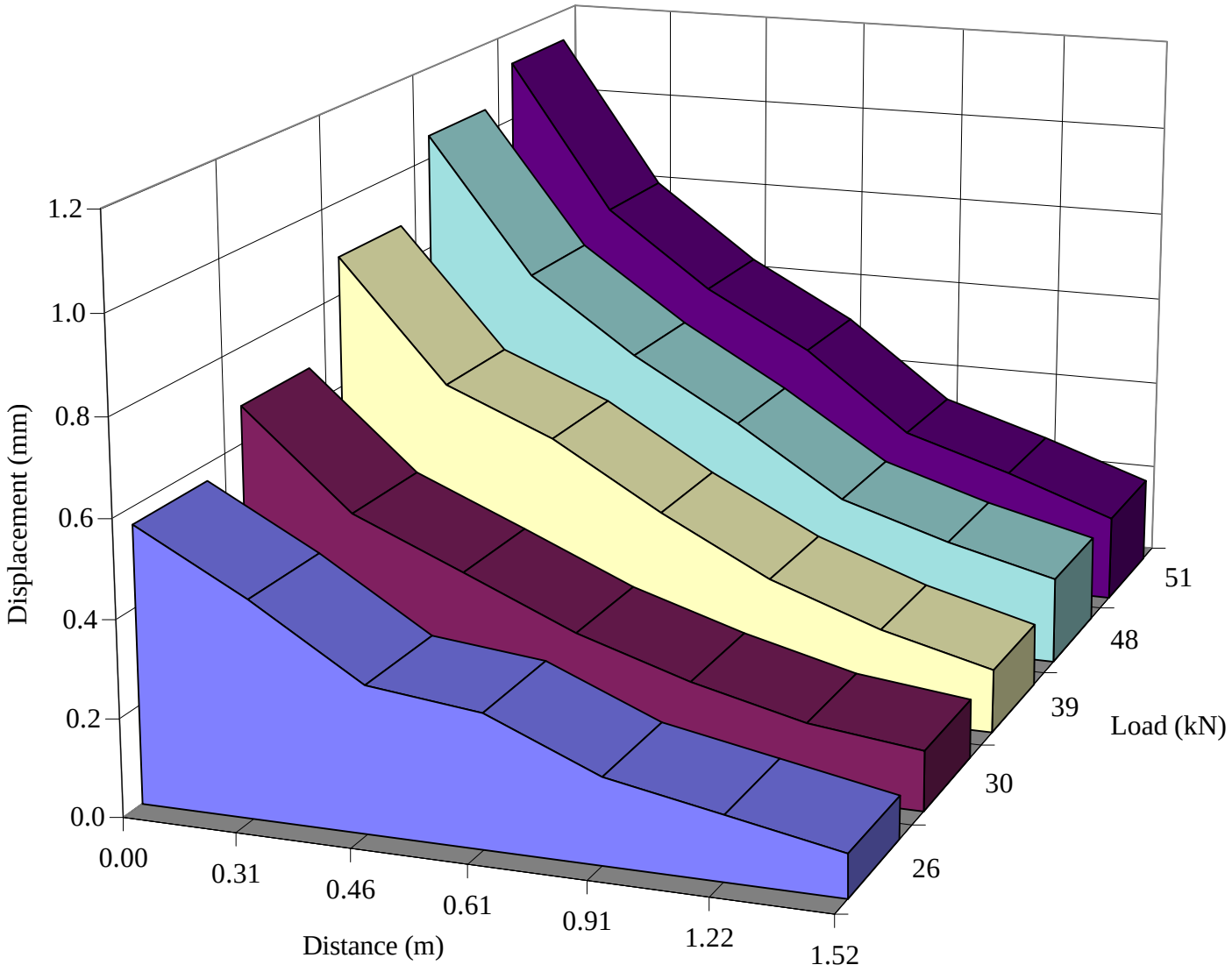

Figure B 58 Displacement as a function of distance for different FWD load levels (January 1997, section 4)

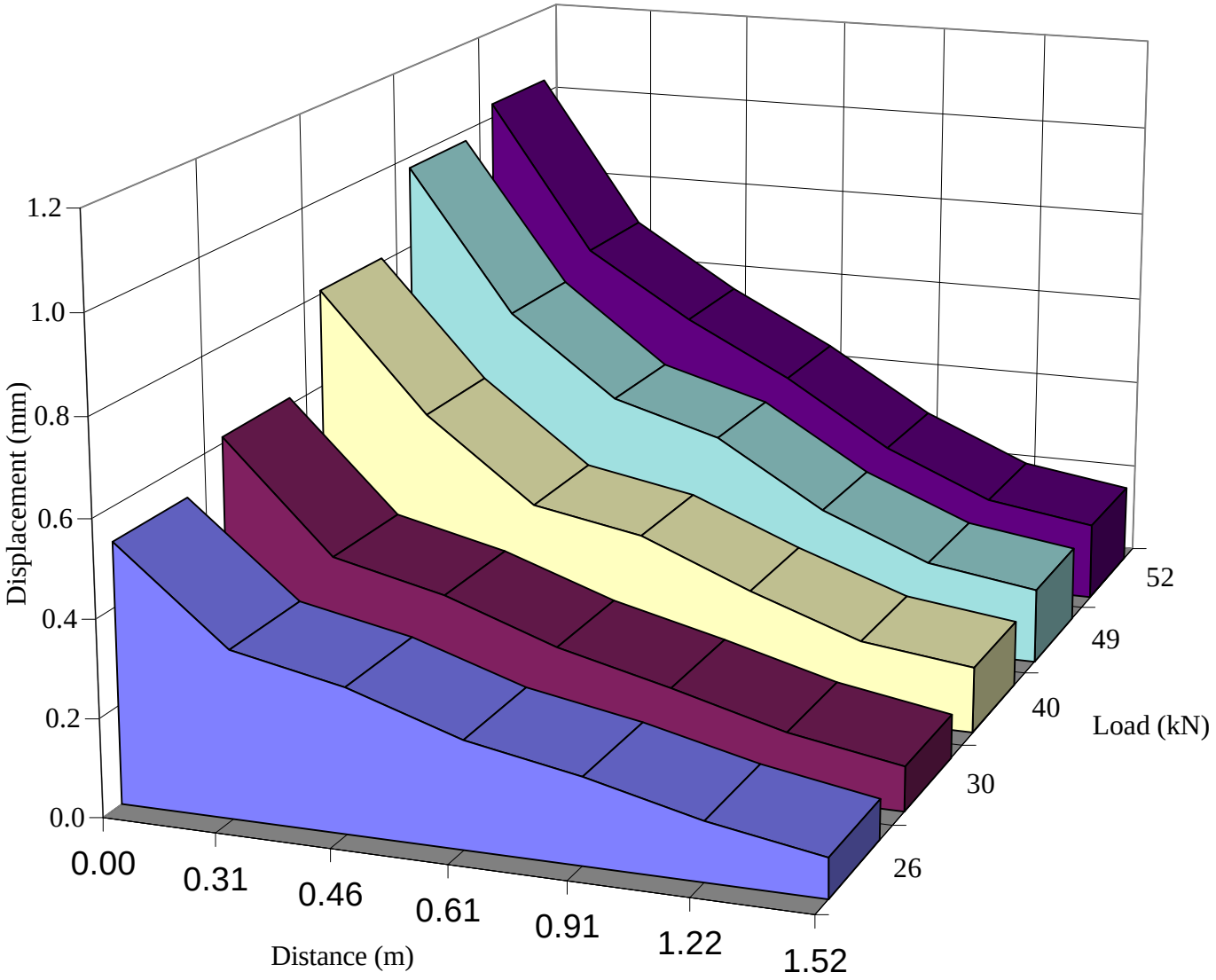

Figure B 59 Displacement as a function of distance for different FWD load levels (January 1997, section 5)

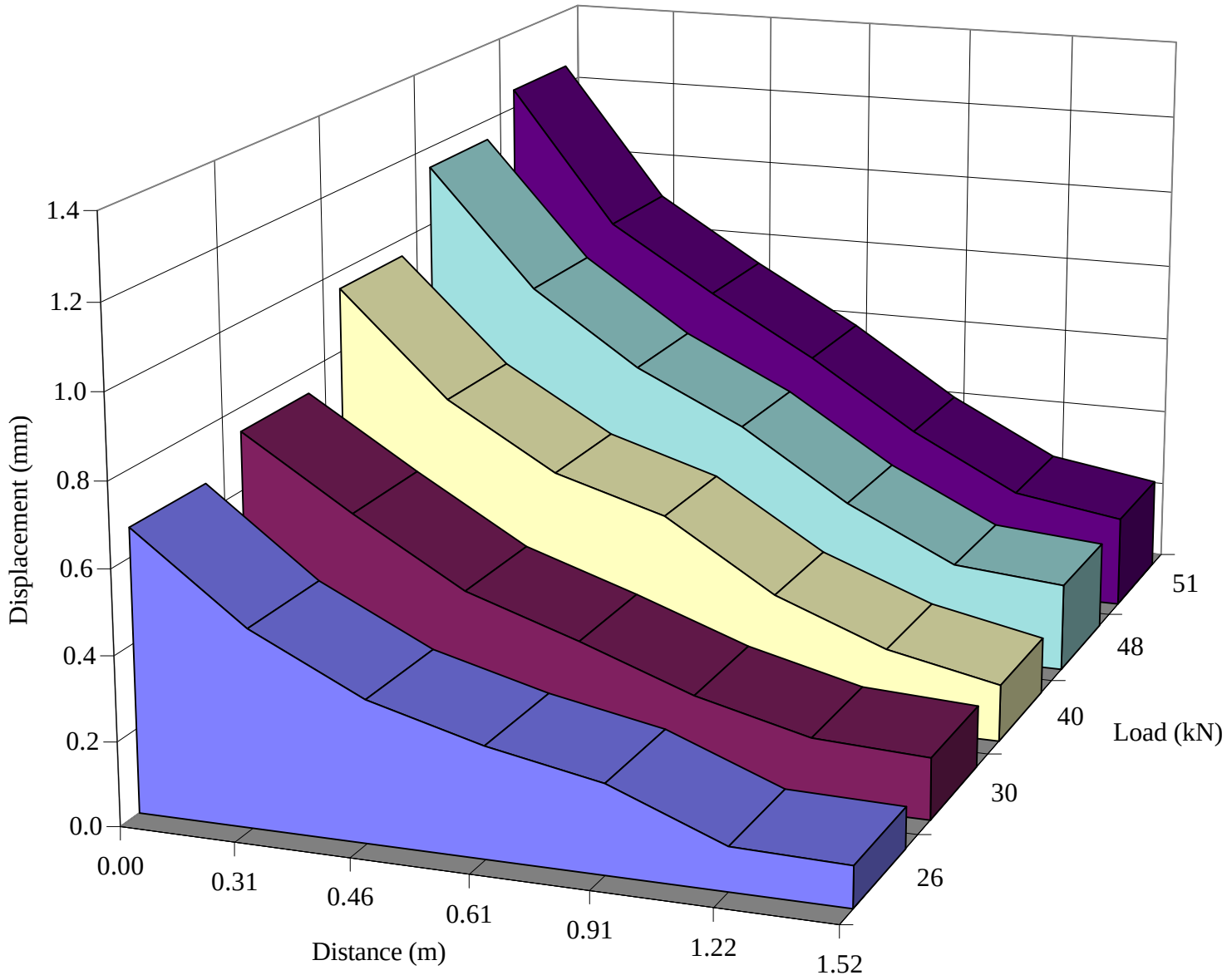

Figure B 60 Displacement as a function of distance for different FWD load levels (January 1997, section 6)

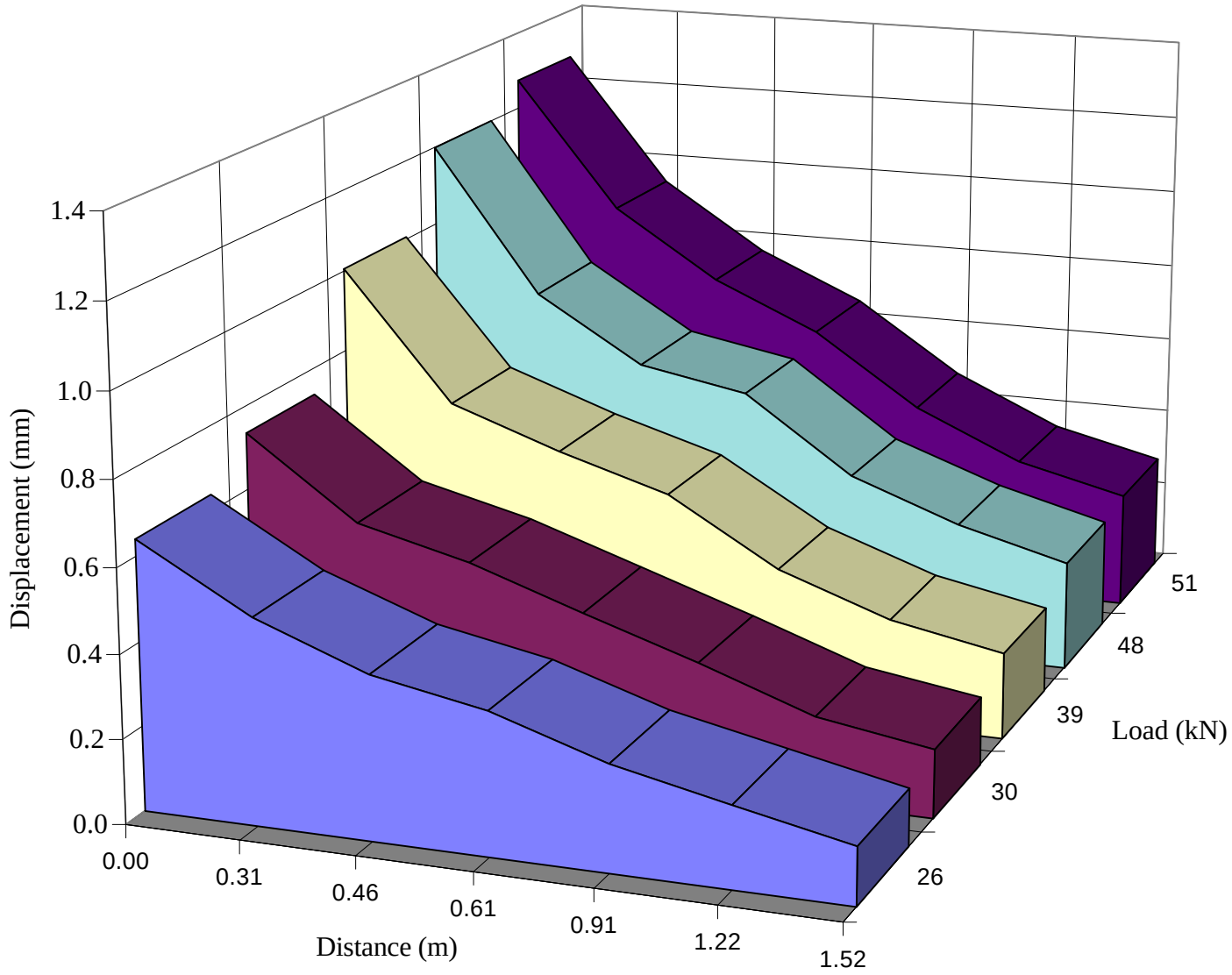

Figure B 61 Displacement as a function of distance for different FWD load levels (January 1997, section 7)

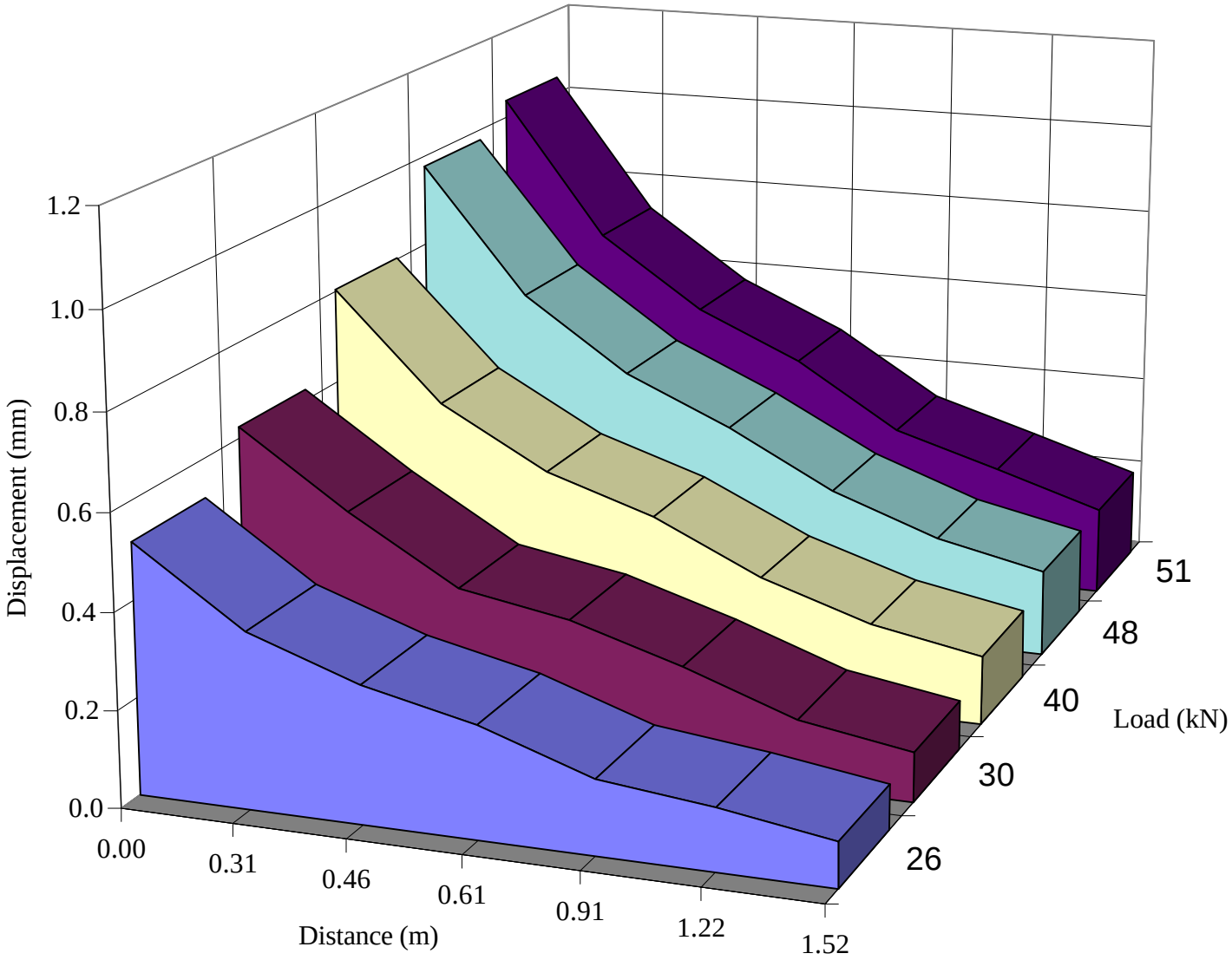

Figure B 62 Displacement as a function of distance for different FWD load levels (January 1997, section 8)

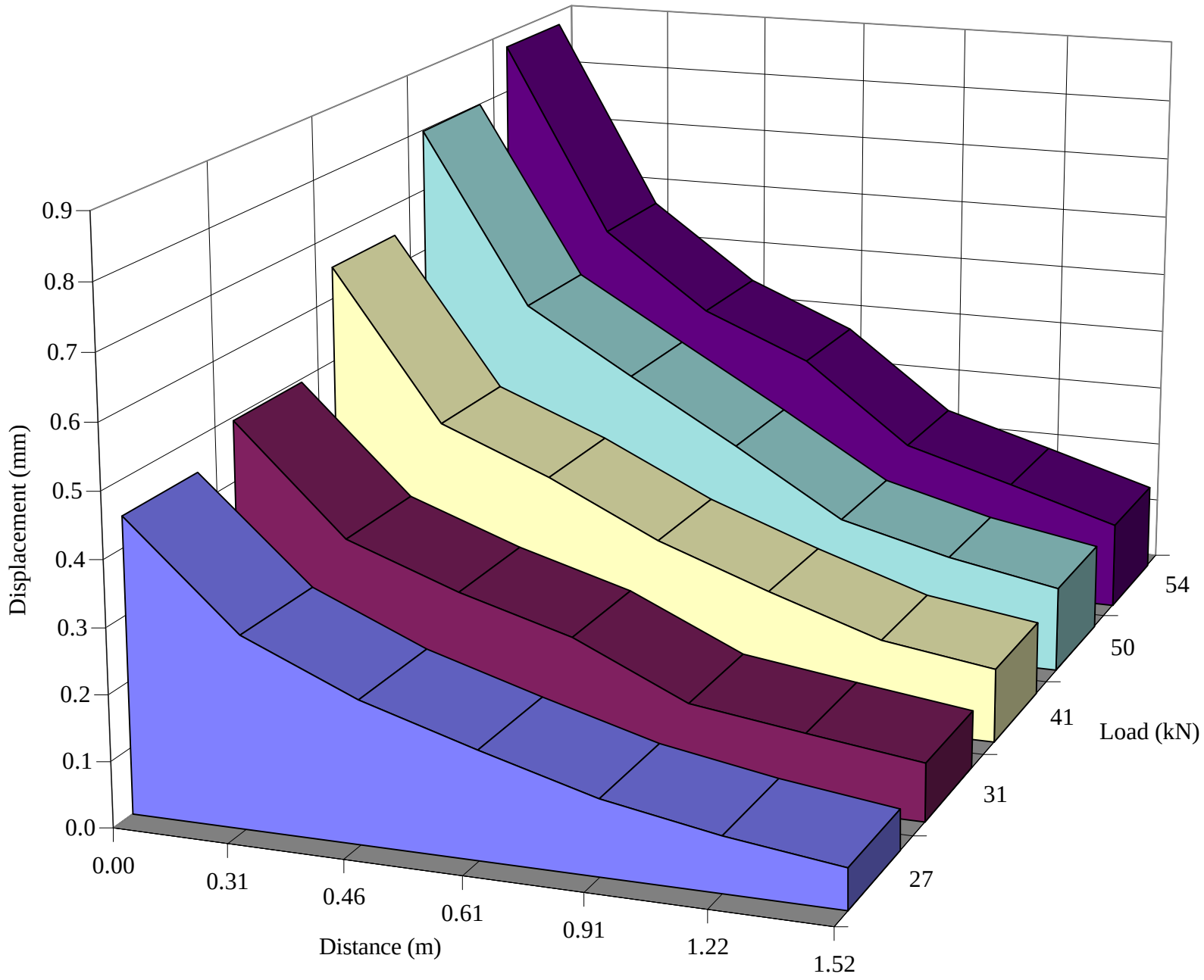

Figure B 63 Displacement as a function of distance for different FWD load levels (January 1997, section 9)

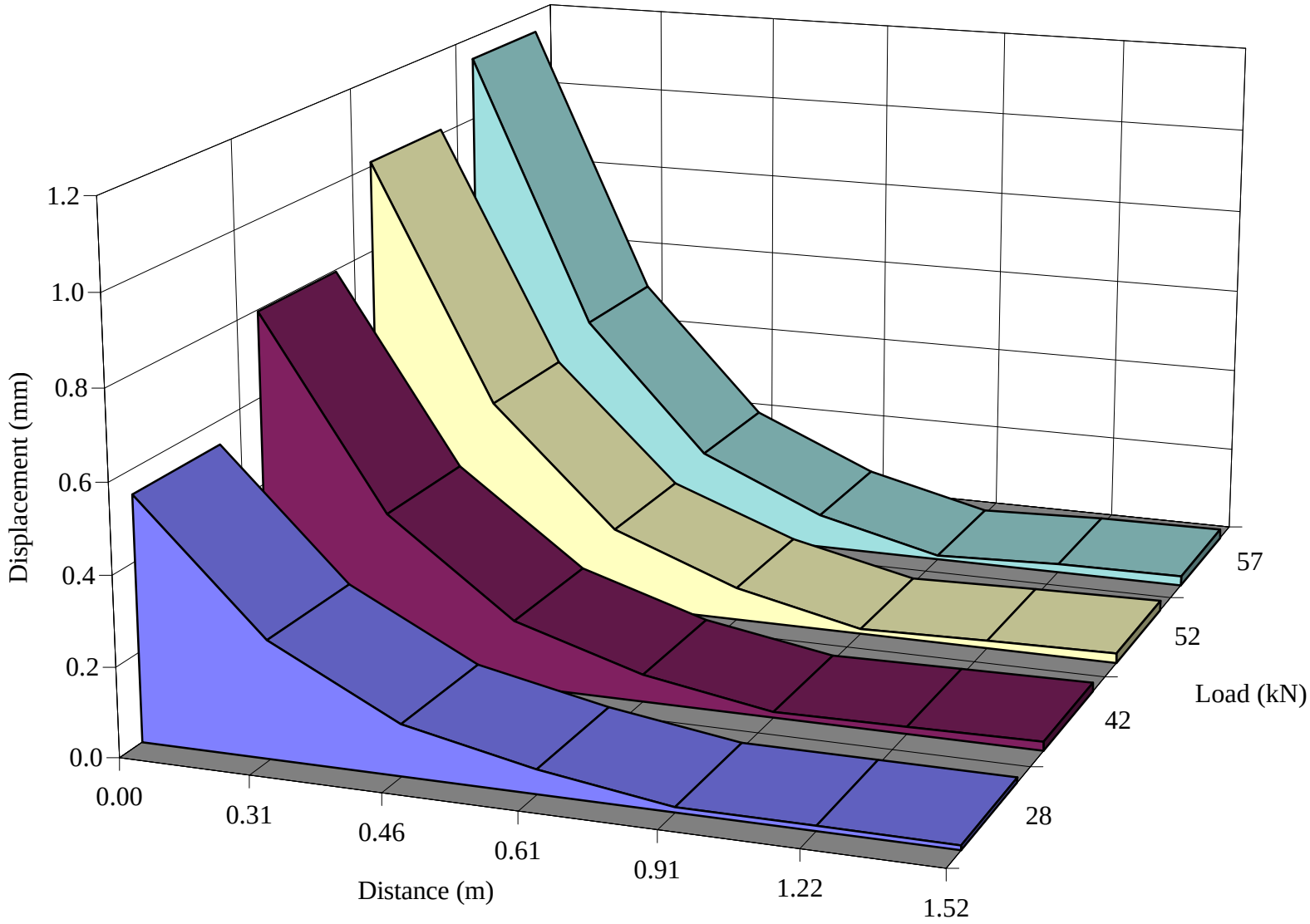

Figure B 64 Displacement as a function of distance for different FWD load levels (April 1997, section 1)

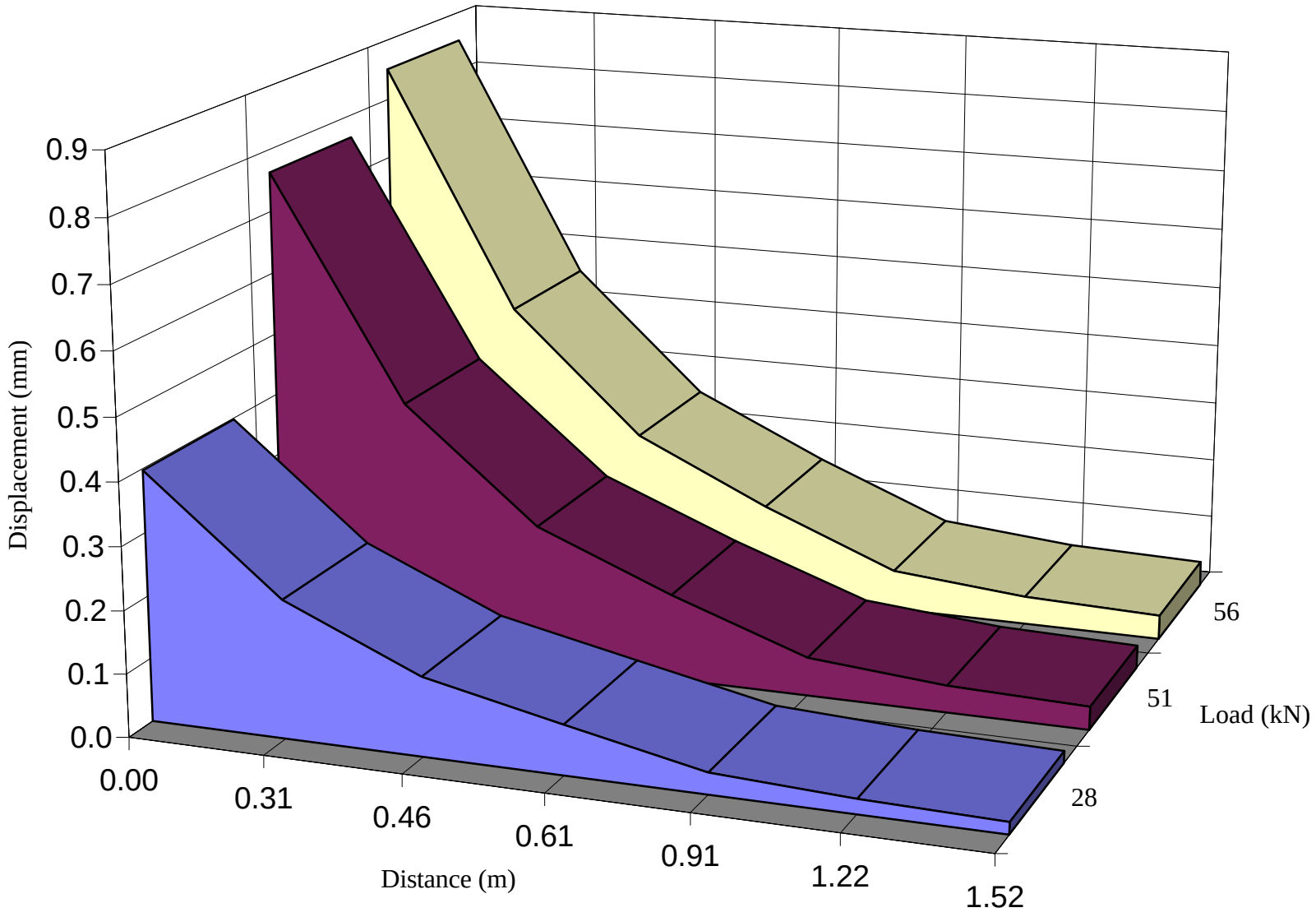

Figure B 65 Displacement as a function of distance for different FWD load levels (April 1997, section 2)

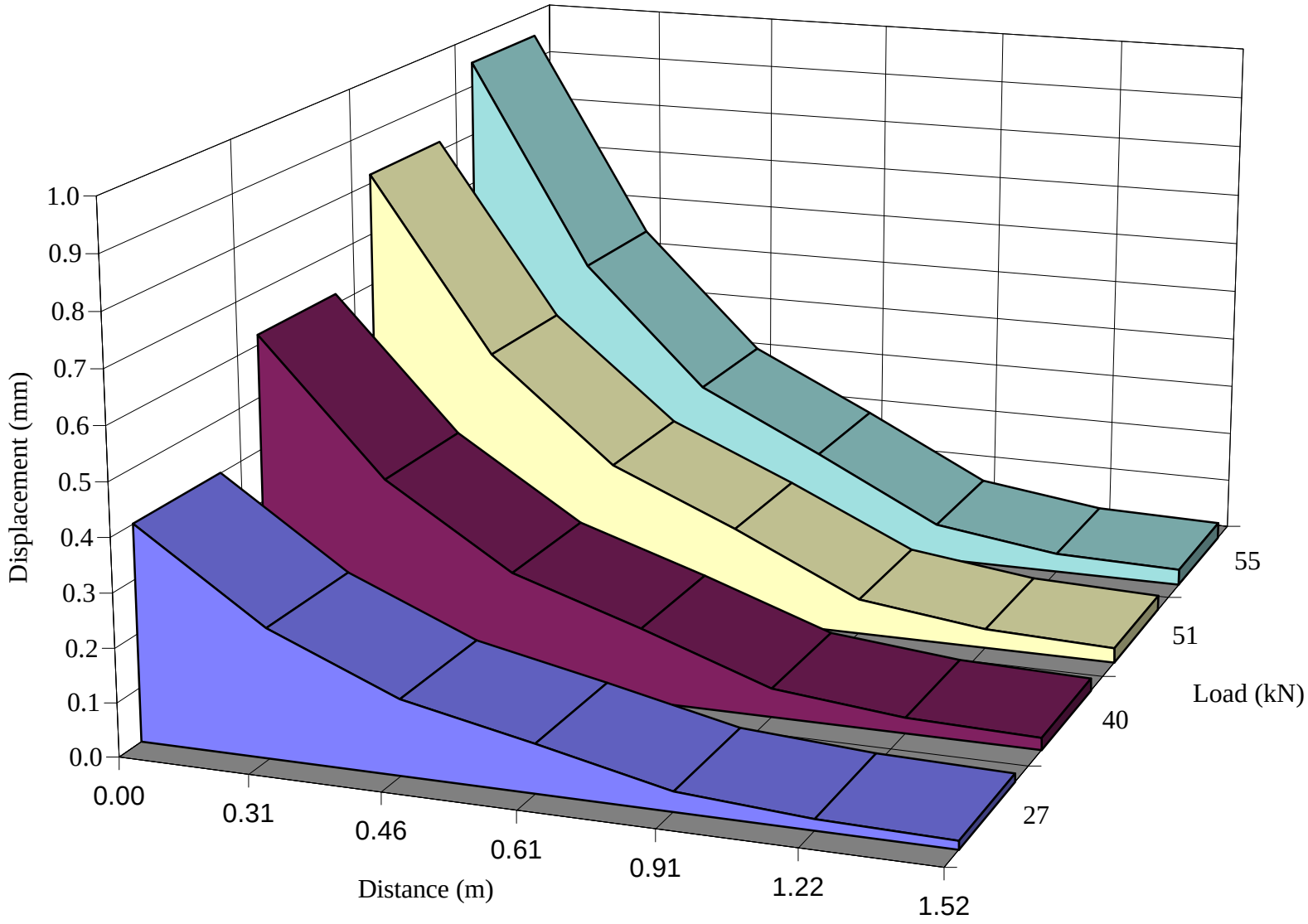

Figure B 66 Displacement as a function of distance for different FWD load levels (April 1997, section 3)

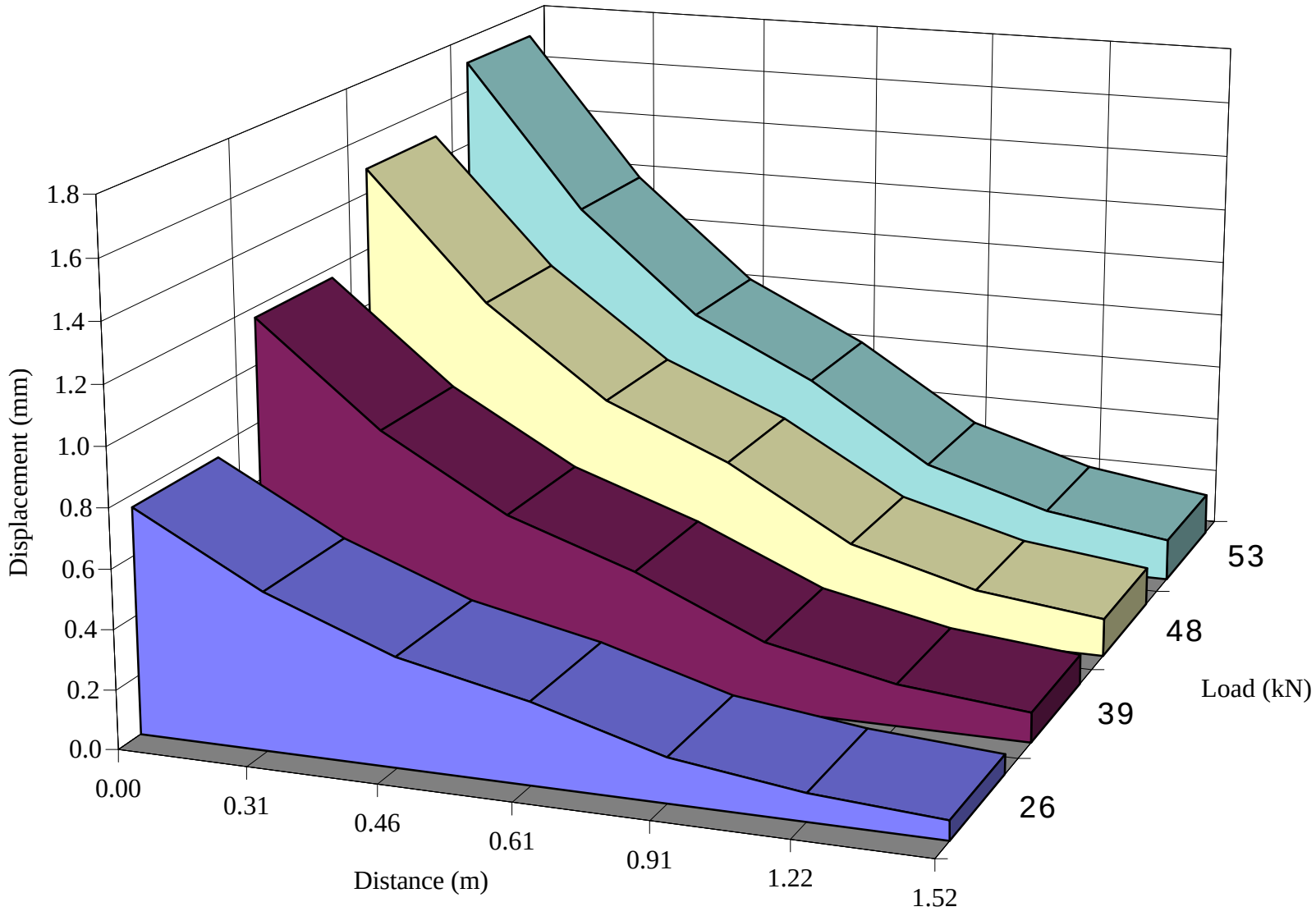

Figure B 67 Displacement as a function of distance for different FWD load levels (April 1997, section 4)

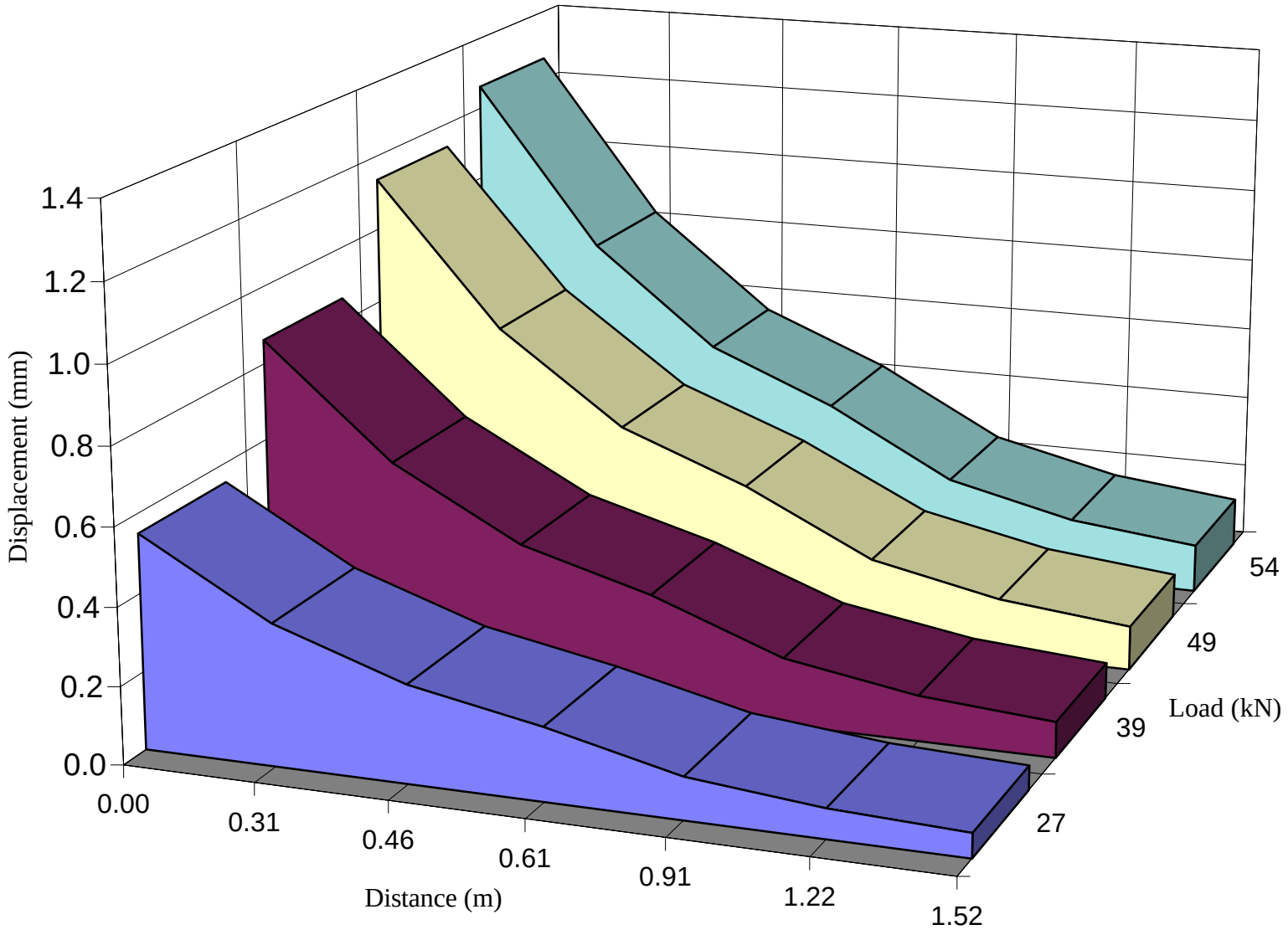

Figure B 68 Displacement as a function of distance for different FWD load levels (April 1997, section5)

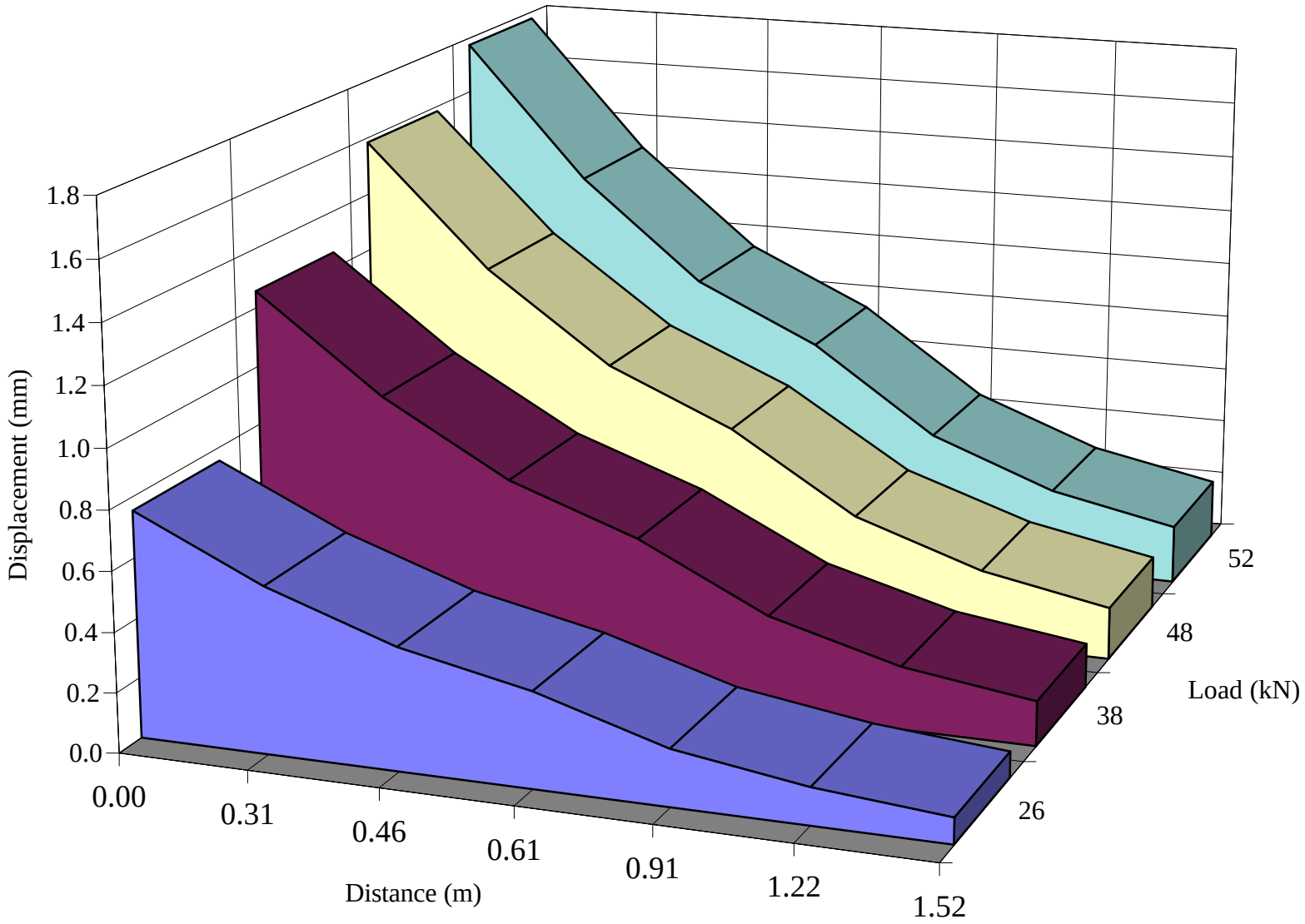

Figure B 69 Displacement as a function of distance for different FWD load levels(April 1997, section 6)

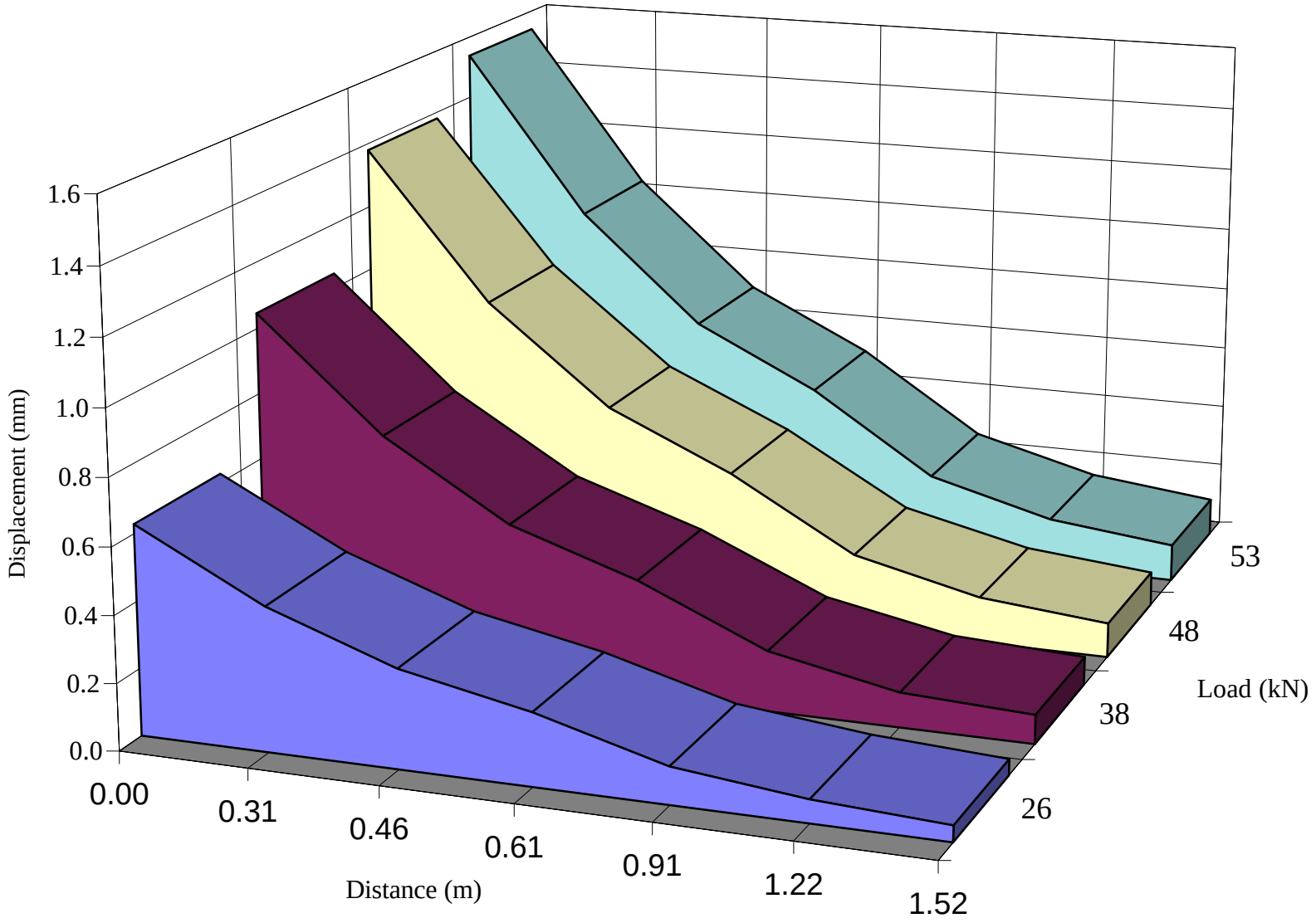

Figure B 70 Displacement as a function of distance for different FWD load levels (April 1997, section 7)

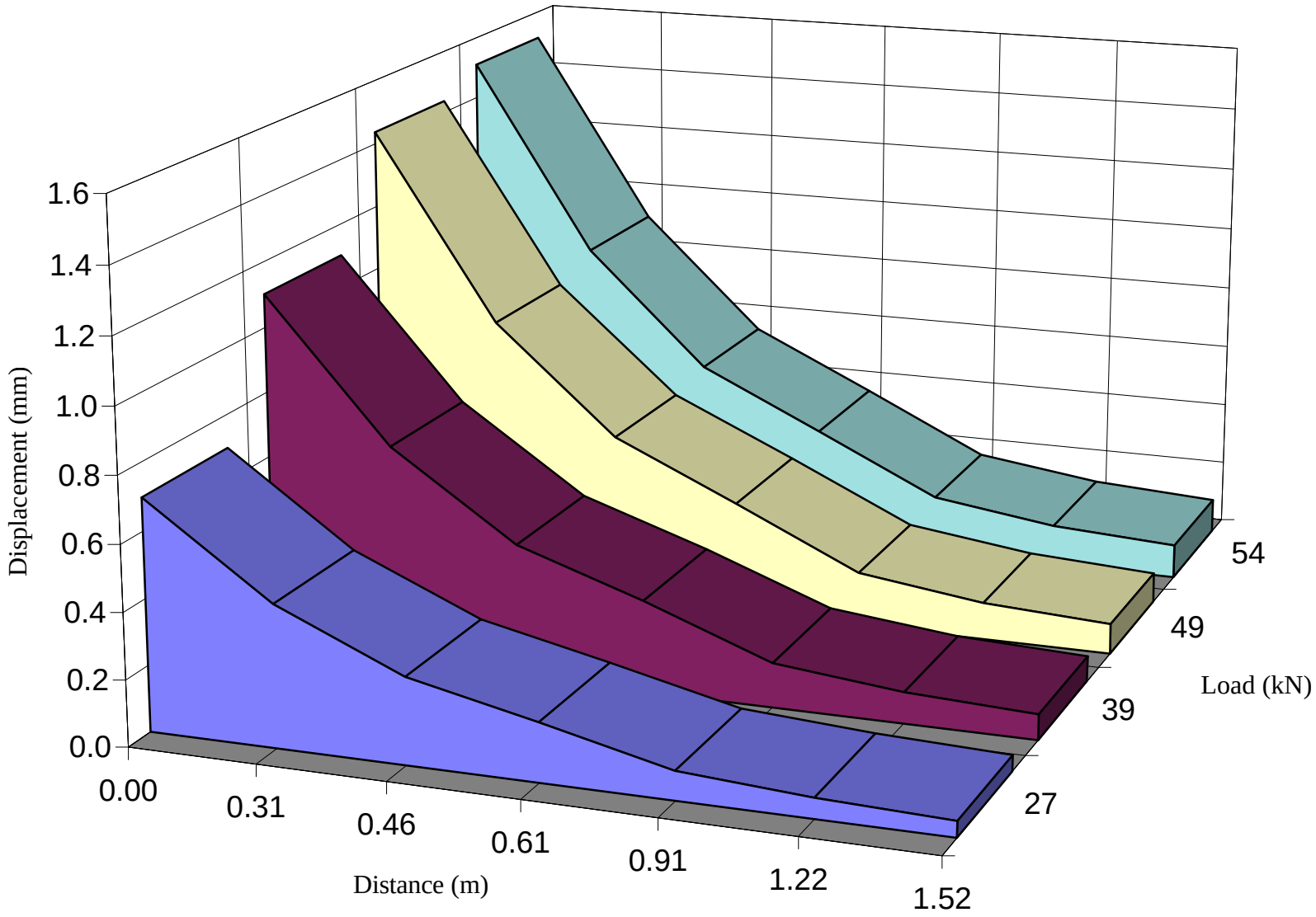

Figure B 71 Displacement as a function of distance for different FWD load levels (April 1997, section 8)

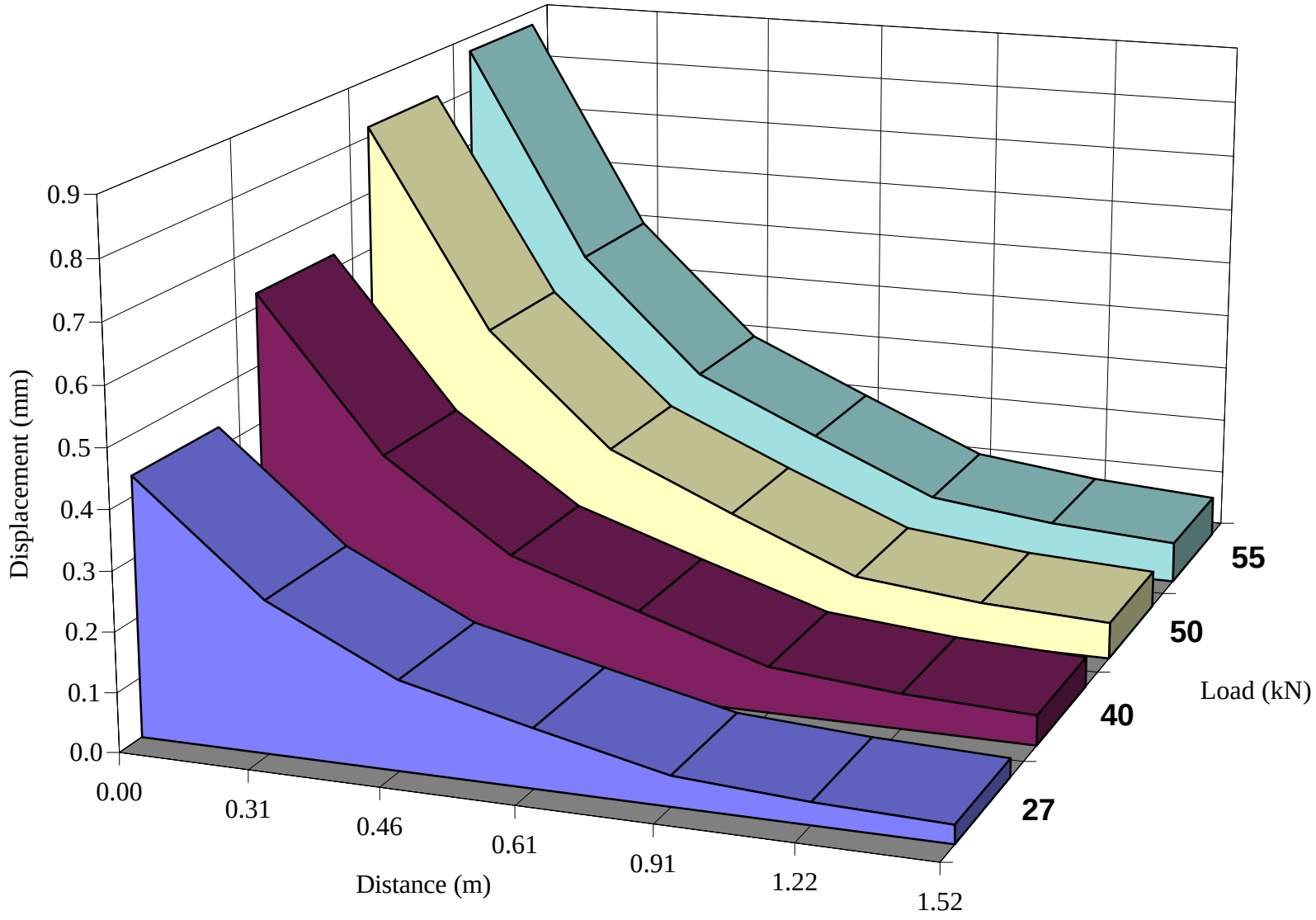

Figure B 72 Displacement as a function of distance for different FWD load levels (April 1997, section 9)

APPENDIX C

Table C1 Subgrade moduli and depth of Bedrock in October (1994)

Section	Subgrade Modulus (MPa)	Error (%)	Depth of Bed Rock (mm)
1	124	43	2000
2	125	15	3750
3	103	19	2750
4	39	13	3250
5	50	16	3750
6	34	10	4500
7	32	18	2125
8	46	26	3000
9	124	14	3750

Table C 2 Subgrade moduli and depth of Bedrock in March (1995)

Section	Subgrade Modulus (MPa)	Error(%)	Deth of Bed Rock(mm)
1	98	16.0	950
2	115	15.2	1375
3	116	10.5	1875
4	66	18.2	3750
5	57	8.7	4000
6	50	6.5	5000
7	40	9.5	2825
8	42	18.6	2300
9	118	15.3	4500

Table C 3 Subgrade moduli and depth of Bedrock in August (1995)

Section	Subgrade Modulus (MPa)	Error (%)	Depth of Bed Rock (mm)
1	105	35	1200
2	110	16	1725
3	92	11	1725
4	60	26	2500
5	75	23	3250
6	63	16	5000
7	57	30	2500
8	73	36	3000
9	103	23	1400

Table C 4 Subgrade Moduli and depth of Bedrock in April (1996)

Section	Subgrade Modulus (MPa)	Error (%)	Depth of Bed Rock (mm)
1	35	4.3	7500
2	58	7.3	5800
3	45	5.9	7500
4	31	4.4	7500
5	41	6.5	4250
6	31	6.8	7500
7	28	3.9	7500
8	39	6.4	6425
9	38	7.3	7500

Table C 5 Subgrade Moduli and depth of Bedrock in July (1996)

Section	Subgrade Modulus (MPa)	Error (%)	Depth of Bed Rock (mm)
1	37	5.4	7500
2	63	6.4	5725
3	42	5.2	7000
4	23	3.8	7500
5	32	5.8	6425
6	26	3.9	7500
7	27	5.4	5550
8	30	3.8	6150
9	33	3.9	7500

Table C 6 Subgrade Moduli and depth of Bedrock in October (1996)

Section	Subgrade Modulus (MPa)	Error (%)	Depth of Bed Rock (mm)
1	57	40	750
2	103	18	2000
3	88	8.2	2000
4	39	8.2	2000
5	51	5.1	4600
6	37	2.6	4425
7	27	8.4	1750
8	30	13.9	1500
9	84	12	2250

Table C7 Subgrade Moduli and depth of Bedrock in January (1997)

Section	Subgrade Modulus (MPa)	Error (%)	Depth of Bed Rock
1	54	6.5	7500
2	83	21.4	4475
3	78	16.0	4025
4	39	10.6	5975
5	47	14.0	5500
6	35	9.8	3800
7	28	9.2	6600
8	40	9.1	7025
9	42	10.2	6250

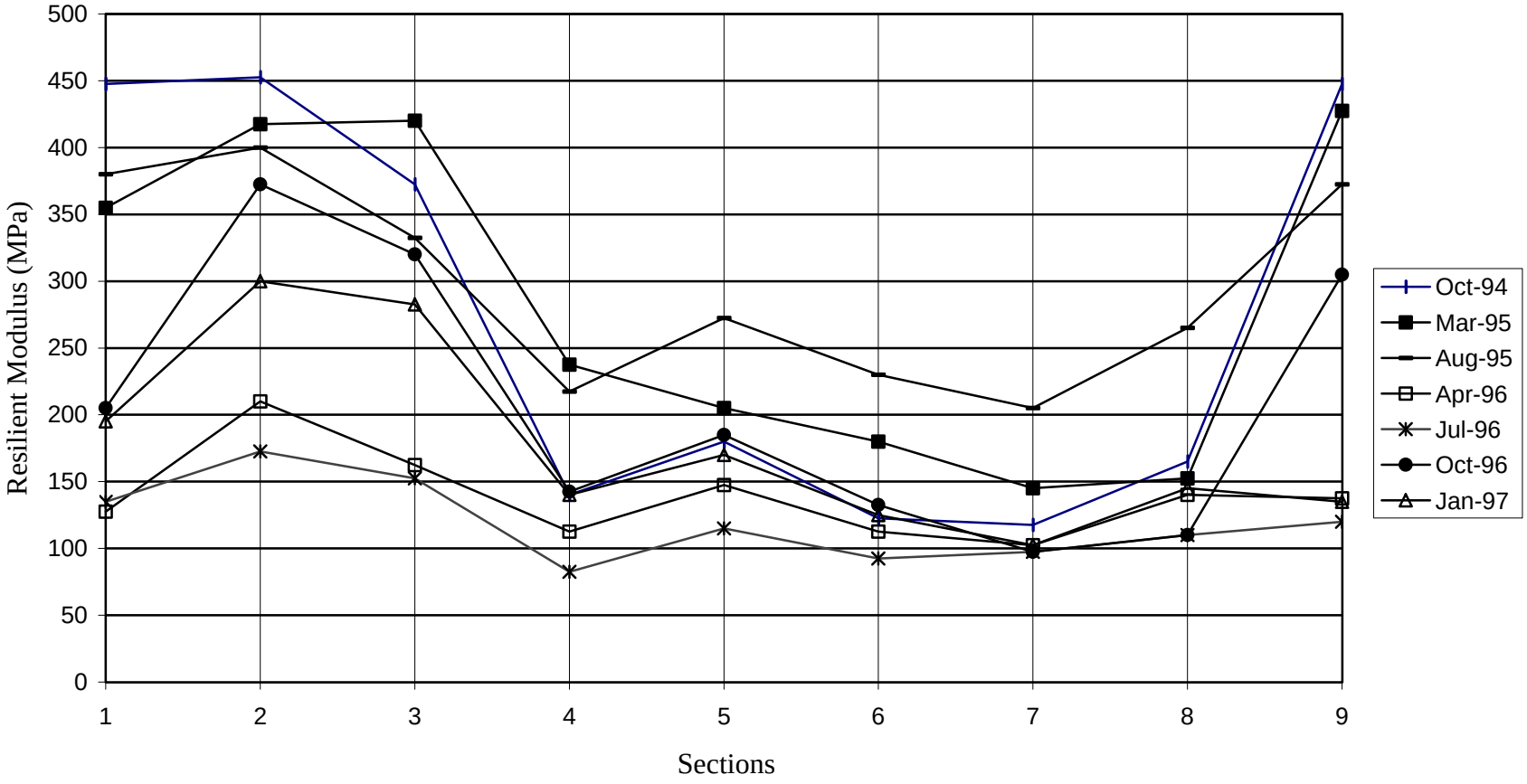

Figure C 1 Apparent subgrade resilient modulus variation over time

APPENDIX D

Table D 1 Surface deflection for 40 kN loading (ELSYM5) and pressure responses from Calibrations 1 and 2.

Aug-95

Section No.	Deflection * FWD (μm)	Deflection Elsym 5 (μm)	Vertical Stress (ELSYM 5) @ top of Subgrade (kPa)	Vertical Stress (ELSYM 5) @ Base (kPa)	Calib1 @ 56 km/hr (kPa)	Calib2 @ 56 km/hr (kPa)	Calib1 @ 64 km/hr (kPa)	Calib2 @ 64 km/hr (kPa)
1	712				218		210	
2	590	540	110	200	117	110	143	148
3	675				122	116	150	141
4	1038				93	90	103	101
5	887	645	74.0	204	88	84	104	96
6	1011				100	95	100	99
7	1108							
8	1164	620	59	215				
9	498				99	95	101	102

Calibration 1 and 2 at 40 kN load and 550 kPa tire pressure

Table D 2 Surface deflection for 40 kN loading (ELSYM5) and pressure responses from Calibrations 1, 2 and 3.

Apr-96

Section No.	Deflection * FWD (mm)	Deflection Elsym 5 (mm)	Vertical Stress (ELSYM 5) @ top of Subgrade (kPa)	Vertical Stress (ELSYM 5) @ Base (kPa)	Calib1 @ 56 km/hr (kPa)	Calib2 @ 56 km/hr (kPa)	Calib1 @ 64 km/hr (kPa)	Calib2 @ 64 km/hr (kPa)	Calib3 @ 56 km/hr (kPa)	Calib3 @ 64 km/hr (kPa)
1	1187				218		210			
2	1455	805	78		117	143	110	148	112	115
3	948				122	150	150	141		
4	1092				93	103	103	101	113	102
5	861	925	68		88	104	84	96		
6	1117				100	95	95	99	128	101
7	1055									
8	802	890	42							
9	873				99	95	101	102	101	92

Calibration 1, 2 and 3 at 40 kN load and 550 kPa tire pressure

Table D 3 Surface deflection for 40 kN loading (ELSYM5) and pressure responses from Calibrations 1 and 2.

Mar-95

Section No.	Deflection * FWD (μm)	Deflection Elsym 5 (μm)	Vertical Stress (ELSYM 5) @ top of Subgrade (kPa)	Vertical Stress (ELSYM 5) @ Base (kPa)	Calib1 @ 56 km/hr (kPa)	Calib2 @ 56 km/hr (kPa)	Calib1 @ 64 km/hr (kPa)	Calib2 @ 64 km/hr (kPa)
1	526				218		210	
2	501	525	112	186	117	110	143	148
3	449				122	116	150	141
4	600				93	90	103	101
5	823	770	82.1	177	88	84	104	96
6	820				100	95	100	99
7	1010							
8	896	853	49	172				
9					99	95	101	102

Calibration 1 and 2 at 40 kN load and 550 kPa tire pressure

Table D 4 Surface deflection for 40 kN loading (ELSYM5) and pressure responses from Calibrations 1, 2 and 3.

Apr-96

Section No.	Deflection * FWD (mm)	Deflection Elsym 5 (mm)	Vertical Stress (ELSYM 5) @ top of Subgrade (kPa)	Vertical Stress (ELSYM 5) @ Base (kPa)	Calib1 @ 56 km/hr (kPa)	Calib2 @ 56 km/hr (kPa)	Calib1 @ 64 km/hr (kPa)	Calib2 @ 64 km/hr (kPa)	Calib3 @ 56 km/hr (kPa)	Calib3 @ 64 km/hr (kPa)
1	1061				218		210			
2	879	940	74	161	117	143	110	148	112	115
3	995				122	150	150	141		
4	1302				93	103	103	101	113	102
5	1041	1105	46	168	88	104	84	96		
6	1231				100	95	95	99	128	101
7	1029									
8	971	1040	41	159						
9	933				99	95	101	102	101	92

Calibration 1, 2 and 3 at 40 kN load and 550 kPa tire pressure

Table D 5 Surface deflection for 40 kN loading (ELSYM5) and pressure responses from Calibrations 1 and 2.

Oct-96

Section No.	Deflection * FWD (μm)	Deflection Elsym 5 (μm)	Vertical Stress (ELSYM 5) @ top of Subgrade (kPa)	Vertical Stress (ELSYM 5) @ Base (kPa)	Calib1 @ 56 km/hr (kPa)	Calib2 @ 56 km/hr (kPa)	Calib1 @ 64 km/hr (kPa)	Calib2 @ 64 km/hr (kPa)
1	734				218		210	
2	725	513	110		117	110	143	148
3	610				122	116	150	141
4					93	90	103	101
5		645	74.0		88	84	104	96
6	1011				100	95	100	99
7	1010							
8	1002	1035	59	38				
9					99	95	101	102

Calibration 1 and 2 at 40 kN load and 550 kPa tire pressure

Table D 6 Surface deflection for 40 kN loading (ELSYM5) and pressure responses from Calibrations 1 and 2.

Oct-94

Section No.	Deflection * FWD (μm)	Deflection Elsym 5 (μm)	Vertical Stress (ELSYM 5) @ top of Subgrade (kPa)	Vertical Stress (ELSYM 5) @ Base (kPa)	Calib1 @ 56 km/hr (kPa)	Calib2 @ 56 km/hr (kPa)	Calib1 @ 64 km/hr (kPa)	Calib2 @ 64 km/hr (kPa)
1	564				218		210	
2	389	137		148	117	110	143	148
3					122	116	150	141
4					93	90	103	101
5		645			88	84	104	96
6					100	95	100	99
7								
8								
9	424				99	95	101	102

Calibration 1 and 2 at 40 kN load and 550 kPa tire pressure

Table D 7 Deflection readings from 40 kN, 27 kN and 50 kN of FWD load.

Section No.	40 kN (SG)	27 kN (SG)	50 kN (SG)
1			
2	53.9		460
3	235		378
4		186	385
5			
6			
7			
8			326
9	280	258	635

* Deflection values (mm)

Table D 8 Deflection readings from 40 kN, 27 kN and 50 kN of FWD load.

Section No.	40 kN (SG)	27 kN (SG)	50 kN (SG)
1		1151	
2			
3			
4			
5			
6			
7	940	707	1080
8			
9	280		

* Deflection values (mm)

APPENDIX E

Table E 1a Deflection and stress results at subgrade/base from varying transition thicknessess and transition layer resilient moduli using ELSYM5

Mar-95 Sections 1 and 3

x Deflection on HMA surface
\- Stress in Base
\+ Stress in Subgrade

Deflection (μm)		Stress (kPa)	
Defl(1)	635	Stress(1)	210.4
Defl(3)	1905	Stress(3)	117.3

	Transition Layer resilient modulus (kPa)						
Contamination (mm)	**13800**	**27600**	**34500**	**55200**	**69000**	**82800**	**103500**
2.5	358.14 x	414.0	457.2	497.8	513.1	523.2	533.4
	195.96 -	198.7	199.4	200.1	200.8	200.8	201.5
	110.4 +	111.1	111.1	111.1	111.1	111.1	111.1
5.0	421.6	467.4	482.6	510.5	520.7	528.3	535.9
	189.8	194.6	196.0	198.0	198.7	199.4	200.1
	109.7	111.1	111.1	111.1	111.8	111.8	111.8
12.5	576.6	556.3	551.2	546.1	546.1	543.6	543.6
	176.0	185.6	187.7	192.5	193.9	195.3	196.7
	92.4	95.4	96.0	96.6	96.6	97.2	97.2
25.0	642.6	596.9	586.7	569.0	563.9	558.8	553.7
	157.3	171.1	175.3	182.9	185.6	188.4	191.1
	102.1	108.3	109.7	111.1	111.8	1117.8	111.8
37.5	693.4	629.9	614.7	589.3	579.1	571.5	563.9
	140.1	158.0	162.8	173.2	178.0	181.5	185.6
	99.4	107.6	109.0	111.8	112.5	112.5	112.5
50.0	741.7	662.9	642.6	609.6	596.9	586.7	574.0
	127.0	147.0	153.2	27.6	171.1	175.3	180.8
	97.3	107.0	109.0	111.8	113.2	113.2	113.2

Table E 2a Deflection and stress results at subgrade/base from varying transition thicknessess and transition layer resilient moduli using ELSYM5

Mar-95 Sections 7 and 9

x Deflection on HMA surface
\- Stress in Base
\+ Stress in Subgrade

Deflection (μm)		Stress(kPa)	
Defl(7)	1010	Stress(7)	361
Defl(9)	1123	Stress(9)	

	Transition Layer resilient modulus (kPa)						
Contamination (mm)	**13800**	**27600**	**34500**	**55200**	**69000**	**82800**	**103500**
12.5	939.8 x	901.7	891.54	873.76	868.68	863.6	861.06
	196.65 -	198.03	198.72	199.41	199.41	200.1	201.48
	44.229 +	44.781	44.85	44.919	111.09	44.919	44.85
25.0	934.72	911.86	906.78	894.08	889	886.46	881.38
	189.75	193.2	193.89	195.96	196.65	197.34	198.72
	44.02	45.06	45.193	44.988	45.333	45.264	45.195
37.5	965.2	934.72	927.1	911.86	904.24	899.16	894.08
	182.85	186.99	188.37	191.82	193.2	194.58	195.96
	38.28	39.48	39.66	39.84	39.78	39.72	39.54
50.0	1003.3	960.12	949.96	929.64	919.48	911.86	904.24
	174.57	180.78	182.16	186.99	189.06	191.13	193.2
	44.16	45.816	46.092	46.299	46.23	46.092	45.816
62.5	1041.4	988.06	972.82	947.42	934.72	924.56	914.4
	165.6	173.19	175.26	181.47	184.23	184.92	186.3
	44.367	46.368	46.644	46.851	46.713	46.575	46.23

Table E 3a Deflection and stress results at subgrade/base from varying transition thicknessess and transition layer resilient moduli using ELSYM5

Aug-95 Sections 1 and 3

x Deflection on HMA surface
\- Stress in Base
\+ Stress in Subgrade

Deflection (μm)		Stress(kPa)	
Defl(1)	723.7	Stress(1)	210.5
Defl(3)	685.5	Stress(3)	143.2

	Transition Layer resilient modulus (kPa)						
Contamination (mm)	**13800**	**27600**	**34500**	**55200**	**69000**	**82800**	**103500**
2.5	215.392 x	416.6	475.0	510.5	528.3	538.5	548.6
	193.89 -	196.7	197.3	198.7	198.7	199.4	199.4
	74.52 +	73.8	73.8	73.8	73.8	73.8	73.1
5.0	429.3	477.5	495.3	525.8	535.9	543.6	551.2
	188.4	193.2	194.6	196.7	197.3	198.0	198.0
	75.9	74.5	74.5	73.8	73.8	73.8	73.8
12.5	589.3	571.5	566.4	561.3	561.3	558.8	558.8
	174.6	183.5	186.3	190.4	192.5	193.2	194.6
	76.6	75.9	75.2	74.5	74.5	73.8	73.8
25.0	657.9	612.1	602.0	584.2	579.1	574.0	569.0
	155.9	169.1	173.2	180.8	184.2	186.3	189.1
	75.9	76.7	76.6	75.9	75.2	75.2	74.5
37.5	706.1	645.2	629.9	604.5	594.4	586.7	579.1
	139.4	156.6	160.1	171.8	176.0	179.4	183.5
	75.2	76.6	767.3	76.6	76.6	75.9	75.2
50.0	756.9	678.2	657.9	624.8	612.1	602.0	589.3
	125.6	145.6	151.1	163.5	169.1	173.2	178.7
	74.5	78.0	78.0	78.0	77.3	76.6	75.9

Table E 4a Deflection and stress results at subgrade/base from varying transition thicknessess and transition layer resilient moduli using ELSYM5

x Deflection on HMA surface
- Stress in Base
+ Stress in Subgrade

Aug-95 Sections 4 and 6

Deflection (μm)		Stress (kPa)	
Defl(4)	1054	Stress(4)	103.5
Defl(6)	1027	Stress(6)	101

	Transition Layer resilient modulus (kPa)						
Contamination(mm)	**13800**	**27600**	**34500**	**55200**	**69000**	**82800**	**103500**
12.5	660.4 x	662.9	662.9	665.5	665.5	668.0	668.0
	71.76 +	73.1	73.8	73.8	73.8	73.8	73.8
25.0	736.6	703.6	698.5	685.8	680.7	675.6	673.1
	70.4	73.1	73.8	74.5	74.5	74.5	74.5
37.5	779.8	731.5	721.4	701.0	693.4	688.3	680.7
	69.0	73.1	73.8	74.5	74.5	74.5	74.5
62.5	866.1	789.9	772.2	739.1	723.9	713.7	701.0
	68.0	73.1	74.5	75.9	75.9	75.9	75.9
75.0	911.9	823.0	800.1	759.5	741.7	731.0	713.7
	67.9	73.8	75.2	76.6	76.6	76.6	76.6
87.5	962.7	856.0	828.0	779.8	779.8	744.2	723.9
	68.1	74.5	75.9	77.3	77.3	78.0	78.0
100.0	1013.5	889.0	858.5	802.6	777.2	759.5	739.1
	68.5	75.2	77.3	78.7	78.7	78.7	78.0
112.0	1064.3	924.6	889.0	825.5	797.6	777.2	751.8
	70.4	77.3	78.7	80.0	80.0	80.0	79.4

Table E 5a Deflection and stress results at subgrade/base from varying transition thicknessess and transition layer resilient moduli using ELSYM5

Apr-96 Sections 1 and 3

x Deflection on HMA surface
\- Stress in Base
\+ Stress in Subgrade

Deflection (μm)		Stress(kPa)	
Defl(1)	1188	Stress(1)	112
Defl(3)	948		

	Transition Layer resilient modulus (kPa)						
Contamination(mm)	**13800**	**27600**	**34500**	**55200**	**69000**	**82800**	**103500**
2.5	711.2 x	782.3	805.2	830.6	838.2	843.3	845.8
	159.39 -	160.8	161.5	162.2	162.2	162.2	162.2
	79.35 +	79.4	80.0	80.0	80.0	80.0	80.0
5.0	764.5	805.2	815.3	835.7	840.7	843.3	845.8
	155.9	158.7	159.4	160.1	160.8	160.8	161.5
	79.4	80.0	80.0	80.0	80.0	80.0	80.0
12.5	868.7	853.4	8470.9	848.4	845.8	845.8	843.3
	146.3	151.1	152.5	155.3	1536.6	157.3	158.0
	68.4	69.6	69.6	69.6	69.6	69.6	69.6
25.0	929.6	894.1	883.9	868.7	863.6	858.5	853.4
	131.1	140.1	142.1	147.0	149.0	151.1	153.2
	78.0	80.0	80.7	81.4	81.4	81.4	80.7
37.5	980.4	927.1	914.4	891.5	881.4	876.3	866.1
	118.0	129.0	131.8	138.7	142.1	144.9	147.7
	77.3	80.7	81.4	82.1	82.1	82.1	82.1
50.0	1031.2	962.7	944.9	914.4	901.7	891.5	881.4
	106.3	119.4	123.5	131.8	135.9	139.4	1406.2
	77.3	81.4	82.8	83.5	83.5	82.8	82.8
62.5	1082.0	998.2	977.9	939.8	922.0	909.3	896.6
	98.0	112.5	117.3	127.0	131.8	135.2	140.1
	77.3	82.8	83.5	84.9	84.9	84.2	84.2

Table E 6a Deflection and stress results at subgrade/base from varying transition thicknessess and transition layer resilient modulus using ELSYM5

Apr-96 Sections 4 and 6

x Deflection on HMA surface
\- Stress in Base
\+ Stress in Subgrade

Deflection (μm)		Stress in kPa	
Defl (4)	1093	Stress (4)	101.4
Def (6)	1117	Stress (6)	93.84

	Transition Layer resilient modulus (kPa)						
Contamination (mm	13800	27600	34500	55200	69000	82800	103500
12.5	973 x	972.8	970.6	978.8	972.8	842.8	845.8
	52.5 +	53.5	53.7	53.8	53.8	162.2	163.0
25.0	1031.2	1005.8	1000.7	990.6	985.5	843.2	845.9
	53.9	54.1	54.2	54.4	55.7	160.8	161.5
37.5	1076.9	1038.9	1028.7	1010.9	1003.3	845.8	843.3
	53.6	54.7	54.9	55.1	54.9	157.3	158.1
50.0	1122.7	1071.9	1056.6	1033.7	1021.1	1013.4	1003.3
	53.4	55.4	55.7	55.9	55.8	55.5	147.6
62.5	1170.9	1089.7	1089.6	1056.6	1041.4	1031.2	1016.5
	54.0	56.7	56.6	56.7	56.6	56.3	56.6
75.0	1224.3	1143.0	1122.7	1082.1	1064.3	1049.1	1031.2
	54.6	57.7	57.6	57.8	57.5	57.1	56.6
87.5	3.0	1182.4	1155.7	1107.4	1084.6	1069.3	1061.8
	55.5	58.4	58.8	58.9	58.5	58.1	58.3

Table E 7a Deflection and stress results at subgrade/base from varying transition thicknessess and transition layer resilient moduli using ELSYM5

Apr-96 Sections 7 and 9

x Deflection on HMA surface	Deflection (μm)	Stress in kPa
- Stress in Base	Defl (7) 1055	Stress
+ Stress in Subgrade	Defl (9) 873	Stress 92

	Transition Layer resilient modulus (kPa)					
Contamination (mm)	**13800**	**27600**	**55200**	**69000**	**82800**	**103500**
12.5	970.28 x	934.7	911.9	906.8	901.7	899.2
	41.745 +	42.2	42.4	423.7	423.0	42.3
25.0	972.8	950.0	932.2	929.6	924.6	922.0
	41.7	42.5	42.8	42.7	42.7	42.6
37.5	1003.3	972.8	950.0	944.9	939.8	932.2
	41.7	42.9	43.2	43.1	43.1	42.9
50.0	1038.9	998.2	967.7	960.1	952.5	942.3
	41.9	43.4	43.7	43.6	43.5	43.3
62.5	1079.5	1026.2	988.1	975.4	965.2	952.5
	42.2	43.9	44.3	44.2	44.0	43.6
75.0	1120.1	1056.6	1031.2	993.1	980.4	965.2
	42.6	44.6	44.9	44.7	44.5	44.1

Table E 8a Deflection and stress results at subgrade/base from varying transition thicknessess and transition layer resilient moduli using ELSYM5

Jul-96 Sections 1 and 3

x Deflection on HMA surface
- Stress in Base
+ Stress in Subgrade

Deflection (μm)
Defl(3) 995.3

Stress in kPa

	Transition Layer resilient modulus (kPa)						
Contamintion (mm)	**13800**	**27600**	**34500**	**55200**	**69000**	**82800**	**103500**
5.0	889 x	932.2	944.9	962.7	967.7	972.8	972.8
	150.4 -	152.5	153.2	1538.7	154.6	154.6	155.3
	72.45 +	73.1	73.1	73.1	73.1	73.1	73.1
12.5	988.1	977.9	975.4	972.8	970.3	967.7	965.2
	141.5	145.6	147.0	149.0	149.7	151.1	151.8
	72.5	73.8	73.8	73.8	73.8	73.8	73.8
25.0	1051.6	1016.0	1008.4	993.1	988.1	983.0	977.9
	127.0	134.6	136.6	140.8	142.8	144.2	146.3
	63.0	64.8	64.8	64.8	64.8	64.8	64.8
37.5	1104.9	1054.1	1041.4	1018.5	1008.4	1003.3	993.1
	113.9	123.5	126.3	132.5	135.2	138.0	141.5
	72.5	75.2	75.9	75.9	0.0	75.9	75.2
50.0	1158.2	1092.2	1074.4	1043.9	1031.2	1021.1	1008.4
	102.1	113.9	118.0	125.6	129.0	132.5	136.6
	73.1	76.6	76.6	77.3	77.3	76.6	76.6
87.5	1211.6						
	98.7						

Table E 9a Deflection and stress results at subgrade/base from varying transition thicknessess and transition layer resilient moduli using ELSYM5

Jul-96 Sections 4 and 6

x Deflection on HMA surface
\- Stress in Base
\+ Stress in Subgrade

Deflection (μm)	Stress in kPa
Defl (4) 1302	Stress (4) 98.7
Defl (6) 1231	Stress (6) 91.84

	Transition Layer resilient modulus (kPa)						
Contamination (mm)	**13800**	**27600**	**34500**	**55200**	**69000**	**82800**	**103500**
12.5	1153.16 x 47.472 +	1153.2 47.9	1155.7 48.0	1155.7 48.0	1153.2 48.0	1153.2 48.0	1150.6 47.8
25.0	1211.6 47.8	1188.7 48.6	1183.6 48.7	1170.9 48.7	1165.9 48.7	1163.3 48.6	1155.7 48.4
37.5	1262.4 48.3	1224.3 49.4	1214.1 49.5	1196.3 49.5	1188.7 49.4	1181.1 49.3	1170.9 49.0
50.0	1313.2 49.0	1262.4 50.3	1249.7 50.5	1224.3 50.4	1211.6 50.2	1201.4 50.0	1176.0 49.5
62.5	1366.5 49.8	1303.0 51.3	1285.2 51.5	1252.2 51.4	1234.4 51.1	1221.7 50.4	1211.6 50.2
75.0	1424.9 50.7	1343.7 52.6	1323.3 52.6	1280.2 52.4	1259.8 52.1	1259.8 51.7	1221.7 51.7

Table E 10a Deflection and stress results at subgrade/base from varying transition thicknessess and transition layer resilient moduli using ELSYM5

Jul-96 Section 7and 9

x Deflection on HMA surface
- Stress in Base
+ Stress in Subgrade

Deflection (μm)
Defl (9) 933

Stress in kPa
Stress (9) 74.8

	Transition Layer resilient modulus (kPa)			
Contamination (mm)	13800	27600	34500	55200
12.5	1109.98 x	1074.4	1064.3	1051.6
	189.06 -	190.4	191.1	191.8
	36.915 +	37.3	37.3	37.3
25.0	1117.6	1097.3	1092.2	1082.0
	182.9	185.6	186.3	187.7
	37.1	37.7	37.7	37.8
37.5	1143.0	1125.2	1117.6	1102.4
	176.0	179.4	180.8	183.5
	32.5	33.2	33.3	33.3
50.0	1193.8			
	168.4			
	37.8			

Table E 1b Deflection and stress results after varying base resilient modulus using ELSYM5
for 100mm base layer Mar-95

285163	241500	207000	172500	138000	103500	69000	55200
551.0	564.1	579.5	594.2	617.0	645.0	691.5	719.2
744.0	732.2	716.4	699.3	676.5	645.5	599.5	572.3
404.0	411.3	419.0	424.0	429.0	432.5	427.3	422.5

Deflections (μm)
Stress in kPa

Table E 2b Deflection and stress results after varying base resilient modulus using ELSYM5
for 200mm base layer Mar-95

252464	241500	207000	172500	138000	103500	69000	55200
871.2	878.8	914.4	955.0	1003.3	1069.3	1163.3	
201.5	198.7	189.1	178.0	165.6	150.4	131.1	
44.8	45.4	47.4	49.6	52.1	54.7	57.2	

Deflections (μm)
Stress in kPa

Table E 3b Deflection and Stress results after varying base resilient modulus using ELSYM5
for 100mm base layer
Aug-95

285163	241500	207000	172500	138000	103500	69000	55200
551.2	563.9	579.1	594.4	617.2	645.2	690.9	
202.2	198.7	194.6	189.8	183.5	175.3	162.8	
109.7	318.8	113.9	115.2	116.6	117.3	115.9	

Deflections (μm)
Stress in kPa

Table E 4b Deflection and Stress results after varying base resilient modulus using ELSYM5 for 150mm base layer

Aug-95

272543	241500	207000	172500	138000	103500	69000	55200
655.32	673.1	693.42	721.36	751.84	795.02	861.06	899.16
73.83	75.9	77.97	80.04	82.11	83.49	84.87	84.18

Deflections (μm)

Stress in kPa

Table E 5b Deflection and Stress results after varying base resilient modulus using ELSYM5 for 100mm base layer

Apr-96

282900	241500	207000	172500	138000	69000	55200
828.1	845.8	863.6	883.9	906.7	982.9	899.2
163.5	159.4	155.9	151.9	146.3	130.4	84.2
79.4	81.4	83.5	84.9	86.9	89.1	98.72

Deflections (μm)

Stress in kPa

Table E 6b Deflection and Stress results after varying base resilient modulus using ELSYM5 for 150mm base layer

Apr-96

270045	241500	207000	172500	138000	103500	82800	69000
935	957.5	985.5	1017.5	1057.5	1107.5	1145	1177.5
53.1	54.6	56.5	58.6	60.9	63.2	64.8	65.1

Deflections (μm)

Stress in kPa

Table E 7b Deflection and stress results after varying base resilient modulus using ELSYM5 for 200mm base layer

Apr-96

303345	276000	241500	207000	172500	138000	103500	82800
255	265	267.2	272.5	284.9	1030	1095	1142.5
39.8	41.1	46.4	48.7	52.0	49.3	51.8	53.3

Deflections (μm)

Stress in kPa

Table E 8b Deflection and stress results after varying base resilient modulus using ELSYM5 for 100mm base

Jul-96

282900	241500	207000	172500	138000	103500	69000	55200
932.5	952.5	972.5	995.0	1020.0	1055.0	1100.0	1127.5
157.3	153.2	149.7	144.9	140.1	133.2	124.9	120.1
73.1	74.5	76.6	78.7	80.0	82.1	82.8	82.8

Deflections (μm)

Stress in kPa

Table E 8b Deflection and stress results after varying base resilient modulus using ELSYM5 for 100mm base

Jul-96

1025000	875000	750000	625000	500000	375000	250000	55200
995.0	1020.0	1042.5	1067.5	1100.0	1140.0	1195.0	49.1
180.1	176.0	171.8	167.7	162.2	154.6	144.9	140.1
81.4	84.2	86.3	88.3	91.1	93.2	95.2	95.2

Deflections (μm)

Stress in kPa

Table E 9b Deflection and Stress results from varying Base Resilient Modulus using ELSYM5 for 200mm Base

Jul-96

282900	241500	207000	172500	138000	103500	69000	55200
1007.5	1047.5	1087.5	1135.0	1192.5	1267.5	1370.0	1392.5
200.8	190.4	180.8	169.7	156.6	141.5	122.8	119.6
35.7	37.7	39.5	41.6	44.0	46.6	49.4	52.1

Deflections (μm)

Stress in kPa

Table E 10b Deflection and Stress results from varying Base Resilient Modulus using ELSYM5 for 200mm Base

Jul-96

282900	**241500**	**207000**	**172500**	**138000**	**103500**	**69000**
1007.5	1047.5	1087.5	1135.0	1192.5	1267.5	1370.0
200.8	190.4	180.8	169.7	156.6	141.5	122.8
35.7	37.7	39.5	41.6	44.0	46.6	49.4

Deflections (μm)

Stress in kPa

Table E 11 A summary of Thickness of intermixing layer and elastic modulus (MPa) using ELSYM5 analysis

	Date			
	Mar-95	**Aug-95**	**Apr-96**	**Jul-96**
Section	**Transition Layer thickness, mm (Resilient Modulus, MPa)**			
1	12.5 (82.8-103.5 MPa)	50.0 (13.8-27.6 MPa)	62.5 (13.8-34.5)	62.5 (13.8-27.6) 50.0 (34.5-55.2)
3	2.5 (27.6-34.5)	25 (27.6-34.5) 37.5 (13.8-27.6)	50.0 (13.8- 27.6) 62.5 (34.5- 55.2)	50.0 (27.6- 34.5)
4		112.5 (13.8- 27.6)	62.5 (13.8- 27.6)	
6		112.5 (13.8 - 27.6)	62.5 (34.5 -55.2)	50.0 (27.6 - 55.2) 62.5 (55.2)
7	62.5 (13.8- 27.6)		75.0 (13.8- 27.6) 62.5 (13.8 - 27.6)	12.5(69 -82.8)

APPENDIX F

Table F 1 Deflection and stress results at subgrade/base from varying transiton thicknessess and transition layer resilient moduli using KENLAYER

Mar-95 Sections 1and 3
Deflection (μm) Stress in kPa
Defl (1) 526 Stress (1) 210
Defl (3) 448.5 Stress (3) 117.3

x Deflection on HMA surface
- Stress in Base
+ Stress in Subgrade

59°F

	Transition Layer resilient modulus (kPa)						
Contamination (mm	**13800**	**27600**	**34500**	**55200**	**69000**	**82800**	**103500**
2.5	799.75 x 102.396 -	792.8 102.3	791.3 102.3	789.0 102.2	788.3 102.2	787.8 102.2	787.0 102.1
5.0	813.5 102.7	800.0 102.6	797.3 102.6	792.8 102.5	791.3 102.4	790.0 102.4	789.0 102.3
13.0	852.5 103.4	821.5 103.6	814.8 103.5	804.0 102.9	800.3 103.2	797.5 103.1	794.8 102.9
25.0	913.0 104.0	855.8 105.0	843.0 105.0	823.0 104.7	815.3 104.5	810.0 104.3	803.8 103.8

Table F 2 Deflection and stress results at subgrade/base from varying transiton thicknessess and transition layer resilient moduli using KENLAYER

Mar-95 Sections 1and 3

Deflection (μm) Stress in kPa

Defl (1) 526 Stress (3) 210

Defl (3) 448.5 Stress (3) 117.3

x Deflection on HMA surface

\- Stress in Base

\+ Stress in Subgrade

70°F

	Transition Layer resilient modulus (kPa)						
Contamination (mm)	**13800**	**27600**	**34500**	**55200**	**69000**	**82800**	**103500**
2.5	861.25 x 117.714 -	852.8 117.4	851.0 117.4	848.5 117.2	847.5 117.2	847.0 117.2	843.3 117.1
5.0	877.8 118.3	861.5 117.9	858.3 117.9	852.8 117.6	851.0 117.5	849.8 117.4	848.5 117.4
13.0	924.5 119.9	887.3 119.5	879.0 119.3	866.3 118.7	861.5 118.5	858.3 121.5	855.0 118.1
25.0	999.8 122.0	929.8 122.0	914.0 121.6	888.8 120.8	879.8 120.3	860.8 119.9	864.0 119.4

Table F 3 Deflection and stress results at subgrade/base from varying transiton thicknessess and transition layer resilient moduli using KENLAYER

Mar-95 Section 7and 9

	Deflection (μm)
x Deflection on HMA surface	Defl (7) 1010

Stress in kPa

Stress (7) 940

- Stress in Base
+ Stress in Subgrade

70°F

	Transition layer resilient modulus (kPa)						
Contamination(mm)	**13800**	**27600**	**34500**	**55200**	**69000**	**82800**	**103500**
13.0	1170.2 x 38.9 +	1161.8 39.4	1159.8 39.5	1156.0 39.6	1154.5 39.6	1153.3 39.6	1151.8 39.6
25.0	1196.0 39.8	1178.5 39.6	1174.3 39.7	1167.0 39.9	1163.8 39.9	1161.0 39.9	1158.3 39.8
38.0	1194.3 38.6	1176.8 39.5	1172.8 39.6	1165.5 39.8	1162.3 39.8	1159.5 39.8	1156.8 39.7
50.0	1192.3 38.5	1175.3 39.4	1171.3 39.5	1163.8 39.7	1160.8 39.7	1157.8 39.6	1155.3 35.0
63.0	1276.5 38.5	1232.5 40.3	1222.0 40.9	1205.5 40.8	1196.8 40.7	1189.5 40.3	0.0 40.8

Table F 4 Deflection and stress results at subgrade/base from varying transiton thicknessess and transition layer resilient moduli using KENLAYER

Aug-95 Sections 1 and 3

Deflection (μm)	Stress in kPa
Defl (1) 713	Stress (1) 210
Defl (3) 675	Stress (3) 143

x Deflection on HMA surface
\- Stress in Base
\+ Stress in Subgrade

70°F

	Transition Layer resilient modulus (kPa)						
Contamination (mm)	**13800**	**27600**	**34500**	**55200**	**69000**	**82800**	**103500**
2.5	632 x 91.22 +	627.5 91.8	625.5 91.9	625.0 92.4	625.0 92.1	624.5 92.2	624.2 92.1
5.0	641.2 90.3	632.5 91.4	630.7 91.6	627.8 92.0	626.5 92.1	625.7 92.1	625.5 92.1
12.5	666.5 87.8	647.0 90.5	642.7 91.0	635.8 91.8	633.0 92.0	631.3 92.0	629.5 92.2
25.0	704.8 84.1	670.8 89.2	662.8 90.1	649.5 91.5	644.5 91.9	640.5 92.1	636.5 92.3
38.0	741.3 81.4	694.0 88.0	682.5 89.4	663.3 91.4	655.7 92.0	650.5 92.3	644.3 92.5
50.0	775.3 92.9	716.5 87.9	702.3 88.8	677.3 91.4	667.5 92.2	660.8 92.6	651.8 92.9

Table F 5 Deflection and stress results at subgrade/base from varying transiton thicknessess and transition layer resilient moduli using KENLAYER

Aug-95 Sections 4 and 6

x Deflection on HMA surface
\- Stress in Base
\+ Stress in Subgrade

Deflection (μm) Stress in kPa
Defl(4) 1038 Stress(4) 103.5
Defl(6) 1011 Stress(6) 101

70°F

	Transition Layer resilient modulus (kPa)						
Contamination (mm)	**13800**	**27600**	**34500**	**55200**	**69000**	**82800**	**103500**
12.5	820 x 61.6 +	806.3 62.9	803.3 63.1	797.8 63.3	796.0 63.5	794.5 63.6	792.8 63.6
25.0	851.8 60.1	825.8 62.5	818.2 62.9	810.8 63.0	810.6 63.2	810.2 63.5	809.5 63.9
38.0	882.5 59.0	846.5 62.3	837.8 62.9	822.0 63.8	816.0 64.0	811.3 64.0	813.8 64.0
63.0	947.3 57.5	888.8 62.2	874.3 63.1	874.3 65.4	872.9 64.6	870.1 63.5	866.5 63.0
75.0	980.8 57.1	911.3 62.2	894.3 63.4	883.0 64.2	879.5 64.9	877.5 65.6	872.1 66.9